DEPARTMENT OF
CIVIL, CHEMICAL, ENVIRONMENTAL, AND MATERIALS ENGINEERING - DICAM

SECOND CYCLE DEGREE

ENVIRONMENTAL ENGINEERING

CYCLIC TESTING OF NORTH SEA SANDS SUBJECT TO LOADS FROM OFFSHORE WIND TURBINE FOUNDATIONS

Supervisor
Prof. Barbara Zanuttigh

Co-Supervisor
Prof. Bruno Stuyts

Defended by
Shahriar Mokhtari

December/ 2023

Academic Year 2022/2023

Abstract

This thesis investigates the cyclic behaviour of North Sea sands under dynamic loads from offshore wind turbine foundations, addressing a key challenge in the shift towards renewable energy. It emphasizes the geotechnical aspects, particularly soil-pile system degradation, essential for the stability and sustainability of offshore wind structures.

The research methodology involved comprehensive undrained static and cyclic simple shear tests on various North Sea sands under different geotechnical conditions, including both dry and saturated states. These tests, accounting for variables like consolidation stresses, relative densities, and cyclic shear stresses, simulated real marine environmental conditions, primarily cyclic loads from waves, wind, and rotor action. The approach provided insights into the soils' behaviour under static and cyclic loading, with detailed shear strain contours and average pore pressure ratio (APPR) contours aiding a comparative analysis with existing models like Andersen's (2015) predictive models. The method also considered key factors such as fine content and drying methods, crucial in predicting the mechanical behaviour of sands under cyclic stresses. Additionally, replicating the cyclic DSS test conditions as outlined in the Fugro report for a Belgian offshore wind farm at Ghent University validated the consistency of test results, thereby further enhancing the empirical robustness of this study.

This study's key findings reveal an inverse relationship between Cyclic Stress Ratio (CSR) and failure cycles, consistent across different sands and significantly influenced by the relative density of the sands. Particularly, this relationship is more pronounced at higher CSR levels, suggesting significant influences of loading severity on soil deformation and failure mechanisms. The effect of relative density was observed to play a crucial role in the cyclic strength and behaviour of the sands, with denser sands demonstrating increased resistance to cyclic loading. Deviation from Andersen's (2015) predictive models, particularly at lower CSR and shear strain ranges, suggests a diverse response in North Sea sands, highlighting the need for model recalibration based on empirical data. These insights underscore the importance of considering CSR and local soil characteristics in offshore wind turbine foundation design, advocating for a tailored approach to ensure a comprehensive understanding of soil behaviour under varying conditions.

Acknowledgement

This thesis is the outcome of an extensive year of research, including a 10-month residency at Ghent University. During this time, many invaluable people have offered their assistance, which adds to the challenge of expressing my gratitude in this acknowledgement. Additionally, heartfelt appreciation is owed to those loved ones who have supported me wholeheartedly and behind the scenes.

I would like to extend my sincere thanks to my supervisor at Bologna University, Professor Barbara Zanuttigh, whose support was always precise, timely, and incredibly helpful.

My gratitude also goes to my co-supervisor at Ghent University, Professor Bruno Stuyts. His vision through problems exemplified wisdom and awareness, and his kindness has always been the motivation for me to proceed, especially when things were not going well.

I want to express my deepest thanks to my mother, Sheyda, and my sister, Sepide, who both tolerated the distance between us and accompanied me with their good wishes throughout this journey.

I am immensely grateful to my fellow traveller, Maria Teresa Monaciello, whose love and patience have been the essence of every moment, making this journey not only bearable but also joyful.

I also want to thank all the staff and fellow students at both universities who facilitated my journey and contributed significantly to my academic experience. A special acknowledgement is extended to the Erasmus+ program for its generous funding and support, which was instrumental in enabling my research and academic endeavours.

In conclusion, from the bottom of my heart, I want to acknowledge everyone who played a part in the transition to the new person I have become. If it were possible, I would thank each one of you individually for your invaluable contribution to my growth and development.

Contents

1 Introduction and Background

1.1 Overview of the Offshore Wind Industry

The global energy landscape has undergone significant changes in recent years, heavily influenced by geopolitical and environmental factors. The aftermath of events, such as Russia's invasion of Ukraine, added to the volatility in fossil fuel markets, accelerating the global shift towards more sustainable and reliable energy sources. Consequently, clean energy investments have soared, with a remarkable 24% increase between 2021 and 2023, outpacing the growth in fossil fuel investments. This momentum has not only been driven by the fluctuating fossil fuel prices but also by strong policy support from major economies like the US, Europe, China, and Japan. The alignment of energy security with climate goals, especially in import-dependent economies, further underscores the importance of this transition [1].

1.1.1 Significance and Growth of Offshore Wind Energy

By 2023, the wind energy sector is approaching a symbolic achievement: reaching 1 terawatt (TW) in operation, with expectations to double this by 2030. Such tremendous growth showcases the transformation of an industry that, four decades ago, saw limited installations in select European countries and parts of the US. Today, wind energy -especially offshore- extends its footprint to numerous countries worldwide, revolutionized by advancements like floating foundations that have expanded the horizons of the deployment [2].

However, 2022 proved a challenging year. 8.8 GW of new offshore wind was fed into the grid last year. The new additions are 58% lower than the bumper year of 2021(21 GW) but still make 2022 the second-highest year in offshore wind history. A confluence of factors—including unproductive government policies, increased logistics costs, and project delays—saw the unusual situation where fossil fuel ventures profited more than their renewable counterparts [2].

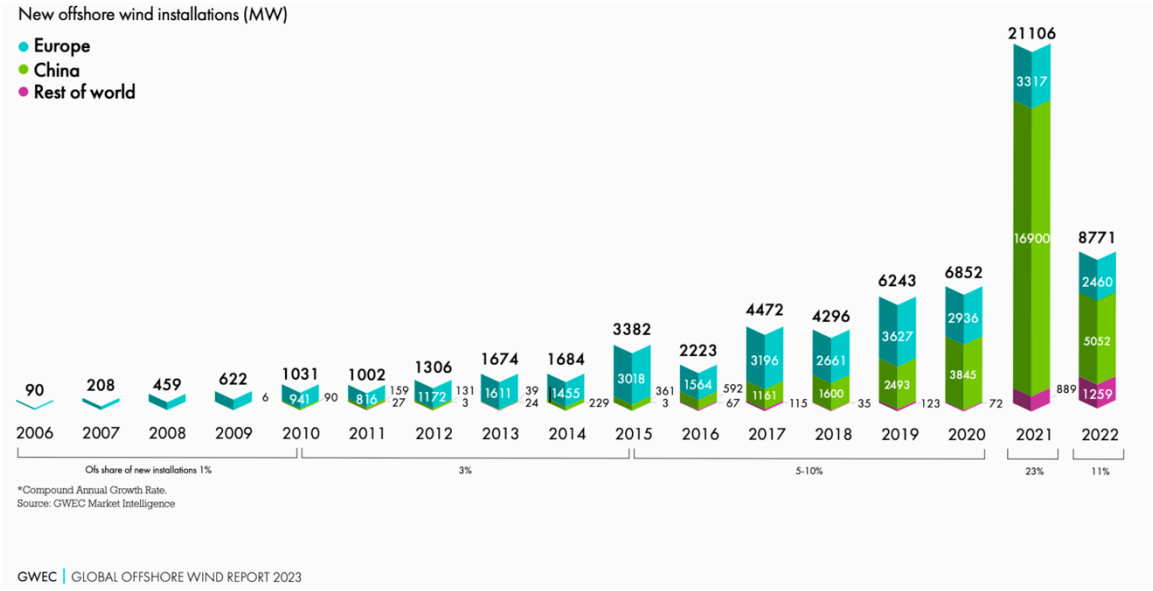

Figure 1-1 Compound Annual Growth Rate[2].

The wind industry's journey, from its early emphasis on reliability to cost reduction, now pivots towards achieving ambitious installation targets. The International Energy Agency (IEA) predicts the dominance of renewables, notably wind, in electricity generation from 2022 to 2025. Onshore wind is slated for annual installations surpassing 100 GW by 2024. In contrast, offshore wind targets over 25 GW in 2025. With an anticipated 680 GW added globally by 2027, offshore installations will contribute 130 GW. This narrative of acceleration is also marked by challenges. Several countries remain under the shadow of inhibitive policies. However, the vast benefits of wind energy—including

industrial growth, job creation, and environmental preservation—are pushing governments like the US and Europe towards supporting its proliferation through policies like the Inflation Reduction Act and REPowerEU [2].

Nevertheless, with the ambitious roadmap set for the wind industry, there are inherent challenges. Meeting the industry's demands, especially for offshore wind, necessitates robust investment in supply chains. While onshore wind has somewhat favourable projections, the offshore segment could face bottlenecks, particularly in Europe, by 2026. The industry must also address anticipated shortages in key components, such as blades and generators, by the decade's latter half [2].

1.1.2 The North Sea's Role in Offshore Wind Installations

As Europe intensifies its shift towards green energy to counter the challenges of global warming and climate change, the North Sea has emerged as a cornerstone in this transition. Notably, it's home to the world's largest offshore wind farm, completed in 2020, with an impressive capacity of 1218 MW from 174 turbines. Furthermore, the North Sea currently hosts over 41 wind farms with a combined capacity nearing 100,133 MW, encompassing around 2630 turbines. The strategic position of the North Sea, replete with key maritime ports and vital trade routes, amplifies its significance, making it an epicentre for offshore wind energy endeavours in Europe [1].

Beyond just wind energy, the North Sea's potential extends to fostering synergies between wind farms and wave farms. The existing wind farm infrastructures could be utilized to enhance the economic efficiency of upcoming wave farms. As offshore wind energy technology evolves, the trend is leaning towards harnessing deeper waters. While monopile structures currently dominate due to their cost benefits and installation ease, the future may see a shift towards floating structures, especially designed for the deeper waters of the North Sea. Supported by comprehensive certification and classification standards, the North Sea continues to be pivotal for Europe's renewable energy aspirations [1].

Europe's move to renewable energy highlights the importance of the North Sea, both for its wind energy potential and its unique marine environment. A study by Beermann et al. shows the significance of the south-eastern North Sea's sublittoral sandbanks. These underwater areas are not only crucial feeding zones for many marine species but are also unique in their composition and conditions. Although these sandbanks face challenges from activities like bottom trawling, they are still home to a variety of marine life. While some parts of the North Sea, like the Dogger Bank, are well-researched, the south-eastern section needs more attention. Given their environmental significance, these sandbanks emphasize the need for marine conservation in the North Sea [3].

1.2 Cyclic Loading of Soil in Offshore Wind Turbine Systems: Impacts of Waves, Wind, and Rotor Action

Offshore wind turbines are continually subjected to numerous environmental conditions, primarily cyclic loads from waves, wind, and rotor action. It is essential to thoroughly understand these cyclic loads as they directly impact the integrity and functionality of these turbines.

In offshore environments, wind turbines are mounted on foundations that face continual cyclic loads from varied sources. These cyclic loads do more than just exert repeated forces; they bring about a degradation in the soil-pile system's performance. This degradation manifests as a decline in the strength and stiffness of the soil, leading to a progressive reduction in the foundation's bearing capacity and an increase in its settlement. Basak's study on lateral cyclic loading on offshore pile foundations in oceanic conditions elaborates on this phenomenon, emphasizing that the degradation is influenced by factors such as the number of load cycles, frequency, and amplitude [4].

Chen et al. (2022) presented an extensive study on the effect of local cyclic loadings on shear strength in soils, especially in landslide-prone areas like the Three Gorges Reservoir Area (TGRA). Their findings underline that local cyclic loading leads to significant reductions in the shear stress of soil compared to monotonic loading. Such reductions, as indicated by historical events, have the potential

to induce landslides with devastating consequences. The insights from TGRA shed light on the importance of understanding stress-strain characteristics under such cyclic loading conditions, vital for maintaining stability and designing protective structures [5].

For offshore wind turbines in challenging environments like the North Sea, Möller et al. spotlighted the implications of soil liquefaction during high-intensity seismic ground movements. The liquefaction can dramatically diminish the inherent soil strength and stiffness. Their research emphasized the significant impact that low-frequency components of seismic shear waves can have, especially during extensive soil liquefaction. Wind turbine towers could be particularly vulnerable during intense seismic events due to significant nonlinearity in the soil surrounding their monopile foundations [6].

Sun et al. (2023) further delved into the subject by studying the effects of horizontal loads on the monopile foundations of offshore wind turbines. Their results revealed a clear degradation in the ultimate uplift-bearing capacity of the pile after horizontal cyclic loading, a crucial consideration, especially in dense soils. They proposed a semi-empirical model to predict this bearing capacity, emphasizing the need to account for these loads during offshore wind turbine installations [7].

1.2.1 Challenges in Conducting Cyclic Soil Tests

Performing cyclic soil tests using a cDSS apparatus as part of my master's research was no straightforward task, yet the challenges were successfully met to ensure that the tests met high accuracy standards. Achieving full sample saturation was especially nuanced; it required a meticulous process to make sure every particle was properly saturated, as anything less could compromise the integrity of the results. Another hurdle was determining the maximum and minimum density for the soil samples, particularly in cases where resources were limited.

Calibration was another area that posed challenges. This step was essential not just for meeting academic standards, but also for ensuring that the measurements were reliable. Calibrating the apparatus required a blend of in-depth scientific understanding and practical skills. The consolidation process also presented its own set of issues. The rate at which the soil was consolidated, pre-sheared, or sheared needed to be finely tuned; if it was too high, it could introduce inconsistencies and difficult to prepare the sample which might skew the test results. This meant spending a considerable amount of time preparing the samples and performing the tests to achieve the right balance.

Lastly, the uniformity of the sample bag could not be overlooked. Ensuring that the soil was evenly distributed throughout the bag was essential, as uneven soil could affect the reliability of the entire test. So, from start to finish, each step of the process had to be performed with a high level of care to ensure the results were as accurate and reliable as possible. [Author's Work].

1.3 General of Research

1.3.1 Effect of Sample Preparation on Shear Stress/Strain Tests

In the field of geotechnical engineering, achieving reliable test results is multifaceted. Not only does it depend on the precision of the equipment and adherence to standard procedures, but also on the meticulous preparation of the samples. With North Sea sand samples being the focal point of this thesis, understanding their unique characteristics during preparation is paramount to achieving consistent results. This study also aims to assess how variations in sample preparation influence the outcomes of shear stress and shear strain tests, especially when employing the cyclic direct simple shear (cDSS) apparatus at Ghent University. Kodicherla et al. (2018) properly remarked on how the method of sample preparation substantially dictates fabric anisotropy and packing density in reconstituted sand samples [8].

One area that proves to be particularly important is the quality and preservation of the samples. Andersen et al (2015) has highlighted the challenges of obtaining high-quality samples of sand and silt that genuinely reflect in-situ conditions. Often, when "intact" samples are significantly disturbed, specialists resort to reconstituting the soil, but this might deviate from authentic in-situ conditions.

The cyclic shear strength of sand and silt can be profoundly influenced by how the sample is prepared [9]. It further underscores the importance of understanding the inherent challenges in sample preparation to ensure consistent and accurate results.

In this research, three distinct techniques are employed for preparing North Sea soil samples:

- Dry tamping under constant volume conditions
- Moist tamping under constant stress conditions
- Wet pluviation under constant stress conditions

These methods are chosen to scrutinize how different preparation procedures affect the mechanical properties of the samples, such as undrained shear strength. Of particular interest is the dry technique under constant volume conditions. This approach is predicated on existing research by R. Dyvik (1987), and Bjerrum & Landva (1966), which suggests that controlling volume during dry testing can simulate the change in vertical stress equalling pore water generation. This is thought to be reflective of real-world, fully saturated offshore conditions. Using the cyclic direct simple shear (cDSS) apparatus at Ghent University, the aim is to validate whether this dry, constant-volume approach indeed mirrors the behavior of soil in offshore settings. While the dry tamping technique is particularly used for cyclic tests, all three methods offer valuable insights into the broader range of mechanical properties under different conditions [10], [11].

In this study, metal rings are used to limit radial deformation during the tests, approximating real-world conditions where soil experiences undrained shear while keeping a constant volume. This methodology is corroborated by recent research from Sun et al. (2023), emphasizing that the initial soil fabric, set during sample preparation, significantly impacts the soil's response to shifts in the principal stress axis [7].

1.3.2 Effect of Saturation

In addition to the above methods, the study also involves the implementation of post-saturation techniques to simulate realistic scenarios. Once the sample is assembled in the cDSS apparatus, it is saturated using a specialized setup involving a tank and hydraulic gradient. This approach ensures that the behavior of the soil under both dry and fully saturated conditions is captured, particularly relevant to offshore settings where a saturated sample is present. The post-saturation process is monitored meticulously until no air bubbles are observed exiting the drainage channels, ensuring full saturation of the soil sample. This saturation process aims to offer a nuanced understanding of the soil's mechanical properties, especially its shear strength, under conditions commonly found in offshore environments.

1.3.3 Effect of Fine Content

The influence of fine content isn't just theoretical; it has practical implications that can significantly affect the accuracy and reliability of soil tests. For instance, during the sample drying process in the testing procedures, a high fine content led to the sample forming noticeable lumps. These lumps seemed to adhere to each other but could be easily broken apart by hand. This phenomenon inevitably introduced an element of error into the results. To mitigate this issue, sieving the samples to remove them was resorted to, but this came at the cost of reducing the sample size substantially. Furthermore, the presence of a high proportion of fines can make the saturation process for soil samples more challenging and time-consuming.

Fine content in soil significantly impacts its mechanical properties, particularly shear strength, and its liquefaction susceptibility. The presence of fines can affect various aspects of soil behaviour, including the outcomes of static tests. In static shear strength measurements, the preparation method of soil samples, such as whether they are 'intact' or 'reconstituted,' can yield different results, and these discrepancies are amplified with variations in fine content. Factors like in situ relative density and water content also become less predictable with increasing levels of fines [9].

In cyclic loading conditions, the fines content can dramatically decrease a soil's resistance to liquefaction, a phenomenon that can have catastrophic implications for structural stability during seismic events. Specifically, the amount of fine content can act as a marker for a soil's liquefaction resistance, with low and high fine levels generally increasing soil's resistance to liquefaction and moderate levels of fine content could diminishing it. The fines block the drainage paths in the soil, thereby preventing efficient drainage and facilitating the build-up of pore pressure, which in turn decrease the soil's resistance to liquefaction. This effect becomes even more significant in conditions where the soil has low relative density and is under low confining pressure. Beyond its impact on liquefaction resistance, fine content also has significant ramifications for the criteria used to evaluate a soil's susceptibility to liquefaction. While traditional factors like clay content, liquid limit, and water content are commonly assessed, the inclusion of plasticity-based criteria can offer a more comprehensive evaluation [12], [13].

2 Literature Review

2.1 Standard Practice for Constant Volume Static and Cyclic DSS Testing

2.1.1 Direct Simple Shear (DSS) Test

The Direct Simple Shear (DSS) test is an integral part of geotechnical engineering, offering invaluable insights into soil properties. Originating as a means to evaluate the shear strength of soil, the DSS test has evolved into a versatile tool also capable of assessing stiffness degradation during cyclic loads [14].

In a DSS test, a soil disc is exposed to a specified normal stress while being sheared. A series of stacked rings surround the sample to ensure the rotation of the principal axes throughout the test. One of the unique features of DSS testing is its control system that maintains a constant sample volume, essentially imposing an undrained shearing condition on the soil. As a result, the maximum shear stress recorded during the constant volume DSS test is indicative of the undrained shear strength of the sample [14].

Cyclic loading can cause excess pore pressure to build up, leading to a decrease in the soil's shear modulus. The level of degradation depends on several factors including the initial state of the soil, the magnitude of applied average and cyclic shear stresses, and the number of applied stress cycles [14].

The cyclic variant of the DSS test, known as cDSS, is particularly useful for understanding how soil behaves under undrained cyclic loading conditions. cDSS tests don't measure excess pore pressures directly due to the absence of a back-pressure system for sample saturation. However, the change in vertical stress observed during cDSS testing is considered to be analogous to the excess pore pressure that would develop in a saturated sample. The test setup is shown in Figure 2-1 [14].

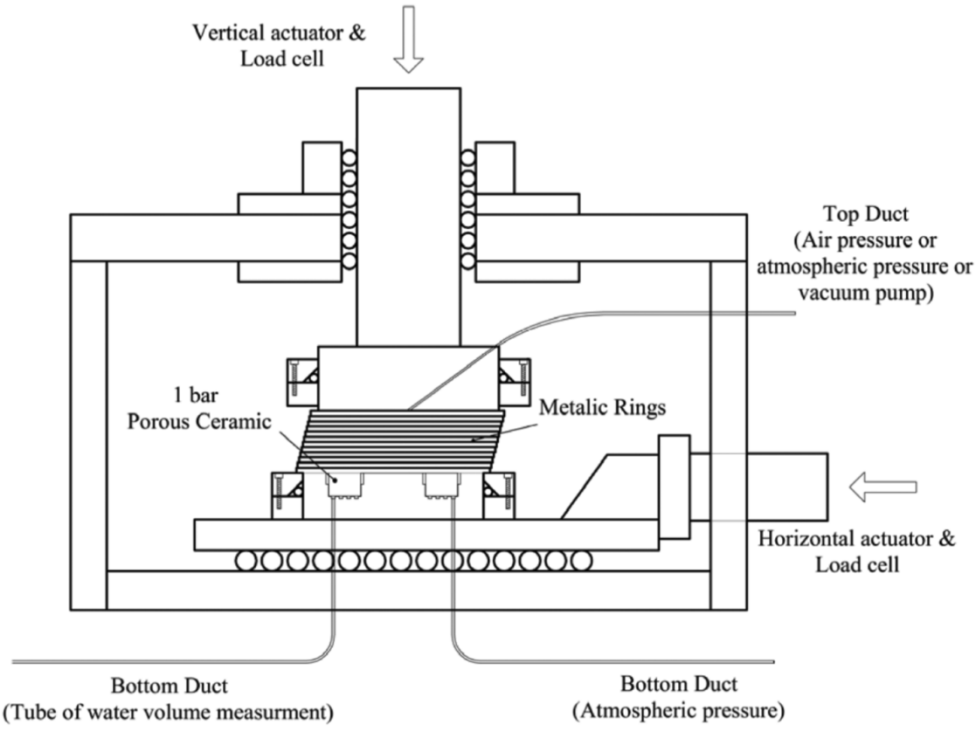

Figure 2-1. Test setup for a direct simple shear (DSS) test [14]

A typical cDSS test involves consolidating a thin soil disc under a representative vertical pressure. The bottom of the sample is then moved cyclically relative to the top. The use of shear stress oscillation between a specified minimum and maximum value is common, and a series of tests with varying shear stress amplitudes is performed to thoroughly characterize the cyclic response of the soil. For instance, a study conducted on a sandy clay from the Hollandse Kust Zuid OWF displayed the growth in cyclic

shear strains as the vertical effective stress on the sample reduced due to the build-up of apparent excess pore pressure (Stuyts, 2023).

2.1.2 Sample Preparation

Direct Simple Shear (DSS) test is paramount for understanding the shear characteristics of soils. However, DSS tests are deeply rooted in the sample preparation. The way a soil sample is prepared can profoundly influence its physical and mechanical attributes, ranging from its density and porosity to its permeability, strength, and stiffness. Given these implications, the selection of an appropriate sample preparation method becomes pivotal. This method should not only mirror the field conditions but also ensure the extraction of reliable test results.

The choice of sample preparation method in Direct Shear Tests on sand significantly influences test outcomes, including void ratios and shear strength. The literature highlights the nuanced differences in results based on whether one uses tamping or pluviation, and whether these methods are applied in a wet or dry state. In a study by Raghunandan et al. (2012), it was shown that void ratios in samples prepared by dry and moist tamping differed noticeably, even when varying parameters like the number of layers or the drop height of the tamper were considered. Likewise, in the pluviation method, factors like mass-flow rate and the height through which sand particles are rained into a mould had varying impacts on the void ratio. Particularly noteworthy is the observation that wet pluviated samples did not exhibit dilation in drained triaxial tests, unlike their dry pluviated counterparts. Moist tamped samples were also found to dilate less than dry tamped samples. These variations in sample behaviour underscore the importance of methodical sample preparation, as they lead to differences in mechanical responses like shear strength and volumetric strain, which can be critical in geotechnical engineering applications.[15]

In the research conducted by Abdullah Talib Al-Yasir and Abbas Jawad Al-Taie, a new sand raining technique was developed with the objective of preparing larger sand specimens more effectively and quickly. This "sand raining" is a laboratory method to prepare sand samples, and the relative density (RD) of these samples is affected by various factors such as the falling height (HF) of the sand and deposition intensity (DI). The study introduced a novel system called the trapped air raining device (TARD), which significantly enhances the RD of the sand samples. Importantly, how samples are prepared can directly influence the characteristics of the soil grains. Traditional techniques risk breaking sand grains, while the raining method avoids this and allows for the fast preparation of large samples. Moreover, the RD of the soil samples is critical because it determines soil characteristics like porosity, void ratio, and grain collision dynamics. This new TARD system, by controlling both the height of rain and the DI simultaneously, achieves a very high RD, reducing sample preparation time by over 90% in comparison to traditional methods [16].

Andersen (2015) points out the difficulty in obtaining high-quality samples that genuinely represent these conditions. The choice between using 'intact' and reconstituted samples significantly affects outcomes; reconstituted samples can offer lower strength than their 'intact' counterparts. However, it's essential to note that sample reconstitution can be problematic, especially when the silt content is high or when fines include clay. The inherent complexities in determining the in situ relative density or water content also add to the challenge, with both metrics proving difficult to estimate confidently. External factors, such as preshearing—a process involving cyclic loading with drainage—can also influence the cyclic shear strength of a sample. While preshearing can enhance cyclic shear strength, its impact on sample preparation hasn't been widely studied. Andersen also suggests that when reconstituting sand, the target density should be based on estimated in situ metrics. However, there are inherent uncertainties, such as variations in calibration chambers or the potential inaccuracies in correlating in situ relative density through CPT. Laboratory measurements, like water content, can provide a more defined parameter, but factors like the determination of maximum and minimum dry densities introduce further uncertainties [9].

One such enlightening research is the "Effects of preparation methods on inherent fabric anisotropy of reconstituted sand samples". This study delves deep into the distinctions brought about by different preparation methods - dry tamping, moist tamping, dry pluviation, and wet pluviation. These methods,

analogous to those in previous research, induce varying degrees of inherent fabric anisotropy in reconstituted sand samples. It was discerned that the method of sample preparation not only impacts the physical characteristics, such as porosity and void ratio, but also the internal grain structure and alignment. These subtleties in grain arrangement can precipitate significant variations in soil behaviour, affecting parameters like shear strength, dilation tendencies, and stiffness. Dry and moist tamping, for instance, showed differing grain alignments leading to contrasted mechanical properties. Wet pluviation, on the other hand, introduced unique fabric arrangements, distinct from its dry counterpart. Such intricate variations echo the assertions from Raghunandan et al. (2012) and Al-Yasir & Al-Taie (2023) about the profound implications of the sample preparation techniques. This study reaffirms the pivotal role of the preparation method in deriving reliable, consistent, and representative results that mirror real-world soil behaviours [8].

There are four main sample preparation methods for soil mechanics: wet pluviation, dry pluviation, dry tamping, and moist tamping which are described in the following.

Dry pluviation

Dry pluviation is one possible sample preparation method for soil mechanics [17]. This method involves pouring dry soil particles into a mould through a funnel from a specific height, producing relatively loose samples with low density and high porosity. The benefits of this method include its ability to create specimens with different densities and stress states while avoiding particle segregation and crushing. However, it may not accurately represent the natural soil structure and fabric and requires careful control of the pouring parameters [15], [18].

Wet Pluviation

Another common method for preparing soil samples for mechanical tests is wet pluviation [17]. This method requires pouring water-saturated soil through a funnel onto a porous base plate within a cylindrical mould. The soil particles rearrange due to the falling water and form a loose deposit with uniform density and moisture content. This method can produce large samples with minimal disturbance and can simulate natural deposition processes. However, it may not be suitable for very fine-grained soils, it could cause soil particle segregation, and it may not represent the in-situ stress conditions of the soil [15], [18].

Moist tamping

Moist tamping is a common technique for preparing soil samples for laboratory testing, especially for investigating the liquefaction properties of sandy soils. The moist tamping method involves compacting soil samples layer by layer in a mould with a tamper. The soil is mixed with water to achieve a certain moisture content before tamping. The number of layers, the height of each layer, the weight of the tamper, and the number of blows per layer are some of the parameters that affect the specimen preparation. The main advantage of this method is its convenience and ease of application. It can also produce specimens with uniform density and moisture content throughout the sample ([15], [19], [20]).

However, the moist tamping method also has some drawbacks and challenges. One of them is the non-uniformity of the soil fabric and structure induced by the compaction process. The soil particles tend to align in a certain direction due to the repeated blows of the tamper, resulting in an inherent fabric anisotropy in the specimen. This anisotropy can affect the mechanical behaviour of the soil under loading conditions, such as its strength, stiffness, and liquefaction resistance. Another challenge is the difficulty in controlling the exact moisture content and density of the specimen, as they depend on various factors such as the initial water content, the compaction energy, and the soil gradation. Moreover, the moist tamping method may not be suitable for soils with high fine content or plasticity, as they may exhibit different compaction characteristics and require different moisture contents [20], [21].

Dry Tamping

Dry tamping is a common method for preparing soil samples for laboratory tests, especially for sand-clay mixtures. It involves compacting dry soil into a mould by applying a series of blows with a hammer. The advantages of dry tamping are that it can produce uniform and repeatable samples with a desired density and water content and that it does not alter the soil structure or fabric. However, dry tamping also has some limitations, such as requiring a large amount of soil, being time-consuming and labour-intensive, and being sensitive to variations in soil gradation and moisture [20].

Dry tamping is a technique for preparing soil samples for laboratory tests, such as triaxial compression or direct shear tests. It involves compacting dry soil particles into a mould by applying a series of blows with a hammer. (ASTM D698, 2012). The key advantage of this method lies in its ability to create uniform specimens with a loose structure. Dry tamping does not form metastable structures that can potentially influence the soil's mechanical behaviour [20].

Nonetheless, it's worth noting that dry tamping may not be ideal for all soil types. Specifically, well-graded soils or soils with a high content of fines might not be suited to this method as it could lead to segregation or inadequate particle-to-particle contact [22].

2.1.3 Effects of Consolidation

The phenomenon of increasing soil strength over time, particularly noticeable in clays due to secondary compression in addition to consolidation, has been well-studied, resulting in the concept of an apparent preconsolidation stress. However, similar effects in sands and silts have garnered less scholarly focus. Notably, even clean sands display long-term increases in strength related to consolidation time, as evident in an oedometer test on very dense clean sand, illustrated in Figure 2-2. [9].

Example of measured and calculated vertical strains with best-fit parameters in oedometer test on clean sand.

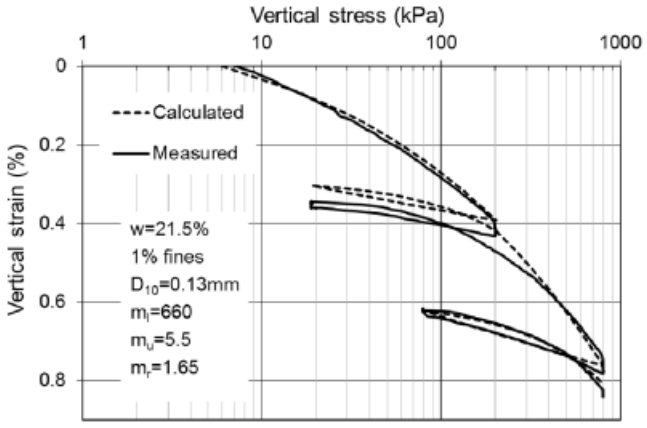

Figure 2-2. Example of measured and calculated vertical strains with best-fit parameters in oedometer test on clean sand.

The relationship between cyclic shear strength and time has been visualized, as shown in Figure 2-3 [9].

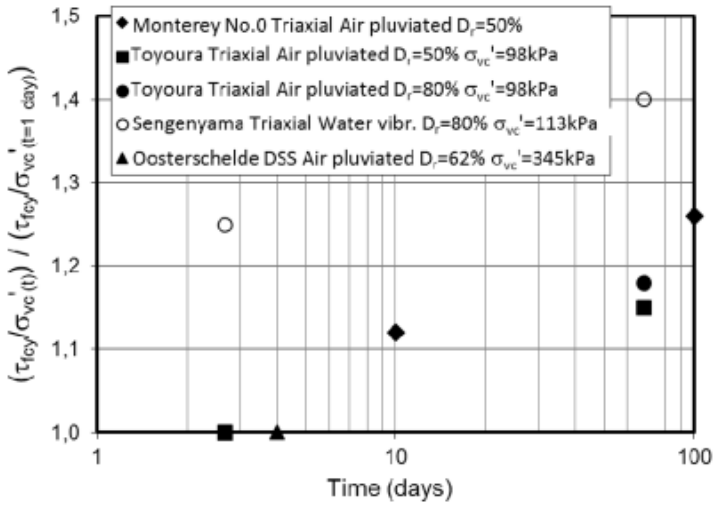

Figure 2-3. Increase in cyclic shear strength as a function of consolidation time.

In examining the temporal effects on the cyclic shear strength of sand, various studies offer insightful perspectives. According to Andersen (2015), Tatsuoka et al. (1986a) discovered a 15–20% increase in the cyclic strength of isotropically consolidated triaxial tests on Toyoura sand with no fines after 68 days, for relative densities of both 50 and 80%[9].

Tatsuoka et al. (1986a) delve deeper into the multifaceted factors affecting cyclic undrained behaviour. Their study focused on Toyoura Sand, scrutinizing a range of variables including loading frequency, the method of pluviating sand, and the duration of sustained compression among others. Their findings show the cyclic undrained triaxial strength increased significantly when the specimen was compressed for approximately 68 days. The study indicates that strength can be affected by long periods of sustained compression, but they found negligible differences in strength with respect to shorter sustained compression periods between 6 minutes and 64 hours. In essence, this reinforces the complexity of time as a variable in cyclic shear strength [23].

Building on their earlier research, Tatsuoka et al.'s 1988 paper further explores the effects of consolidation on the strength and resistance of sand to undrained cyclic loading—a key factor in assessing susceptibility to liquefaction. Their findings revealed that a 68-day period of sustained pressure or over-consolidation with an OCR (Over-Consolidation Ratio) of about two both led to similar increases in strength. They hypothesized that these gains in strength may be due to the same underlying mechanism, potentially the rearrangement of sand grains into more stable configurations. This discovery could negate the need for complex interventions like preloading. The study also found that sands with some fines displayed greater strength increases compared to cleaner sands. These findings underscore the significant role that consolidation history, whether long-term or short-term, plays in affecting the mechanical behaviour of sand, thereby influencing both test outcomes and the inferences made from them [24].

It's worth noting that for many conventional projects, replicating long-term effects in a lab setting may be unfeasible. Andersen suggests allowing the final consolidation stress to act overnight and emphasizes that effects resulting from longer consolidation times should be assessed based on expert judgment and past experiences. It's also crucial to consider the type of sample being used. Andersen points out that reconstituted samples without preshearing were used in his examples, implying that intact or presheared samples may exhibit different behaviours. Moreover, any aging effects could potentially be reversed if samples are consolidated beyond their apparent pre-consolidation pressure.

This nuanced understanding of sample behaviour aligns well with our study's findings and serves as a valuable consideration for future research[9].

2.1.4 Preshearing Phase

Preshearing is often carried out after the soil specimen has reached its specified consolidation stresses but before monotonic or cyclic loading begins. Andersen (2015) presents the criteria for preshearing, stating that soil samples should undergo this process if subjected to cyclic loading with drainage before or during the main event. On the other hand, intact samples already affected by pre-sampling cyclic loading don't require additional preshearing[9].

Transitioning from the theoretical framework, Andersen (2015) provides practical insights, estimating that in applications like offshore gravity platforms on dense sand, preshearing has been about 400 cycles at a normalized cyclic shear $\frac{\tau_{cy}}{\sigma'_{ref}} = 0.04$. As illustrated in Figure 2-4 (included in this section) from Andersen (2015), preshearing can enhance a soil sample's cyclic shear strength by approximately 5% to 25% when compared to non-presheared samples. Notably, this figure incorporates data from various test types like DSS, shaking tables, and triaxial tests, indicating that the impact of preshearing is consistent across different testing methodologies. Adding to the complexity, the volume reduction in the soil during preshearing is generally small, suggesting that increased density alone does not account for the enhanced cyclic resistance[9].

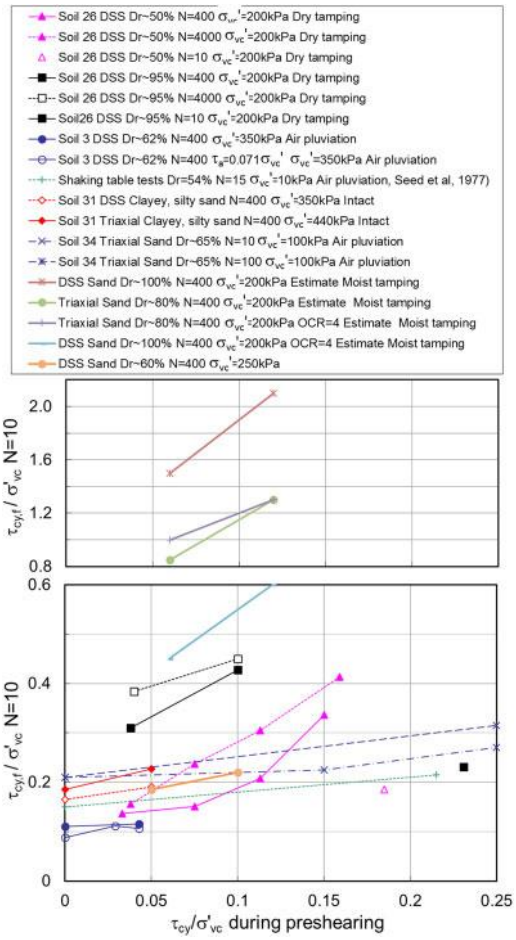

Figure 2-4 Effect of preshearing on undrained cyclic shear stress at failure in triaxial and DSS tests on sand and silty sand [9].

One key challenge in implementing preshearing is determining the in situ relative density (D_r), which is often estimated based on Cone Penetration Test (CPT) correlations. These correlations, however, come with limitations such as the effects of sand type, fines content, and preconsolidation. For overconsolidated soils, the impact of preshearing can be different. In Drammen clay, for instance, preshearing increased resistance in normally consolidated clay but reduced it in overconsolidated clay [9].

Building upon Andersen's work, Quinteros et al. (2017) focus on the drained strength and stiffness of dense sands, an area that had been relatively understudied. Their research involved drained triaxial compression tests performed on a North Sea sand specimen, both with and without preshearing. They discovered that preshearing did not significantly influence either the drained strength or stiffness of the sand, but may mitigate seating issues, thus allowing for better initial test conditions. This is significant for designing offshore structures exposed to a variety of cyclic loads. Interestingly, the findings by Quinteros et al. (2017) deviate from earlier studies, which were mainly concerned with the effects of preshearing in liquefaction scenarios involving loose sands[25].

The study by Pan, Yang, and Xu (2018) further extends the discourse by specifically investigating the impact of preshearing on undrained anisotropy and shear characteristics of saturated sand. Their experimental program revealed that static preshearing at drained compression and extension conditions significantly influences the undrained behaviour of saturated sand, with noticeable differences between triaxial compression and extension tests. They found that both initial effective stress path and pore-pressure responses are markedly influenced by the direction and magnitude of static preshearing. Moreover, their research emphasized that stiffness anisotropy can be attributed to evolving microstructures due to static preshearing and that the effects of static preshearing on undrained strength and brittleness during subsequent loadings are consequential[26].

2.1.5 Shearing Phase

The Direct Simple Shear (DSS) test forms a crucial part of our understanding of soil behaviour under shear stress. In this test, a disk of soil is subjected to a predetermined normal stress while being sheared. The stacking of rings around the sample ensures rotation of the principal stress axes throughout the experiment. To maintain a constant sample volume, a control system is utilized, effectively imposing undrained, constant volume shearing conditions on the soil sample. The variation of shear stress with respect to increasing shear strain is meticulously recorded. It has been conventionally accepted that the maximum shear stress reached during this constant-volume shearing phase represents the undrained shear strength of the soil sample[14].

Continuing from this foundational understanding, recent studies have prompted a re-evaluation of the assumptions that underlie the interpretation of the DSS test's shearing phase. Bernhardt-Barry et al. (2021) employed Discrete Element Method (DEM) models and discovered notable discrepancies between the stress states within the soil sample and those inferred from boundary measurements. Their research indicated that while shear stresses derived from boundary measurements can be representative of the central zone of the specimen, there is a more significant divergence in the normal effective stresses. This divergence calls for caution in interpreting DSS results, particularly when dealing with dense specimens [27].

Moreover, their study challenges conventional paradigms regarding the distribution of stress on various planes within the sample during shearing. Contrary to traditional thought, Bernhardt-Barry et al. (2021) found that the maximum shear stress ratio does not occur uniformly across all planes; rather, it is reached at different strain levels depending on the orientation of the plane within the sample[27].

2.2 Cyclic Soil Behaviour

When it comes to the behaviour of soil under cyclic loading, especially around foundations, it's crucial to understand that the stress conditions are multifaceted. Andersen (2015) simplifies this complex reality by outlining the shear stresses along a possible failure surface below a shallow

foundation. The soil elements along this plane are exposed to diverse stress paths like compression, Direct Simple Shear (DSS), and extension. This leads to variations in both average shear stress, τ_a, and cyclic shear stress, τ_{cy}. Figure 2-5 below shows the shear stresses along a potential failure surface in the soil beneath a shallow foundation.

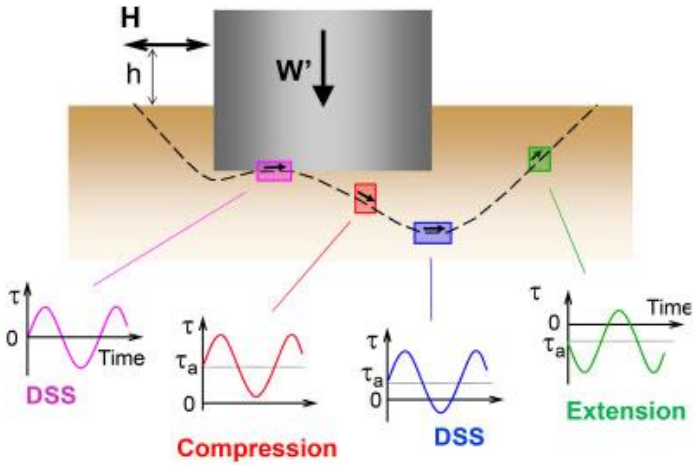

Figure 2-5 Simplified stress conditions for typical elements along a potential failure surface beneath a shallow foundation[9].

In Andersen's study, τ, represents the shear stress observed on the 45-degree plane in compression and extension elements and on the horizontal plane in DSS tests. Such cyclic loading is stress-controlled to accurately model cyclic events, particularly those defined in terms of applied loads. A significant part of understanding this behaviour lies in the quantification of average shear stress, τ_a, which is expressed as the sum of τ_0 and $\Delta\tau_a$. Here, τ_0 is the initial shear stress in the soil before any structural installation and acts under drained conditions. On the other hand, $\Delta\tau_a$ is the additional shear stress induced by the submerged weight of the structure and average environmental loads [9].

These components of average shear stress can act under either drained or undrained conditions, heavily influenced by the soil type and drainage characteristics. For example, in sandy soils, drainage occurs relatively quickly, leading to rapid consolidation under the weight of the structure. Conversely, for clays, it's often conservatively assumed that significant consolidation may not happen before a design storm hits, thereby affecting the soil's cyclic shear strength [9].

The cyclic shear stress, τ_{cy}, is particularly influenced by fluctuating environmental loads. These loads can vary from one cycle to the next, resulting in a non-uniform cyclic shear stress. In a laboratory setting, soil samples are first consolidated to in situ effective stresses and subsequently subjected to shear stresses that approximate as closely as possible the in-situ stress conditions during cyclic loading. Though no existing laboratory equipment can perfectly reproduce all in situ conditions, Andersen (2015) argues that both triaxial and DSS tests offer reasonable approximations for crucial stress conditions. These tests are therefore widely used in design calculations for their practical utility.[9]

2.2.1 Soil Behaviour under Undrained Cyclic Loading

Cyclic loading generally degrades the soil structure and fosters a tendency for volumetric compression. For saturated soils under undrained conditions, these volumetric changes are restrained by water's low compressibility compared to the soil skeleton. This shift effectively transfers part of the soil's normal stresses to the pore water, causing a decrease in effective stresses in the soil. Figure 2-6 shows the effective stress path for undrained tests with monotonic and cyclic loading in contracting soil [9].

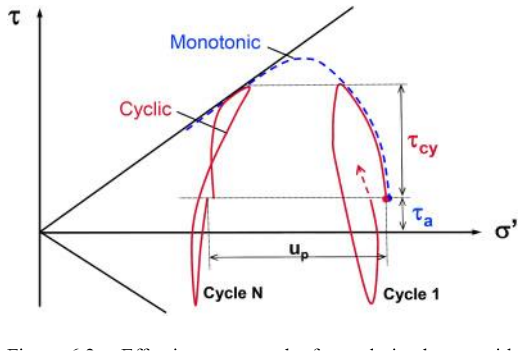

Figure 2-6 Effective stress paths for undrained tests with monotonic and cyclic loading in a contracting soil

In the framework of effective stress paths, Andersen contrasts monotonic and cyclic loading. In monotonic loading, the soil first exhibits a peak shear stress and subsequently softens, aligning with the failure envelope. However, under cyclic loading, the soil incurs incremental pore pressure changes with each cycle, eventually reaching the failure envelope. Notably, soils like dense sand, which possess strong dilative properties, can maintain limited shear strains even when the effective stresses are near zero, though this capacity tends to degrade over repeated cycles.

Andersen introduces parameters to quantify the development of pore pressure and shear strain over time for soil subjected to undrained cyclic loading. These parameters include permanent pore pressure (u_p), cyclic pore pressure (u_{cy}), and average pore pressure (u_a), along with their corresponding shear strains (γ_p, γ_{cy}, and γ_a). Hysteretic damping, an essential aspect in this context, is defined by the area within the stress-strain loop.

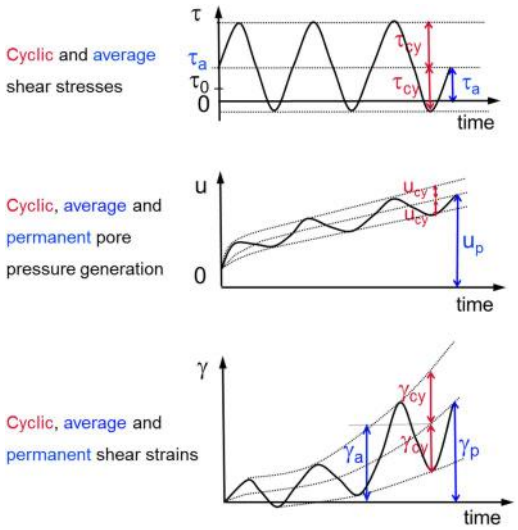

Figure 2-7 Pore pressure and shear strain as functions of time under undrained cyclic loading[9].

The permanent pore pressure is critical for assessing the cumulative effect of cyclic loading, particularly in sandy soils, where pore pressure dissipation and generation can occur simultaneously. On the other hand, cyclic shear strain serves as a primary parameter for calculating cyclic displacements and soil spring stiffnesses. The average shear strain is needed to compute the maximum shear-induced displacement during the cyclic loading event.

The pore pressure and shear strain components are defined as follows: [9]

– The permanent pore pressure, u_p, and the permanent shear strain, γ_p, are the values at the end of a cycle when the shear stress returns to the shear stress at the start of the cycle

– The cyclic pore pressure, u_{cy}, and the cyclic shear strain, γ_{cy}, are the single amplitude values, i.e., half the peak-to-peak values within a cycle

– The average pore pressure, u_a, and the average shear strain, γ_a, are the average of the high and low peak values within a cycle

Furthermore, Andersen (2015) discusses the importance of the permanent shear strain for calculating residual displacements after the cyclic event has concluded. However, this parameter has traditionally not been the focus of specific studies and is often assumed to be the same as the average shear strain.

2.2.2 Characterization of stiffness degradation during cyclic load

The increment of excess pore pressure during cyclical loading has the potential to decrease the soil's shear modulus. The extent to which this degradation occurs is influenced by several variables, such as the soil's initial conditions, the applied mean and cyclic shear stresses, and the total number of stress cycles experienced by the soil. In the following section, the geotechnical lab tests commonly employed for evaluating the soil's cyclic behavioral traits are detailed.

Cyclic Direct Simple Shear Testing (cDSS)

Beyond determining the basic strength and stiffness parameters of soil under monotonic loading, laboratory-based geotechnical tests also serve to monitor the incremental build-up of excess pore pressure in soil subjected to cyclic, undrained loading conditions. When such pore pressure accumulation occurs, there is a corresponding deterioration in soil stiffness. This is especially critical when piles transfer significant cyclical loads to the adjacent soil, leading to a possible weakening of the pile-soil stiffness over time[14].

The cDSS test is instrumental in capturing the evolution of shear strains and the subsequent pore pressure increases in soil under undrained cyclic loading. Here, a thin soil disc is consolidated under a vertically applied stress that is representative of the in-situ conditions. Post-consolidation, the sample's bottom is moved in a cyclical manner relative to its top. It is worth mentioning that the test configuration lacks a back-pressure system for saturating the sample; hence, pore pressures are indirectly inferred. The test is conducted on a dry soil sample, and the changes in vertical stress observed during the test are assumed to be synonymous with the excess pore pressures that would develop in a fully saturated sample. To mimic undrained conditions, a control algorithm is utilized to maintain either constant volume or equivalently, constant height. The cDSS test generally employs a load control mechanism, allowing for specified fluctuations in shear stress between established minimum and maximum thresholds. A series of tests, characterized by varying cyclic shear stress amplitudesτ_{cy}, is commonly executed to gauge the soil's cyclic response. The shear modulus decay is quantified by examining the measured $(\tau - \gamma)$ relationships and calculating the secant stiffness for each cycle. The damping attributes are calculated from the hysteresis loop areas in each $(\tau - \gamma)$ cycle [14].

In Figure 2-8, an example cDSS test result is showcased for sandy clay sourced from Hollandse Kust Zuid OWF. This sample was consolidated under a vertical effective stress of 150 kPa and subjected to a shear stress amplitude of 30 kPa. The data indicates that as cyclical loading persists, there is a consistent increase in the amplitude of the cyclic shear strains, while the vertical effective stress drops due to the accumulation of (apparent) excess pore pressures. This decrement is consistent up to approximately 300 cycles, after which a noticeable acceleration occurs. At this juncture, excess pore pressure reaches about 75% of the initial consolidation pressure. While the test is conducted under fully undrained conditions, it should be noted that allowing the excess pore pressures to dissipate would result in a restoration of the sample's strength. In the context of monopile design, it becomes crucial to evaluate both the drainage scenarios and the likelihood of cyclic degradation under the imposed shear stresses[14].

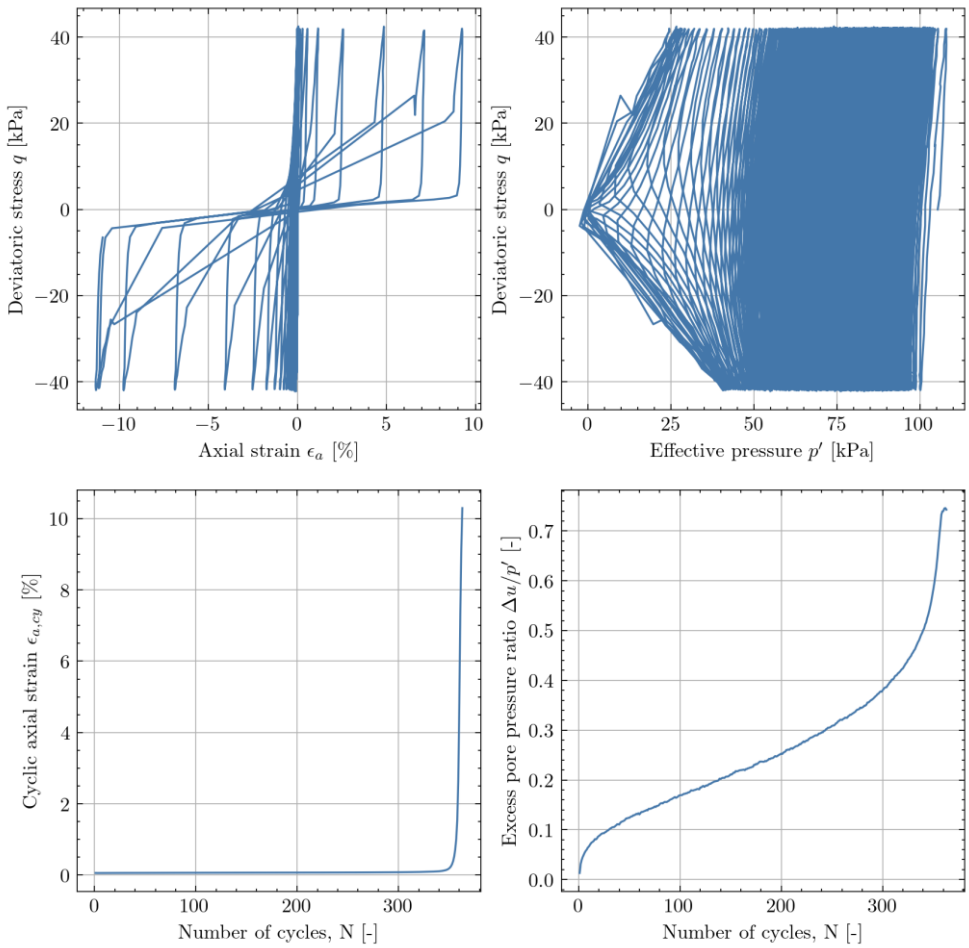

Figure 2-8 Example cyclic triaxial results showing the development of axial strains and excess pore pressures with increasing cycle numbers for a fine sand isotropically consolidated to 105kPa [14].

2.2.3 Damping

The damping coefficient, often denoted by (D), is influenced by several factors such as the average and cyclic shear stresses, the number of stress cycles, and the type of stress path (whether it's triaxial or DSS). Although this aspect of cyclic soil behaviour hasn't been explored as extensively as others, there is some data available. These data points are graphed as a function of cyclic shear strain in Figure 2-9, which primarily draws on findings from stress-controlled two-way cyclic DSS tests that had a 10-second loading period, as well as resonant column tests conducted on Great Belt Clay with an OCR value of 3. The graphical representation in Figure 2-9 reveals that the damping coefficient's value can vary based on the number of cycles [9].

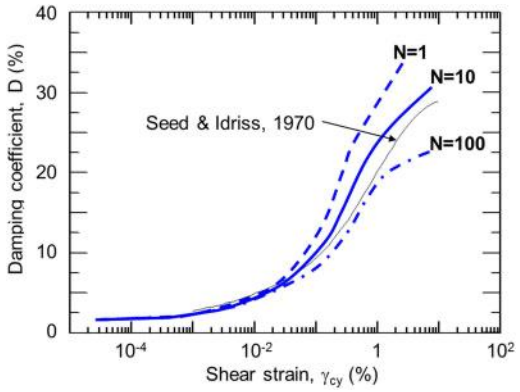

Figure 2-9 Damping coefficient as determined in stress-controlled two-way cyclic DSS tests.

The damping behaviour of soil plays an integral role in offshore wind turbine structures, significantly affecting their foundation lifetime. Stuyts et al. argue that understanding soil damping is complex, given its dependency on various elements like soil stiffness, shear strains in the subsoil, and pile-soil interaction models [28]. Their study underlines the importance of employing more precise, site-specific pile-soil interaction models to evaluate soil damping. They found that conventional models often fall short in explaining the observed variations in soil damping, emphasizing the need for improved methods.

In addition to its strain-dependent nature, soil damping is further complicated by the soil's plasticity index and effective stress levels. Stuyts et al. conducted tests on both cohesive and cohesionless soils, revealing that existing empirical models sometimes overestimate or underestimate damping ratios. This highlights the necessity for alternative formulae and a more comprehensive approach to capture the dependency of soil damping on various factors [28]

3 Test methodology

3.1 Soil Materials

In this study, sand samples from various locations within the North Sea region, including Mol, Wemmel, Beach Sand, and Eemian sands, were analyzed. These samples were collected from boreholes within the Belgian Offshore Wind Farm. Due to limited stock availability, a diverse set of sand samples was employed. This approach not only enabled the completion of all required tests but also facilitated a broader understanding of the specific geological characteristics of different soil samples from the North Sea region.

3.1.1 Mol Sand

Mol sand samples were acquired in a dry state and subjected to specific tests for soil characterization, including particle size distribution and density evaluations. Mol sand is an onshore material. It is used as a reference material because it is a clean silica sand with uniform grain size and well-rounded grains.

3.1.2 Wemmel Sand

Wemmel sand samples were extracted from BELWIND II OFFSHORE WIND FARM BH-103 at two specific depths: 66.1m and 74.2m. These samples initially were not dry and required drying for testing. The geological characteristics of the samples are as follows:

- The 66.00m to 66.45m depth range consists of dark greenish-grey, very silty silica fine sand. Shell fragments are abundant from 66.00m to 66.10m but fewer from 66.10m to 66.45m. A thin lamina of clay was also observed at 66.20m.

- The 74.00m to 74.38m depth range consists of dark greenish-grey, very silty silica fine sand as well.

The drying process was executed under three different conditions: air drying, oven drying at 60 degrees Celsius, and oven drying at 105 degrees Celsius. After drying, the samples underwent particle size distribution analyses and density measurements to ascertain the maximum and minimum dry density. This information serves as the input for calculating the soil volume needed to achieve the desired relative density.

In Figure 3-1 one can see Sample Photographs BH-103

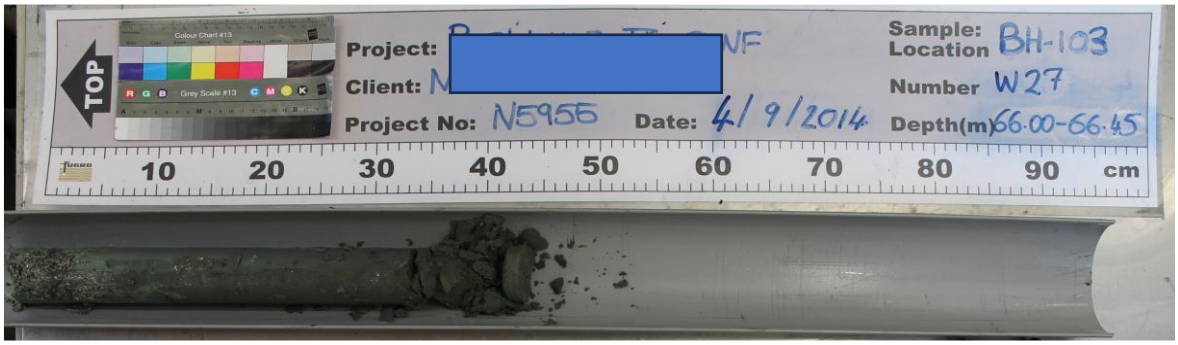

Figure 3-1 Sample W27 from Bore Hole (BH) 103 elevation 66.00 to 66.45m

3.1.3 Beach Sand

Beach Sand samples were also acquired in a dry state. These samples were subjected to ASTM D4253 standard tests, including evaluations for maximum and minimum dry densities. A vibration table was used for agitating the sand samples, and particle size distribution was assessed. Cyclic direct simple shear loading tests were performed on this sand to investigate cyclic degradation.

3.1.4 Eemian Sand:

Eemian sand samples were initially not dry and were obtained from borehole number 102 at the BELWIND II OFFSHORE WIND FARM, located at an elevation of 3 meters below the seafloor [29]. The samples are characterized by their light olive brown colour and are slightly silty, containing fine to medium silica sand, as well as shells and shell fragments. To prepare them for testing, these samples were dried at 60 degrees Celsius.

Post-drying, the Eemian sand samples underwent the Standard Proctor Compaction Test and the Sand Replacement Test for soil characterization. Cyclic direct simple shear loading tests were specifically conducted on these samples to investigate both cyclic degradation and the effects of drying on shear strength parameters.

Moreover, the diverse characteristics inherent in the different samples from the North Sea region form an integral part of the methodology. This diversity enriches the dataset and allows for a more effective achievement of the study's aim: to conduct cyclic testing of North Sea sands that are subject to loads from offshore wind turbine foundations.

3.2 Sample Preparation

Sample preparation is critical for achieving reliable and accurate results in control-volume (CV) and control-stress (CS) tests. The choice between CV and CS aims to replicate in-situ conditions. For monotonic tests on dry samples, CV is employed, maintaining a constant sample height and allowing adjustments in vertical stress. This is vital as these variations can be interpreted as pore water pressure generation within the sample.

Conversely, for saturated samples, CS tests are used. The study aims to investigate the feasibility of using saturated samples in monotonic tests within the cyclic direct shear (cDSS) apparatus. Various sample preparation techniques, such as moist tamping, wet pluviation, and dry tamping, are combined with post-saturation in the cDSS setup. This aims to verify if CV tests on dry samples yield results comparable to CS tests on saturated samples, as theoretically expected. [10], [11] Notably, the cDSS apparatus doesn't measure excess pore pressures directly due to a lack of a back-pressure system, necessitating additional assemblies[14].

For the second part of the study, which focuses on the impact of drying on shear strength, exclusively dry conditions were employed, aligning with the conventional usage of the cyclic direct simple shear (cDSS) apparatus. Here, samples were prepared using dry tamping, a method commonly used in geotechnical laboratory tests [20], [22].

The third and main objective of study involves investigating the cyclic degradation of North Sea sand. Here, the focus was on variables such as confining stress (σ'_{vo}), relative density (D_r), and Cyclic Shear Stress Ratio (CSR). Samples were prepared using dry tamping. Constant Volume (CV) conditions were employed during the consolidation and preshearing phases, switching to Constant Stress (CS) conditions for the shearing phase to mimic in-situ conditions.

While test procedures are meticulously designed to minimize errors, it's important to acknowledge that various factors like sample heterogeneity, equipment calibration, and even minor variations in test conditions can introduce some level of uncertainty into the results. Throughout the testing period, data were continually re-analyzed to identify and eliminate potential sources of error. For instance, challenges were encountered related to controlling vertical displacement in Direct Simple Shear (DSS) tests. The test system software offers two options for controlling vertical displacement during the consolidation phase: the first is based on data from an internal sensor ('vertical displacement'), and the second uses data from the Linear Variable Differential Transformer (LVDT) ('vertical extension'). Depending on which option is selected, the system attempts to maintain a constant value for either the internal sensor or the LVDT, affecting the test's ability to accurately simulate in-situ conditions. This issue highlights the kinds of complexities that can arise in experimental settings and underlines the importance of vigilant data monitoring.

3.2.1 Sample Preparation Methods

In the following sections, the sample preparation methods employed in this study for both CV and CS tests are detailed. They provide insights into their respective applications, effectiveness, and limitations.

Wet Pluviation

For the control-stress tests, the wet pluviation method was employed, accompanying post-saturation of the sample in alignment with ASTM D4253 standards. In this technique, a funnel positioned above a porous base plate is used to pour water-saturated soil into a cylindrical mould. The soil particles naturally settle due to gravitational forces as the water drains through the base plate. This results in a uniform deposit with controlled density and moisture content. This method was selected for its effectiveness in simulating natural deposition processes [15], [18]. However, it should be noted that wet pluviation may not be appropriate for very fine-grained soils or for capturing in-situ stress conditions.

Moist Tamping

For the control stress tests, moist tamping was also applied. The soil samples were first mixed with water to achieve a specific moisture content, typically 5%. Samples have been prepared using a tamping rod attached to a 50 mm diameter circular footing with 35cm height. The part that can fall from different elevations is a circular metallic with a weight of 0.750 kg, worth mentioning that the bottom part diameter is the same dimension as the DSS apparatus mould. The total weight of the tamping arrangement was about 1.2 kg. The number of blows was varied to prepare homogeneous samples. Despite its convenience and the uniformity it brings to samples, this method can introduce fabric anisotropy, affecting the soil's mechanical behaviour under different loadings [21].

Dry Tamping

Both CV and CS tests utilized dry tamping. This method closely resembles moist tamping but differs in sample moisture content. Here, samples are first oven-dried at 60°C to eliminate moisture and then sieved to remove particles larger than 2 mm, such as shells. The dry soil is filled into a mould in 3-4 equal layers to satisfy the desired relative density (D_r), each receiving a varying number of blows to create a homogeneous sample. Although effective in maintaining constant volume, this method can be time-consuming and may not suit soils with well-graded particles or high fine content [22].

3.2.2 Sample Saturation

As an exploratory facet of the study, the impact of sample saturation on test outcomes was investigated, both post-sample preparation and, in the case of wet pluviation, during sample preparation. This was accomplished using a straightforward yet effective setup: an elevated tank positioned approximately one meter above the sample within the cyclic direct simple shear (cDSS) apparatus. A hydraulic gradient facilitated water flow from the tank to the sample, with flow rates controlled through valves. The completion of the saturation process was determined by the absence of air bubbles exiting the drainage channels, ensuring thorough saturation of the samples.

This methodical approach to saturation was instrumental in replicating field conditions as closely as possible within a laboratory setting. The careful control of the saturation process allowed for the observation and analysis of the impact of this critical step on soil behavior under simulated conditions. The saturation step, detailed below, was crucial for ensuring a high fidelity of the laboratory simulations to real-world scenarios.

Figure 3-2 Elevated Tank Setup

The elevated tank system, positioned strategically above the cDSS apparatus, showcases methodical approach. The image highlights the hydraulic setup and the precision of the flow control, essential for effective sample saturation.

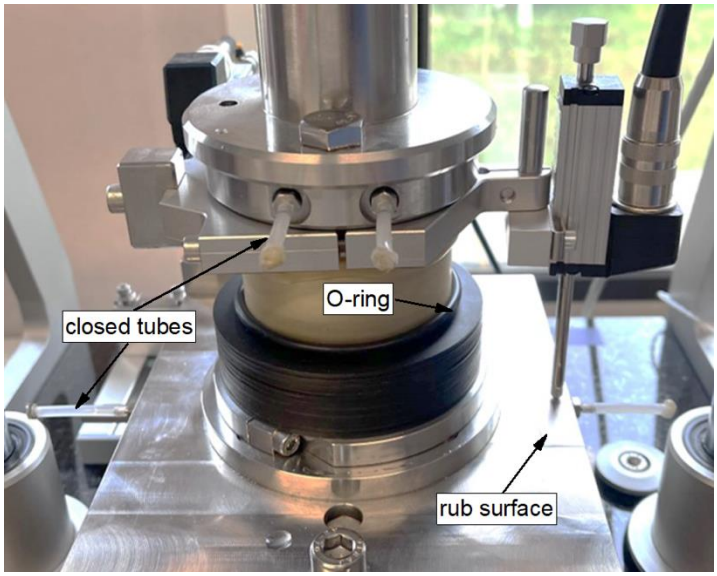

Figure 3-3 Sample Undergoing Saturation

This photograph displays the sample in the saturation phase, capturing the critical moment when saturation nears completion, marked by the absence of air bubbles, indicating the success of the process in mirroring field conditions. During the shearing process, all openings in the apparatus were meticulously sealed to ensure undrained condition, as depicted in Figure 3-3. The use of O-rings placed strategically near the top of the ring stacks was a key adaptation to minimize changes in membrane volume, further ensuring the reliability and accuracy of the test results.

Comparing Dry and Saturated Conditions:

A subsidiary goal of the study was to evaluate the level of agreement between results obtained under saturated conditions in CS tests and those achieved under dry conditions in CV tests. It is noteworthy

that differences in outcomes were observed, emphasizing the importance of moisture content in affecting test results.

Due to these variations, the focus shifted towards conducting tests under dry conditions, a practice more traditionally in line with the use of the cyclic direct simple shear (cDSS) apparatus. These discrepancies also raised questions about the apparatus's capabilities to accurately replicate in-situ conditions when moisture is involved or potentially highlighted limitations in the initial setup.

3.2.3 Sample Drying

Drying soil samples is a crucial step in the study, mainly because moisture content can profoundly affect the test outcomes. The samples of Wemmel sand and Eemian sand were not initially dry, making this step essential for meeting the objective of performing the tests in dry conditions.

Before procceding with the test methodology, it's important to note that three distinct soil drying methods were employed to prepare the samples for testing: Air Drying, Oven Drying at 60°C, and Oven Drying at 105°C. Each method was carefully chosen to investigate its respective impact on the particle size distribution and shear strength, while also considering the potential for altering the soil's mechanical properties.

Air Drying

In this method, soil samples are placed in a spherical glass container along with two humidifiers. The container is sealed to create a controlled environment. Air drying relies on natural evaporation, assisted by the humidifier bags that help reduce the ambient humidity inside the container.

This method is gentle on the soil, preserving its original properties. However, the drying time can be lengthy and may vary based on initial moisture content and fine particle content.

Oven Drying at 60°C.

Samples are placed in a laboratory oven set at a controlled temperature of 60°C and are left to dry until they reach a constant weight, typically in three days.

This method provides a more consistent drying environment and is faster than air drying. However, it may lead to the loss of some fine particles and cause minor alterations to the soil's mechanical properties.

Oven Drying at 105°C.

For this method, soil samples are placed in a laboratory oven set to 105°C for a duration of 24 hours to achieve a constant weight.

This method is the quickest for removing moisture but may alter the soil properties significantly, especially if the soil contains organic or clayey materials. Changes in particle coloration could signify such alterations.

3.2.4 Static Test Methodology

Static testing plays a crucial role in this study, examining the effects of various factors such as sample preparation, drying, and saturation on the mechanical properties of soil, particularly shear strength. The Direct Simple Shear (DSS) test, a standard laboratory method, serves to measure these soil characteristics. DSS is pivotal for simulating slow-loading conditions and long-term stability scenarios in soil mechanics, relevant to structures like slopes, foundations, or embankments [27]. Two specific types of static tests, Constant Volume, and Constant Stress tests are utilized to scrutinize the impact of sample preparation on the shear strength of soils.

Constant Volume Tests

In Constant Volume tests, dry tamping is employed as the method for sample preparation, as supported by the literature review. Dry tamping was selected due to its minimal alteration of the soil's inherent properties and its ability to create a sample with different relative densities. Metal rings are utilized to prevent radial deformation of the sample during the test, thus maintaining the sample in a K0 condition (a condition where lateral earth pressure remains constant during soil deformation) and simulating shearing under undrained conditions.

Procedure:

1. **Prepare and Place the Soil Sample in the Mould**: Utilizing a standardized mould with a diameter of 71.67 mm and a height of 22.27 mm, prepare the soil sample using dry tamping, then place it in the mould.
2. **Apply an Initial Vertical Stress of 5 kPa**: This step ensures proper seating of the soil sample within the apparatus and facilitates effective interaction with the DSS device.
3. **Constant Normal Stress for Consolidation**: Using the DSS apparatus, apply a constant normal stress for consolidation at a predetermined rate (e.g., 5 kPa/min) until the desired consolidation stress level is reached. The sample will only deform vertically due to the metal rings, simulating one-dimensional consolidation.
4. **Gradually Increase Shear Stress**: Consistent with pre-set conditions, shear stress is incrementally raised until the sample fails.
5. **Continuous Monitoring of Shear Stress and Strain**: Record shear stress and strain until the sample reaches its point of failure.
6. **Horizontal Shear Stress Application**: In a displacement-controlled mode, apply horizontal shear stress at a constant rate of 0.1 mm/min, halting the test when a shear strain of 15% is attained.

Constant Stress Tests

For Constant Stress tests, the sample preparation methods vary and include Dry Tamping, Moist Tamping, and Wet Pluviation, with a notable step of post-saturation of the sample before applying any load. The inclusion of post-saturation is designed to more accurately emulate the in-situ conditions present at the sample site. Because water is less compressible than soil, the vertical stress is primarily absorbed by the water within the sample.

Procedure:

1. **Prepare and Place the Soil Sample in the Mould**: Utilizing a standardized mould with a diameter of 71.67 mm and a height of 22.27 mm, prepare the soil sample with Dry Tamping, moist tamping, and wet pluviation methods, then place it in the mould.
2. **Post-Saturation of the Sample**: Before any mechanical loading, saturate the soil sample via a hydraulic gradient facilitated by a water tank situated about one meter above the cDSS apparatus. Valves manage the water flow, and saturation is verified when no bubbles are observed exiting the drainage channels.
3. **Apply an Initial Vertical Stress of 5 kPa**: This step ensures proper seating of the soil sample and its effective interaction with the DSS apparatus.
4. **Constant Normal Stress for Consolidation**: Implement a constant normal stress on the sample for consolidation, which is critical for simulating real-world, water-saturated conditions.
5. **Gradually Increase Shear Stress**: Employ a shear stress increment that adheres to the pre-set stress conditions, gradually increasing until the sample fails.
6. **Continuous Monitoring of Shear Stress and Strain**: Record these variables until the sample reaches its failure condition.

7. **Horizontal Shear Stress Application**: Using displacement-controlled mode, apply horizontal shear stress at a constant rate of 0.1 mm/min, ceasing the application when a shear strain of 15% is achieved.

The static test methodology consists of both Constant Volume and Constant Stress tests. These tests are carefully designed to investigate the effects of various factors such as sample preparation, drying, and saturation on the mechanical properties of soils, particularly shear strength. These methods have been optimized to closely simulate real-world conditions, ensuring that the findings will have direct implications for the understanding of soil structures.

3.2.5 Cyclic Test Methodology

The samples for the cyclic direct simple shear (cDSS) tests were prepared from Eemian and Beach Sand using the dry tamping method, closely following the procedures given in reference reports ((FEBV), 2014a) (Andersen, 2015) (FGCB, 2015) (Fugro, 2014).

In the dry tamping method, the mould is filled by gently raining sand particles through a funnel. The required mass of sand for each sample was accurately calculated, as detailed in the following section. These calculations were designed to achieve the target relative density and considered the known volume of the sample mould.

Preparing the samples for cyclic direct simple shear (cDSS) testing is a meticulous process, which requires careful calculation, as well as consideration of phase relations and previous relevant literature. In following the calculation procedures used for determining the sample mass for a given sand relative density (based on minimum and maximum dry density), as well as a calculation procedure for the selection of cyclic shear stress for a given vertical effective stress. Python programming language was utilized for these calculations.

Test specification:

Specimens subjected to cyclic loading in a stress-controlled manner were exposed to a sinusoidal shear stress with a load period of 10 seconds (i.e., a frequency of 0.1 Hz). This load period and waveform are broadly representative of the primary cyclic loading (wave loading) expected for offshore foundation design (Fugro, 2014). Each sample was tested under two-way loading conditions (i.e., symmetrically) at a prescribed cyclic shear stress ratio ($\frac{\tau_{cy}}{\sigma'_{ref}}$). Reference effective stresses (σ'_{ref}) applied for normalization of the cyclic shear stresses were derived from the results of Andersen's work on Cyclic soil parameters for offshore foundation design. (Andersen, 2015)

A total of forty-eight CSS tests were performed. The CSS testing program included both stress-controlled CSS tests and is summarised on Plates, which show the post-failure state of the soil specimens tested.

The procedures employed for stress-controlled cyclic simple shear tests on disturbed soil specimens are presented below.

Procedures for Stress-Controlled Cyclic Simple Shear Tests

Below are the procedures employed for stress-controlled cyclic simple shear tests on disturbed soil specimens.

Sample Mass Determination

During cDSS testing, the sand sample is mounted in a known volume. This volume can be calculated from the measured diameter and height of the confining rings of the cDSS device. In this case, the mould diameter was found to be 71.67 mm, and the height was 22.27 mm. The sample's cross-sectional area and volume were determined using the equations 3-1 and 3-2:

$$Sample\ Area\ = \frac{\pi * Diametr^2}{4}\ \ (mm^2) \qquad 3\text{-}1$$

$$Sample\ Volume = \ Sample\ Area\ *\ Height\ \ (mm^3) \qquad 3\text{-}2$$

The amount of material needed was then determined based on the minimum and maximum dry unit weight of the material as established through ASTM D4254 and ASTM D4253.

The specific gravity of the sand grains, G_s, was measured via the pycnometer test for Beach Sand in accordance with ASTM D854-02. The specific gravity was 2.65. This dry unit weight was converted into void ratio using the specific gravity and the known unit weight of water (γ_w) equal to 9.81 ($\frac{KN}{m^3}$), as follows:

$$e_{max} = G_s * (\gamma_w / \gamma_{dmin}) - 1 \quad 3\text{-}3$$

$$e_{min} = G_s * (\gamma_w / \gamma_{dmax}) - 1 \quad 3\text{-}4$$

Using these minimum and maximum void ratios, the dry unit weight for a given relative density (D_r) was calculated as:

$$D_r = 1 - (\gamma_d - \gamma_{dmin}) / (\gamma_{dmax} - \gamma_{dmin}) \quad 3\text{-}5$$

The required mass was then calculated by multiplying this density by the sample volume and converting the units as appropriate:

$$Mass = 1e^{-3} * \rho_d * Sample\ Volume \quad 3\text{-}6$$

This mass is the exact quantity that needs to be weighed for sample preparation.

Selection of Cyclic Shear Stress Ratio

The Cyclic Shear Stress Ratio (CSR) is defined as ($\frac{\tau_{cy}}{\sigma'_{ref}}$) . The selection of cyclic shear stress in this study was based on a test program with three different shear stress ratios, equal to 0.1, 0.15, and 0.2.

Knut Andersen's keynote paper from 2015 discusses the laboratory testing performed to collect this data (Andersen, 2015).

Vertical effective stress for the test was selected based on the test program (σ'_{vo}).

The reference stress (σ'_{ref}) was calculated using the following formula:

$$\sigma'_{ref} = pa * (\frac{\sigma'_{vo}}{pa})^n \quad 3\text{-}7$$

where n is a stress exponent typically selected as 0.9 for sand and silt, and pa is the atmospheric pressure (100 kPa).

Andersen (2015) provided diagrams for selecting the cyclic stress ratio, ($\frac{\tau_{cy}}{\sigma'_{ref}}$), for different sand relative densities and fine contents. These diagrams indicated the cyclic stress ratio that would lead to failure in 10 cycles, known as the failure shear stress (τ_f).

The data in Figure 3-4 show cyclic shear strength decreasing with increasing fine content. Estimated curves for fines content less than 5% and fines content of 20% and 35% are included in the figure. The curve for 35% fine content in Figure 3-4 is uncertain because relative density determination is questionable for such high fine content, and a lack of data on relative density for tests with fine content above 23%.

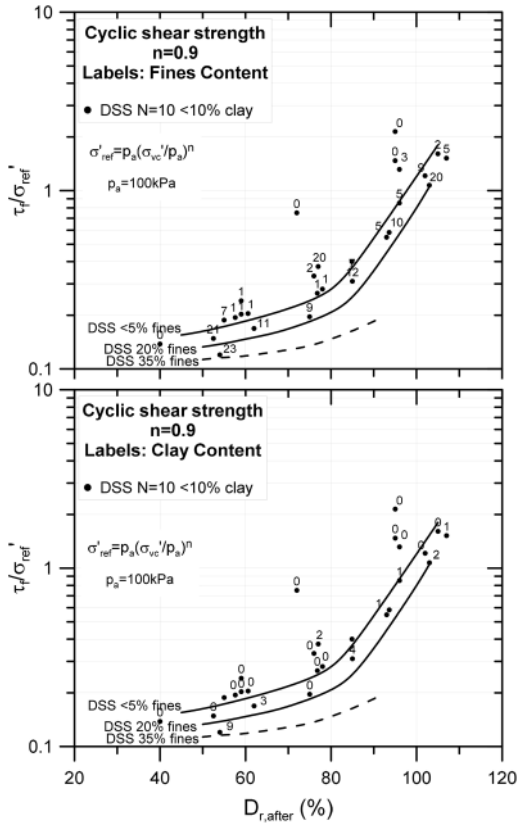

Figure 3-4 Metrical cyclic loading in DSS tests on normally consolidated sand and silt as a function of relative density after consolidation. Upper: Fines content. Lower: clay content [9].

By using these graphs and knowing both the fine content and the desired relative density, it was possible to estimate the shear strength that would lead to failure after 10 cycles.

Referring to the provided graph, it depicts the cyclic shear strength in relation to the relative density, D_r, for different fines and clay contents. The graphs clearly differentiate among samples with less than 5% fines, 20% fines, and 35% fines. This distinction is essential for understanding the cyclic behaviour of sands with varying granular compositions. The top plot emphasizes the fines content, while the bottom plot centers on the clay content.

In this study, the primary focus was on sands containing fines. Both Eemian Sand and Beach Sand, with fines contents of less than 5%, were the primary samples under examination. Observing the top plot of the graph, it is noted that for sands with less than 5% fines and an assumed relative density of 80%, the shear stress ratio resulting in 10 cycles is less than 0.2. Given these insights, assessing three distinct shear stress ratios: 0.1, 0.15, and 0.2, was a rational decision to explore the degradation of the sample under cyclic loading.

To estimate the required shear stress ratio for other cycle numbers, the failure stress ratio ($\frac{\tau_f}{\sigma'_{ref}}$) can be assessed and combined with one of the cyclic contour diagrams proposed by Andersen (2015).

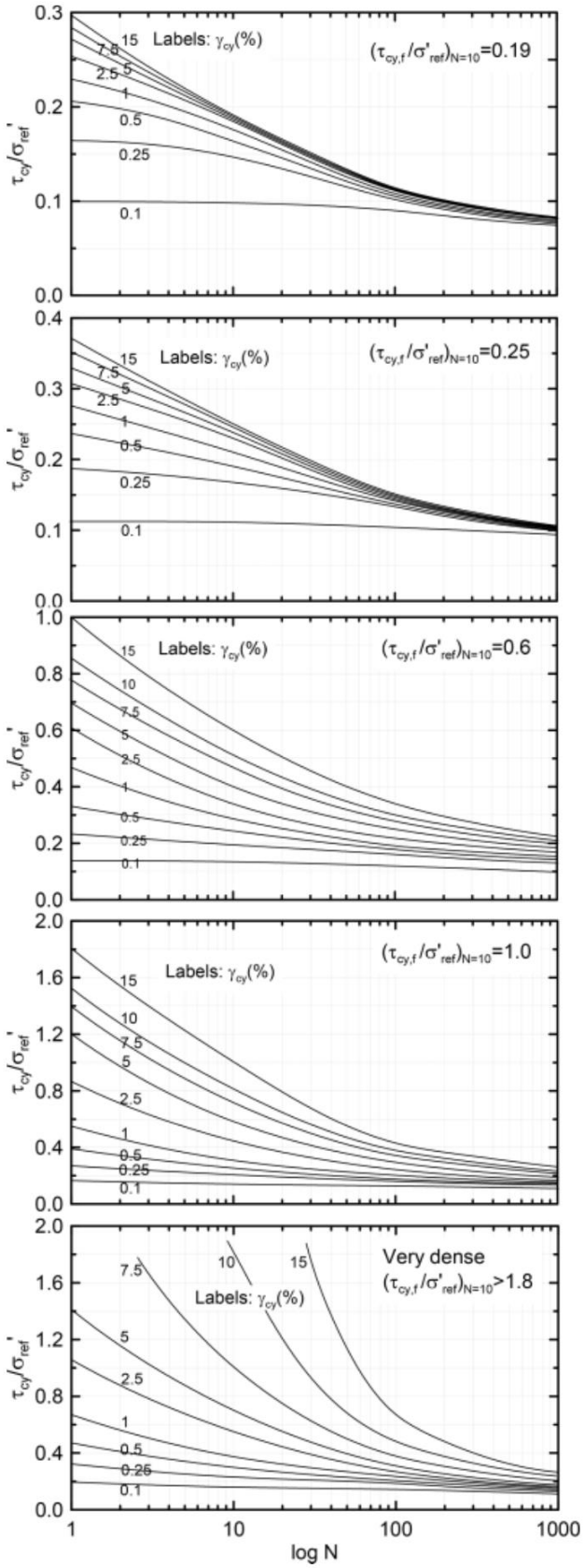

Figure 3-5 Cyclic contour diagrams according to Andersen (2015)

The cyclic stress ratio for reaching failure in e.g. 100 cycles can be read from the selected chart. For the example with a relative density of 75% and 20% fines content, the top panel would need to

be selected. Reading from the chart, the cyclic shear stress ratio would have to be equal to 0.115 to reach failure in 100 cycles [9].

Consolidation

The consolidation phase is an integral part of the cDSS testing process, serving to approximate the in-situ conditions of the soil specimen. This phase is pivotal for ensuring the reliability and accuracy of the subsequent cyclic shearing tests.

In this phase, a specified vertical load is applied to the soil specimen, effectively compressing the soil grains and bringing them closer together. The specimens, originally prepared via the dry tamping method, undergo this consolidation under variable confining stresses, set in line with test program.

The confining stresses applied range from 100 to 500 kPa, specifically at 100, 150, 250, and 500 kPa. These values were chosen to represent a variety of potential real-world conditions and are maintained to ensure a constant vertical effective stress throughout the consolidation process.

For this study, specimens were prepared at two distinct relative densities: 55% and 80%. These figures capture a range of field conditions, from loose to dense sand formations, and have a marked impact on the soil's response to cyclic loads—a primary focus of the research.

Preshearing

Preshearing serves as a crucial step in the cyclic direct simple shear (cDSS) tests, particularly aimed at closely mimicking the real-world conditions that North Sea sands are subjected to in the offshore wind industry. The process involves cyclic loading with drainage either during or after the loading phase, typically applied after the specimen has been consolidated to the specified levels (Andersen, 2015).

For cohesionless specimens like the sand samples in this study, cyclic preshearing is employed to simulate the densification of soil under low-amplitude wave loading. Upon the completion of the consolidation phase, a low amplitude of cyclic shear stress is denoted as (τ_{cy}), and is applied under constant vertical stress conditions, as per foundation considerations and specimen depth (Fugro, 2014).

Maintaining constant vertical stress creates a state akin to a ‘drained condition’ for saturated specimens. This is achieved by continuously adjusting the height of the specimen during the shearing process, ensuring that the vertical stress remains unchanged (Fugro, 2014).

All sand specimens underwent 400 cycles of stress-controlled preshearing under these constant vertical stress conditions. This stage aims to replicate any potential densification or preferential particle alignment that might occur under low-magnitude cyclic loading events, such as during operational or minor storm loading (Fugro, 2014).

For large offshore platforms built on dense sands, preshearing is usually estimated to involve 400 cycles at a stress ratio of $\frac{\tau_{cy}}{\sigma'_{ref}} = 0.04$. In this formula, ($\tau_{cy}$) represents the cyclic shear stress applied to the soil, while (σ'_{ref}) denotes the reference effective normal stress. This ratio is deemed to represent conditions likely to occur during a design storm's build-up phase or during previous smaller storms. In seismic zones, the soil might have experienced smaller quakes over time (Andersen, 2015).

Through the integrated process of specimen preparation, consolidation, and preshearing, the test samples are adequately conditioned to undergo cyclic shearing as described in the following.

Shearing Phase in Stress-Controlled Conditions

Having completed the preceding steps of sample preparation, consolidation, and preshearing, the pivotal phase of stress-controlled shearing was then proceeded to. These tests were executed using the cyclic direct simple shear (cDSS) apparatus at Ghent University's laboratory.

Stress-controlled cyclic simple shear (CSS) tests were performed using the cDSS apparatus. Failure is established when either the accumulated shear strain (γ_a) or the cyclic shear strain (γ_{cy}) reaches 15%. Another criterion for terminating the test is reaching 1000 cycles—the maximum number of

allowable cycles. During the tests, there was a consistent increase in cyclic shear strain, (γ_{cy}), as cyclic loading proceeded [9], [29].

After the consolidation and preshearing stages, the specimen undergoes a combination of initial (average) shear stress (τ_{av}), and cyclic shear stress (τ_{cy}) (Fugro, 2014). These stresses are further elaborated and graphically represented in the figure 3-5.

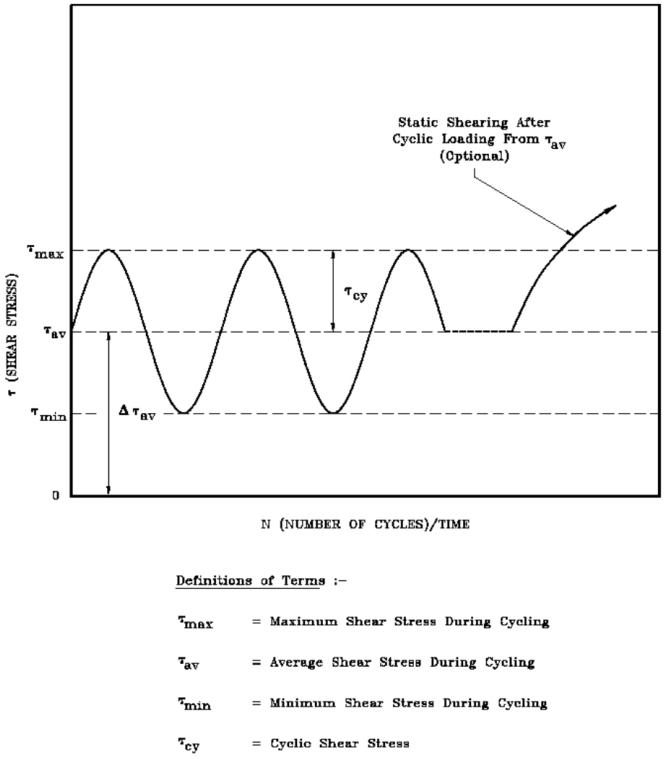

Figure 3-6 Shear stress versus time

In this study, shear tests under cyclic loading were conducted under constant volume conditions, which is analogous to undrained conditions for saturated specimens. To maintain this state, the vertical stress on the specimen was continually adjusted during shearing to ensure constant height. This practice is in line with the widely accepted understanding that the variation in vertical stress during shearing equates to the change in pore water pressure one would expect in a genuinely undrained test [29].

To further clarify, it's worth noting that in the aftermath of the preshearing phase, the specimens often have some level of residual shear stress. This residual stress can be interpreted as the initial shear stress, τ_{av}, for the subsequent cyclic loading tests. To standardize the test conditions and ensure symmetric shear application, this initial stress is reset to zero. This adjustment enhances the test's accuracy and representing the results.

3.2.6 Damping Calculation

Damping values are calculated for each cyclic test to evaluate the energy dissipation behaviour of the soil samples under cyclic loading conditions. This evaluation is critical in assessing the soil's performance for applications like offshore wind installations that are subjected to dynamic loads.

Damping ratio, often denoted as ξ, provides a dimensionless measure of energy dissipation in a material subjected to cyclic loading. For this research, the damping ratio is obtained using the following methodology:

- The stress-strain hysteresis loop generated during cyclic loading is first analysed. This loop provides insights into soil behaviour for each cycle.
- The area enclosed by the stress-strain hysteresis loop, termed r_e, is computed. This area gives a measure of the energy dissipated by the material during the cyclic loading. Essentially, it quantifies the amount of energy lost in the form of heat or other internal processes during a cycle. This is a direct indication of the material's damping capacity[30], [31]
- The product of the tangential stress and its corresponding shear strain within the loop, which represents the maximum energy stored in the material during cyclic loading, is also calculated. This product is denoted by p_e

Using the above parameters, the damping ratio, ξ, is computed using the formula:

$$\xi = \frac{r_e}{4\pi p_e} \qquad 3\text{-}8$$

It should be noted that the damping ratio can be understood as a ratio of the energy dissipated to the energy stored in the material during cyclic loading.

By systematically computing the damping ratios across different cyclic tests, the research aims to provide insights into how the soil dissipates energy. These insights can be valuable for ensuring the structural stability of offshore installations and can be used in numerical simulations for design optimization. Moreover, the damping ratio serves as an additional parameter for comparative evaluations between different soil types and preparation methods.

3.2.7 Test Program Overview

To provide a comprehensive understanding of the material properties and behaviour under different conditions, a series of both static and cyclic tests were conducted. Below are tables summarizing the test program, describing the various parameters involved in each test.

Static Tests

The following table provides an overview of the static tests carried out. Two different types of sand, MOL Sand and Wemmel Sand, were used in these tests. Various methods for sample preparation and drying were employed to evaluate their impact on the results. Each test was performed under a constant consolidation pressure of 150 kPa and with a relative density of 80%. The phase for all static tests is either Constant Shear (CS) or Constant Volume (CV).

Table 3-1 Overview of Static Shear Tests on MOL and Wemmel Sands

Test No.	Sample	Sample Preparation	Drying method	Consolidation Pressure	Relative Density	Phase	Static/Cyclic
1	MOL Sand	Dry Tamping	post saturation	250	80	CS	Static
2	MOL Sand	Dry Tamping	post saturation	250	80	CS	Static
3	MOL Sand	Moist Tamping	post saturation	250	80	CS	Static
4	MOL Sand	Moist Tamping	post saturation	250	80	CS	Static
5	MOL Sand	Wet Pluviation	pre and post saturation	250	80	CS	Static
6	MOL Sand	Wet Pluviation	pre and post saturation	250	80	CS	Static
7	MOL Sand	Dry Tamping	Oven Drying at 60°C	250	80	CV	Static
8	MOL Sand	Dry Tamping	Oven Drying at 60°C	250	80	CV	Static
9	MOL Sand	Dry Tamping	Oven Drying at 60°C	250	80	CV	Static
10	Wemmel Sand	Dry Tamping	Oven Drying at 60°C	250	80	CV	Static
11	Wemmel Sand	Dry Tamping	Oven Drying at 60°C	250	80	CV	Static
12	Wemmel Sand	Dry Tamping	Oven Drying at 60°C	250	80	CV	Static
13	Wemmel Sand	Dry Tamping	Oven Drying at 105°C	250	80	CV	Static
14	Wemmel Sand	Dry Tamping	Oven Drying at 105°C	250	80	CV	Static
15	Wemmel Sand	Dry Tamping	Air drying	250	80	CV	Static

Cyclic Tests

For the cyclic tests, Eemian and Beach Sand sands were used. These tests were carried out at various consolidation pressures, relative densities, and Cyclic Stress Ratios (CSR). Similar to the static tests, various methods for sample preparation and drying were used.

Table 3-2 Overview of Cyclic Shear Tests on Eemian and Beach Sands

Test No.	Sample	Sample Preparation	Drying method	Consolidation Pressure	Relative Density	CSR	Static/Cyclic
1	Eemian	Dry tamping	Oven Drying at 60°C	100	80	0,1	Cyclic
2	Eemian	Dry tamping	Oven Drying at 60°C	100	80	0,15	Cyclic
3	Eemian	Dry tamping	Oven Drying at 60°C	100	80	0,2	Cyclic
4	Eemian	Dry tamping	Oven Drying at 60°C	150	80	0,1	Cyclic
5	Eemian	Dry tamping	Oven Drying at 60°C	150	80	0,15	Cyclic
6	Eemian	Dry tamping	Oven Drying at 60°C	150	80	0,2	Cyclic
7	Eemian	Dry tamping	Oven Drying at 60°C	250	80	0,1	Cyclic
8	Eemian	Dry tamping	Oven Drying at 60°C	250	80	0,15	Cyclic
9	Eemian	Dry tamping	Oven Drying at 60°C	250	80	0,2	Cyclic
10	Eemian	Dry tamping	Oven Drying at 60°C	500	80	0,1	Cyclic
11	Eemian	Dry tamping	Oven Drying at 60°C	500	80	0,15	Cyclic
12	Eemian	Dry tamping	Oven Drying at 60°C	500	80	0,2	Cyclic
13	Eemian	Dry tamping	Oven Drying at 60°C	100	55	0,1	Cyclic
14	Eemian	Dry tamping	Oven Drying at 60°C	100	55	0,15	Cyclic
15	Eemian	Dry tamping	Oven Drying at 60°C	100	55	0,2	Cyclic
16	Eemian	Dry tamping	Oven Drying at 60°C	150	55	0,1	Cyclic
17	Eemian	Dry tamping	Oven Drying at 60°C	150	55	0,15	Cyclic
18	Eemian	Dry tamping	Oven Drying at 60°C	150	55	0,2	Cyclic
19	Eemian	Dry tamping	Oven Drying at 60°C	250	55	0,1	Cyclic
20	Eemian	Dry tamping	Oven Drying at 60°C	250	55	0,15	Cyclic
21	Eemian	Dry tamping	Oven Drying at 60°C	250	55	0,2	Cyclic
22	Eemian	Dry tamping	Oven Drying at 60°C	500	55	0,1	Cyclic
23	Eemian	Dry tamping	Oven Drying at 60°C	500	55	0,15	Cyclic
24	Eemian	Dry tamping	Oven Drying at 60°C	500	55	0,2	Cyclic

Test No.	Sample	Sample Preparation	Drying method	Consolidation Pressure	Relative Density	CSR	Static/Cyclic
25	Beach Sand	Dry tamping	Oven Drying at 60°C	100	80	0,1	Cyclic
26	Beach Sand	Dry tamping	Oven Drying at 60°C	100	80	0,15	Cyclic
27	Beach Sand	Dry tamping	Oven Drying at 60°C	100	80	0,2	Cyclic
28	Beach Sand	Dry tamping	Oven Drying at 60°C	150	80	0,1	Cyclic
29	Beach Sand	Dry tamping	Oven Drying at 60°C	150	80	0,15	Cyclic
30	Beach Sand	Dry tamping	Oven Drying at 60°C	150	80	0,2	Cyclic
31	Beach Sand	Dry tamping	Oven Drying at 60°C	250	80	0,1	Cyclic
32	Beach Sand	Dry tamping	Oven Drying at 60°C	250	80	0,15	Cyclic
33	Beach Sand	Dry tamping	Oven Drying at 60°C	250	80	0,2	Cyclic
34	Beach Sand	Dry tamping	Oven Drying at 60°C	500	80	0,1	Cyclic
35	Beach Sand	Dry tamping	Oven Drying at 60°C	500	80	0,15	Cyclic
36	Beach Sand	Dry tamping	Oven Drying at 60°C	500	80	0,2	Cyclic
37	Beach Sand	Dry tamping	Oven Drying at 60°C	100	55	0,1	Cyclic
38	Beach Sand	Dry tamping	Oven Drying at 60°C	100	55	0,15	Cyclic
39	Beach Sand	Dry tamping	Oven Drying at 60°C	100	55	0,2	Cyclic
40	Beach Sand	Dry tamping	Oven Drying at 60°C	150	55	0,1	Cyclic
41	Beach Sand	Dry tamping	Oven Drying at 60°C	150	55	0,15	Cyclic
42	Beach Sand	Dry tamping	Oven Drying at 60°C	150	55	0,2	Cyclic
43	Beach Sand	Dry tamping	Oven Drying at 60°C	250	55	0,1	Cyclic
44	Beach Sand	Dry tamping	Oven Drying at 60°C	250	55	0,15	Cyclic
45	Beach Sand	Dry tamping	Oven Drying at 60°C	250	55	0,2	Cyclic
46	Beach Sand	Dry tamping	Oven Drying at 60°C	500	55	0,1	Cyclic
47	Beach Sand	Dry tamping	Oven Drying at 60°C	500	55	0,15	Cyclic
48	Beach Sand	Dry tamping	Oven Drying at 60°C	500	55	0,2	Cyclic

4 Test Results and Discussion

4.1 Basic Material Characterization

The following section provides an in-depth look into the fundamental properties and characteristics of different sand samples utilized in this research. A primary concern is the grain size distribution, which plays a pivotal role in understanding the mechanical behavior and properties of these sands. Further on, the specific gravity of soil solids, another critical geotechnical attribute, will also be discussed. Detailed insights and results are segmented by the type of sand under consideration, ensuring a methodical presentation of data.

4.1.1 Grain Size Distribution

The particle size distribution was determined using different sieve numbers, ranging from 0.075 to 4 mm. This test was conducted for a duration of 20 minutes at a frequency of 60 HZ. The results for each sand are as follows:

Wemmel Sand:

The Wemmel sand used for this study originated from borehole 103 in BELWIND II OFFSHORE WIND FARM but was taken from different elevations—specifically, depths of 66.1 m and 74.2 m. This sand underwent various drying methods, which significantly influenced its particle size distribution.

During the sample preparation phase, it was observed that Wemmel sand contained a high percentage of fines, leading to the formation of noticeable lumps. These lumps were not only cohesive but could also be easily broken apart by hand. To better understand this behaviour, particle size distribution was measured under multiple conditions:

1. **Before and after cDSS apparatus use**: The sample was analysed both before and after being subjected to the cDSS apparatus.
2. **Drying Methods**: Three distinct drying methods were used air drying, drying at 60 degrees Celsius, and drying at 105 degrees Celsius. The particle size distribution was determined for each of these drying methods.

Results:

- **Unused 60°C dried sample**:
  This untested sample, dried at 60°C, exhibited a fines content amounting to 11%.
- **Unused air-dried sample:**
  Without any specific drying temperature and prior to any cDSS testing, this sample had 30% fines.
- **60°C dried sample (post-cDSS use, single run):**
  After drying at 60°C and subsequently undergoing a singular cDSS test, the sample contained 22% fines.
- **60°C dried sample (post-cDSS use, multiple runs):**
  Upon being subjected to multiple cDSS tests and post-drying at 60°C, the sand contained 42% fines.
- **105°C dried sample (post-cDSS use):**
  Upon being subjected to multiple cDSS tests and post-drying at 105°C, the sand contained 50% fines.
- **Rehydrated and dried Wemmel sand:**
  After rehydration and subsequent drying at 105°C, fines content was observed to be consistent with the unused 105°C dried sample, at 11%.

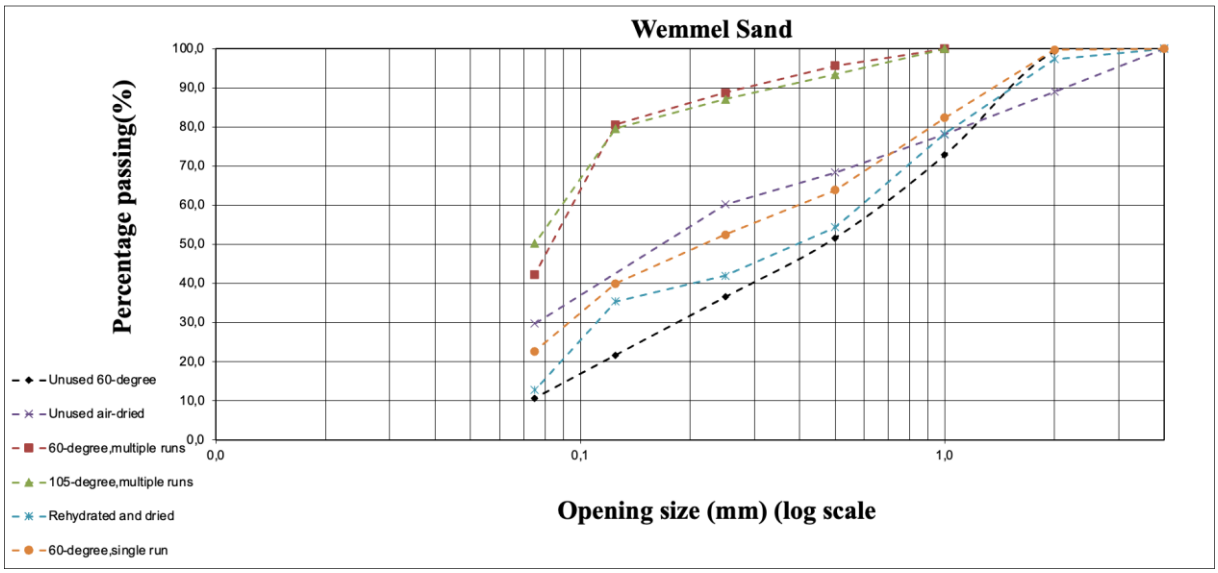

Figure 4-1 Particle Size Distribution of Wemmel Sand Under Various Drying and Testing Conditions, Showing Percentage Passing vs. Particle Size Characterization

Eemian Sand:

Unlike Wemmel sand, Eemian sand did not exhibit the issue of lump formation during the drying process, suggesting it has a minor amount of fine content. As a result, a 60-degree drying process was opted for this type of sand. This choice was informed not only by existing literature that supports the efficacy of intermediate temperature drying but also by the need to balance the risk of lump formation and time efficiency.

Particle size distribution was evaluated for the 60-degree dried samples, and the results confirmed that Eemian sand contains less than 1% fines. This low fine content suggests that Eemian sand possesses different geotechnical properties compared to Wemmel sand, making it a potentially more stable material for certain applications.

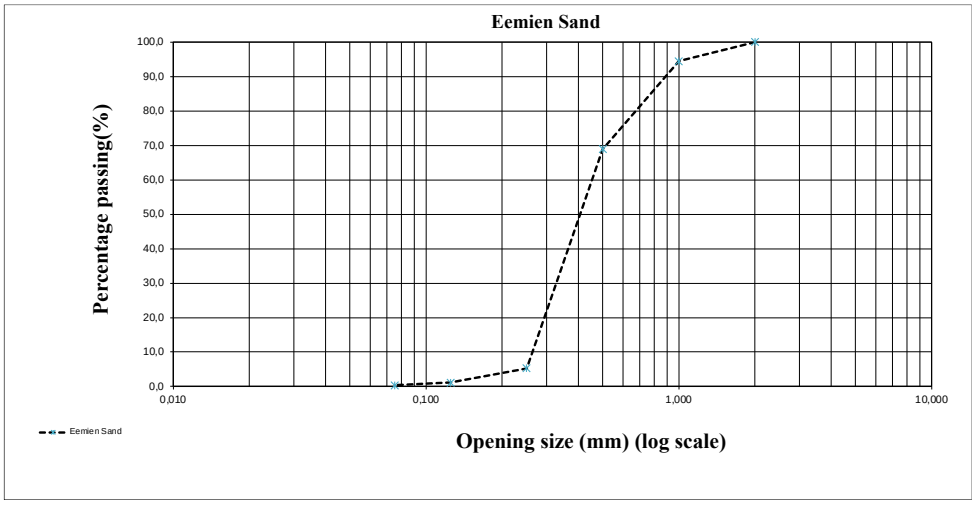

Figure 4-2 Particle Size Distribution of 60-degree Dried Eemian Sand, Showing Percentage Passing vs. Particle Size.

Beach Sand:

The Beach Sand was chosen for cyclic direct simple shear (cDSS) tests due to the availability of a sufficient amount of material, facilitating the smooth execution of the various test plans. Upon receipt, the sand was relatively dry. However, to ensure consistency across all samples, it was subjected to a 60-degree drying process. The drying phase was chosen for this sample to ensure that any residual moisture would be effectively removed, maintaining consistent test conditions.

Particle size distribution tests for the 60-degree dried Beach Sand revealed less than 1% fines, making it suitable for various applications where low fines content is desired.

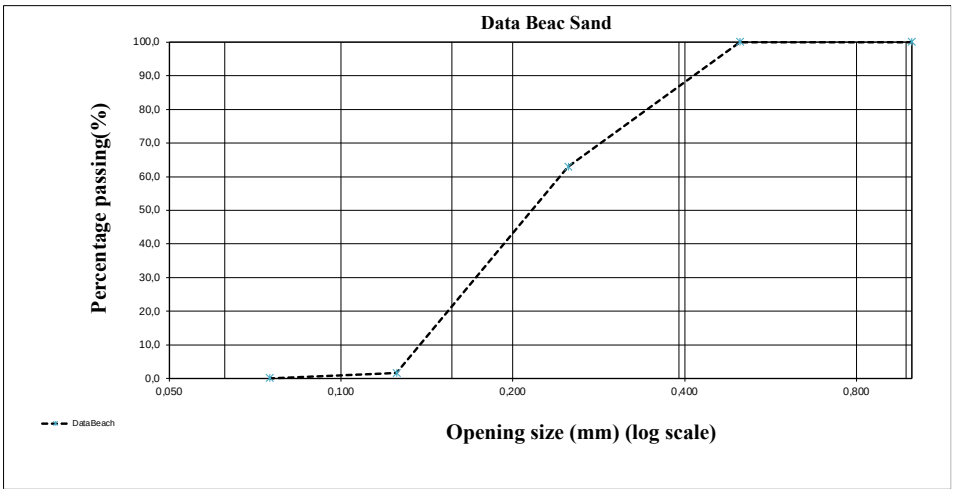

Figure 4-3 Particle Size Distribution of 60-degree Dried Beach Sand, Showing Percentage Passing vs. Particle Size.

Mol Sand:

Mol Sand was primarily used in this study to investigate the effects of saturation. Although the sand was received in a dry state, it was further subjected to a 60-degree drying process in an oven. Same as Eemian Sand this step was taken to eliminate the risk of any residual moisture content that could potentially affect the test results.

Unlike Wemmel sand, Mol Sand contained less than 1% fines, indicating a purely sandy composition. This characteristic makes it a particularly interesting material for studying the effects of saturation, as the absence of fines simplifies the saturation process both in terms of time consumption and accuracy.

Given the lack of fines and the consistent drying process, the grain size distribution for Mol Sand remained stable and was not subject to variations similar to those observed in Wemmel sand. Therefore, Mol Sand can be considered a consistent and stable material suitable for the saturation tests conducted in this study.

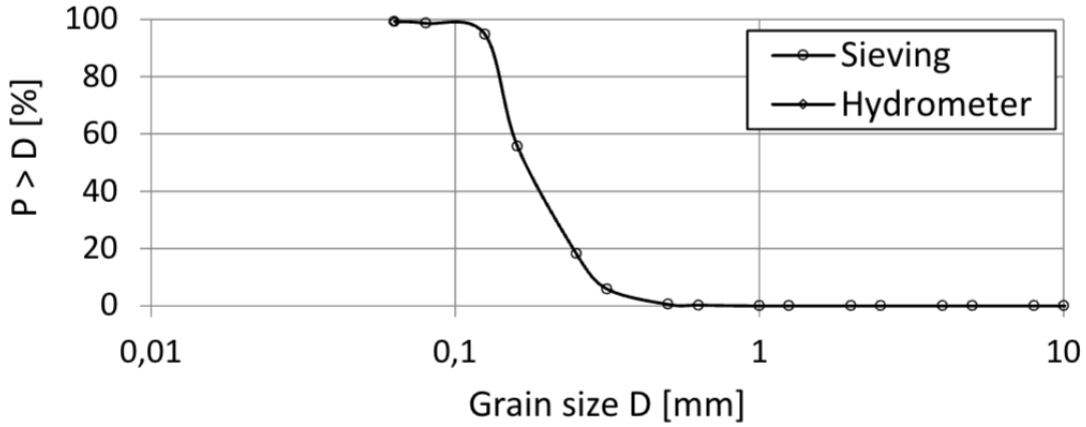

Figure 4-4 Particle Size Distribution of Mol Sand, Showing Percentage Passing vs. Particle Size.

4.1.2 Specific Gravity

The specific gravity of soil solids (G_s) is a fundamental property that influences a range of geotechnical characteristics. Specifically, the accurate determination of G_s is essential for calculating the dry unit weight of the soil, which in turn is critical for determining the sample mass in both static and cyclic tests.

Beach Sand:

For Beach Sand, specific gravity was determined through test procedures based on the ASTM D854 standard. The obtained value was 2.65. The consistency of this value with common ranges for sandy soils further validates the reliability of test procedures and results.

Other Sands:

For Wemmel, Eemian, and Mol sands, a specific gravity of 2.65 was assumed. This assumption was based on its common usage in geotechnical studies and its practicality for sandy soils. The reliability of this assumed value is supported by existing geotechnical literature [14], [32].

4.1.3 Maximum and Minimum Dry Density

Determining the maximum and minimum dry densities of different sands is not just a procedural step but a critical prerequisite for advanced geotechnical calculations. These density values enable us to calculate the required mass for soil samples, facilitating both static and dynamic testing. Various methods, tailored to the sand type and laboratory constraints, were employed in this study.

Vibration Table Method (Beach Sand Sand)

For Beach Sand, the maximum and minimum dry densities were determined using a vibration table method, adhering to the ASTM D854-02 standards. This method involved filling a mould with sand and vibrating it for a duration of 10 minutes to obtain maximum and minimum densities.

$$\textit{Average Maximum Dry Density } \gamma_{dmax\_avg} = 1.7\ Te/m^3 \qquad 4\text{-}1$$

$$\textit{Average Minimum Dry Density } \gamma_{dmin\_avg} = 1.5\ Te/m^3 \qquad 4\text{-}2$$

Manual Layering Technique (Wemmel, Eemian, and Mol Sands)

Due to sample limitations, a manual layering technique was employed for Wemmel, Eemian, and Mol sands. The method included the careful layering and horizontal stroking of sand in a mould.

- For Wemmel sand, the maximum and minimum densities achieved were 1.42 Te/m^3 and 1.07 Te/m^3, respectively.
- For Eemian sand, maximum and minimum densities of 1.7 Te/m^3 and 1.4 Te/m^3, respectively, were obtained.
- For Mol sand, the calculated maximum and minimum densities were 1.5 Te/m^3 and 1.21 Te/m^3, respectively.

To summarize the key findings in the Basic Material Characterization section, a comprehensive table has been compiled. It presents an overview of the four different sands studied: Wemmel, Eemian, Beach Sand, and Mol. The table captures essential parameters, such as grain size distribution, specific gravity, and maximum and minimum dry densities. These values are pivotal for further geotechnical analyses and calculations. The methods employed for determining densities are also outlined to provide context for the reported values.

4-3 Basic Material Characterization of Wemmel, Eemian, Beach, and Mol Sands.

Sand Type	**Grain Size Distribution (% Fines)**	**Specific Gravity (G_s)**	**Max Dry Density (kN/m^3)**	**Min Dry Density (kN/m^3)**	**Method for Density Determination**
Wemmel Sand	11-50% (varies with drying methods and use)	2.65	14.21	10.77	Manual Layering
Eemian Sand	< 1%	2.65	17	14.08	Manual Layering
Beach Sand	< 1%	2.65	1.7	1.5	Vibration Table
Mol Sand	< 1%	2.65	18.2	13	Manual Layering

4.2 Effect of Preparation Methods on Shear Strength

To understand the influence of sample preparation on shear strength in a laboratory setting, three distinct preparation techniques were employed, conducting tests under both constant volume (CV) and constant stress (CS) conditions. Within the cDSS apparatus, the prevalent approach for both static and cyclic shearing typically focuses on maintaining a dry condition. Before initiating cyclic tests, it is aimed to assess the cDSS apparatus's performance under saturated conditions, recognizing its inherent limitation in directly measuring pore pressure. These experiments utilized Mol sand with a relative density of 40% and a confining stress of 100 kPa. The CV tests exclusively used dry tamping on dry samples, while the CS tests employed: dry tamping, moist tamping, and wet pluviation. Each CS test sample underwent post-saturation to ensure full saturation. Dry samples were subjected to monotonic tests under CV conditions, whereas the saturated ones were examined under CS conditions.

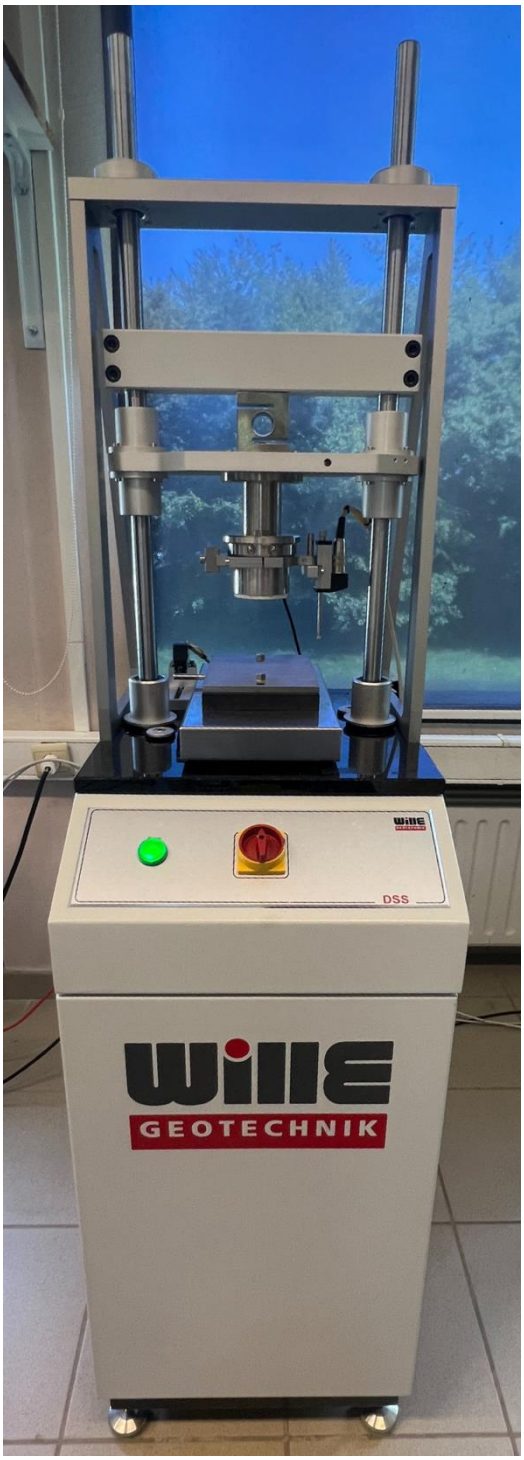

Figure 4-5 The Cyclic Direct Simple Shear (cDSS) Apparatus at UGent University.

It's noteworthy that the cDSS apparatus does not directly measure excess pore pressures due to the absence of a back-pressure system, requiring additional assemblies (Stuyts, 2023). The changes in pore pressure are assumed to be equal to the changes in stress on the axial actuator during cyclic loading at constant volume[10], [11].

Hence, the CV tests are all performed in dry condition. For samples saturated with water, the presence of the pore water ensures the constant volume condition. During such tests on saturated samples, the total stress on the actuator is kept constant (CS condition). The purpose of this research is to investigate the degradation of cyclic testing of North Sea sands. However, a preliminary step is to precisely prepare the samples for tests which comes through an investigation on CV and CS tets.

4.2.1 Comparison of CV and CS Tests

Graphical Interpretation of Undrained Shear Strength Behaviour during monotonic DSS testing

The x-axis displays the percentage of shear strain, measured using a local LDVT (Linear Variable Differential Transformer; an electromechanical sensor that transforms mechanical motion into variable electrical signals) and is employed for displacement measurements. Tests were concluded when a shear strain of 15% was reached. The y-axis displays monotonic shear stress, measured with a load cell inside the cDSS apparatus which is normalized by dividing it by the effective vertical stress (or confining pressure) for uniformity across tests.

The following graph provides a comprehensive visualization of the shear strain and shear stress relationships under different sample preparation techniques and test conditions.

In total, nine tests were conducted: three under constant volume (CV) conditions using dry tamping and six under constant stress (CS) conditions, which were all followed by post-saturation. The CS tests further included two with dry tamping, two with moist tamping, and two with wet pluviation.

Key to Graph Interpretation:

- The first set of letters: CS for control-stress, CV for control-volume.

- The second letter: D for Dry Tamping, M for Moist Tamping, and W for Wet Pluviation.

- The third letter: S stands for post-saturation, indicating that the sample was fully saturated after assembly in the apparatus and U stands for unsaturated phase.

In the graph, the trend lines offer valuable insights:

- CV tests using dry tamping displayed an initial peak in shear strength, which was then followed by a steadier rise.

- CS tests under all preparation methods showed a more consistent increase in shear strength and a higher overall shear strength.

A noteworthy observation is the significant divergence in shear strength at approximately 5% of horizontal shear strain between CV and CS contours presentation. Although the graphs begin to converge as the test precedes, the difference remains considerable.

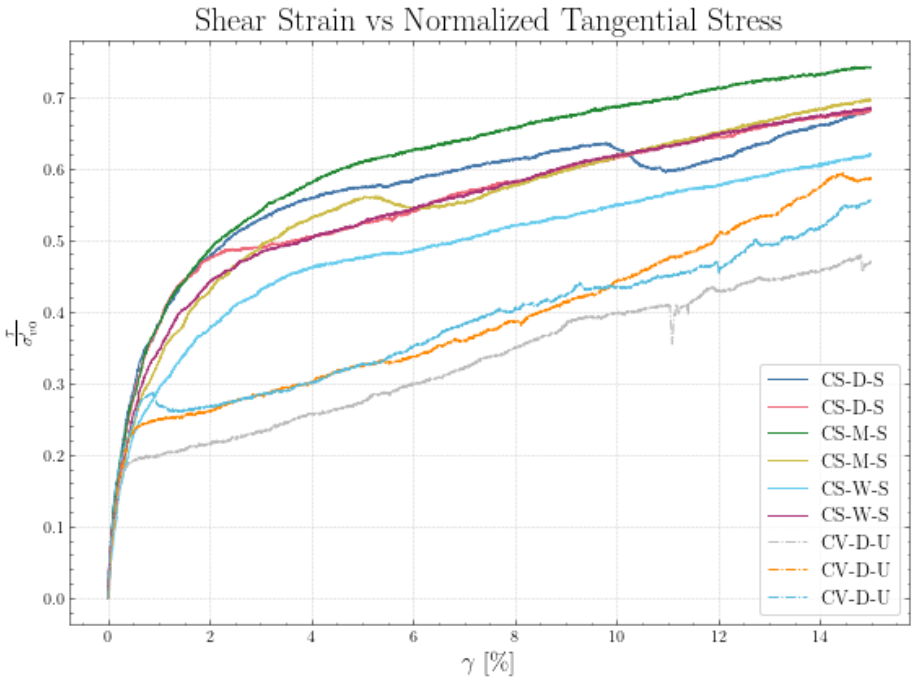

Figure 4-6 Comparative Shear Stress-Shear Strain contours for Different Sample Preparations and Test Conditions. The graph plots normalized shear stress against the percentage of shear strain collected using LDVT. Tests were conducted either under control volume (CV)

4.2.2 Rationale Behind the Preference for Dry Testing

During this research, cyclic direct simple shear (cDSS) tests were executed under both dry and saturated conditions. The outcomes showcased a noticeable variation between constant volume (CV) tests performed dry and constant stress (CS) tests. The graph highlights these differences around the 5% horizontal shear strain. Therefore, understanding the underlying reasons and variables becomes essential.

In this study, the decision to use dry testing was influenced by the cDSS apparatus's limitation. It cannot measure excess pore pressures directly during CS tests without a back-pressure system, especially when water is involved. Dry conditions made the procedure simpler, eliminating the need to maintain constant volume conditions in water, which would have necessitated a more complex setup. To achieve saturation in CS tests, a tank and specific settings to manage water flow to and from the sample, already in the cDSS apparatus, are essential. These additions increase the procedure's complexity and potential for errors. Among the procedure steps is de-aeration, which removes air bubbles from water using suction, adding another layer of precision to the process.

It's worth noting that earlier studies, such as those by Bjerrum & Landva (1966) and Dyvik et al. (1987), suggested that controlling volume during dry testing could emulate changes in vertical stress, analogous to pore water pressure generation.

Opting for dry conditions not only streamlines the sample preparation process, eliminating the need for additional steps like wet pluviation and post-saturation, but it also bolsters efficiency and reproducibility.

4.3 Effect of drying

The selection of drying methods in soil sample preparation significantly influences the outcomes of subsequent soil tests. This is particularly important in the case of Wemmel sand, which has a naturally high fine particle size and moisture content. It has used three distinct drying methods: air drying, oven drying at 60°C, and oven drying at 105°C. These methods were chosen to evaluate their impact on the particle size distribution, shear strength, and other mechanical properties of the soil.

The graph reveals a pattern in Wemmel Sand's particle distribution. After a drying cycle at 60°C, the fine content stands at 11%. Upon one use in the DSS apparatus, this number increases to 22%, and after multiple uses in the machine, it further rises to 42%. This increase might indicate the presence of coagulated particles in the sample, and these coagulated particles broke apart during shearing. It's essential to mention that all samples were sieved using a 2 mm mesh immediately after drying to remove larger particles like shells.

However, a discrepancy is observed with the unused samples dried at 60°C in contrast to those air-dried. The sample dried at 60°C exhibits 10% fine content compared to the air-dried which shows 30%. This observation contradicts the expectation that higher temperatures would increase the aggregation of finer particles, culminating in a larger grain size and thereby a diminished fine content. This difference potentially could highlight the potential impact of variability within a sample.

Lastly, Wemmel Sand naturally has a high fine content. In the 60 and 105-degree drying scenarios, after multiple shearing cycles, the fine content reached 42% and 50%, respectively. This supports the idea that some degree of particle degradation or crushing might be occurring during shearing.

Impact of Drying Temperatures on Shear Strength Testing and Material Characteristics

Shear strength tests were performed on samples dried at both 105°C and 60°C to examine their behaviour under shear stress conditions in the cDSS apparatus. Three tests were conducted for each drying condition, and the results were captured in three distinct graphs.

Graph 1: Shear Stress vs. Shear Strain ($\tau - \gamma$).

In Figure 4-7, both the 105°C and 60°C dried tests revealed a positive correlation between shear strain (γ) on the x-axis and shear stress (τ) on the y-axis. However, the tests dried at 105°C showed a higher shear stress value at each corresponding shear strain point. For example, at a shear strain of 15%, the 60°C tests showed an average τ of 69 kPa, while the 105°C tests exhibited an average τ of 78.8 kPa.

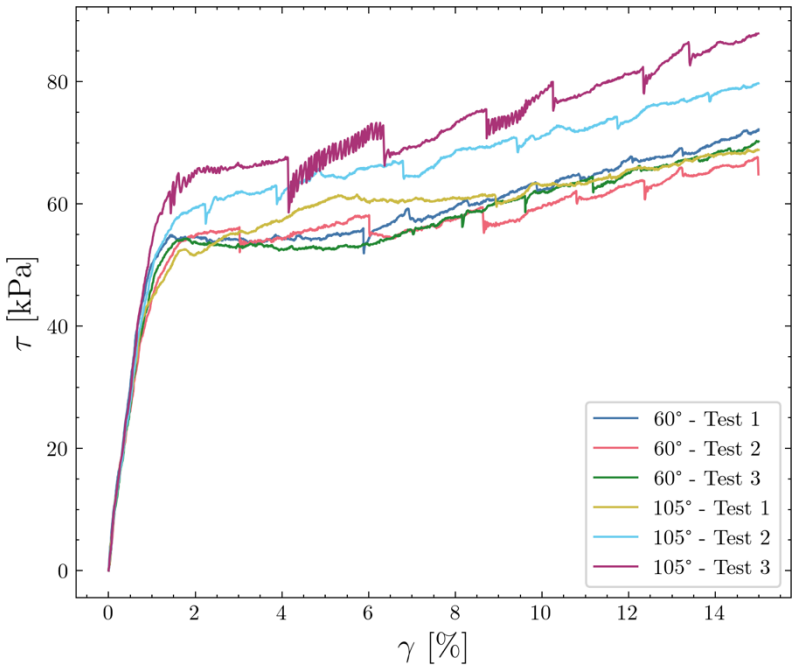

Figure 4-7 Comparison of shear stress τ [kPa] against shear strain γ [%] for samples dried at 105°C and 60°C.

Graph 2: Vertical Effective Stress vs. Shear Stress ($\tau - \sigma'_v$).

Figure 4-8 illustrates the relationship between vertical effective stress (σ'_v) and shear stress (τ). As can be observed, an increase in shear stress corresponds with a decrease in vertical effective stress, which could be indicative of the soil's dilatancy behaviour. The cDSS apparatus likely maintains a constant volume condition by adjusting the vertical effective stress throughout the test.

Utilizing the stress-dilatancy theory by Bolton (1986), if the samples initially behave contractively (indicating a reduction in volume during shearing), it leads to excess pore pressure development, subsequently causing a decrease in the vertical effective stress. This means that the soil samples, especially those prepared at 60°C, exhibited higher dilatancy when subjected to shear.

For instance, in the 60°C dried samples, a rise in shear stress from an average of 55 kPa to 70 kPa correlates with a decline in vertical effective stress from about 178 kPa to 162 kPa. In comparison, for the 105°C dried samples, a shear stress increase from approximately 65 kPa to 80 kPa corresponds with a reduction in vertical effective stress from an average of 190 kPa to around 182 kPa. This suggests that the 105°C dried samples, which display a more gradual decline in vertical

effective stress with increasing shear stress, might have a different dilatancy behaviour compared to the 60°C dried samples.

Moreover, the evident difference in the behaviour between 60°C and 105°C dried samples can be attributed to the varied particle arrangements and possible agglomerations induced by different drying temperatures. It is also discernible that the 105°C dried samples' contours are consistently higher than those of the 60°C dried samples, which may further indicate differences in their volumetric responses under shearing.

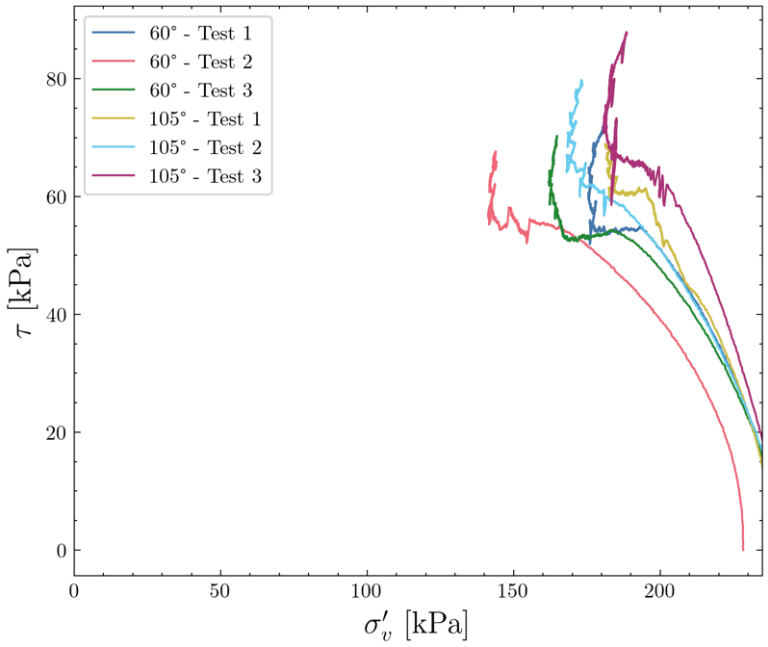

Figure 4-8 Vertical effective stress (σ'_v) [kPa] versus shear stress τ [kPa] for samples dried at 105°C and 60°C.

Graph 3: Pore Water Pressure vs. Shear Strain ($\frac{\Delta U}{\sigma'_{v0}} - \gamma$).

Figure 4-9 presents the relationship between shear strain (γ) on the x-axis, represented as a percentage (%), and the change in normalized excess pore water pressure ($\frac{\Delta U}{\sigma'_{v0}}$) on the y-axis, which is dimensionless. As shear strain increases, as illustrated in Figure 4-9, there's a clear rise in normalized pore pressure ratio for all tests. This behaviour implies a corresponding reduction in vertical effective stress, a trend that is also evident from Figure 4-8 where, with the increase in shear stress, a decrease in vertical effective stress is observed.

It should be noted that the excess pore pressure presented here is an apparent excess pore pressure calculated from the change in vertical stress on the vertical actuator during a CV test.

For the tests conducted at 60°C, the graph shows that as the shear strain approached 15%, the normalized pore water pressure values ranged between approximately 0.25 and 0.37. On the other hand, for the tests performed at 105°C, the normalized pore water pressures varied between 0.16 to 0.31 when the shear strain was at the same level.

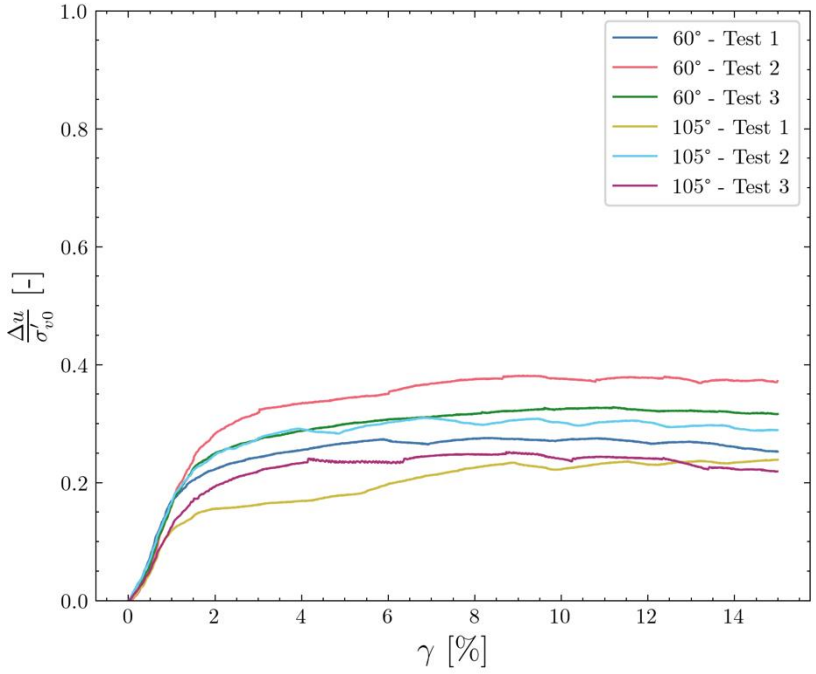

Figure 4-9 Normalized pore water pressure $\frac{\Delta U}{\sigma'_{v0}}$ versus shear strain γ [%] for samples dried at 105°C and 60°C.

4.3.1 Microscopic Examination of Dried Samples

To further understanding of the influence of drying methods on Wemmel sand, microscopic examinations were performed on samples dried at both 60°C and 105°C. These microscopic analyses aimed to elucidate the variations in soil microstructure that could affect its mechanical properties.

Under the microscope, some differences were observed between the 60°C and 105°C dried samples. The samples dried at 60°C displayed a more uniform distribution of particles and fewer agglomerations. In contrast, the samples dried at 105°C revealed increased particle agglomeration and clump formation. Figure 4-10 present the microscopic images of the 60°C and 105°C dried samples, respectively.

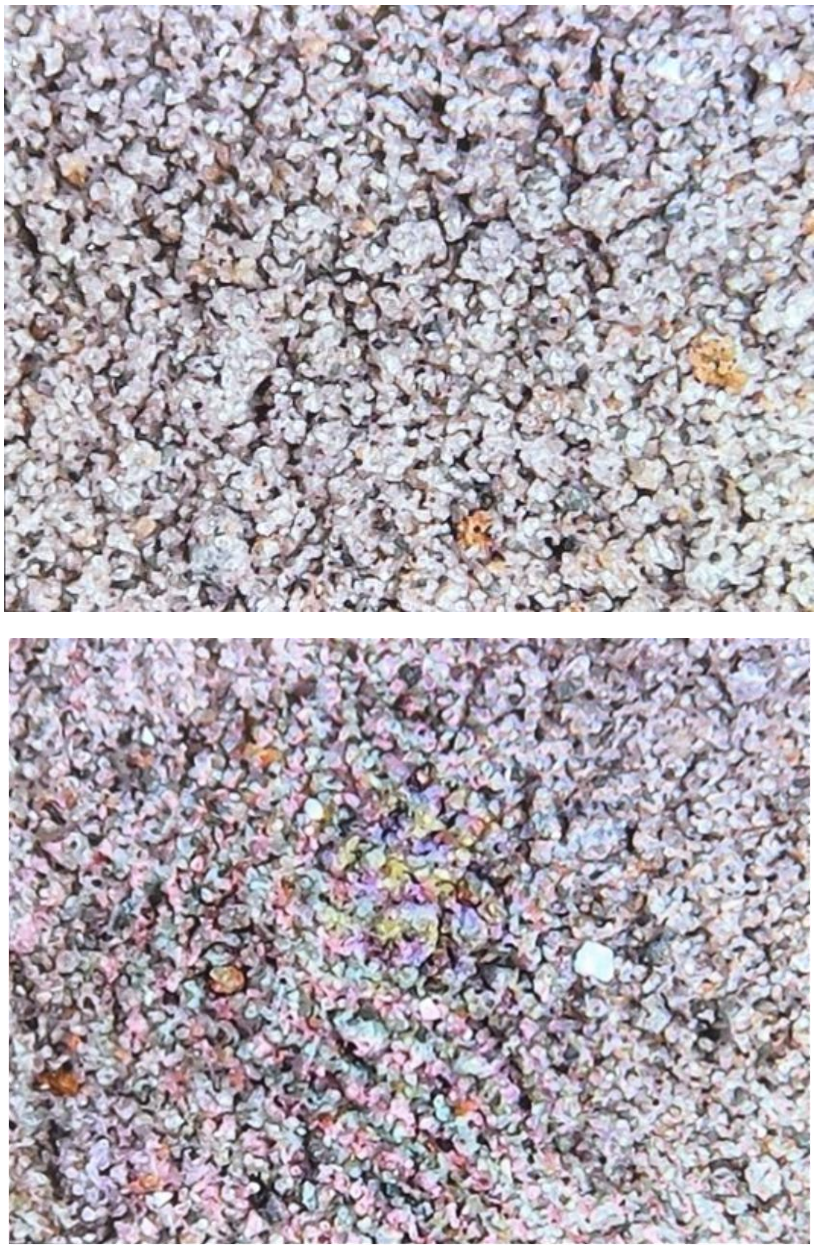

Figure 4-10 Microscopic examination of Wemmel sand dried at 60°C (top) and 105°C (down).

4.3.2 Material Loss During Drying

Both 105°C and 60°C drying methods led to a noticeable formation of lumps, which had the characteristics of being cohesive and easily broken apart by hand. The soil was sieved to remove these lumps before testing to avoid affecting the results.

It is critical to note the significant sample loss during the drying and sieving process. For ongoing studies requiring multiple tests runs on the same sample, as well as in the case of a lack of materials, this material loss can be a significant concern. For instance, Eemian Sand Sample showed considerable loss after drying at 60°C and sieving to remove shells and lumps.

Figure 4-11 Material Wastage in Eemian Sand Sample BH103 after drying at 60°C.

4.4 Cyclic Characterization of North Sea Sand

The primary objective of this section is to investigate the cyclic degradation of North Sea sands when subjected to loads from offshore wind turbine foundations. Two distinct types of soil samples, Beach Sand and Eemian Sand, were selected for this study due to their specific relevance to the North Sea offshore wind farms. Both sand types contained less than 1% fines content. To maintain material consistency across all tests, samples were dried at a uniform temperature of 60°C. Sample preparation exclusively employed dry tamping.

Test Variables

The experimental design included the following key variables:

- **Consolidation Pressures:** Tests were performed at four different consolidation pressures: 100, 150, 250, and 500 kPa.
- **Relative Densities:** Two levels of relative density were examined; 55% to represent medium dense sand and 80% to represent dense sand.
- **Cyclic Stress Ratio (CSR):** CSR values of 0.1, 0.15, and 0.2 were investigated regarding cyclic loading.

For these tests, Cyclic Direct Simple Shear (cDSS) testing was employed at the laboratory of Ghent University to assess the soil samples' cyclic response under symmetrical loading conditions. Each sample underwent 400 cycles of stress-controlled preshearing under constant vertical stress conditions, simulating the densification of soil under low-amplitude loading, as detailed in the test methodology. After this preshearing stage, each sample was subjected to varying consolidation pressures, relative densities, and CSR values. It's important to note that the shear tests under cyclic loading were conducted under constant volume conditions, analogous to undrained conditions for saturated specimens. The vertical stress on the specimen was continually adjusted during shearing to ensure a consistent height, reflecting genuine undrained test conditions. Additionally, after the preshearing phase, the specimens often possess some level of residual shear stress, which is reset to zero to ensure symmetric shear application and standardize the test conditions.

Given these variables, a total of 48 tests were conducted. The criteria for test termination were either reaching 1,000 cycles or achieving a 15% shear strain, whichever occurred first. Data concerning the soil's cyclic behaviour, such as the number of cycles to failure and horizontal shear stress at different levels of shear strain and average pore pressure were rigorously recorded. Changes in confining stress, serving as an indicator of pore water pressure, will be explained and presented in the following sections through graphs.

4.4.1 Graphical Presentation of Cyclic Test Results

This section delineates the cyclic behaviour of North Sea sands, visually represented through four distinct graphs. Each graphic is designed to convey specific characteristics of the soil samples, primarily focusing on consolidation pressures, relative densities, and Cyclic Stress Ratios (CSR). Data for these graphical results have been sourced from an experimental series of 48 cyclic tests, emphasizing variables such as cyclic shear stress amplitude, cyclic shear strain amplitude, excess pore pressure, and damping.

First Plot: Shear Strain vs. Tangential Stress ($\boldsymbol{\gamma_{cy} - \tau_{cy}}$)

This primary plot examines the relationship between shear strain (γ_{cy}) and tangential stress (τ_{cy}). The x-axis represents shear strain, derived from the horizontal Linear Variable Differential Transformer (LVDT) sensor and adjusted for any pre-shear deviations. Meanwhile, the y-axis illustrates tangential stress in kPa calculated from the horizontal load cell. By plotting the real-time interaction between stress and strain across test cycles, this representation offers a granular view of soil behaviour under cyclic shear. It sets the foundation for interpreting more intricate stress-strain dynamics highlighted in the subsequent plots. The test results that as the cyclic loading progresses, the achieved shear strain during each cycle increases until a limit shear strain is reached (typically 15%). The shear modulus G as a function of strain level can be calculated by dividing the maximum shear stress by the maximum strain achieved. This shows a reduction of shear modulus with strain level, a strain-softening behaviour.

Second Plot: Vertical Stress vs. Tangential Stress during Cyclic Shear ($\boldsymbol{\sigma'_v - \tau_{cy}}$)

This plot focuses on the interplay between vertical effective stress (σ'_v) and tangential stress (τ_{cy}), both measured in kPa. The vertical stress, illustrated on the x-axis, begins from the initial effective vertical stress and undergoes adjustments as the test proceeds. On the y-axis, the amplitude of cyclic tangential stress, which is fixed during the cyclic test, is found. As the soil sample is subjected to cyclic shear stress in constant volume conditions, this graph explicitly captures the evolving relationship between effective vertical stress and cyclic tangential stress.

The test results that during cyclic loading, the vertical effective stress reduces. This indicates a build-up of (apparent) excess pore pressure until the failure line is reached. Once the failure line is reached, the test data exhibits a so-called *butterfly* shape, in which the sample does not show sudden failure but instead continues to accumulate strain at very low effective stress.

Third Plot: Cycle Number vs. Cyclic Shear Strain Amplitude and Damping ($\boldsymbol{N - \gamma_{cy}}$) $\boldsymbol{and}$ ($\boldsymbol{N - D}$)

This graph sheds light on the cyclic behaviour of the soil sample, focusing on two key parameters: Cyclic Shear Strain Amplitude (γ_{cy}) and Damping. The primary y-axis illustrates the Cyclic Shear Strain Amplitude, marked as a percentage. These values are determined by taking the average of the maximum and minimum shear strains for each cycle. The x-axis counts the number of cycles following the pre-shear stage. The example test results show that the rate of cyclic strain amplitude increase is low for the initial cycles. However, once the vertical effective stress is sufficiently reduced, the rate of accumulation accelerates until the maximum allowed shear strain amplitude is exceeded.

A secondary y-axis on the right displays Damping values, derived from the hysteresis loops created by the shear strain and tangential stress within each cycle. The damping ratio, ξ, a dimensionless measure of energy dissipation, is computed by first calculating the area enclosed by the stress-strain hysteresis loop, known as r_e. This area quantifies the amount of energy dissipated during the cyclic loading. The maximum product of tangential stress and its corresponding shear strain within the loop

is then computed, denoted by p_e, which is halved to calculate the damping ratio ζ using the formula $\xi = \frac{r_e}{4\pi p_e}$. By contrasting Damping values (depicted as a red dashed line) with the Cyclic Shear Strain Amplitude, one can observe their mutual evolution over cycles.

Understanding Damping Variations in Cyclic Loads:

The figure 4-12 related to sample test (Beach Sand under CSR of 0.1, Consolidation Pressure of 100 kPa, and Relative Density of 55%) demonstrates the simultaneous plotting of maximum tangential stress, corresponding shear strain, and damping over numerous cycles. One can easily observe the abrupt changes in damping which correspond to certain cycles. A closer inspection of these cycles offers noteworthy observations:

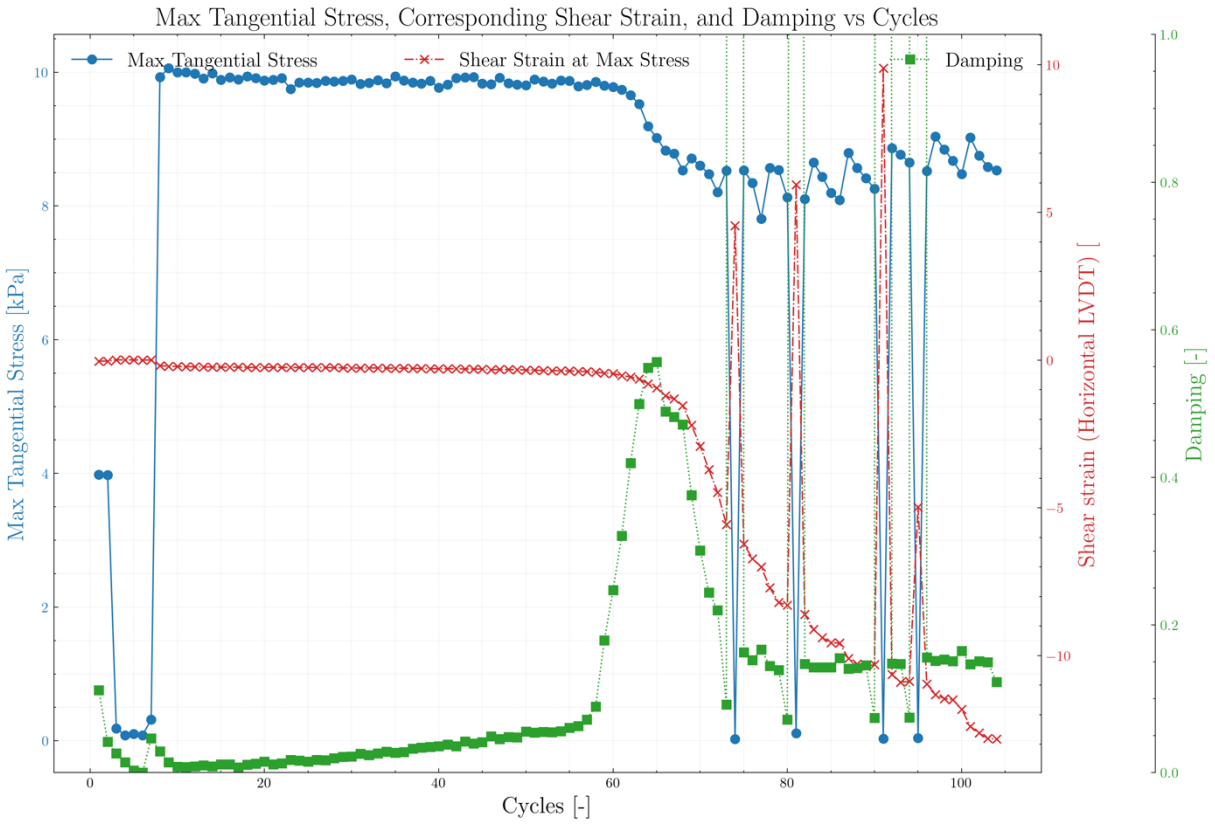

Figure 4-12 Cyclic Shear Strain Amplitude and Damping Behaviour of Beach Sand Under Cyclic Loading.

1. **Zero Shear Stress Points**: The graph reveals specific cycles where the tangential shear stress approximates zero. These points also coincide with a distinct change in the maximum shear strain value, specifically its sign.
2. **Shear Strain Accumulation**: In the initial 73 cycles, a progressive accumulation in shear strain is evident. It attains a value of approximately 5.5% by cycle 73. However, in the immediate next cycle (cycle 74), the shear strain exhibits a surprising change not only in magnitude but also in sign, dropping to -4.5%. This sudden variation is transient as the shear strain reverts to its original pattern by cycle 75, registering a value of 6.2%.

The sudden drop in damping is directly associated with these abrupt changes in shear strain. Such behaviour can be rationalized through the lens of soil behaviour under cyclic loading. As the soil undergoes repeated cyclic loads, modifications in its behaviour emerge, resulting in transformations in the hysteresis loop and the consequent energy dissipation. Over multiple cycles, the microstructure of the soil may undergo adjustments, which can potentially influence the damping

values (Hardin & Drnevich, 1972). Moreover, past literature emphasizes that the damping ratio can be affected by alterations in the soil structure, which evolve over time due to continuous cyclic loading.

Fourth Plot: Cycle Number vs. Average Pore Pressure Ratio ($\boldsymbol{N - \frac{\Delta U}{\sigma'_{v0}}}$)

The last plot focuses on the Average Pore Pressure Ratio and its progression across the cycles. The x-axis counts the cycles during the shearing stage. The y-axis, ranging from 0 to 1, indicates the Average Pore Pressure Ratio. This ratio is extracted by measuring the absolute difference between the mean vertical stress of each cycle and the initial effective vertical stress ($\sigma'_{v_{mean}} - \sigma'_{v_0}$), then normalizing this difference by the initial effective vertical stress (σ'_{ref}). When this ratio reaches 1, a liquefaction condition is effectively observed.

This ratio offers insights into the relative shifts in pore pressure during the cyclic test. The trend is important for understanding how pore pressure is generated in the soil body during cyclic shearing. When comparing the excess pore pressure generation with the cyclic shear strain accumulation, it can be observed that the cyclic strain development accelerates one an excess pore pressure ratio of 50% to 60% is reached.

For the full set of graphical results that complement the discussions in this chapter, please see Appendix A.

Test 1: Cyclic Behaviour of Beach Sand under CSR of 0.1, Consolidation Pressure of 100 kPa, and Relative Density of 55%

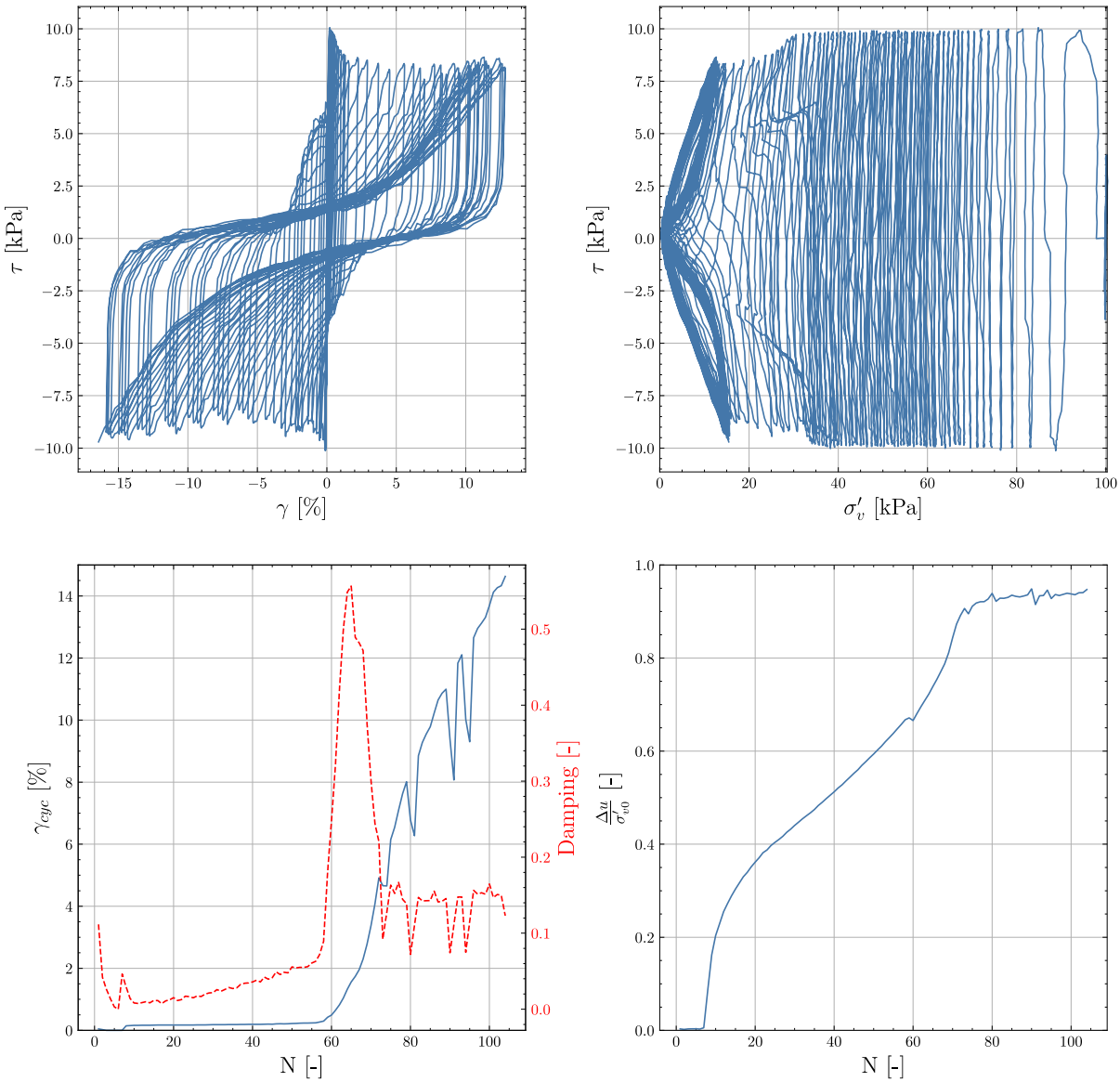

Figure 4-13 Multifaceted Cyclic Response of Beach Sand - Integrating shear stress-strain behaviour, stress evolution, damping characteristics, and pore pressure ratio development.

4.5 Key Observations from Cyclic Tests:

In the following table, key observations from cyclic tests on Eemian and Beach Sand samples are summarized. The table illustrates the number of cycles required to reach certain thresholds of cyclic shear strain and excess pore pressure ratio, under varying consolidation pressures, relative densities, and Cyclic Stress Ratios (CSRs). Note that a dash ("-") in the table indicates that the specific shear strain or pore pressure ratio was not reached, even after extending the test to 1000 cycles.

Table 4-1 Cyclic Test Thresholds for Eemian and Beach Sand Samples.

					Number of cycles for reaching cyclic strain of				**Number of cycles for reaching excess pore pressure ratio of**				
Test No.	**Sample**	p_0' **[kPa]**	**Relative Density**	**CSR**	**1%**	**5%**	**10 %**	**15 %**	**0,05**	**0,1**	**0,25**	**0,6**	**0,9**
1	Eemian	100	80	0,1	-	-	-	-	39	45	290	-	-
2	Eemian	100	80	0,15	16	21	23	27	11	12	13	19	20
3	Eemian	100	80	0,2	1	2	4	7	1	1	2	2	-
4	Eemian	150	80	0,1	119	129	137	151	16	16	24	93	132
5	Eemian	150	80	0,15	7	12	18	21	5	5	6	7	12
6	Eemian	150	80	0,2	5	8	13	19	4	4	5	7	-
7	Eemian	250	80	0,1	73	93	101	109	16	17	20	57	103
8	Eemian	250	80	0,15	50	68	75	78	19	19	25	63	73
9	Eemian	250	80	0,2	38	44	48	50	36	37	37	43	-
10	Eemian	500	80	0,1	1	5	10	15	6	7	31	-	-
11	Eemian	500	80	0,15	58	68	79	83	18	19	20	31	-
12	Eemian	500	80	0,2	20	23	26	30	20	20	21	22	-
13	Eemian	100	55	0,1	230	259	266	270	7	7	21	197	260
14	Eemian	100	55	0,15	1	5	10	15	5	5	6	10	27
15	Eemian	100	55	0,2	38	39	41	42	38	38	39	40	-
16	Eemian	150	55	0,1	-	-	-	-	4	4	21	716	-
17	Eemian	150	55	0,15	7	12	18	21	2	2	3	8	21
18	Eemian	150	55	0,2	5	9	13	15	4	4	5	11	-
19	Eemian	250	55	0,1	67	73	78	84	18	19	34	245	349
20	Eemian	250	55	0,15	20	26	32	36	6	7	8	20	-
21	Eemian	250	55	0,2	7	8	9	10	7	7	7	8	-
22	Eemian	500	55	0,1	344	378	385	389	10	10	20	239	234
23	Eemian	500	55	0,15	12	17	21	24	3	4	5	12	47
24	Eemian	500	55	0,2	4	7	10	14	5	6	6	6	9
25	Beach Sand	100	80	0,1	173	189	226	245	8	8	17	129	184
26	Beach Sand	100	80	0,15	23	34	52	76	12	12	13	23	56
27	Beach Sand	100	80	0,2	7	10	19	36	6	6	6	8	-
28	Beach Sand	150	80	0,1	203	234	266	323	4	5	13	74	102
29	Beach Sand	150	80	0,15	8	16	51	161	58	59	62	189	346
30	Beach Sand	150	80	0,2	38	39	42	49	37	37	37	39	-
31	Beach Sand	250	80	0,1	92	115	138	176	18	19	34	245	349
32	Beach Sand	250	80	0,15	10	12	14	17	9	9	10	12	-
33	Beach Sand	250	80	0,2	3	4	6	7	3	3	3	4	8

Test results

					Number of cycles for reaching cyclic strain of				Number of cycles for reaching excess pore pressure ratio of				
Test No.	**Sample**	**p'_0 [kPa]**	**Relative Density**	**CSR**	**1%**	**5%**	**10 %**	**15 %**	**0,05**	**0,1**	**0,25**	**0,6**	**0,9**
34	Beach Sand	500	80	0,1	339	354	380	393	18	19	38	255	378
35	Beach Sand	500	80	0,15	58	68	76	83	44	45	46	60	-
36	Beach Sand	500	80	0,2	6	8	10	13	6	6	7	8	-
37	Beach Sand	100	55	0,1	62	72	85	100	8	9	12	51	73
38	Beach Sand	100	55	0,15	3	5	7	10	2	22	3	4	9
39	Beach Sand	100	55	0,2	5	6	7	10	5	5	5	6	-
40	Beach Sand	150	55	0,1	178	183	188	192	7	8	22	140	184
41	Beach Sand	150	55	0,15	13	14	24	33	11	12	12	14	35
42	Beach Sand	150	55	0,2	8	10	15	24	8	8	8	10	25
43	Beach Sand	250	55	0,1	67	73	78	84	5	5	11	53	79
44	Beach Sand	250	55	0,15	13	14	15	16	11	11	12	14	-
45	Beach Sand	250	55	0,2	6	7	8	11	6	6	7	8	-
46	Beach Sand	500	55	0,1	212	220	229	235	2	3	15	150	234
47	Beach Sand	500	55	0,15	50	53	57	60	40	41	42	50	-
48	Beach Sand	500	55	0,2	4	7	10	14	4	4	5	8	-

4.5.1 Effect of Sand Type

In this section, the results derived from the cyclic tests conducted on North Sea sands with different relative densities, 55% and 80%, are graphically presented. This section focused on two primary sand types: Eemian Sand and Beach Sand. Both sands, originating from the North Sea region, contain less than 1% fine content. The Average Maximum Dry Density for both sands is 1.7 Te/m^3. The Average Minimum Dry Density is 1.5 Te/m^3 for the Eemian Sand and 1.4 Te/m^3 for the Beach Sand.

The graphical representations are designed with a y-axis indicating the average number of cycles, plotted in a logarithmic scale (Log N). The x-axis combines CSR (Cyclic Stress Ratio) and shear strain values, providing a comprehensive view of the relationship between them and the average number of cycles needed to achieve specific shear strain benchmarks. For each distinct CSR value - 0.1, 0.15, and 0.2 - separate bars illustrate the average number of cycles necessary to meet the established shear strain thresholds for both sand types, at their respective relative densities. The bars are color-coded for differentiation: green for the Eemian Sand and red for the Beach Sand.

Based on the data presented, it is anticipated sands with comparable properties would exhibit a similar number of cycles to reach specific shear strain limits, as clearly showcased by the graphical representations, especially at higher CSR values for both relative densities. For instance, at a relative density of 55% and a CSR of 0.2, the Eemian Sand required 20 cycles to reach a shear strain of 15%, whereas the Beach Sand needed 15 cycles. This close behaviour emphasizes their similar constitutive nature. Moreover, at an increased relative density of 80%, both Eemian and Beach sands necessitated 26 cycles to achieve the 15% shear strain under a CSR of 0.2.

Upon examining the overall behaviour of the Eemian Sand compared to the Beach Sand, a noticeable pattern emerges. The Eemian Sand consistently demonstrates a slightly superior cyclic strength when confronted with similar conditions. This is evident from the number of cycles the sand can endure before reaching predetermined shear strain benchmarks.[33]

Comparative Analysis of Average Number of Cycles for Eemian and Beach Sands at Different CSR and Shear Strain Values for Relative Densities of 55% and 80%

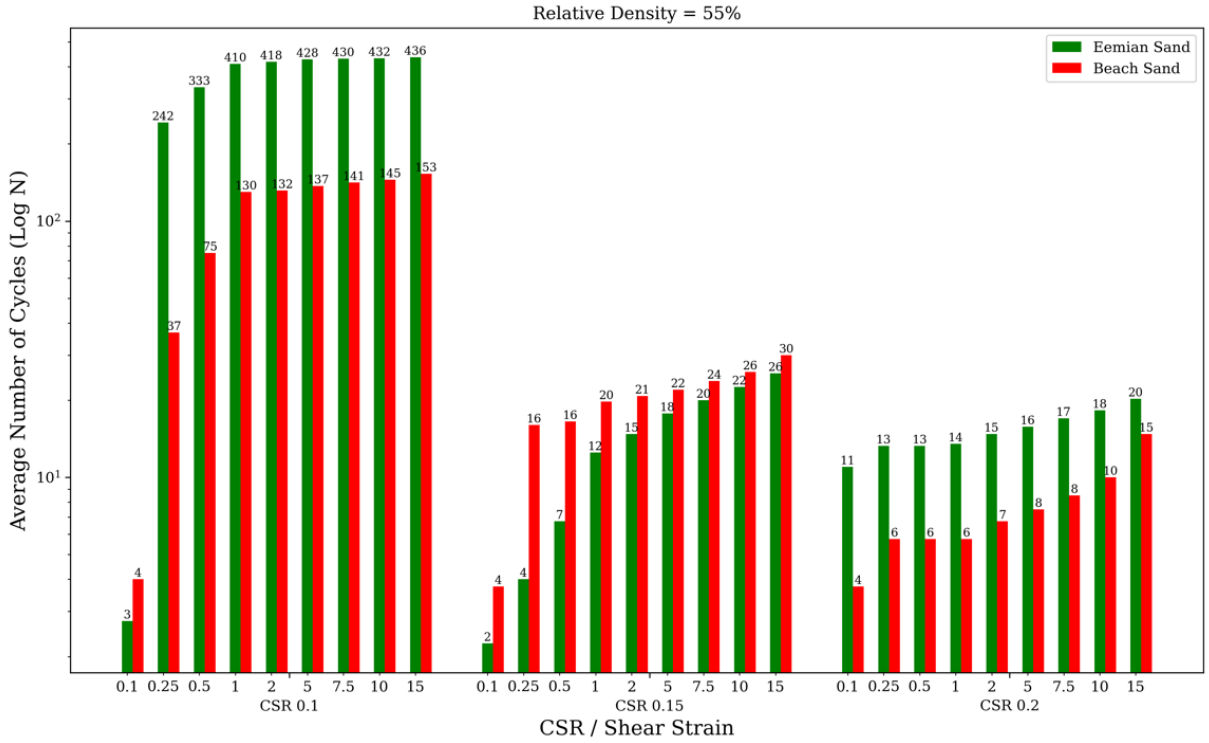

Figure 4-14 Comparative Cyclic Resistance of Eemian and Beach Sand for Relative Densities of 55%.

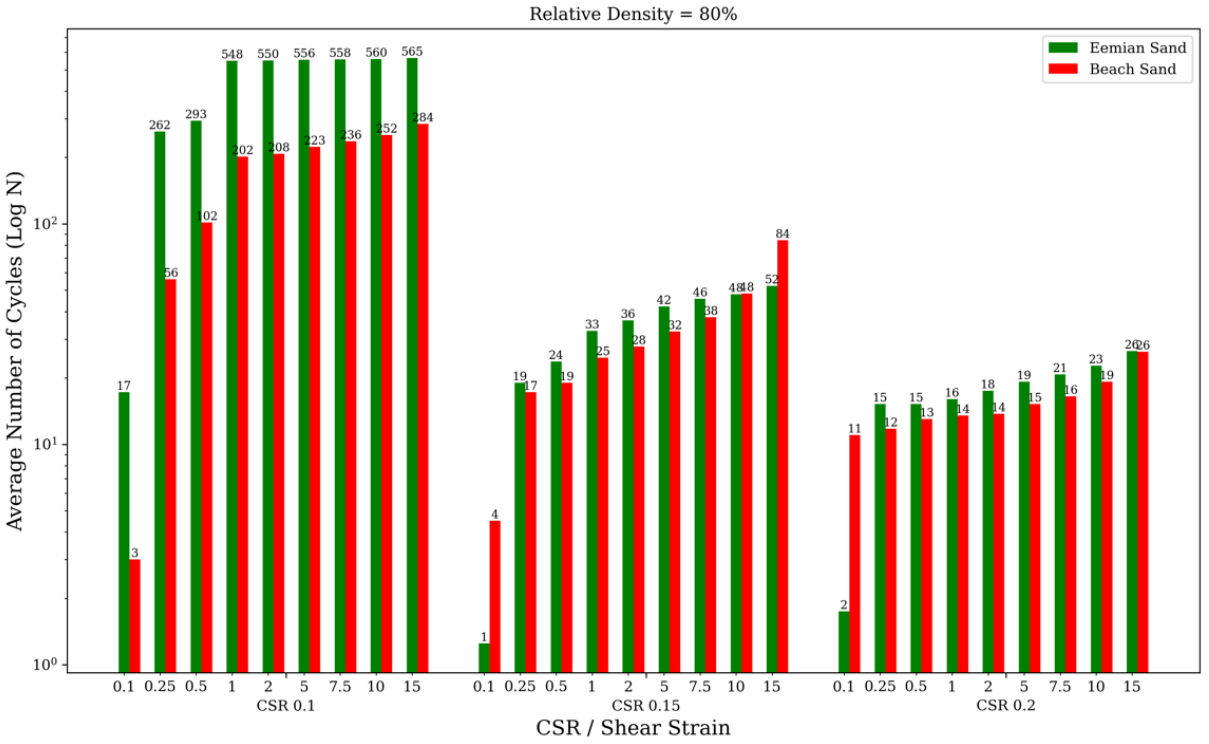

Figure 4-15 Comparative Cyclic Resistance of Eemian and Beach Sand for Relative Densities of 80%.

4.5.2 Effect of Relative Density

In this section, the influence of relative density on the cyclic behaviour of North Sea sands is detailed. The focus is primarily on Eemian Sand and Beach Sand samples. The graphical representations serve to elucidate how the number of cycles is influenced by both the average pore pressure ratios and shear strain levels for two levels of relative density—55% and 80%. It is imperative to underscore that a higher relative density markedly enhances the cyclic strength of the sands. This is manifested as an increased number of cycles (N) necessary to reach a given strain or excess pore water pressure level. This core finding is evident across the various CSR levels and stress conditions tested.

The visualizations are generated for three distinct CSR (Cyclic Stress Ratio) levels—0.1, 0.15, and 0.2. For ease of discussion, the red bars are representative of a relative density of 55%, while the green bars show a relative density of 80%.

The X-axis of each graph can present either the Average Pore Pressure Ratio ($\frac{\Delta U}{\sigma'_{v0}}$) or shear strain percentages, depending on the specific focus of the evaluation. For the Average Pore Pressure Ratio graphs, the X-axis ranges over four selected values—0.05, 0.1, 0.25, and 0.6. Conversely, when focusing on shear strain, the X-axis ranges over—0.1, 0.25, 0.5, 1, 2, 5, 7.5, 10, and 15 percent. The Y-axis in both cases is logarithmic in scale and represents the Average Number of Cycles to failure (Log N).

Each bar within the visual representations indicates the average number of cycles to reach a certain pore pressure ratio or shear strain level. The bars are plotted for the two different relative density to highlight the effect of relative density. These averages have been calculated across various vertical stress levels for each CSR—100, 150, 250, and 500 kPa—and the specific sand type. Numerical values displayed atop each bar provide this average, rounded for clarity. For brevity, it will be presented one sample figure here, and one can find the rest in Appendix D.

Building upon examination of relative density effects on cyclic behaviour, it is essential to discuss the justification behind the choice of averaging across distinct consolidation pressures. The reason is the normalization procedure of the shear stress to the specific reference stress, σ'_{ref}, a methodology explained by Andersen (2015). According to Andersen (2015), the cyclic response is subject to consolidation stresses, even after their normalization. Consequently, both static and cyclic behaviours are normalized to a specific reference stress, delineated as $\sigma'_{ref} = pa * (\frac{\sigma'_{vo}}{pa})^n$, with pa representing the atmospheric pressure (fixed at 100 kPa) and n serving as an empirical exponent derived from curve fitting. For current analysis involving sand and silt subjected to cyclic shear, the value of n is determined as 0.9. The important rationale behind using this methodology, especially in the context of sand and silt, is to align as closely as possible with the reference stress, given that the definition of undrained shear strength often borders ambiguity in dense, dilatant terrains of sand and silt [9]. The reference stress mainly comes from the vertical stresses, so horizontal stress is not estimated in the DSS tests. Using this method, based on Andersen's research, makes the averaging approach reliable and consistent.

For tests that did not meet the defined criteria even after 1,000 cycles, these have been assumed to indicate a completion at 1,000 cycles. Table below specifies these tests.

Table 4-2 Summary of Tests Not Meeting Criteria at Defined Cycle Thresholds.

NO.	Sand Type	Relative Density (RD %)	Vertical Stress (kPa)	Criterion Not Met
1	Eemian Sand	80%	500 kPa	Did not achieve average pore pressure ratio of 0.6 at CSR 0.1
2	Eemian Sand	80%	100 kPa	Did not achieve average pore pressure ratio of 0.6 at CSR 0.1
3	Eemian Sand	80%	500 kPa	Did not exceed shear strain of 1% at CSR 0.1
4	Eemian Sand	80%	100 kPa	Did not exceed shear strain of 0.5% at CSR 0.1
5	Eemian Sand	55%	150 kPa	Did not exceed shear strain of 0.5% at CSR 0.1

Effect of Relative Density on Cyclic Strength of Eemian Sand and Beach Sands at Different CSR Levels

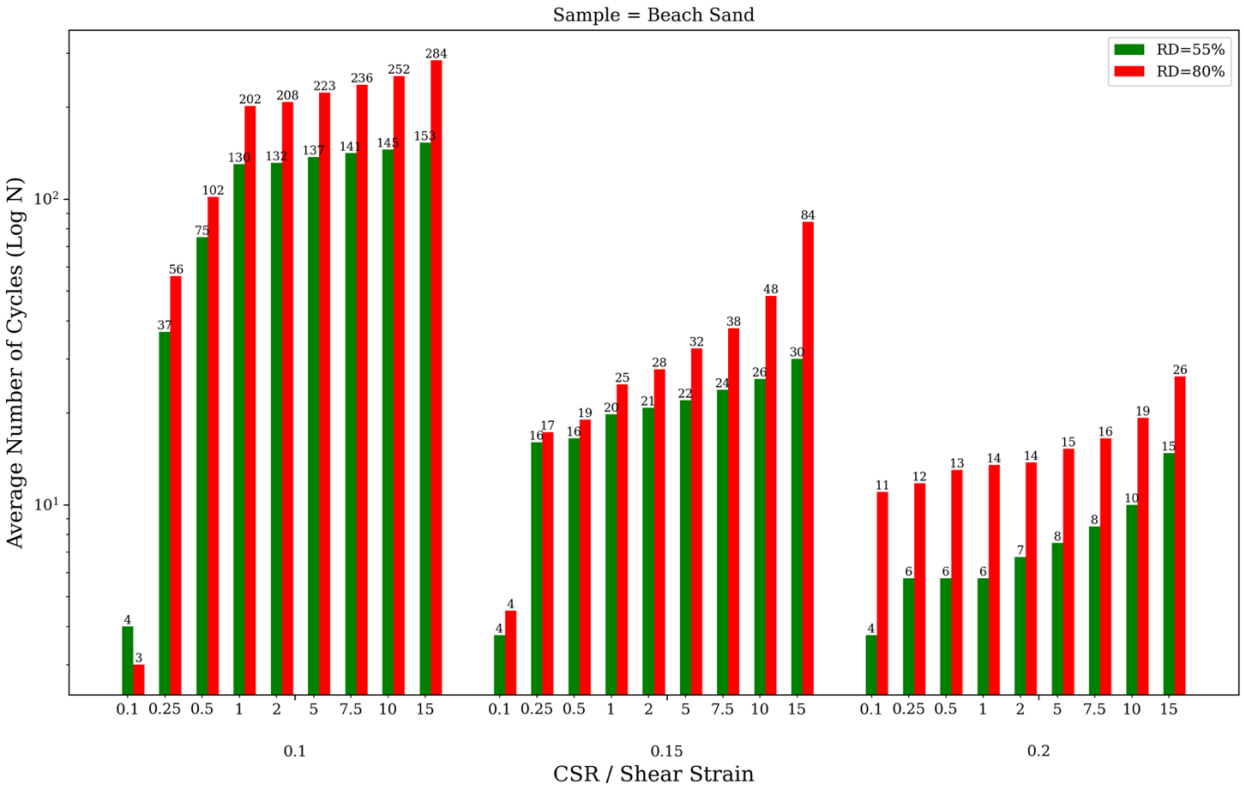

Figure 4-16 Average Number of Cycles for Beach Sand at Different CSR Levels and Relative Densities.

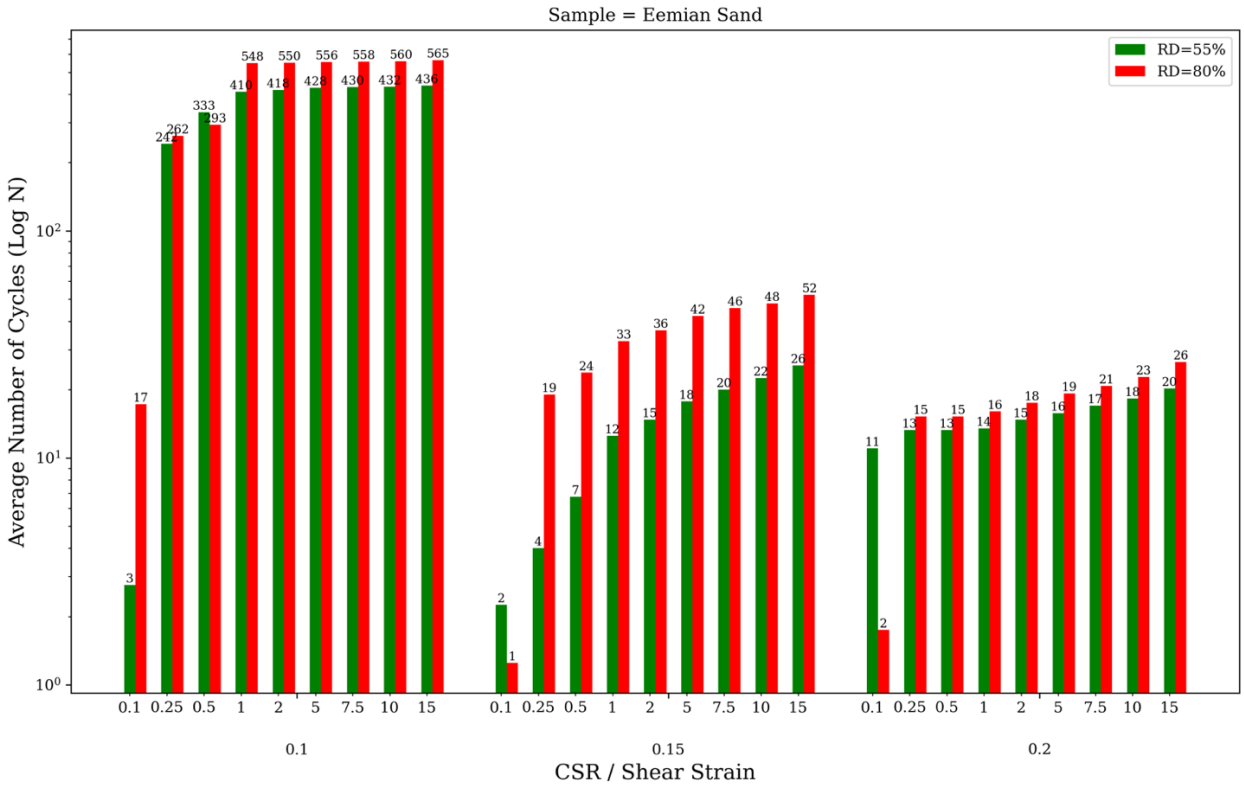

Figure 4-17 Average Number of Cycles for Eemian Sand at Varying CSR Levels and Relative Densities.

4.5.3 Effect of Cyclic Stress Ratio (CSR) on Cyclic Behaviour

In the current section, the role of varying CSR on the cyclic behaviour of North Sea sands, specifically the Eemian Sand and Beach Sand, is explored. Drawing parallels with the prior section on relative density, the graphical representations in this section further illustrate how different loading conditions (i.e., CSR levels) influence the key parameters: Shear Strain and Average Pore Pressure ratios. For a clear analysis, three specific CSR levels—0.1, 0.15, and 0.2—are spotlighted.

To elucidate these relationships, two distinct sets of graphs are employed. One set is dedicated to shear strains, while the other serves for average pore pressure ratios. Each sand type—Eemian Sand and Beach Sand—has its own individual plot for both 55% and 80% relative densities. The aim is to unravel how varied CSR levels impact the number of cycles needed to achieve the defined shear strain or average pore pressure ratios.

For those graphs homing in on shear strains, the X-axis captures a range of predefined values—0.1, 0.25, 0.5, 1, 2, 5, 7.5, 10, and 15 percent. On the other side, when assessing average pore pressure ratios, the X-axis extends across four crucial values—0.05, 0.1, 0.25, and 0.6. Importantly, an average pore pressure ratio, say 0.6, implies that the pore water pressure has reached a substantial 60% of the initial vertical effective stress. Regardless of the graph or the specific parameter being analyzed, the Y-axis consistently uses a logarithmic scale, denoting the Average Number of Cycles to failure (Log N).

In every graph, data points, connected by lines to illustrate trends, display the average number of cycles required to hit the desired shear strain or average pore pressure ratio across varied CSR levels. These averages are derived from different vertical stress levels—100, 150, 250, and 500 kPa—and each is distinguished by sand type and relative density.

The CSR levels, indicative of the loading conditions, are instrumental in determining the cyclic response of the foundation soils. Adjusting the CSR is vital for gauging soil resilience under varied intensities of cyclic loading, which is essential for the analysis of foundation soils subjected to both operational functions and extreme environmental conditions.

The experimental outcomes clearly demonstrate the impact of CSR on the cyclic strength of the sands. With an increment in CSR from 0.1 to 0.2, there is a notable reduction in the number of cycles needed to reach a specific shear strain or pore pressure ratio, observed consistently across both Eemian and Beach Sand samples, irrespective of their relative densities. This inverse relationship between CSR and the number of cycles to reach failure is accentuated at elevated CSR levels, suggesting a significant influence of loading severity on the progression of soil deformation and the subsequent failure mechanisms.

Effect of CSR on the Cyclic Resistance of Eemian Sand and Beach Sands at Different Shear Strain Levels

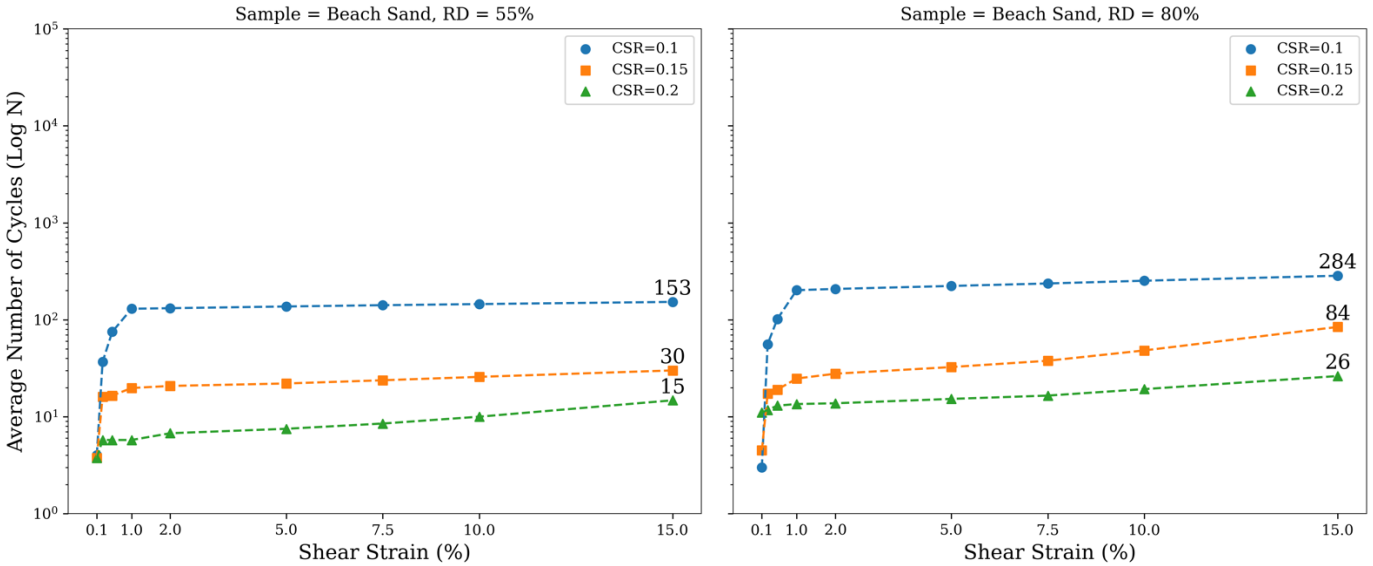

Figure 4-18 Effect of CSR on Shear Strains in Beach Sand

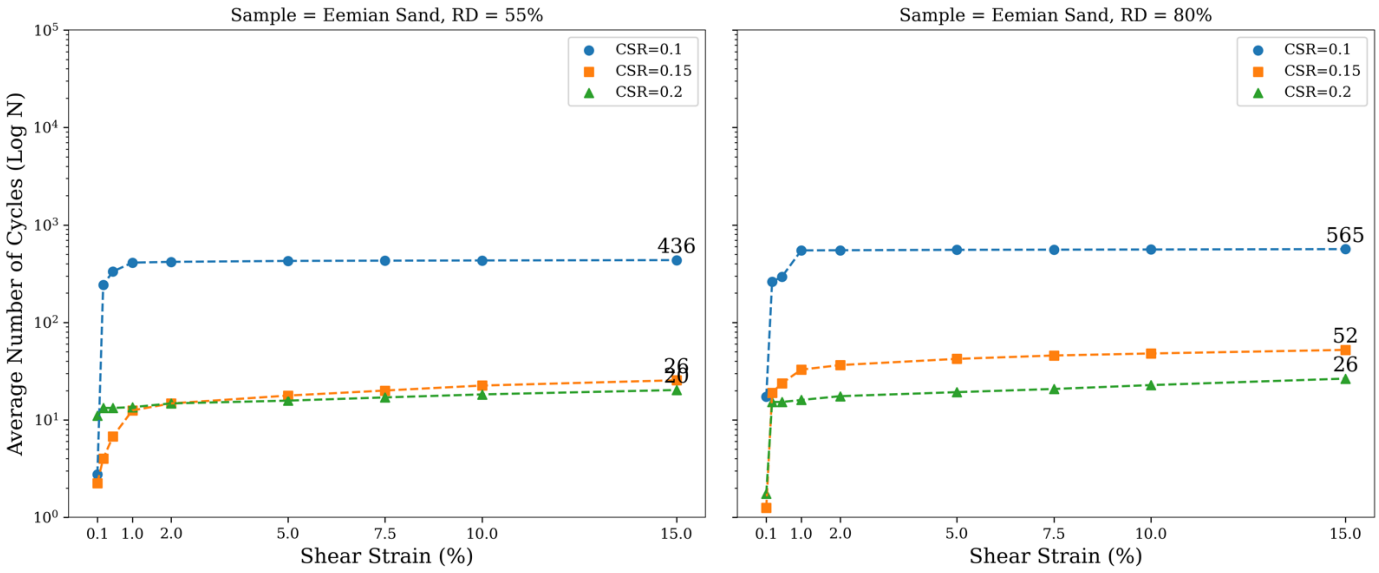

Figure 4-19 Effect of CSR on Shear Strains in Eemian Sand.

Effect of CSR on the Cyclic Resistance of Eemian Sand and Beach Sands at Different Pore Pressure Ratios

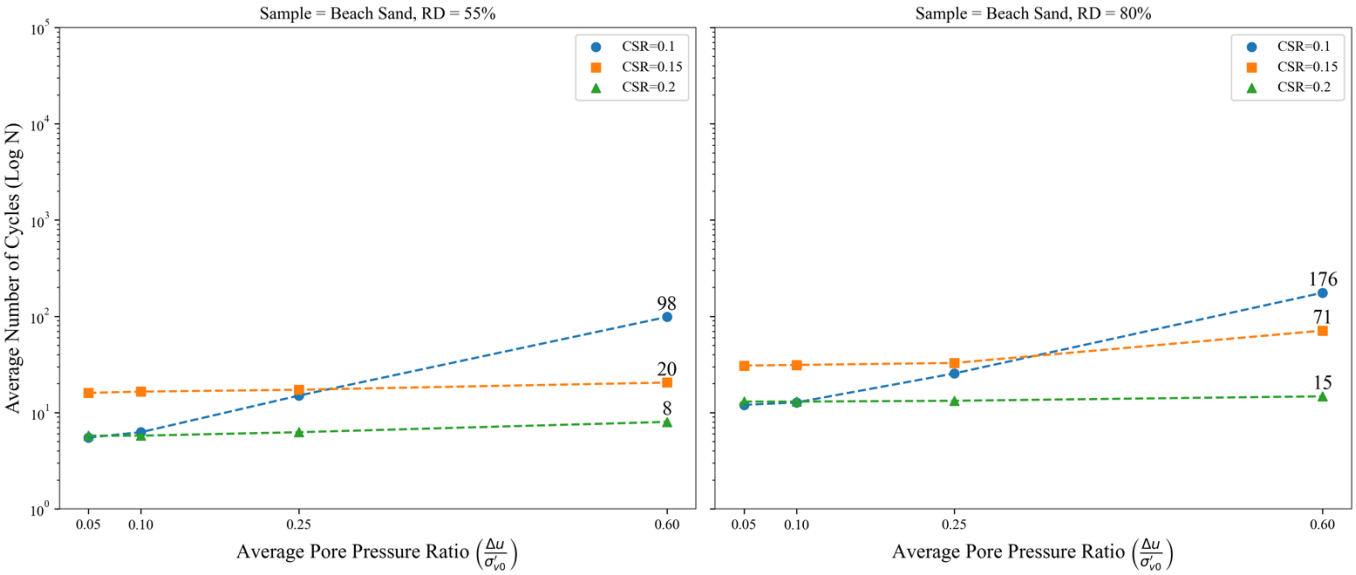

Figure 4-20 Effect of CSR on Pore Pressure Development in Beach Sand.

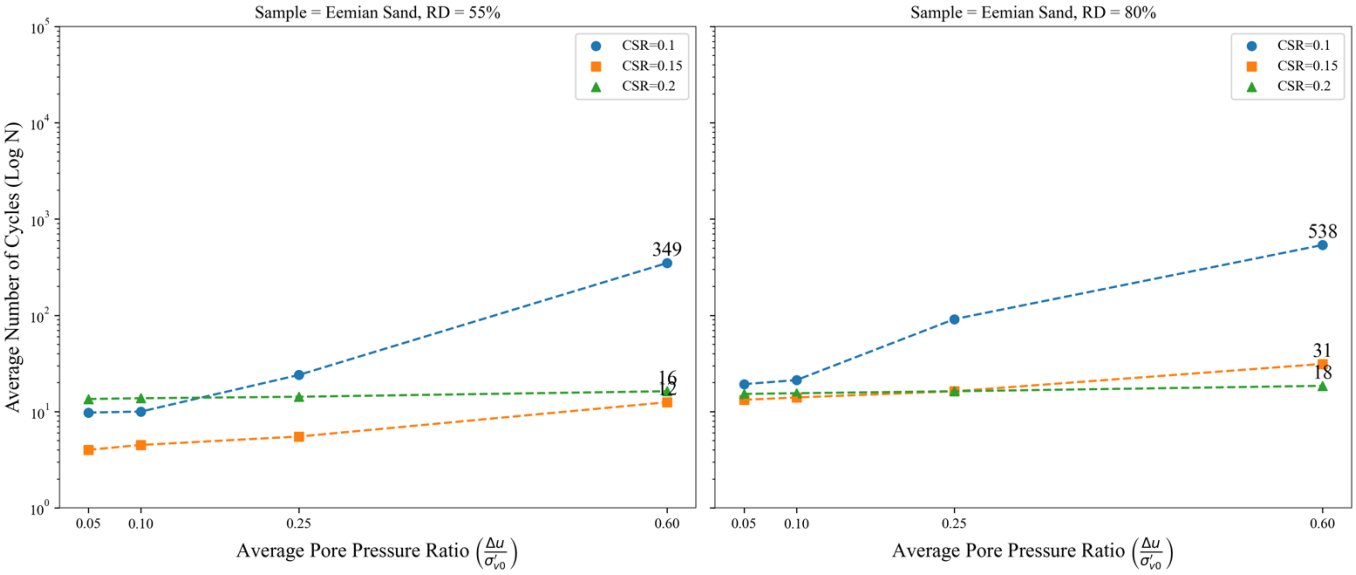

Figure 4-21 Effect of CSR on Pore Pressure Development in Eemian Sand.

4.5.4 Strain Contours

This section presents the outcomes of cyclic tests on North Sea sands, focusing on Beach Sand and Eemian Sand. These results are based on a set of tests for each sand type, with consistent conditions of vertical stress and relative density, but varying Cyclic Stress Ratio (CSR) values of 0.1, 0.15, and 0.2.

The x-axis displays the logarithmic representation of the number of cycles (Log N), while the y-axis showcases the CSR. These plots meticulously detail the soil's behaviour under cyclic loading, taking into consideration factors like consolidation pressures, relative densities, and differing shear stress amplitudes. The divisions are further refined based on certain shear strain benchmarks, as suggested by [9].

For each conducted test, the cycles required to attain designated shear strain thresholds (γ =[0.1, 0.25, 0.5, 1, 2, 5, 7.5, 10, 15]) are meticulously documented. In aggregate, 16 graphs emerge from 48 distinct tests, offering a comprehensive insight into the cyclic response of the soil under diverse stress scenarios. For brevity, it will be discussed one sample figure here, and the complete set can be found in Appendix B.

A clear trend is discerned when examining the relationship between CSR and N. An inverse correlation is consistently observed for CSR values at the extremes of 0.1 and 0.2; as CSR intensifies, indicating stronger shear forces applied to the sample, the number of cycles to reach a specific shear strain diminishes. This underscores the fundamental concept that increased shear stresses expedite failure under static conditions.

Nevertheless, at a CSR of 0.15, the expected pattern does not always hold true. Assuming identical conditions, such as vertical stress and relative density, one might anticipate that results at CSR 0.1 would manifest more cycles than at CSR 0.15, and results at CSR 0.2 would exhibit fewer cycles than at CSR 0.15. However, the data occasionally defies this rationale.

Several factors might account for this inconsistency. The closeness of cyclic shear ratios, such as 0.15, 0.1, and 0.2, means even minor variations during testing stages become more pronounced. A critical phase is sample preparation in Direct Simple Shear (DSS) testing where minor discrepancies can significantly sway the outcomes. These minor differences, which may be negligible at more distinct CSR levels like 0.1 and 0.2, become more pronounced when evaluating closely spaced values.

It is crucial to highlight that while the expected inverse relationship between CSR levels and the number of cycles is generally observed at higher shear strains, some exceptions are noted at lower shear strains, particularly below 1%. This could be attributed to variations in particle configuration during sample preparation, and possibly, to slight differences in the fine content of the samples. As testing progresses to larger shear strains, the anticipated trend of reduced cycles with increased CSR becomes more pronounced, aligning with the foundational principles of soil mechanics under cyclic loading conditions.

Beach Sand (RD = 80%, Vertical Stress = 100)

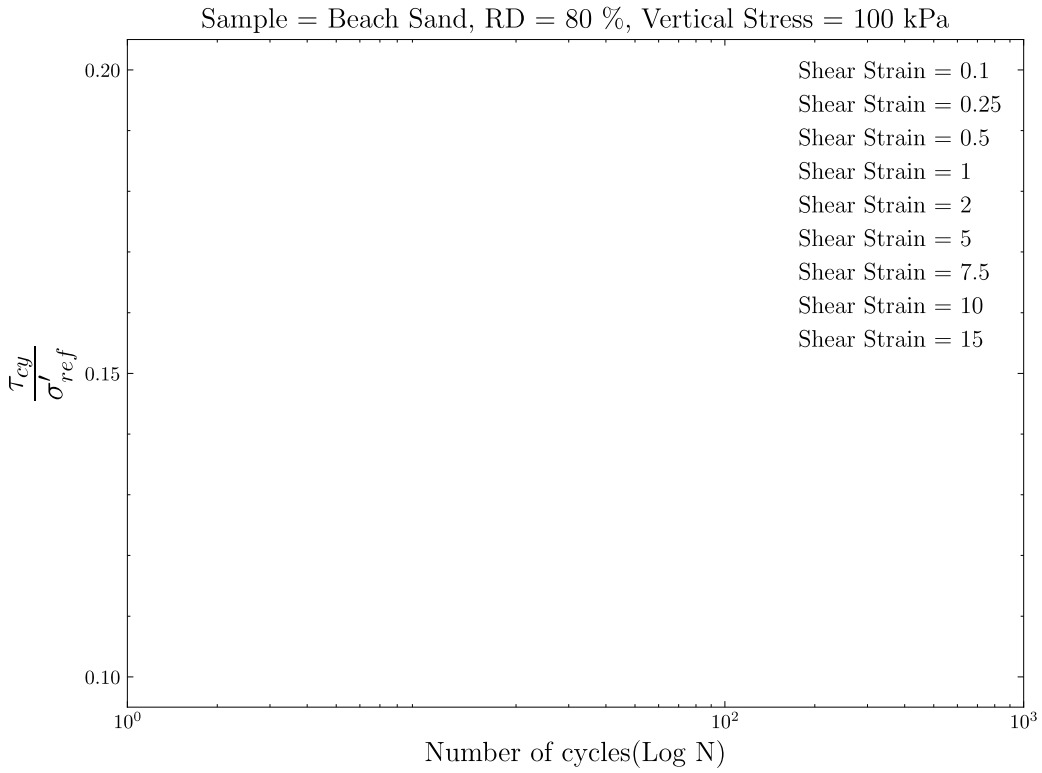

Figure 4-22 Cyclic Stress Ratio (CSR) and Shear Strain Response for Beach Sand at 80% Relative Density.

4.5.5 Average Pore Pressure Ratio contours

The study of North Sea sands' response under cyclic loading conditions reveals not just strain behaviours but also how they influence Average Pore Pressure Ratio (APPR) contours. The methodology remains consistent with that of the strain contours, employing three cyclic tests for each sand type. The maintained consistency in vertical stress and relative density across samples allows for a focused examination of the CSR's influence, which is varied at 0.1, 0.15, and 0.2 to observe its effects on pore pressure buildup.

Graphical representations in this context are similarly structured, with the x-axis plotting the logarithm of the number of cycles to failure (Log N) and the y-axis detailing the CSR. These plots serve to deepen the understanding of how cyclic loads affect pore pressure responses in soils, especially under controlled shear stress and consolidation conditions. Specific APPR benchmarks – 5%, 10%, 25%, and 60% – anchor the presentation of data, illustrating the soil's tendency towards pore pressure accumulation under cyclic stresses. For brevity, it will be discussed one sample figure here, and the complete set can be found in Appendix C.

The collected data across 48 tests are synthesized into 16 graphs, providing a broad perspective on pore pressure evolution and its correlation with cyclic loading intensity. A single representative graph is discussed in detail within this section, with the entire suite available in Appendix C for comprehensive review.

Patterns observed align with those from the strain contours, with a clear negative correlation at CSR values of 0.1 and 0.2 — as CSR increases, pore pressures accumulate more rapidly, indicating a more pronounced soil response to higher loading intensities. At CSR 0.15, however, the trend is disrupted by anomalies that suggest potential variances in the experimental process, particularly during sample preparation for Direct Simple Shear (DSS) testing. These minute variances, while seemingly insignificant, can significantly impact results, especially when CSR values are closely juxtaposed.

Intriguingly, despite the general trend of CSR inversely affecting cycle counts at higher APPR benchmarks, anomalies are evident at lower pore pressure ratios, similar to the trends observed with shear strains. These irregularities could hint at the nuances in particle arrangement and the soil's fine content, among other intrinsic properties of the sand. As the soil is subjected to higher APPR benchmarks, the relationship between increased CSR and accelerated pore pressure build-up solidifies, aligning with the expected mechanical behaviour under cyclic loads.

Beach Sand (RD = 80%, Vertical Stress = 100 kPa)

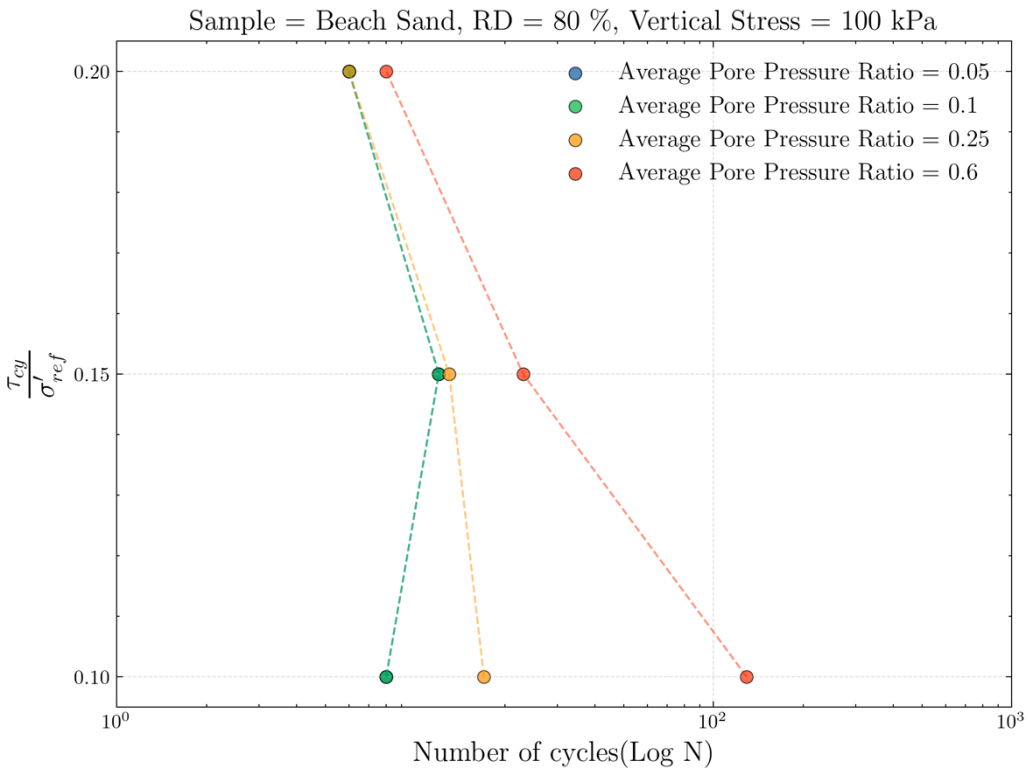

Figure 4-23 CSR and Average Pore Pressure Ratio Response in Beach Sand.

4.5.6 Comparative Analysis of North Sea Sand Behavior with Andersen's Predictive Models

Andersen's comprehensive work on cyclic soil parameters has become a cornerstone in the field of geotechnical engineering, particularly concerning the foundation design for offshore structures. His research provides critical insights into the cyclic resistance of sands under offshore loading conditions through a series of cyclic triaxial and direct simple shear (DSS) tests. This section aims to juxtapose the cyclic behaviour of North Sea sands, specifically Eemian and Beach Sand, against Andersen's predictive models to ascertain their applicability in predicting the number of cycles to failure for these sands.

Andersen's findings, derived from a range of sands with varying relative densities, are manifested in a series of graphs correlating cyclic stress ratios (CSR) with the number of cycles to failure under both drained and undrained conditions. His models provide a baseline for comparison, allowing us to scrutinize the similarities or discrepancies when subjected to similar cyclic loading conditions.

"In the context of North Sea sands, particularly Eemian and Beach Sands, the analysis aimed to assess the applicability of Andersen's predictive models. The test methodology closely mirrored the principles outlined by Andersen, focusing on cyclic direct simple shear (DSS) tests to derive comparable insights into the cyclic behaviour of these sands under various CSR levels and shear strains.

The empirical investigation conducted cyclic DSS tests on Eemian and Beach Sands, with relative densities set at 55% and 80%, across CSR levels of 0.1, 0.15, and 0.2. The tests quantified the average number of cycles required to achieve predefined shear strains of 1%, 5%, 10%, and 15%. These results were then represented in the table 4-3 to facilitate a direct comparison with Andersen's established models.

Table 4-3 Comparative Cyclic Test Results with Andersen's Model.

Relative Density	CSR	Shear Strain (%)	Eemian Avg Cycles	Beach Sand Avg Cycles	Andersen Avg Cycles
55	0,1	1	410	130	159
55	0,1	5	428	137	212
55	0,1	10	432	145	220
55	0,1	15	436	153	225
55	0,2	1	10	20	23
55	0,2	5	15	22	29
55	0,2	10	20	26	31
55	0,2	15	24	30	32
55	0,2	1	14	6	5
55	0,2	5	16	8	7
55	0,2	10	18	10	8
55	0,2	15	20	15	9
80	0,1	1	298	202	1000
80	0,1	5	307	223	1000
80	0,1	10	312	253	1000
80	0,1	15	319	284	1000
80	0,2	1	33	25	75
80	0,2	5	42	33	93
80	0,2	10	49	48	106
80	0,2	15	52	84	113
80	0,2	1	16	14	15
80	0,2	5	19	15	25
80	0,2	10	23	19	29
80	0,2	15	27	26	31

And a sample graph which compares the results for a condition of CSR equal to 0.2 is presented as figure 4-24, and the rest for brevity is presented in Appendix E.

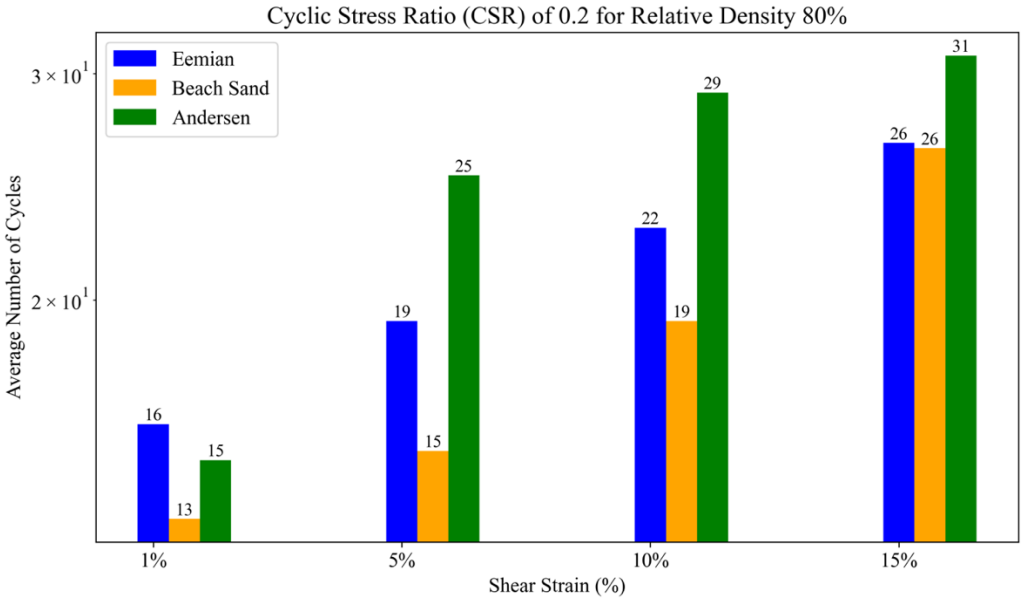

Figure 4-24 Comparative Cyclic Test Results with Andersen's Model

Results Analysis

The graphical analysis reveals a nuanced narrative of sand behaviour under cyclic loading. For both Eemian and Beach Sands, the average number of cycles to failure exhibits an inverse relationship with the CSR levels, a trend that aligns with Andersen's models. However, the comparison is not without its complexities. While the general trend of decreased cycles to failure with increased CSR is consistent with Andersen's predictions, the specific values differ.

For instance, at a CSR of 0.1 and shear strain of 5%, Eemian Sand displayed an average of 427.5 cycles to failure, and Beach Sand had 137 cycles, compared to Andersen's predictive model of 212 cycles for similar conditions. This pattern persists across other CSR levels and shear strains, indicating a potential variance in soil characteristics or test conditions that may influence the outcomes. When examining the data more closely, it is observed that at a CSR of 0.2 for a shear strain of 15%, both Eemian and Beach Sands show an average of 26 cycles to failure, closely mirroring Andersen's prediction of 31 cycles. This suggests that at higher CSR levels, the predictive model is more applicable, potentially due to the more pronounced effects of cyclic loading that overshadow the subtler variances in soil properties.

Eemian Sand, with its higher average cycles to failure at low CSR levels, indicates a slightly stiffer response when compared to Beach Sand, which is more in line with Andersen's models at these lower CSR levels. For example, at a CSR of 0.1 and shear strain of 1%, Eemian Sand required 410.25 cycles on average to fail, whereas Beach Sand needed only 129.75 cycles, against Andersen's model which predicted 159 cycles. This could be indicative of the Eemian Sand's relative robustness against low-level cyclic loading when compared to the predictive model.

The behaviour at higher relative densities presents an intriguing contrast. At 80% relative density, both Eemian and Beach Sands required significantly more cycles to reach failure at lower CSRs compared to Andersen's predictions, with the discrepancy being particularly stark at a CSR of 0.1 across all shear strains. However, as the CSR increases to 0.15 and beyond, the cycles to failure for both sands decrease substantially, aligning more closely with Andersen's predicted values. This trend suggests that the relative density of the sand plays a crucial role in its cyclic resistance, especially as the loading intensity increases.

Furthermore, the sand behaviour is more closely aligned with Andersen's predictions at shear strains of 10% and 15% across higher CSR values. This could indicate that Andersen's models are more representative of sand behaviour under conditions that approach or exceed typical operational thresholds for offshore foundations.

Conclusions

The detailed comparison indicates that Andersen's predictive models offer a valuable framework for understanding cyclic behaviour under DSS tests, particularly at higher CSR levels and shear strains where the effects of cyclic loading are more pronounced. However, the results for North Sea sands demonstrate some deviations, especially at lower CSR levels and lower shear strains. These findings suggest that while Andersen's models can be used as a preliminary reference, the specific characteristics of North Sea sands, such as grain size distribution and mineral composition, must be accounted for in accurate predictions. Therefore, it is concluded that Andersen's graphs serve as a guiding baseline but require calibration against empirical data from the specific sands in question, particularly at lower CSRs, to ensure the reliability of predictions for the cyclic behavior of North Sea sands.

4.5.7 Validation of Cyclic DSS Test Results Against Belgian Offshore Wind Farm Data from the Fugro Report

To enhance the understanding of cyclic results, a comparison with the findings from the Fugro report for a Belgian offshore wind farm is planned [34]. Methodology involved conducting stress control shearing tests under constant volume conditions, following the conditions detailed in the Fugro report. Such an approach facilitates a direct comparison of cyclic test outcomes on North Sea sand. Both Beach Sand and Eemian sands were subjected to these tests to provide a comprehensive comparison. This section details the specific conditions governing these tests and presents the results obtained from re-constructed test conditions, against the Belgian offshore wind farm report's data. Notably, the tests focused on samples labelled as 21BAGA from borehole BH-103, extracted from 4 m depth.

Test description on Sample 21BAGA Test CSS12

1. The sample was initially consolidated to 500 kPa.
2. This was subsequently decreased to 40 kPa, which served as the confining stress during both the pre-shearing and shearing phases.
3. During the pre-shearing phase, the sample underwent 400 cycles of stress-controlled cyclic loading under constant vertical stress. This was done with a frequency of 0.1 Hz and a cyclic stress amplitude of 2 kPa.
4. The stress-controlled cyclic loading in the constant volume phase utilized a frequency of 0.1 Hz, and the cyclic stress was set at 79 kPa.
5. The sample has reached 15% shear strain after 19 cycles.

A detailed description of the cyclic test on Test CSS12 is provided below:

Table 4-4 Summary of Consolidated Cyclic DSS Test CSS12.

VISUAL DESCRIPTION
Olive silica fine to coarse SAND with shell fragments.

GENERAL	
Date test started	15/10/2014
Type of sample	Re-compacted
Specimen orientation	Vertical

INITIAL		
Diameter	[mm]	66.3
Length	[mm]	30.0
Moisture content	[%]	21.4
Bulk density	[Mg/m³]	2.05
Dry density	[Mg/m³]	1.69
Void ratio	[-]	0.567
Degree of saturation	[%]	100
Assumed particle density	[Mg/m³]	2.65
Torvane	[kPa]	-
Pocket penetrometer	[kPa]	-

CONSOLIDATION STAGE 1		
σ'_{vc}	[kPa]	500
Vertical strain	[%]	0.86
Bulk density	[Mg/m^3]	2.06
Dry density	[Mg/m^3]	1.71
Void ratio	[-]	0.554
Moisture content	[%]	20.9

CONSOLIDATION STAGE 2		
σ'_{vc}	[kPa]	40
Vertical strain	[%]	0.54
Bulk density	[Mg/m^3]	2.06
Dry density	[Mg/m^3]	1.70
Void ratio	[-]	0.559
Moisture content	[%]	21.1

STRESS-CONTROLLED CYCLIC PRE-SHEAR – CONSTANT VERTICAL STRESS		
σ'_v	[kPa]	40
Reference stress	[kPa]	40
Mean τ_{av}	[kPa]	0
Mean τ_{cy}	[kPa]	2
Frequency	[Hz]	0.10
Number of cycles applied	(N)	400
Vertical strain	[%]	0.54
Bulk density	[Mg/m^3]	2.06
Dry density	[Mg/m^3]	1.70
Void ratio	[-]	0.559

STRESS-CONTROLLED CYCLIC LOADING – CONSTANT VOLUME		
Reference stress	[kPa]	40
Mean τ_{av}	[kPa]	0
Mean τ_{cy}	[kPa]	79
Frequency	[Hz]	0.10
Number of cycles at failure	(N_f)	19
γ_{av} at N_f	[%]	1.49
γ_{cy} at N_f	[%]	15.35
Shear induced $\Delta\sigma'_v$ at N_f	[kPa]	-23
Vertical strain	[%]	0.54

Results of Test CSS12 based on Fugro report:

1. Shear Strain versus Shear Stress ($\boldsymbol{\gamma_{cy} - \tau_{cy}}$)

The graph plots shear strain ($\boldsymbol{\gamma_{cy}}$), presented as a percentage on the x-axis, against cyclic shear stress ($\boldsymbol{\tau_{cy}}$), measured in kPa on the y-axis. The periodic fluctuations in shear stress highlight the cyclic nature of the applied loads. As the shear strain increases, the shear stress amplitude remains consistent at 79kPa.

2. Normalized Vertical Stress against normalized Shear Stress ($\boldsymbol{\sigma'_v/\sigma'_{v0} - \tau_{cy}/\sigma'_{v0}}$)

The x-axis displays the normalized vertical stress ($\boldsymbol{\sigma'_v/\sigma'_{v0}}$), while the y-axis represents the normalized Shear stress ($\boldsymbol{\tau_{cy}/\sigma'_{v0}}$), with both being dimensionless. A notable feature is the confining stress reaching zero in each cycle, indicating that the excess pore water pressure is equal to vertical effective stress at that point.

3. Cycle Number versus Shear Stress ($\boldsymbol{N\ -\ \tau_{cy}}$)

On the x-axis, the number of cycles (N) is represented, while the y-axis depicts the Shear stress ($\boldsymbol{\tau_{cy}}$) in kPa.This graph showcases the relationship between the number of applied cycles on the x-axis and cyclic shear stress ($\boldsymbol{\tau_{cy}}$) in kPa on the y-axis. Throughout the cycles, the shear stress amplitude remains at 79 kPa.

4. Cycle Number versus Shear Strain ($\boldsymbol{N - \gamma_{cy}}$)

The fourth graph illustrates the number of cycles (N) on the x-axis and the relationship between shear strain ($\boldsymbol{\gamma_{cy}}$) in (%) on the y-axis. There's an evident trend, suggesting that the soil undergoes increased deformation with each subsequent cycle, reaching a shear strain of 15% by cycle 21.

5. Cycle Number versus Shear Induced ($\boldsymbol{N - \frac{\Delta U}{\sigma'_{v0}}}$)

The graph illustrates the relationship between the number of cycles (N) on the x-axis and the Shear Induced ($\boldsymbol{\frac{\Delta U}{\sigma'_{v0}}}$), which is dimensionless and shown on the y-axis. The graph reveals that the Shear Induced reaches a ratio of approximately 2.5 in the first cycle. As testing progresses, this ratio exhibits a marginal decrease, stabilizing around the absolute value of 2.2.

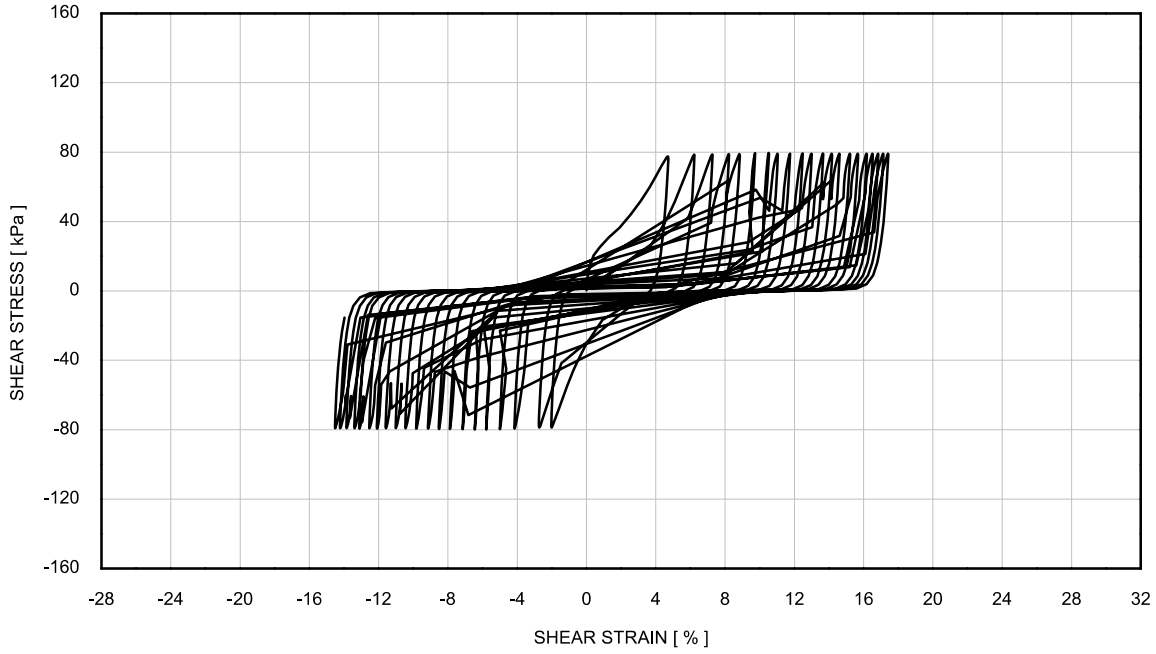

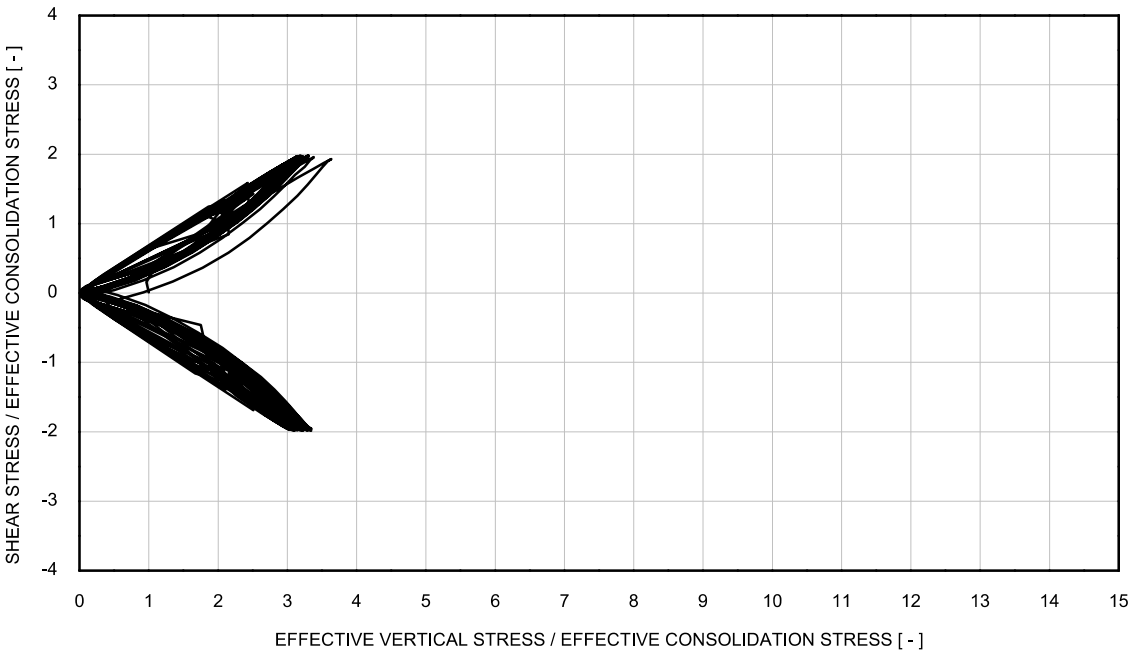

σ'_{vc}	:	40 kPa	Borehole	: BH-103
Mean τ_{av}	:	0 kPa	Sample	: 21BAGA
Mean τ_{cy}	:	79 kPa	Depth [m]	: 4
Frequency	:	0.10 Hz	Test No.	: CSS12

Figure 4-25 Consolidated Cyclic DSS Test

Stress-Controlled Cyclic Loading Stage - Constant Volume

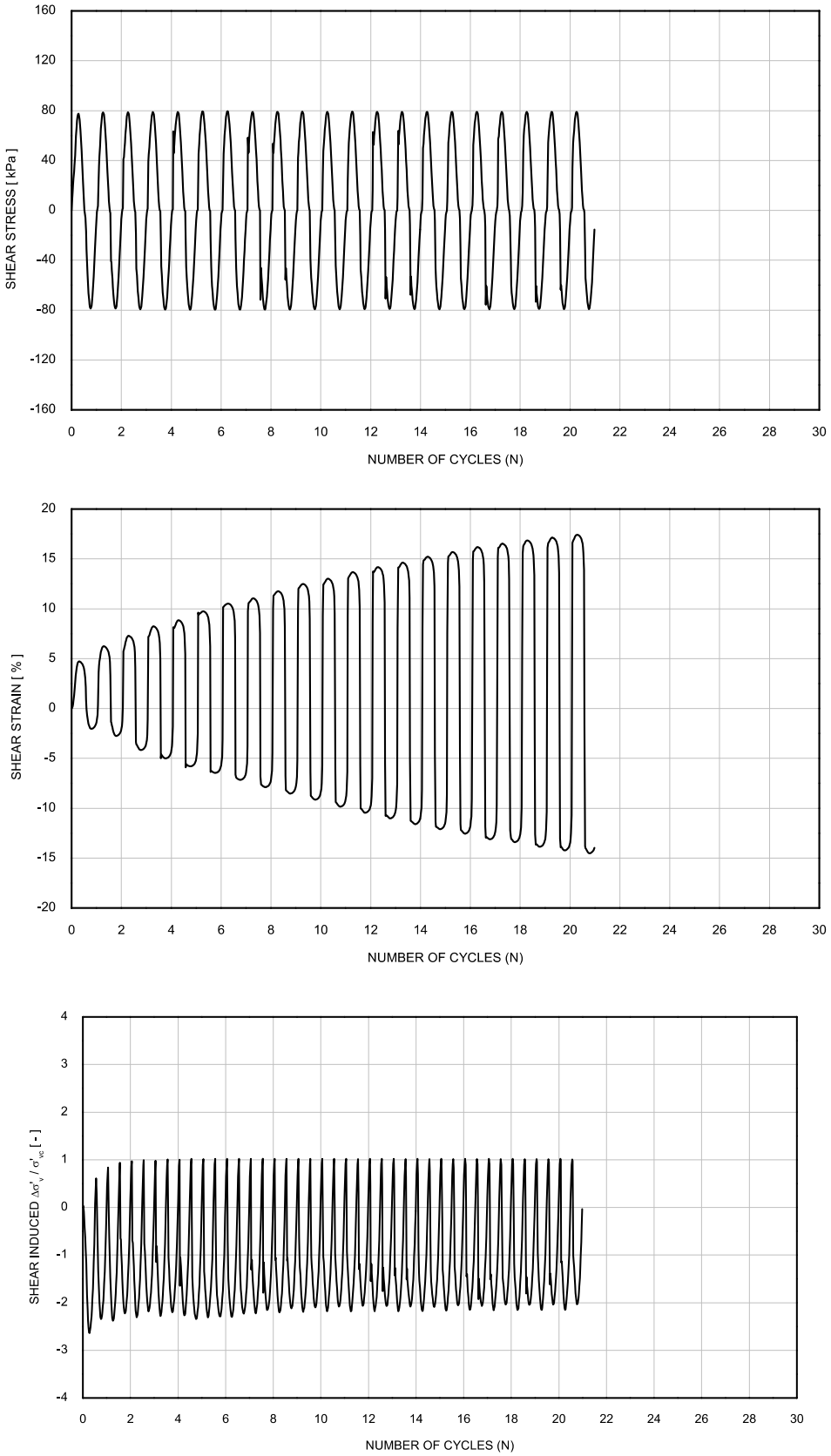

Figure 4-26 Consolidated Cyclic DSS Test

Stress-Controlled Cyclic Loading Stage - Constant Volume.

Results of Beach Sand with Conditions of Sample 21BAGA Test CSS12

Cyclic direct simple shear (cDSS) tests were conducted on Beach Sand, mirroring the conditions of Sample 21BAGA Test CSS12. A comprehensive graphical representation explains the relationships between the various parameters under consideration.

1. Shear Strain versus Tangential Stress ($\boldsymbol{\gamma_{cy} - \tau_{cy}}$)

The relationship between the tangential stress ($\boldsymbol{\tau_{cy}}$) and the shear strain ($\boldsymbol{\gamma_{cy}}$) is presented in the top-left graph. The x-axis showcases the shear strain in percentage, while the y-axis represents the tangential stress in kPa. Notably, the graph reveals a shear stress amplitude corresponding to the original test, 79 kPa, and reaching a 15% shear strain during cycling.

2. Normalized Vertical Stress against normalized Tangential Stress ($\boldsymbol{\sigma'_v/\sigma'_{v0} - \tau_{cy}/\sigma'_{v0}}$)

The top-right graph provides insights into the relationship between the normalized vertical stress ($\boldsymbol{\sigma'_v/\sigma'_{v0}}$) on the x-axis and the normalized tangential stress ($\boldsymbol{\tau_{cy}/\sigma'_{v0}}$) on the y-axis. Both parameters are normalized by dividing them by the vertical effective stress, in accordance with the Fugro report presentation. The normalized shear stress predominantly fluctuates between values of -2 and 2, while the confining stress varies from 0 to 3.4 within each cycle.

3. Cycle Number in relation to Cyclic Shear Strain Amplitude ($\boldsymbol{N - \gamma_{cy}}$)

The bottom-left graph demonstrates the number of cycles (N) on the x-axis and cyclic shear strain amplitude ($\boldsymbol{\gamma_{cy}}$) in % on the y-axis. As the number of cycles increases, the cyclic shear strain amplitude clearly grows, reaching 15% after 70 cycles. The data shows a shear strain equal to 5% by the 4th cycle and 10% by the 39th cycle.

4. Cycle Number versus Average Pore Pressure Ratio ($\boldsymbol{N - \frac{\Delta U}{\sigma'_{v0}}}$)

The last graph, on the bottom right, presents normalized vertical stress ($\boldsymbol{\sigma'_v/\sigma'_{v0}}$) on the x-axis, and on the y-axis, tangential stress ($\boldsymbol{\tau_{cy}/\sigma'_{v0}}$), both dimensionless. It highlights the effect of cyclic loading on increasing pore pressures. This ratio represents the value of pore pressure in relation to the vertical effective stress, with values exceeding 1 pointing towards potential negative pressures. Notably, by the third cycle, there is a pronounced jump to a ratio of 1.2. This ratio remains steady at approximately 0.95 until the soil reaches the failure criteria at cycle 70.

Test results

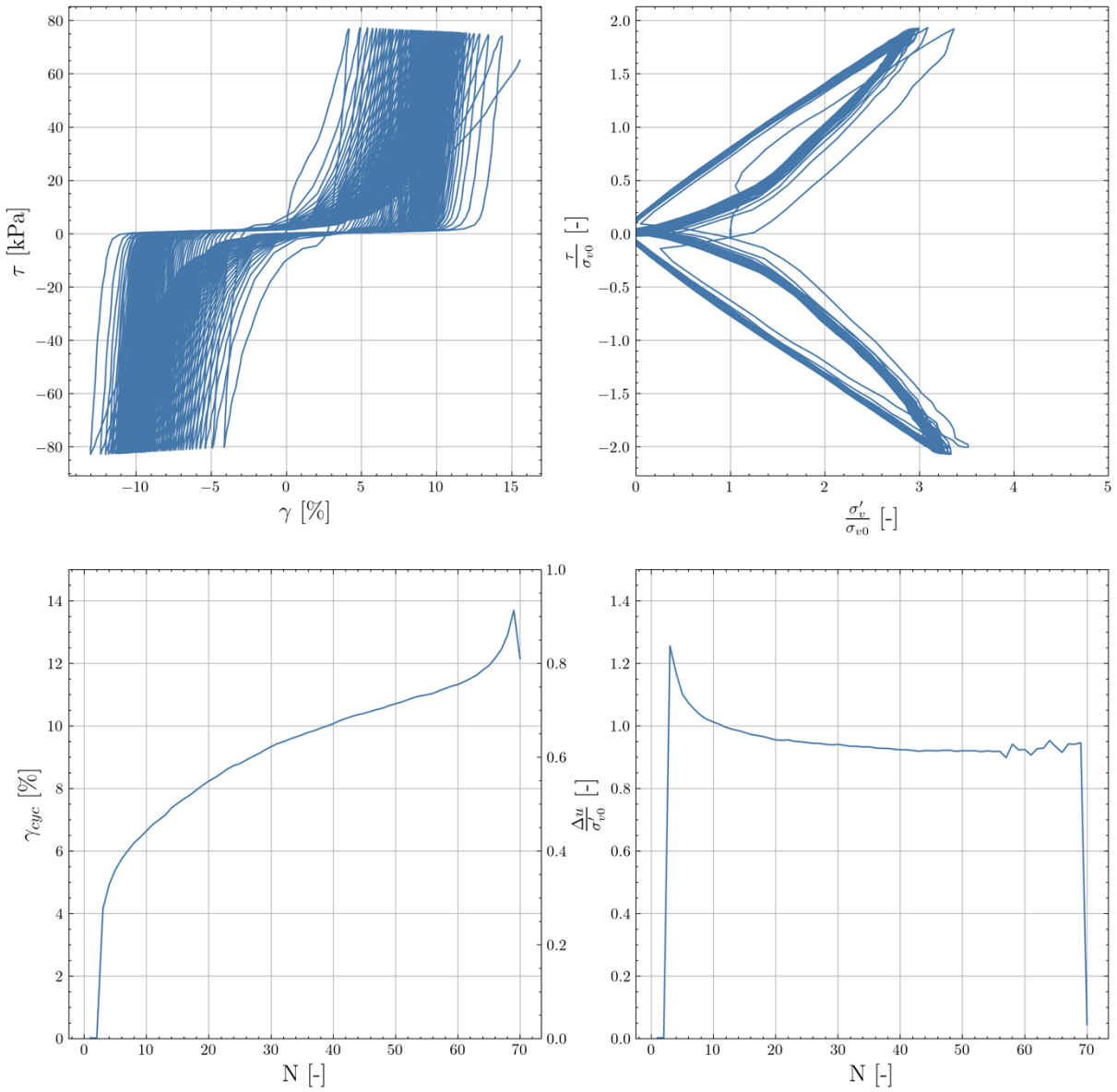

Figure 4-27 Cyclic Behaviour Analysis of Beach Sand Mirroring Test CSS12 Conditions.

Results of Eemian Sand with Conditions of Sample 21BAGA Test CSS12

After conducting cyclic direct simple shear (cDSS) tests on Beach Sand, the Eemian Sand was tested under the conditions of Sample 21BAGA Test CSS12. The graphical interpretations align closely with those previously described for Beach Sand.

The Eemian sand reaches shear strains ($\boldsymbol{\gamma_{cy}}$) of 5%, 10%, and 15% after 4, 11, and 21 cycles, respectively.

The normalized shear stress ($\boldsymbol{\tau_{cy}/\sigma'_{v0}}$) primarily oscillates between -2 and 2, while the normalized confining stress ($\boldsymbol{\sigma'_v/\sigma'_{v0}}$) ranges from 0 to 3.4 within each cycle.

By the third cycle, a significant rise to a pore pressure ratio ($\frac{\boldsymbol{\Delta U}}{\boldsymbol{\sigma'_{v0}}}$) of 1.4 is observed. This ratio descends to 1.1 by the 7th cycle and stabilizes around 1 until the soil meets the failure criteria at cycle 21.

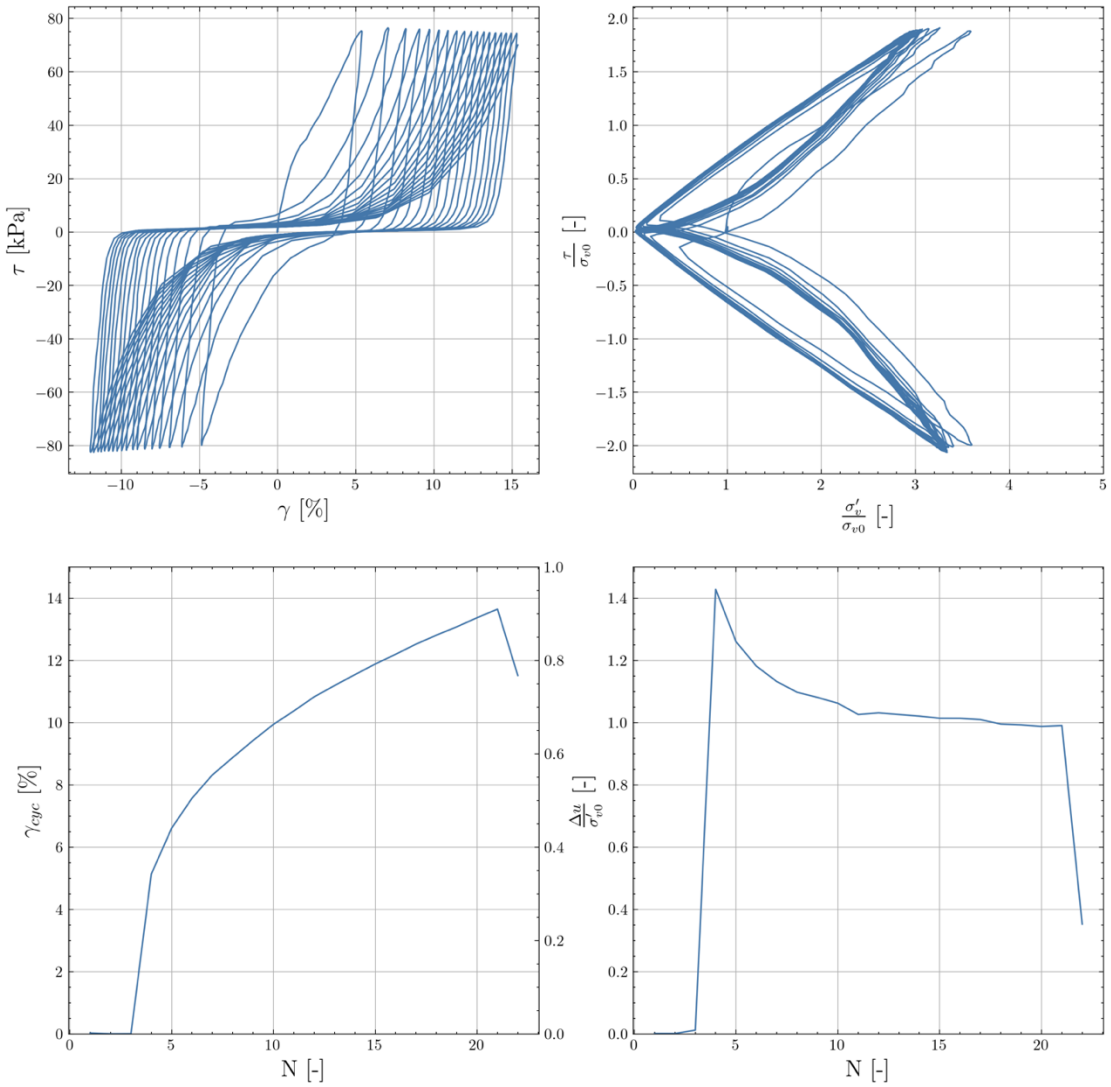

Figure 4-28 Cyclic Behaviour Analysis of Eemain Sand Mirroring Test CSS12 Conditions.

Test description on Sample 21BAGA Test CSS13

1. The sample was initially consolidated to 500 kPa.
2. This was subsequently decreased to 80 kPa, which served as the confining stress during both the pre-shearing and shearing phases.
3. During the pre-shearing phase, the sample underwent 400 cycles of stress-controlled cyclic loading under constant vertical stress. This was done with a frequency of 0.1 Hz and a cyclic stress amplitude of 2 kPa.
4. The stress-controlled cyclic loading in the constant volume phase utilized a frequency of 0.1 Hz, and the cyclic stress was set at 159 kPa.
5. The sample has reached 15% shear strain after 5 cycles.

A detailed description of the cyclic test on Sample 21BAGA Test CSS13 is provided below.

Table 4-5 Summary of Consolidated Cyclic DSS Test CSS13

VISUAL DESCRIPTION
Olive silica fine to coarse SAND with shell fragments.

GENERAL	
Date test started	20/10/2014
Type of sample	Re-compacted
Specimen orientation	Vertical

INITIAL		
Diameter	[mm]	66.3
Length	[mm]	30.0
Moisture content	[%]	21.2
Bulk density	[Mg/m³]	2.06
Dry density	[Mg/m³]	1.70
Void ratio	[-]	0.562
Degree of saturation	[%]	100
Assumed particle density	[Mg/m³]	2.65
Torvane	[kPa]	-
Pocket penetrometer	[kPa]	-

CONSOLIDATION STAGE 1		
σ'_{vc}	[kPa]	500
Vertical strain	[%]	0.66
Bulk density	[Mg/m^3]	2.06
Dry density	[Mg/m^3]	1.71
Void ratio	[-]	0.552
Moisture content	[%]	20,8

CONSOLIDATION STAGE 2		
σ'_{vc}	[kPa]	40
Vertical strain	[%]	0.35
Bulk density	[Mg/m^3]	2.06
Dry density	[Mg/m^3]	1.70
Void ratio	[-]	0.557
Moisture content	[%]	21.0

STRESS-CONTROLLED CYCLIC PRE-SHEAR – CONSTANT VERTICAL STRESS		
σ'_v	[kPa]	40
Reference stress	[kPa]	40
Mean τ_{av}	[kPa]	0
Mean τ_{cy}	[kPa]	2
Frequency	[Hz]	0.10
Number of cycles applied	(N)	400
Vertical strain	[%]	0.34
Bulk density	[Mg/m^3]	2.06
Dry density	[Mg/m^3]	1.70
Void ratio	[-]	0.557

STRESS-CONTROLLED CYCLIC LOADING – CONSTANT VOLUME		
Reference stress	[kPa]	40
Mean τ_{av}	[kPa]	0
Mean τ_{cy}	[kPa]	159
Frequency	[Hz]	0.10
Number of cycles at failure	(N_f)	5
γ_{av} at N_f	[%]	-2.44
γ_{cy} at N_f	[%]	18.03
Shear induced $\Delta\sigma'_v$ at N_f	[kPa]	-103
Vertical strain	[%]	0.34

Results of Test CSS13 based on Fugro report.

1. Shear Strain versus Shear Stress ($\boldsymbol{\gamma_{cy} - \tau_{cy}}$)

The graph plots shear strain ($\boldsymbol{\gamma_{cy}}$), presented as a percentage on the x-axis, against cyclic shear stress ($\boldsymbol{\tau_{cy}}$), measured in kPa on the y-axis. The cyclical variations in shear stress underscore the repetitive nature of the applied loads. Even as the shear strain increases with each cycle, the shear stress amplitude consistently holds at 159kPa.

2. Normalized Vertical Stress against normalized Tangential Stress ($\boldsymbol{\sigma'_v/\sigma'_{v0} - \tau_{cy}/\sigma'_{v0}}$)

The x-axis displays the normalized vertical stress ($\boldsymbol{\sigma'_v/\sigma'_{v0}}$), while the y-axis represents the normalized tangential stress ($\boldsymbol{\tau_{cy}/\sigma'_{v0}}$), with both being dimensionless. During each cycle, the vertical effective stress reduces to zero, indicating that the pore water pressure equals the vertical effective stress at these points.

3. Cycle Number versus Tangential Stress ($\boldsymbol{N - \tau_{cy}}$)

On the x-axis, the number of cycles (N) is represented, while the y-axis depicts the tangential stress ($\boldsymbol{\tau_{cy}}$) in kPa. The third graph illustrates the consistent interplay between cyclic shear stress and the number of cycles. Across all cycles, the shear stress consistently holds at 159 kPa.

4. Cycle Number versus Shear Strain ($\boldsymbol{N - \gamma_{cy}}$)

The fourth graph illustrates the cycle count (N) on the x-axis and the relationship between horizontal strain (displayed in %) on the y-axis. With each successive cycle, the soil undergoes greater deformation, reaching a shear strain of 15% by the fifth cycle.

5. Cycle Number versus Shear Induced ($\boldsymbol{N - \frac{\Delta U}{\sigma'_{v0}}}$)

The graph illustrates the relationship between the number of cycles (N) on the x-axis and the Shear Induced ($\frac{\Delta U}{\sigma'_{v0}}$), which is dimensionless and shown on the y-axis. The pore pressure ratio hits slightly above 6 in the first cycle. It then decreases to around 5.6, before rising again, nearing the ratio of 6.

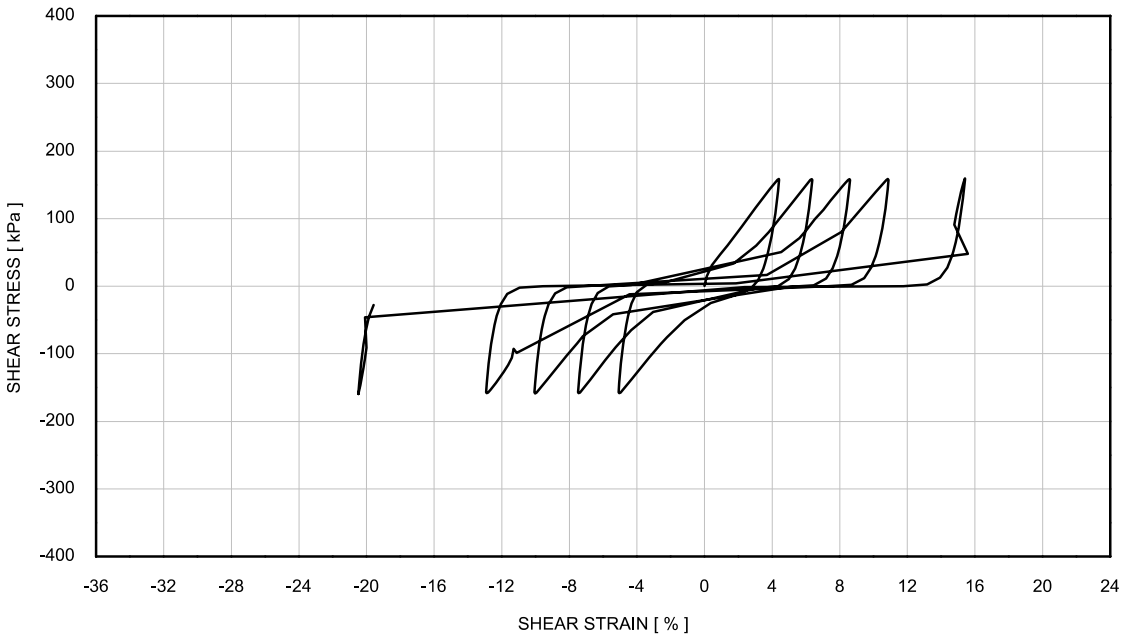

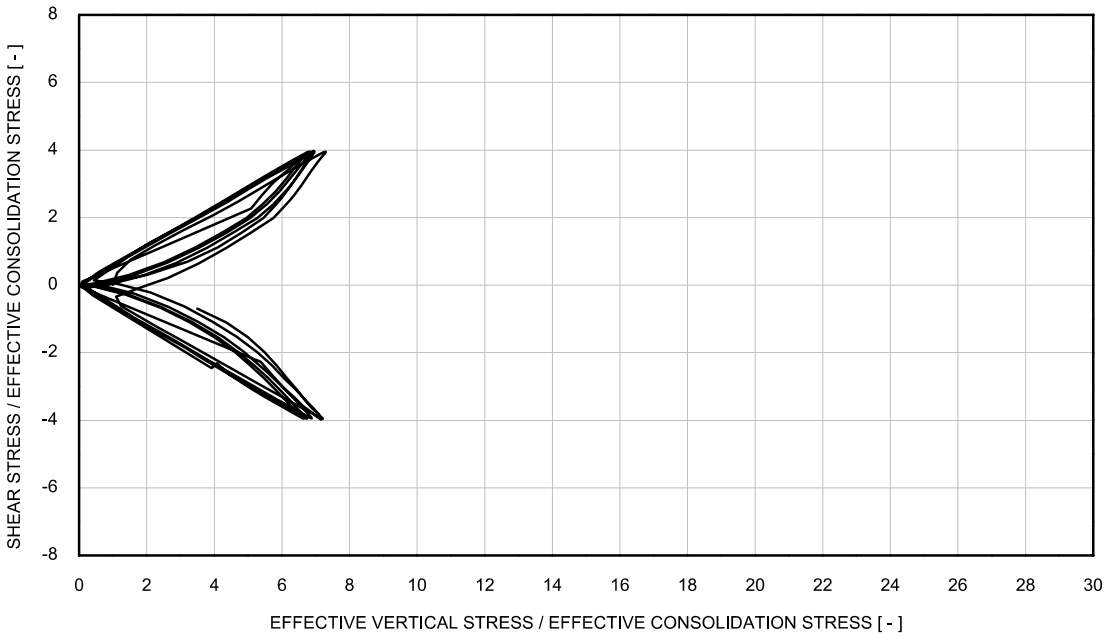

σ'_{vc}	:	40 kPa	Borehole	:	BH-103
Mean τ_{av}	:	0 kPa	Sample	:	21BAGA
Mean τ_{cy}	:	159 kPa	Depth [m]	:	4
Frequency	:	0.10 Hz	Test No.	:	CSS13

Figure 4-29 Consolidated Cyclic DSS Test

Stress-Controlled Cyclic Loading Stage - Constant Volume

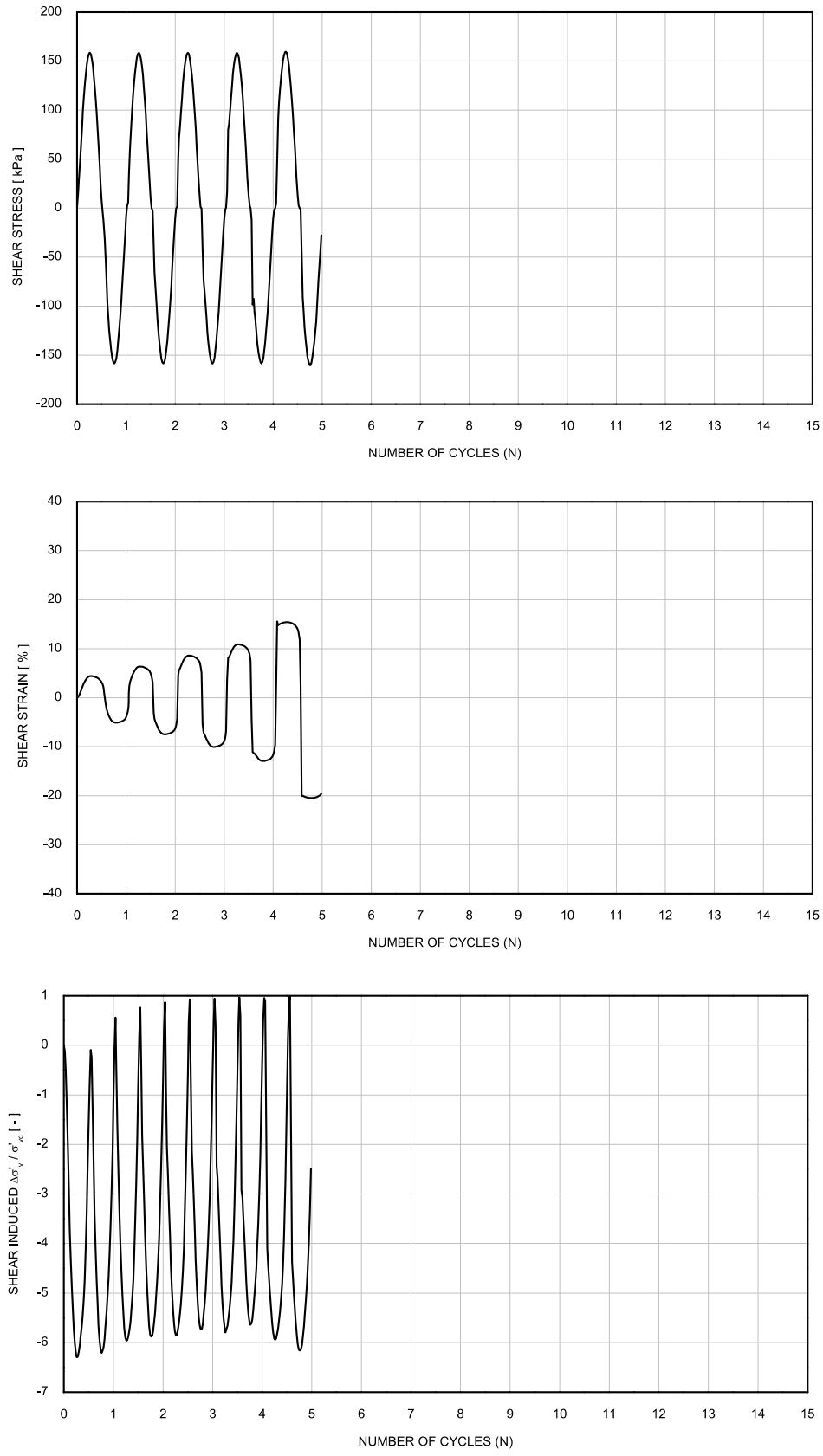

Figure 4-30 Consolidated Cyclic DSS Test Stress-Controlled

Cyclic Loading Stage - Constant Volume

Results of Beach Sand with Conditions of Sample 21BAGA Test CSS13

Cyclic direct simple shear (cDSS) tests were conducted on Beach Sand, mirroring the conditions of sample 21BAGA Test CSS13. A comprehensive graphical representation elucidates the relationships between the various parameters under consideration.

1. Shear Strain versus Tangential Stress ($\boldsymbol{\gamma_{cy} - \tau_{cy}}$)

The top-left graph illustrates the relationship between tangential stress and shear strain. The x-axis displays the shear strain in %, while the y-axis presents the tangential stress in kPa. Significantly, the graph illustrates a shear strain amplitude that aligns with the original test, nearing 159 kPa, and reaching a 15% shear strain through the cycles.

2. Normalized Vertical Stress against Tangential Stress in Cyclic Shear ($\boldsymbol{\sigma'_v/\sigma'_{v0} - \tau_{cy}/\sigma'_{v0}}$)

On the x-axis, the graph presents normalized vertical stress ($\boldsymbol{\sigma'_v/\sigma'_{v0}}$), and on the y-axis, tangential stress ($\boldsymbol{\tau_{cy}/\sigma'_{v0}}$). The top-right graph elucidates the relationship between the normalized vertical stress and tangential stress in cyclic shear. Both variables are normalized by dividing them by the vertical effective stress, consistent with the Fugro report's presentation. The normalized shear stress predominantly fluctuates between values of -4 and 4, while the normalized confining stress varies from 0 to 6.6 within each cycle.

3. Cycle Number in relation to Cyclic Shear Strain Amplitude ($\boldsymbol{N - \gamma_{cy}}$)

On the x-axis, the graph represents the number of cycles (N), and on the y-axis, it presents cyclic shear strain amplitude ($\boldsymbol{\gamma_{cy}}$) in %. The bottom-left graph displays the progression of cyclic shear strain amplitude in relation to the increasing number of cycles. With the increase in cycles, the cyclic shear strain amplitude rises, achieving 15% by the 30th cycle. Specifically, by the 3rd cycle, the shear strain is recorded at 7%, and by the 10th cycle, is 10%.

4. Cycle Number versus Average Pore Pressure Ratio ($\boldsymbol{N - \frac{\Delta U}{\sigma'_{v0}}}$)

The last graph, on the bottom right, shows how the average pore pressure ratio changes with the number of cycles. It highlights the effect of cyclic loading on increasing pore water pressures. This ratio represents the value of pore pressure in relation to the consolidation stress, with values exceeding 1 pointing towards potential negative pressures.

There's a significant leap by the third cycle to the ratio of 3.6. This high value persists through subsequent cycles, maintaining around 3.5. Finally, on the final 30th cycle, which is also the failure point, the pressure drops sharply to 2.

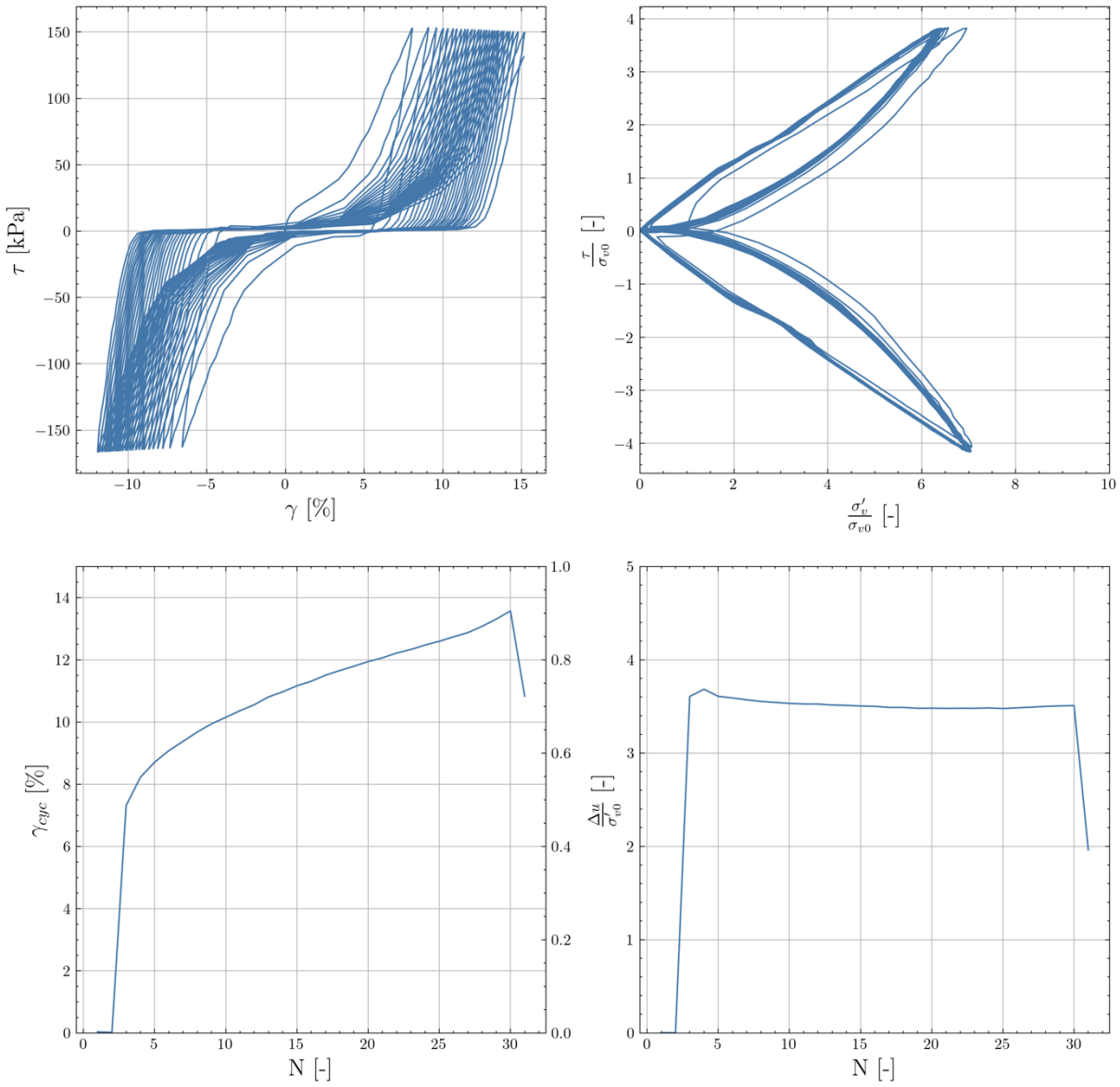

Figure 4-31 Cyclic Behaviour Analysis of Beach Sand Mirroring Test CSS13 Conditions.

Results of Eemian Sand with Conditions of Sample 21BAGA Test CSS13

Following the cyclic direct simple shear (cDSS) tests on Beach Sand, Eemian Sand was similarly tested under the conditions specified for Sample 21BAGA Test CSS13. The resulting graphical interpretations closely resemble those previously observed for Beach Sand.

The Eemian sand reaches shear strains ($\boldsymbol{\gamma_{cy}}$) of 5%, 10%, and 15% after 7, 9, and 15 cycles, respectively.

The normalized shear stress ($\boldsymbol{\tau_{cy}/\sigma'_{v0}}$) changes between -4 and 4, while the confining stress ($\boldsymbol{\sigma'_v/\sigma'_{v0}}$) ranges from 0 to 6.6 within each cycle.

By the third cycle, there's a marked increase in the pore pressure ratio (Shear Induced) ($\frac{\boldsymbol{\Delta U}}{\boldsymbol{\sigma'_{v0}}}$) to 3.7, which then steadies around 3.5 for the rest of the cycles.

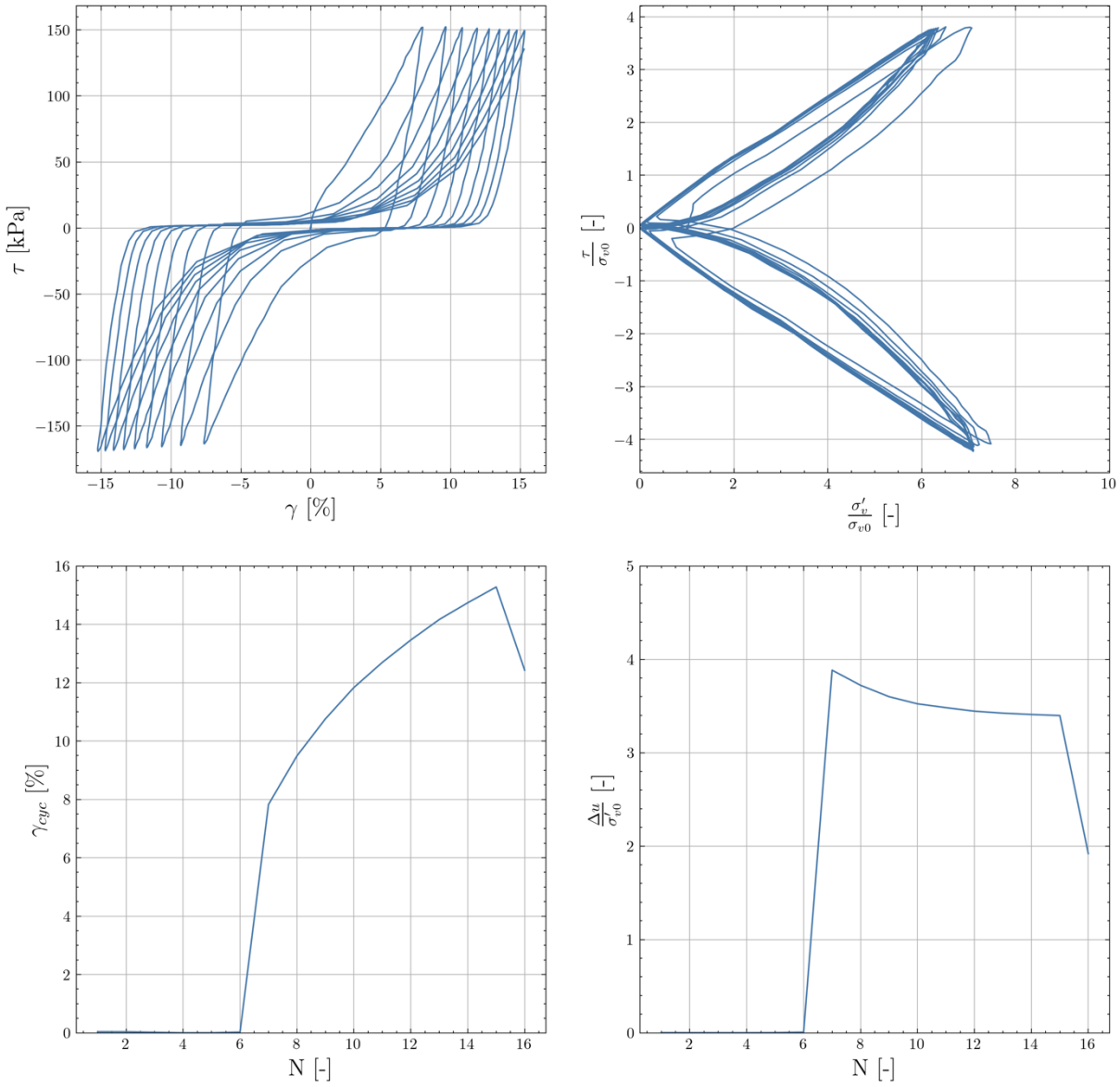

Figure 4-32 Cyclic Behaviour Analysis of Eemian Sand Mirroring Test CSS13 Conditions.

Analysis of Cyclic DSS Test Replications

The replication of the Fugro cyclic DSS test conditions in the Ghent University laboratory was aimed at verifying the consistency of test results with existing data from the Belgian Offshore Wind Farm project. The comparative analysis of tests on 21BAGA, Beach Sand, and Eemian Sand reveals a high degree of replicability, which is commendable in experimental work.

The following table summarizes the number of cycles required to reach a 15% shear strain under different test conditions for the Fugro test, Beach sand, and Eemian sand:

Test Condition	Fugro Report (Cycles to 15% Shear Strain)	Beach Sand (Cycles to 15% Shear Strain)	Eemian Sand (Cycles to 15% Shear Strain)
CSS12 (40 kPa Consolidation, 79 kPa Cyclic Shear)	19	70	21
CSS13 (80 kPa Consolidation, 159 kPa Cyclic Shear)	5	30	15

CSS12 Condition (40 kPa Consolidation Stress, 79 kPa Cyclic Shear Stress):

The Fugro report indicated that 21BAGA sand required 19 cycles to reach a 15% shear strain. Replication with Eemian Sand resulted in a marginally higher 21 cycles to reach the same strain, a difference that falls within the acceptable range of experimental variability. Beach Sand required 70 cycles, reflecting a more significant difference that likely points to intrinsic material properties rather than methodological discrepancies. This variability, while noteworthy, aligns with the expected heterogeneity in soil mechanic behaviours.

CSS13 Condition (80 kPa Consolidation Stress, 159 kPa Cyclic Shear Stress):

The CSS13 condition proved more rigorous, with the Fugro report documenting just 5 cycles for 21BAGA sand to reach 15% shear strain. Eemian Sand needed 15 cycles, and Beach Sand took 30 cycles under the same conditions. Despite the greater disparity, the trend of marginal differences supports the notion of acceptable replication fidelity for sands with similar geotechnical properties.

The Eemian Sand's closer adherence to the Fugro results bolsters the argument for the accuracy of test replication. It implies that while laboratory conditions and sand types introduce some variability, these factors do not significantly detract from the validity of the replication efforts.

In conclusion, achieving exact numerical replication in geotechnical testing is inherently challenging due to the variable nature of soil properties and their response to test conditions. Nonetheless, the outcomes from the Ghent laboratory suggest a successful emulation of the Fugro report's protocols. The observed variations lie within an acceptable range, underscoring the robustness of the employed testing methodologies. Notably, the Eemian Sand's performance closely emulates that reported by Fugro, underscoring confidence in the reproducibility of cyclic DSS tests across different contexts and materials.

5 Conclusion

This thesis represents a significant advancement in the understanding of the complex cyclic behaviour of soils, with a particular focus on the North Sea sands subjected to the dynamic loads of offshore wind turbine foundations. It addresses the crucial need for sustainable energy production amidst the global shift towards renewable energy sources, specifically focusing on the challenges posed by the offshore wind industry in the North Sea. Through extensive cyclic direct simple shear (cDSS) tests, the study has shed light on soil-pile system degradation under cyclic loads, offering invaluable insights for the advancement of geotechnical engineering and practical applications in offshore foundation design.

A pivotal aspect of this research was the exploration of various North Sea sands, including Mol, Wemmel, Beach Sand, and Eemian sands, each exhibiting unique responses to static and cyclic loading. The study uncovered that sands like Wemmel, with higher fine content, presented challenges in sample preparation and behaviour prediction under cyclic loading, particularly influenced by drying methods. Drying at different temperatures notably affected the particle size distribution and mechanical behaviour, with increased fine content suggesting particle breakage and alteration in soil structure. This finding is crucial, as it may indicate significant changes in soil fabric not typically considered in standard predictive models. In contrast, sands with fewer fines, such as Eemian Sand, demonstrated more predictable behaviour, emphasizing the importance of understanding material-specific characteristics. Future studies should aim to systematize drying methods, considering characteristics such as fine content and the effects of particle coagulation during drying at higher temperatures, to enhance the predictability and consistency of soil behaviour analysis.

In addition to conventional methods, this thesis innovatively explored the impact of sample saturation on soil behaviour using the cyclic direct simple shear (cDSS) apparatus. The experiment aimed to simulate in-situ moisture conditions, providing a more realistic understanding of soil responses under cyclic loading. Controlled water flow was introduced to the samples for this purpose. The saturation process was observed to coincide with notable variations in the sands' response to shear stress. This shift to dry testing, despite the initial focus on saturation, was necessitated by the cDSS apparatus's inability to measure pore pressures in saturated samples due to the lack of a back-pressure system. The decision was based on maintaining the reliability and consistency of the methodology and the study's results. This investigation into the effects of saturation has underscored the complexity of moisture's role in soil dynamics. Future research is encouraged to delve deeper into how water presence alters soil behaviour, under both static and cyclic loading conditions. Such studies are vital for enhancing the accuracy and relevance of laboratory testing in geotechnical engineering.

The investigation into sample preparation methods, particularly with Mol sand, revealed a complex relationship between methodology and material response. Techniques like dry tamping, moist tamping, and wet pluviation showed nuanced differences in shear strength behavior under constant volume (CV) and constant stress (CS) conditions. Notably, dry tamping under CV conditions led to an initial peak in shear strength, followed by a gradual increase, contrasting the uniform rises in CS tests. This highlights the challenges of replicating in-situ conditions in a laboratory and the importance of precise methodology. Microscopic examination of dried samples also revealed microstructural changes due to different drying methods, demonstrating the impact of sample preparation on laboratory test outcomes. These findings highlight the sensitivity of soil behavior to preparation methods and drying techniques, underscoring their role in lab test accuracy and reliability. Future research should focus on refining these methods to better replicate in-situ conditions and enhance the validity of laboratory results in geotechnical engineering.

One of the most significant findings of this research was the clear correlation between higher relative densities and increased cyclic strength of sands, particularly evident in the detailed examination of Eemian and Beach Sands. This study reaffirmed the fundamental geotechnical principle that denser soils exhibit greater resistance to cyclic loading, as evidenced by the increased

number of cycles necessary to reach a given strain or excess pore pressure level. This trend, consistent across various CSR levels and stress conditions tested, highlights the pivotal role of soil densification in enhancing the resilience of offshore wind turbine foundations to endure severe conditions of the offshore environment.

Additionally, the study's investigation into the Cyclic Stress Ratio (CSR) revealed distinct behaviours in the cyclic response of North Sea sands. While an inverse relationship between CSR and the number of cycles to reach failure was apparent at the broader levels (CSR of 0.1 compared to 0.2), suggesting increased loading severity leads to quicker soil failure, the nuances became more complex at closer CSR intervals. At these narrower gaps, such as between CSR values of 0.1 and 0.15 or 0.15 and 0.2, unexpected discrepancies emerged. These observed anomalies, particularly at CSR values of 0.15, underscore the sensitivity of sand behaviour to even minor variances in sample preparation or intrinsic sand properties. This highlights the critical importance of meticulous sample preparation and a deeper understanding of material-specific responses in geotechnical testing. Such findings necessitate a deeper look into the sample preparation protocols and the unique behaviour of each sand type to ensure the accuracy of predictive models for soil behaviour under cyclic loads.

The comparative analysis with Andersen's predictive models revealed nuanced relationships between cyclic strength, behaviour, and model predictions. While general trends in cyclic strength and behaviour aligned with Andersen's models, significant deviations were observed, particularly in specific CSR and relative density ranges. For example, at a CSR of 0.1 and RD of 55%, Eemian Sand displayed a stiffer response than Andersen's models suggested, requiring more cycles to reach failure. However, at the same CSR but with RD at 80%, Andersen's models indicated a stiffer response. This pattern changes again at higher CSR values, where the results are closer to Andersen's predictions. These trends underscore the complexity of soil behaviour under cyclic loading and highlight the need for empirical calibration of predictive models, especially at varying CSR levels and relative densities. The findings emphasize the necessity for future research to refine these models for improved predictability and stability of offshore structures' foundations in dynamic marine environments.

A key aspect of this research was replicating cyclic tests based on the conditions described in the Fugro Report for the Belgian Offshore Wind Farm. Conducted at Ghent University, this replication aimed to validate the consistency of test results with those obtained from the Belgian Offshore Wind Farm project. The comparative analysis across Beach Sand, Eemian Sand, and the Fugro report's data demonstrated a high degree of replicability. The observed variability in reaching a 15% shear strain under similar test conditions emphasizes the nuanced responses of these sands to cyclic loading. This highlights the importance of understanding specific sand characteristics for accurate geotechnical assessments, particularly for offshore wind turbine foundations. The close adherence of the Eemian Sand results to the Fugro data reinforces the reliability of this testing approach and exemplifies the successful emulation of industry-standard testing protocols in an academic setting.

This thesis has also pioneered in generating insightful curves that delineate the relationship between shear strain levels and pore pressure ratios under varying cyclic stress ratios (CSR). These curves are not mere representations of data but are valuable analytical tools that provide a multi-dimensional understanding of soil behaviour under cyclic loads. They serve as a testament to the soil’s resilience or susceptibility to such loads, offering a predictive look at how different North Sea sands might behave under the operational stresses of offshore wind turbines. This nuanced understanding is crucial, as it informs the engineering decisions that ensure the long-term stability and integrity of offshore structures amid the dynamic and often harsh marine environment.

In conclusion, this thesis contributes significantly to the field of geotechnical engineering and the renewable energy sector. It emphasizes the importance of tailored geotechnical evaluations and adaptive modelling in developing robust and effective offshore wind energy infrastructure. The findings from this study not only enhance theoretical understanding but also have direct applications in optimizing the design and durability of offshore wind turbine foundations, particularly in adapting to the unique soil characteristics of the North Sea.

6 Bibliography

[1] A.-M. Chirosca, L. Rusu, and A. Bleoju, “Study on wind farms in the North Sea area,” *Energy Reports*, vol. 8, pp. 162–168, Dec. 2022, doi: 10.1016/j.egyr.2022.10.244.

[2] “GWEC,” Global Wind report 2023, 2023.

[3] J. Beermann *et al.*, “Characterization and differentiation of sublittoral sandbanks in the southeastern North Sea,” *Biodivers Conserv*, vol. 32, no. 8–9, pp. 2747–2768, Jul. 2023, doi: 10.1007/s10531-023-02629-4.

[4] S. Basack and S. Dey, “Influence of Relative Pile-Soil Stiffness and Load Eccentricity on Single Pile Response in Sand Under Lateral Cyclic Loading,” *Geotechnical and Geological Engineering*, vol. 30, no. 4, pp. 737–751, Aug. 2012, doi: 10.1007/s10706-011-9490-1.

[5] Q. Chen, D. Cui, Q. Liu, and X. Tao, “Effect of Local Cyclic Loading on Direct Shear Strength Characteristics of Shear-Zone Soil,” *Applied Sciences*, vol. 12, no. 24, p. 13024, Dec. 2022, doi: 10.3390/app122413024.

[6] Stavroula Kontoe, David Taborda, Julia Katharina Moller, and David M Potts, “Resonance in offshore wind turbine systems due to seismic loading and extensive soil liquefaction,” *ISSMGE*, Jul. 2022, doi: 10.53243/NUMGE2023-126.

[7] Y.-X. Sun, Z.-P. Wang, H.-Q. Dou, Z.-F. Qu, B.-L. Xue, and L.-Y. Feng, “Influence of Horizontal Loading in Changing the Ultimate Uplift Bearing Capacity of Monopile Foundation of Offshore Wind Turbine,” *JMSE*, vol. 11, no. 6, p. 1150, May 2023, doi: 10.3390/jmse11061150.

[8] S. P. K. Kodicherla, G. Gong, L. Fan, C. K. S. Moy, and J. He, “Effects of preparation methods on inherent fabric anisotropy and packing density of reconstituted sand,” *Cogent Engineering*, vol. 5, no. 1, p. 1533363, Jan. 2018, doi: 10.1080/23311916.2018.1533363.

[9] K. H. Andersen, Ed., *Cyclic soil parameters for offshore foundation design*. CRC Press, a Balkema book, 2015.

[10] L. Bjerrum and A. Landva, “Direct Simple-Shear Tests on a Norwegian Quick Clay,” *Géotechnique*, vol. 16, no. 1, pp. 1–20, Mar. 1966, doi: 10.1680/geot.1966.16.1.1.

[11] R. Dyvik, T. Berre, S. Lacasse, and B. Raadim, “Comparison of truly undrained and constant volume direct simple shear tests,” *Géotechnique*, vol. 37, no. 1, pp. 3–10, Mar. 1987, doi: 10.1680/geot.1987.37.1.3.

[12] S. Ghani and S. Kumari, “Insight into the Effect of Fine Content on Liquefaction Behavior of Soil,” *Geotech Geol Eng*, vol. 39, no. 1, pp. 1–12, Jan. 2021, doi: 10.1007/s10706-020-01491-3.

[13] J. Liu, “Influence of Fines Contents on Soil Liquefaction Resistance in Cyclic Triaxial Test,” *Geotech Geol Eng*, vol. 38, no. 5, pp. 4735–4751, Oct. 2020, doi: 10.1007/s10706-020-01323-4.

[14] B. Stuyts, “IMPROVED SOIL-STRUCTURE INTERACTION FOR OFFSHORE MONOPILES BASED ON IN-SITU MONITORING DATA,” Doctoral dissertation, Vrije Universiteit Brussel, 2023.

[15] M. Raghunandan, A. Juneja, and B. Hsiung, “Preparation of reconstituted sand samples in the laboratory,” *International Journal of Geotechnical Engineering*, vol. 6, no. 1, pp. 125–131, Jan. 2012, doi: 10.3328/IJGE.2012.06.01.125-131.

[16] A. T. Al-Yasir and A. J. Al-Taie, “A new sand raining technique to reconstitute large sand specimens,” *Journal of the Mechanical Behavior of Materials*, vol. 32, no. 1, p. 20220228, Jan. 2023, doi: 10.1515/jmbm-2022-0228.

[17] ASTM D4253, “Standard Test Methods for Maximum Index Density and Unit Weight of Soils Using a Vibratory Table.” ASTM International, 2016. doi: 10.1520/D4253-16.
[18] Y. Li, Y. Yang, H.-S. Yu, and G. Roberts, “Effect of Sample Reconstitution Methods on the Behaviors of Granular Materials under Shearing,” *J. Test. Eval.*, vol. 46, no. 6, p. 20170126, Nov. 2018, doi: 10.1520/JTE20170126.
[19] A.-B. Huang, W.-J. Chang, H.-H. Hsu, and Y.-J. Huang, “A mist pluviation method for reconstituting silty sand specimens,” *Engineering Geology*, vol. 188, pp. 1–9, Apr. 2015, doi: 10.1016/j.enggeo.2015.01.015.
[20] Z. Zhu, F. Zhang, J.-C. Dupla, J. Canou, E. Foerster, and Q. Peng, “Assessment of tamping-based specimen preparation methods on static liquefaction of loose silty sand,” *Soil Dynamics and Earthquake Engineering*, vol. 143, p. 106592, Apr. 2021, doi: 10.1016/j.soildyn.2021.106592.
[21] L. David Suits, T. Sheahan, J. Frost, and J.-Y. Park, “A Critical Assessment of the Moist Tamping Technique,” *Geotech. Test. J.*, vol. 26, no. 1, p. 9850, 2003, doi: 10.1520/GTJ11108J.
[22] T. Wichtmann and T. Triantafyllidis, “On the influence of the grain size distribution curve on P-wave velocity, constrained elastic modulus Mmax and Poisson’s ratio of quartz sands,” *Soil Dynamics and Earthquake Engineering*, vol. 30, no. 8, pp. 757–766, Aug. 2010, doi: 10.1016/j.soildyn.2010.03.006.
[23] F. Tatsuoka *et al.*, “Some Factors Affecting Cyclic Undrained Triaxial Strength of Sand,” *Soils and Foundations*, vol. 26, no. 3, pp. 99–116, Sep. 1986, doi: 10.3208/sandf1972.26.3_99.
[24] F. Tatsuoka, H. Kato, M. Kimura, and T. B. S. Pradhan, “Liquefaction Strength of Sands Subjected to Sustained Pressure,” *Soils and Foundations*, vol. 28, no. 1, pp. 119–131, Mar. 1988, doi: 10.3208/sandf1972.28.119.
[25] V. Quinteros, T. Lunne, R. Dyvik, L. Krogh, R. Bøgelund-Pedersen, and S. Bøtker-Rasmussen, “Influence of Pre-Shearing on the Triaxial Drained Strength and Stiffness of a Marine North Sea Sand,” in *Offshore Site Investigation Geotechnics 8th International Conference Proceedings*, Society of Underwater Technology, 2017, pp. 338–345. doi: 10.3723/OSIG17.338.
[26] K. Pan, Z. X. Yang, and T. T. Xu, “Impact of Static Preshearing on Undrained Anisotropy and Shear Characteristics of Sand,” *Int. J. Geomech.*, vol. 18, no. 12, p. 04018162, Dec. 2018, doi: 10.1061/(ASCE)GM.1943-5622.0001319.
[27] M. L. Bernhardt-Barry, G. Biscontin, and C. O’Sullivan, “Analysis of the stress distribution in a laminar direct simple shear device and implications for test data interpretation,” *Granular Matter*, vol. 23, no. 3, p. 55, Aug. 2021, doi: 10.1007/s10035-021-01118-1.
[28] B. Stuyts, W. Weijtjens, and C. Devriendt, “Revised Soil Damping Using Realistic Pile-Soil Interaction Models,” in *Proceedings of the 2nd Vietnam Symposium on Advances in Offshore Engineering*, vol. 208, D. V. K. Huynh, A. M. Tang, D. H. Doan, and P. Watson, Eds., in Lecture Notes in Civil Engineering, vol. 208. , Singapore: Springer Singapore, 2022, pp. 441–448. doi: 10.1007/978-981-16-7735-9_49.
[29] Fugro, “ADVANCED LABORATORY REPORT BELWIND II OFFSHORE WIND FARM BLIGH BANK,” Leuven, 2014.
[30] B. O. Hardin and V. P. Drnevich, “Shear Modulus and Damping in Soils: Design Equations and Curves,” *J. Soil Mech. and Found. Div.*, vol. 98, no. 7, pp. 667–692, Jul. 1972, doi: 10.1061/JSFEAQ.0001760.
[31] S. Muthukumar and R. DesRoches, “A Hertz contact model with non-linear damping for pounding simulation,” *Earthquake Engng Struct. Dyn.*, vol. 35, no. 7, pp. 811–828, Jun. 2006, doi: 10.1002/eqe.557.

[32] Fugro, “Geotechnical Engineering Report, Belwind II Offshore Wind Farm, Bligh Bank, Offshore Belgium,” Brussels, FGCB Report No. C922-01 (01), 2015.
[33] C. S. Chang and Z.-Y. Yin, “Micromechanical modeling for behavior of silty sand with influence of fine content,” *International Journal of Solids and Structures,* vol. 48, no. 19, pp. 2655–2667, Sep. 2011, doi: 10.1016/j.ijsolstr.2011.05.014.
[34] Fugro, “Geotechnical Report, Investigation Data Belwind II Offshore Wind Farm Lot 1, Bligh Bank, Offshore Belgium,” Noblewind NV, Leuven, N5955/01, Issue 3, 2014.

List of Figures

List of Tables

7 Appendix

7.1 Appendix A: Comprehensive Graphical Results of Cyclic Test Behavior for North Sea Sands

Test 2: Cyclic Behaviour of Beach Sand under CSR of 0.1, Consolidation Pressure of 100 kPa, and Relative Density of 80%

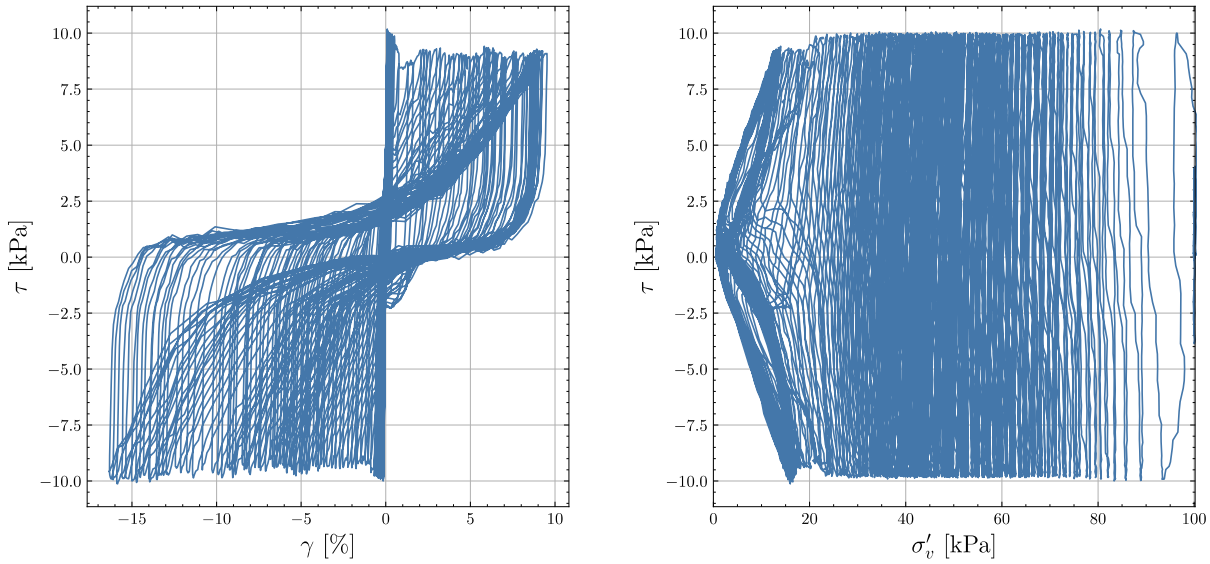

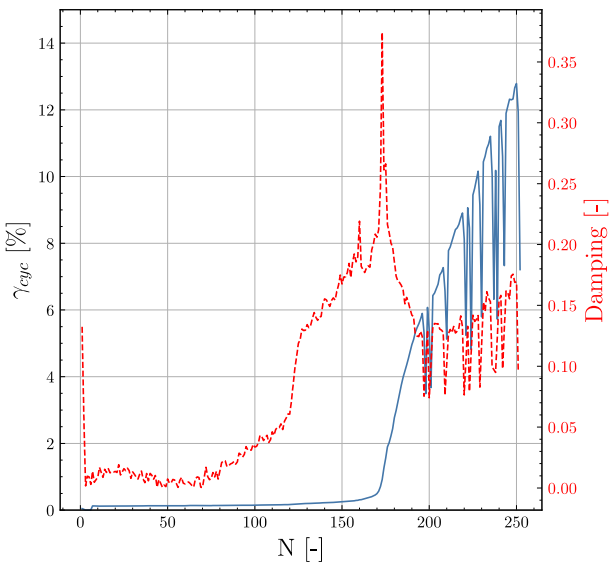

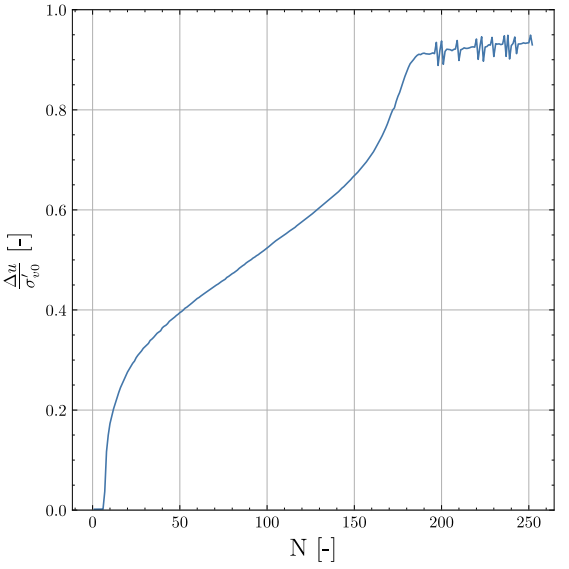

Test 3: Cyclic Behaviour of Beach Sand under CSR of 0.1, Consolidation Pressure of 150 kPa, and Relative Density of 55%

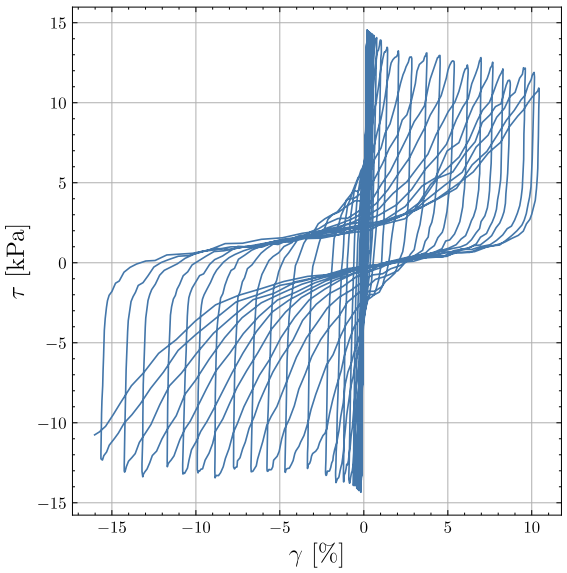

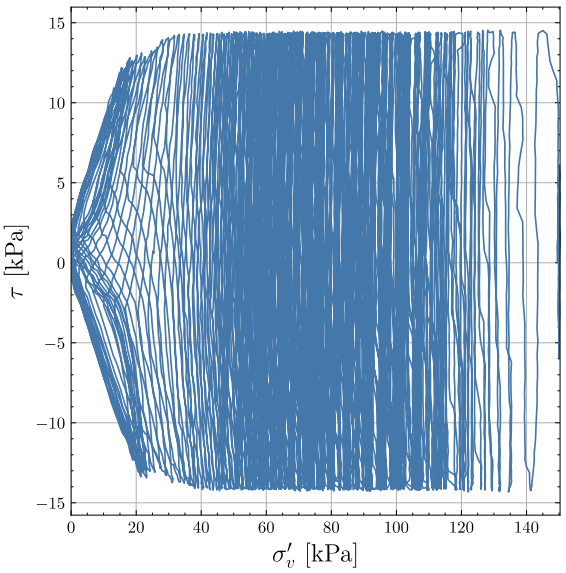

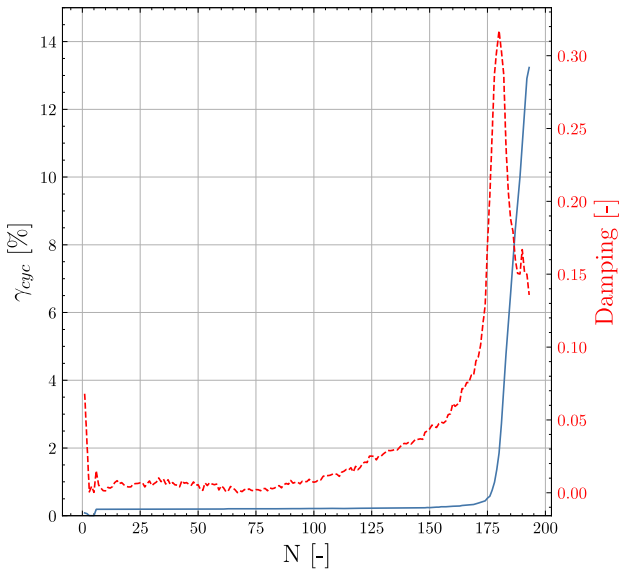

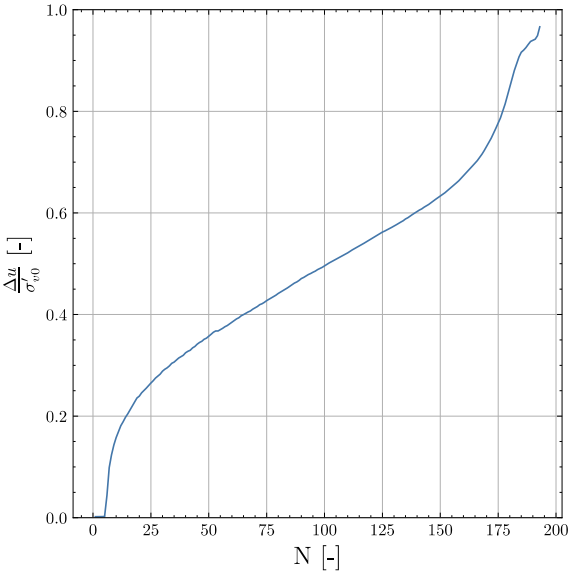

Test 4: Cyclic Behaviour of Beach Sand under CSR of 0.1, Consolidation Pressure of 150 kPa, and Relative Density of 80%

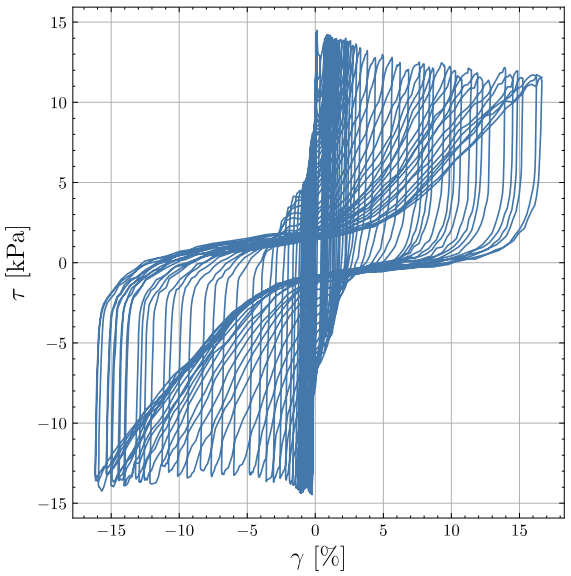

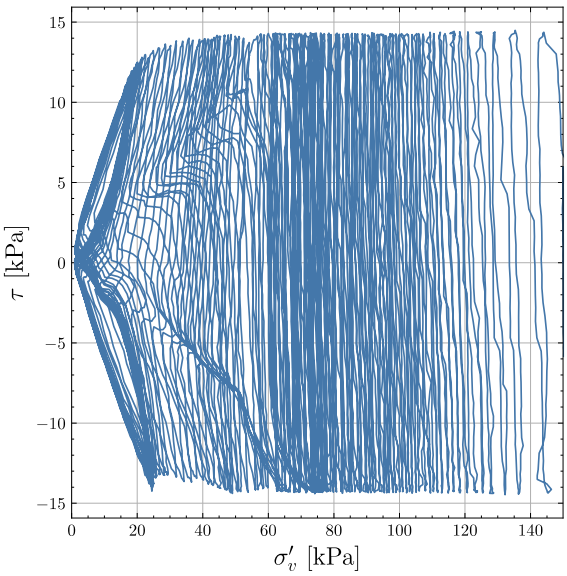

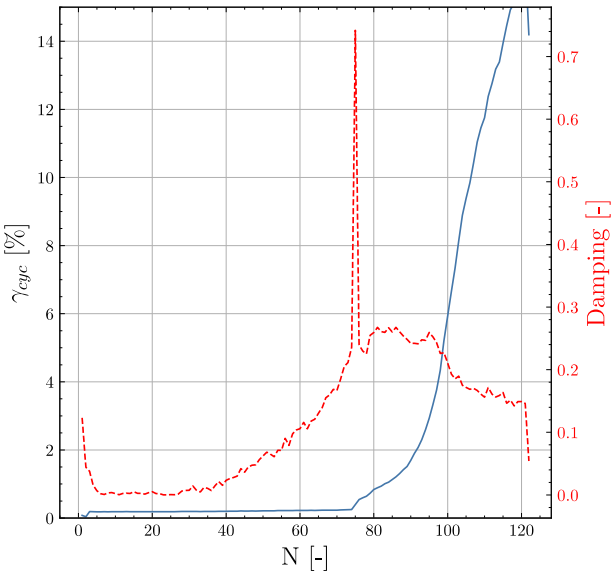

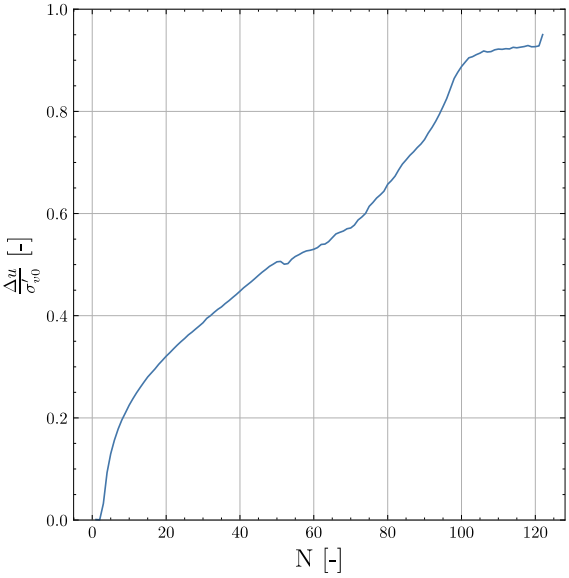

Test 5: Cyclic Behaviour of Beach Sand under CSR of 0.1, Consolidation Pressure of 250 kPa, and Relative Density of 55%

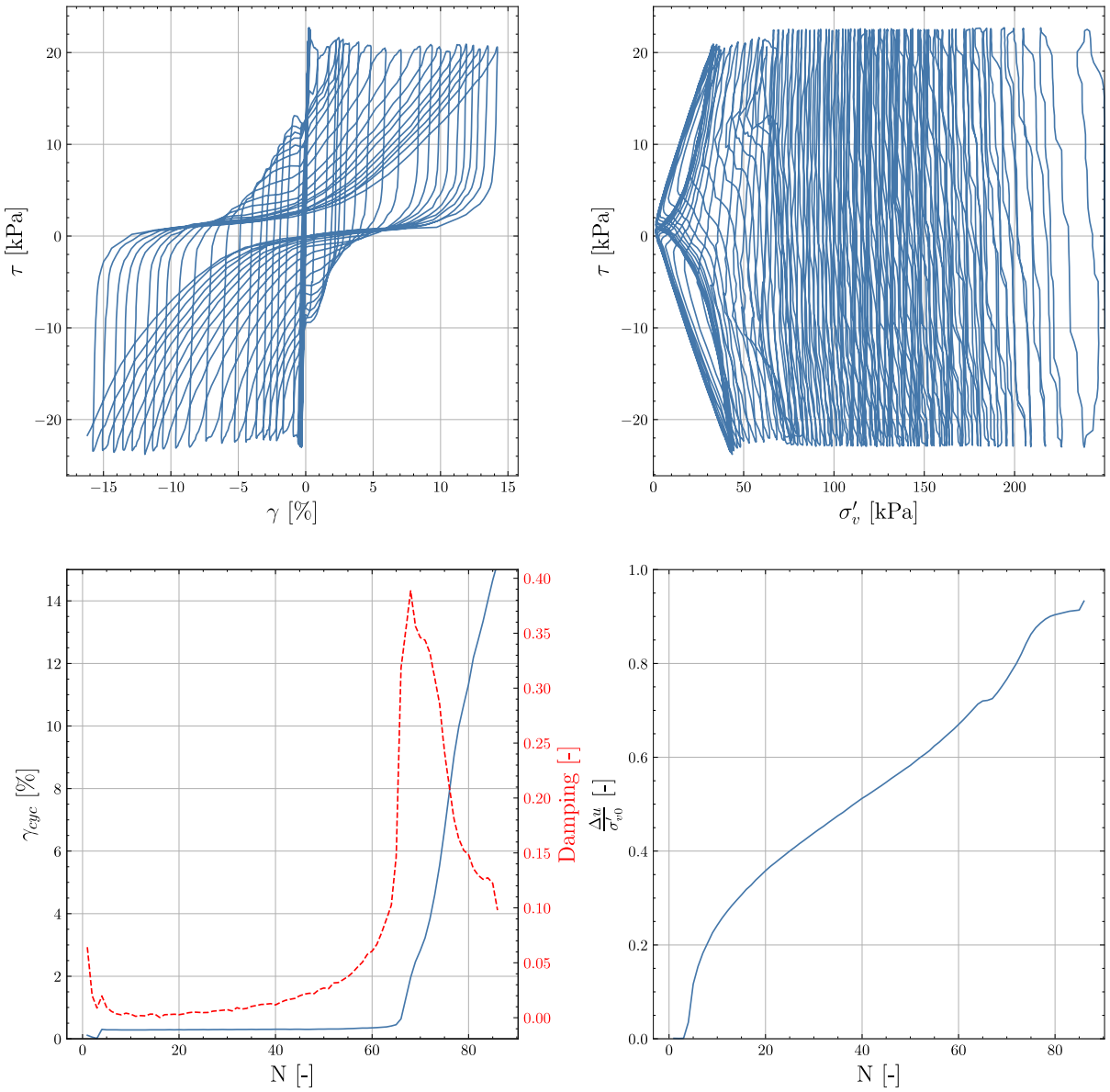

Test 6: Cyclic Behaviour of Beach Sand under CSR of 0.1, Consolidation Pressure of 250 kPa, and Relative Density of 80%

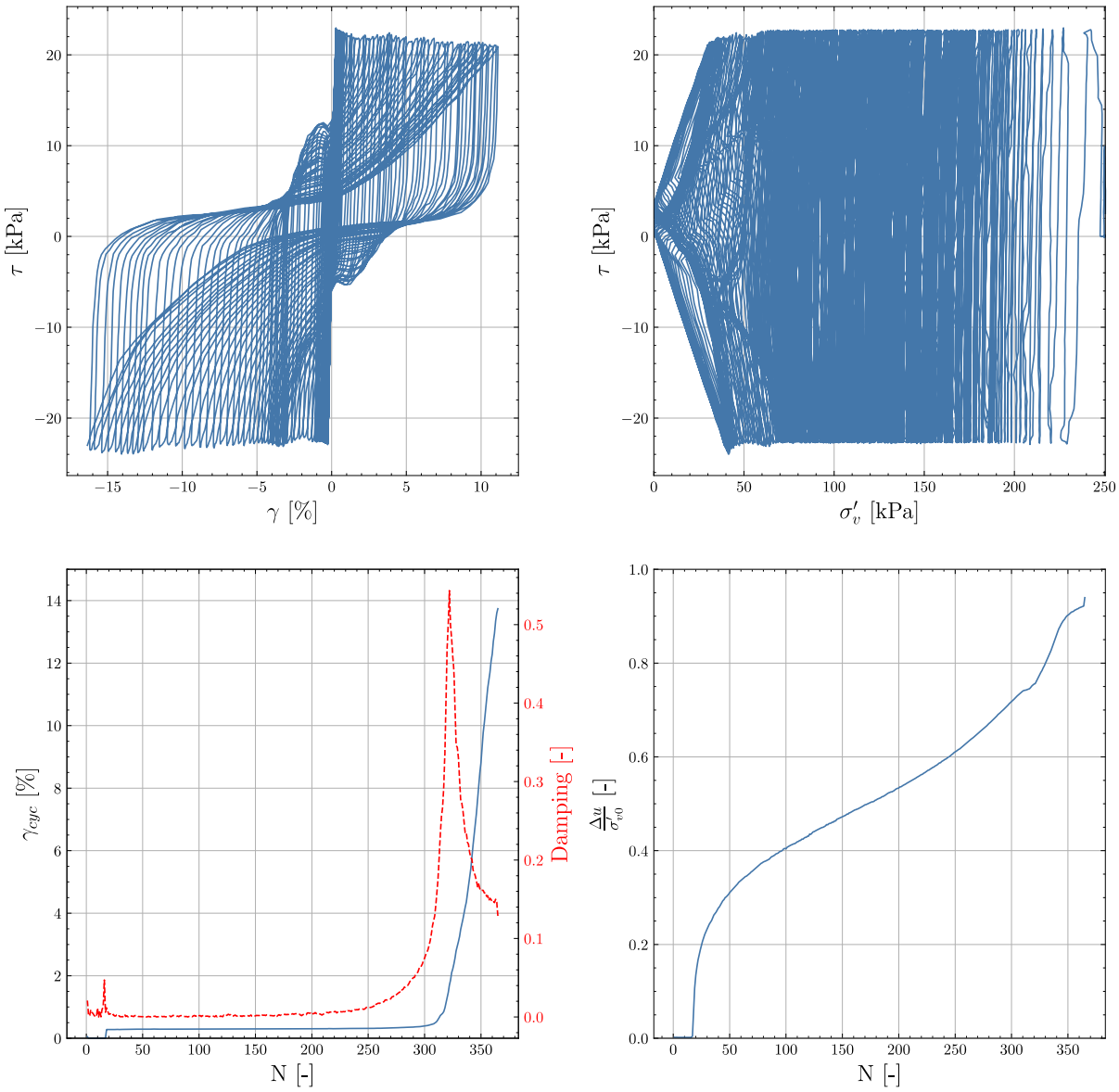

Test 7: Cyclic Behaviour of Beach Sand under CSR of 0.1, Consolidation Pressure of 500 kPa, and Relative Density of 55%

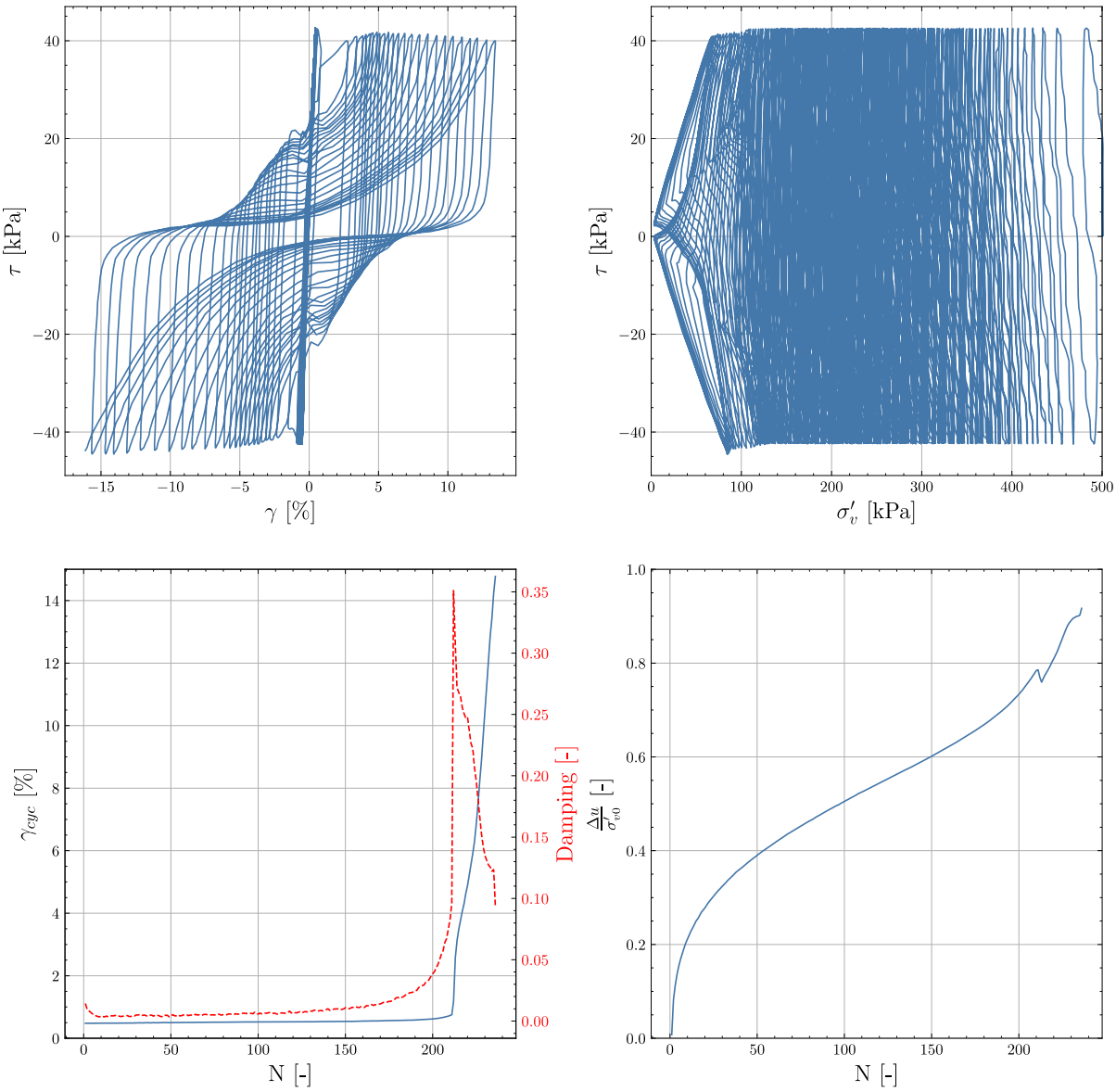

Test 8: Cyclic Behaviour of Beach Sand under CSR of 0.1, Consolidation Pressure of 500 kPa, and Relative Density of 80%

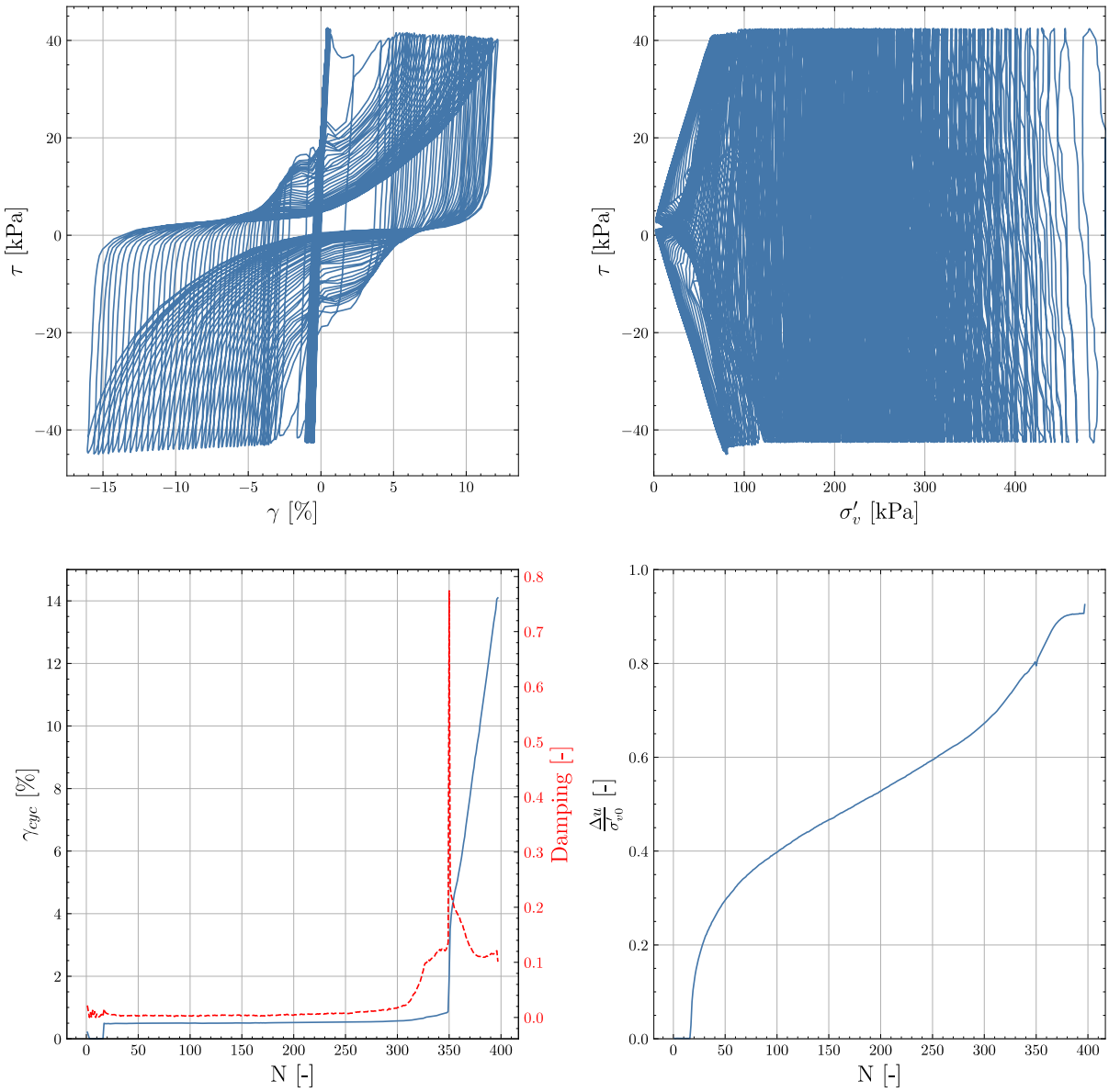

Test 9: Cyclic Behaviour of Beach Sand under CSR of 0.15, Consolidation Pressure of 100 kPa, and Relative Density of 55%

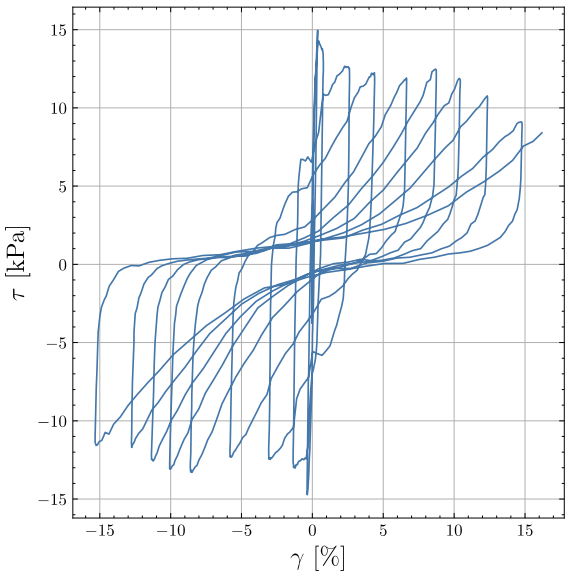

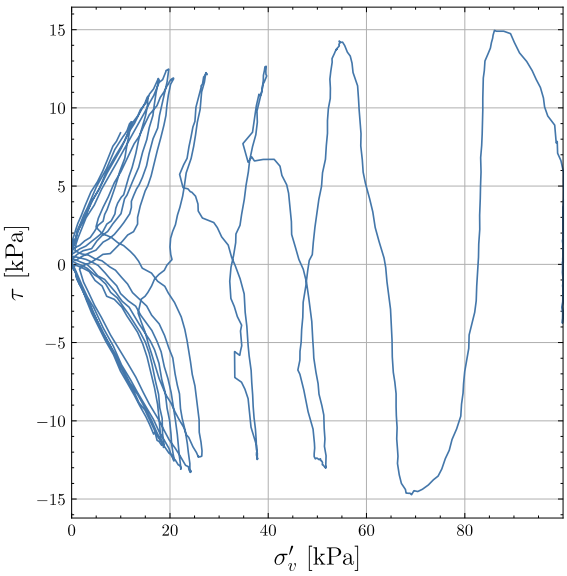

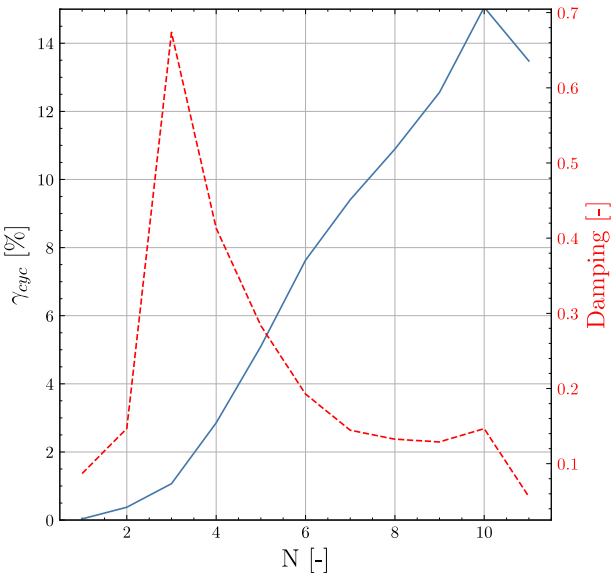

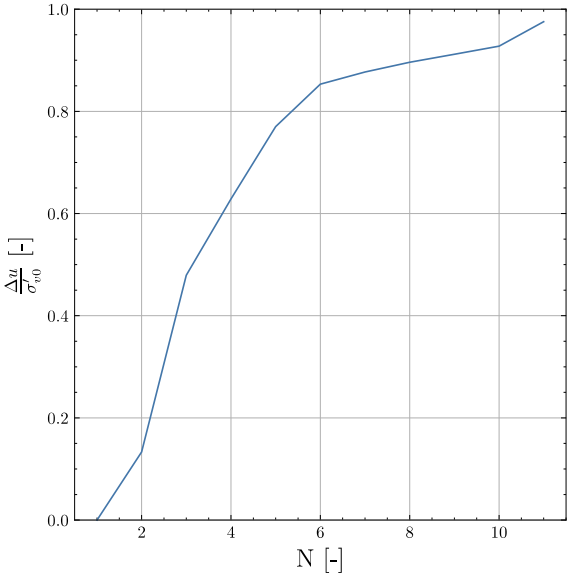

Test 10: Cyclic Behaviour of Beach Sand under CSR of 0.15, Consolidation Pressure of 100 kPa, and Relative Density of 80%

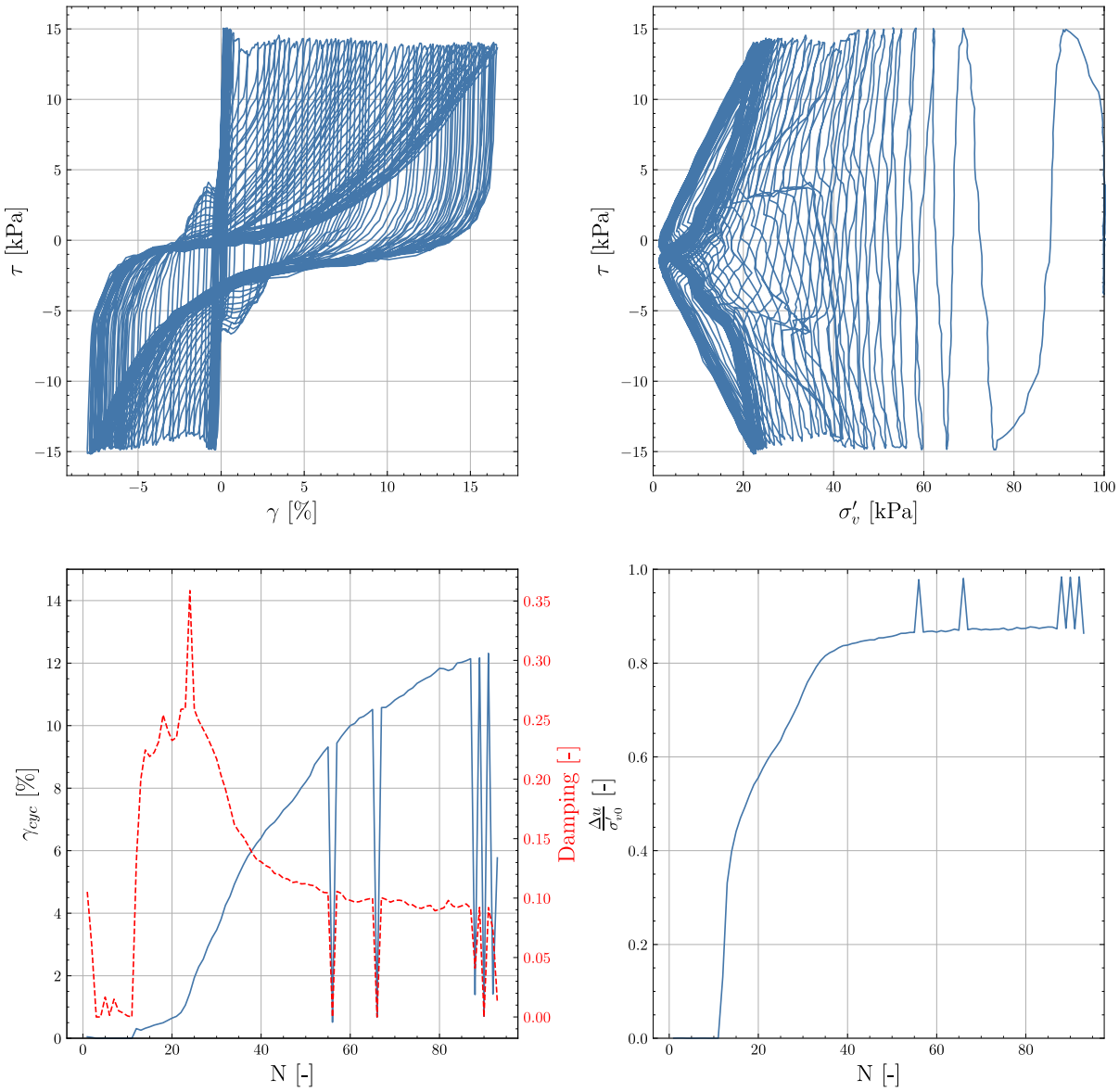

Test 11: Cyclic Behaviour of Beach Sand under CSR of 0.15, Consolidation Pressure of 150 kPa, and Relative Density of 55%

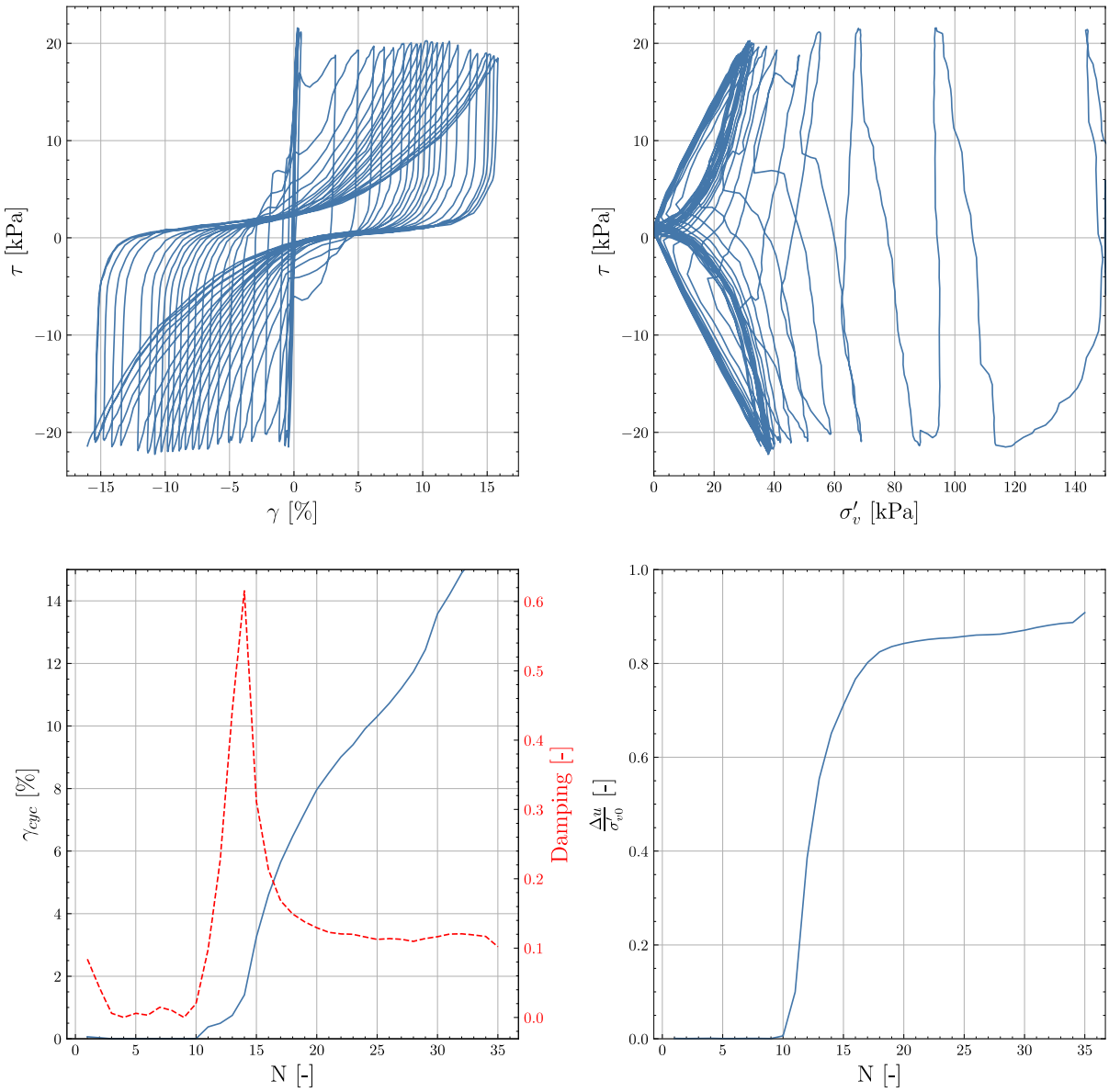

Test 12: Cyclic Behaviour of Beach Sand under CSR of 0.15, Consolidation Pressure of 150 kPa, and Relative Density of 80%

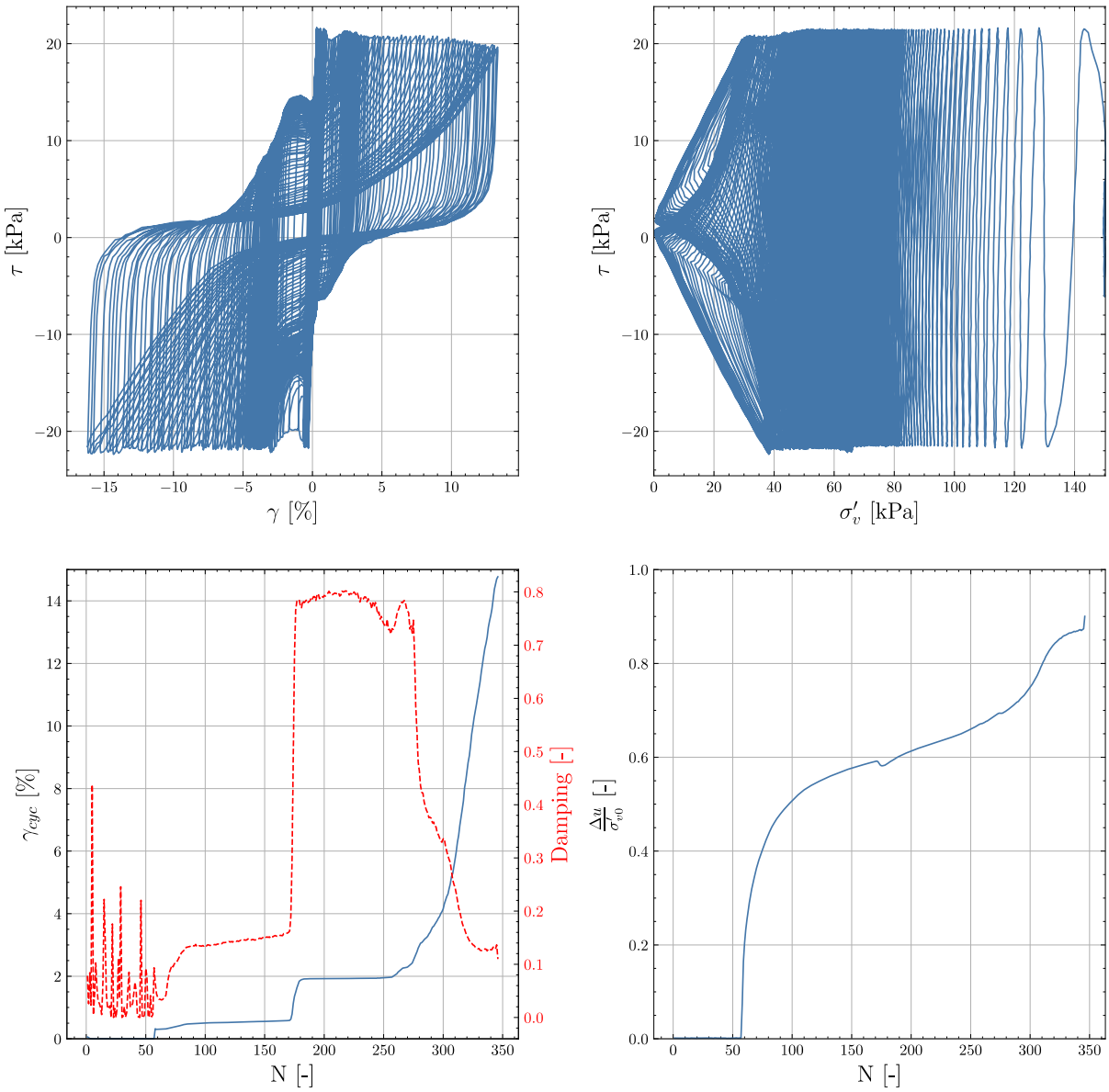

Test 13: Cyclic Behaviour of Beach Sand under CSR of 0.15, Consolidation Pressure of 250 kPa, and Relative Density of 55%

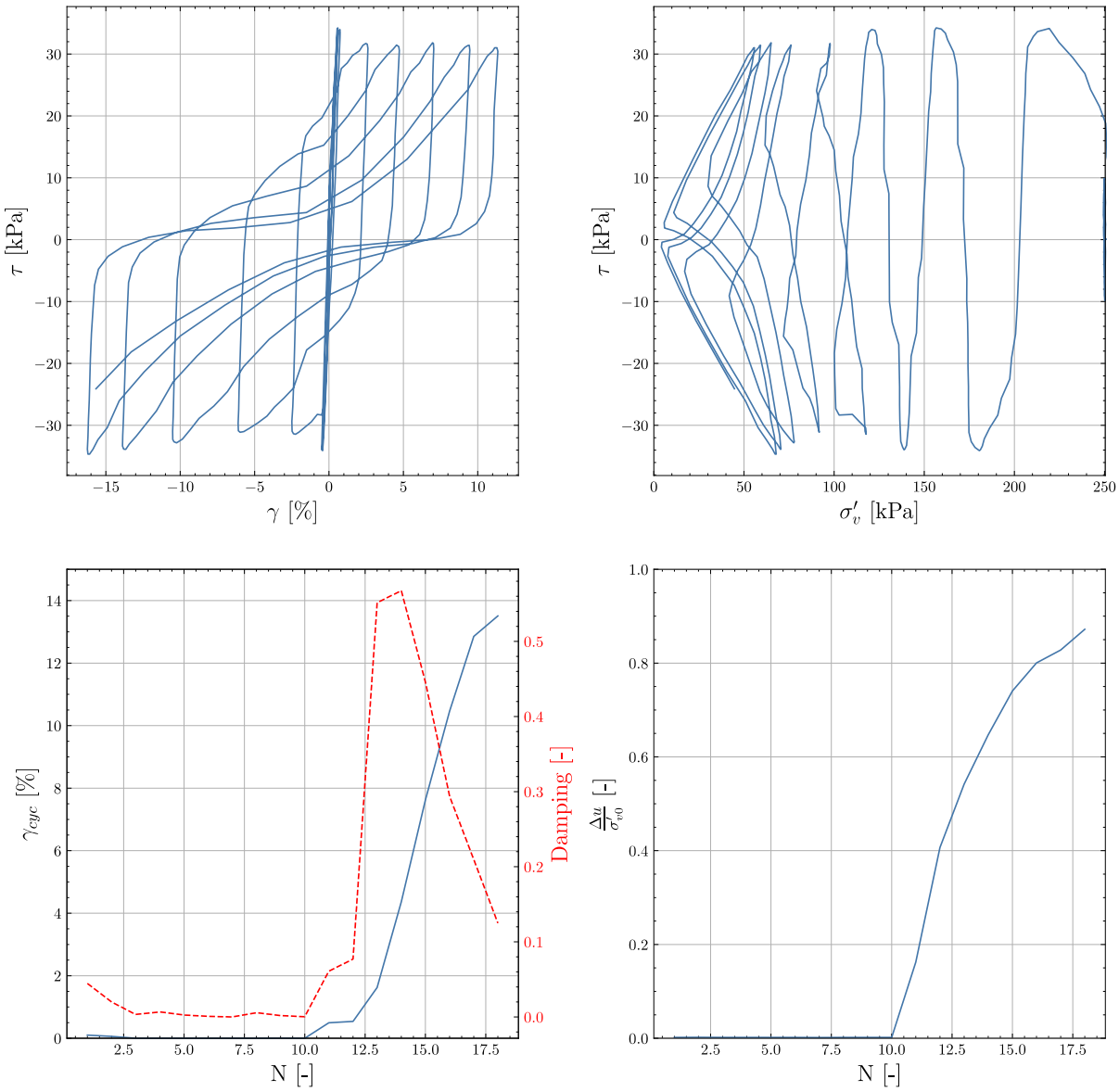

Test 14: Cyclic Behaviour of Beach Sand under CSR of 0.15, Consolidation Pressure of 250 kPa, and Relative Density of 80%

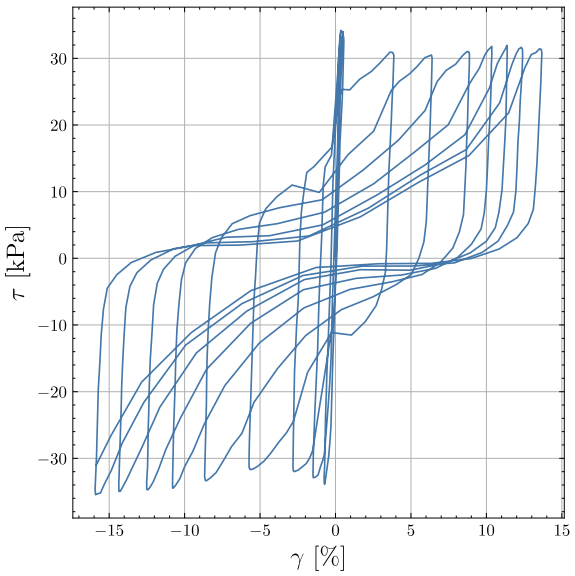

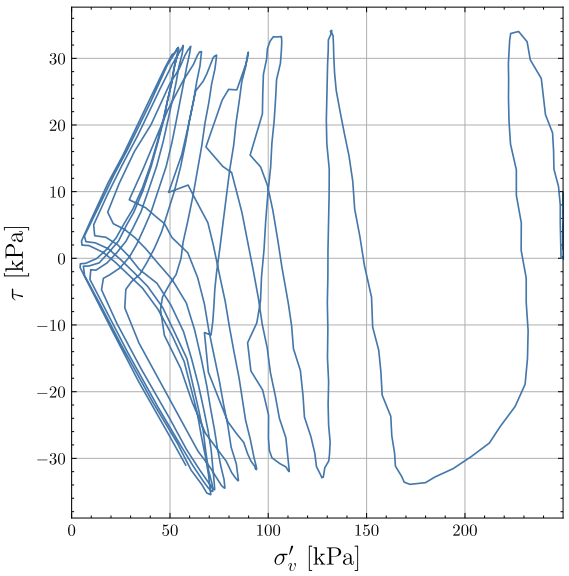

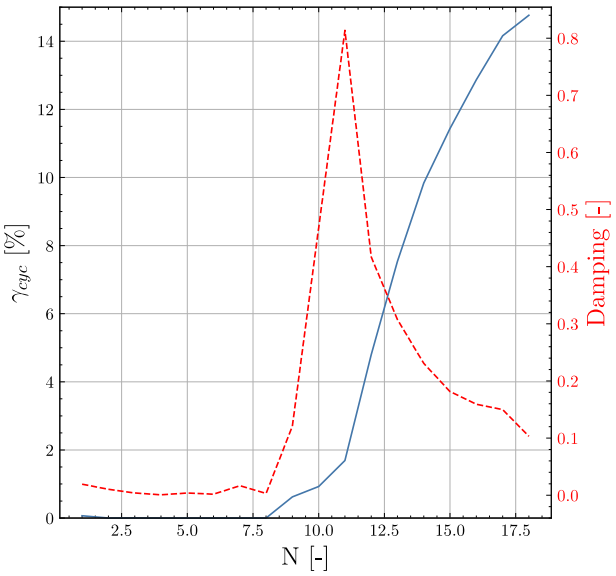

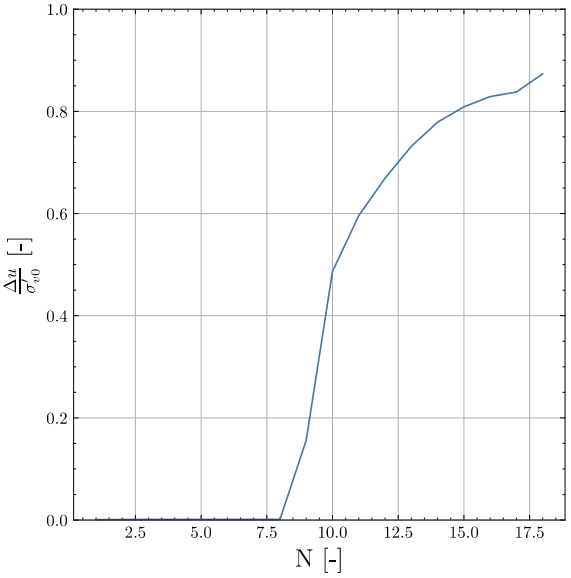

Test 15: Cyclic Behaviour of Beach Sand under CSR of 0.15, Consolidation Pressure of 500 kPa, and Relative Density of 55%

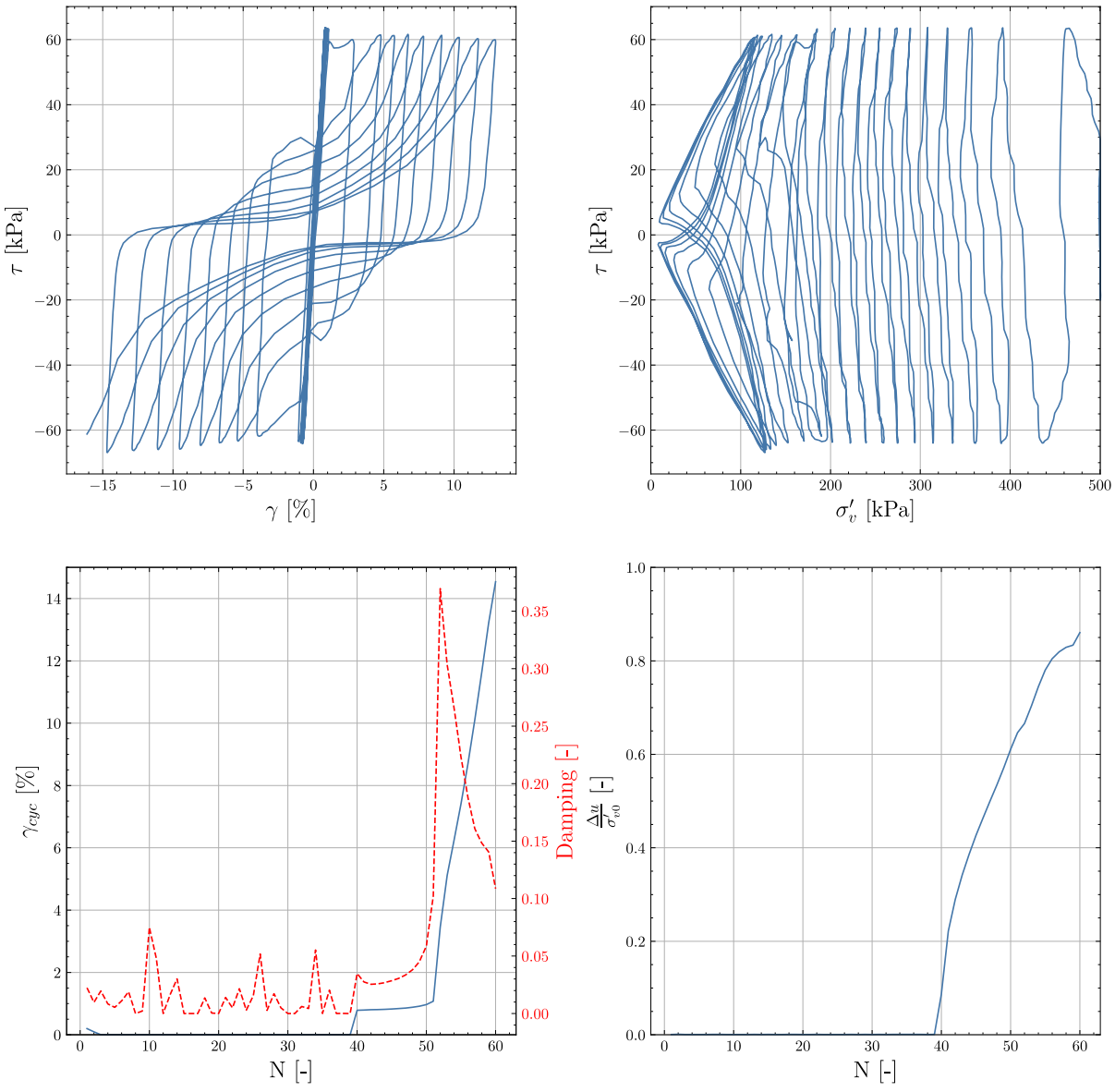

Test 16: Cyclic Behaviour of Beach Sand under CSR of 0.15, Consolidation Pressure of 500 kPa, and Relative Density of 80%

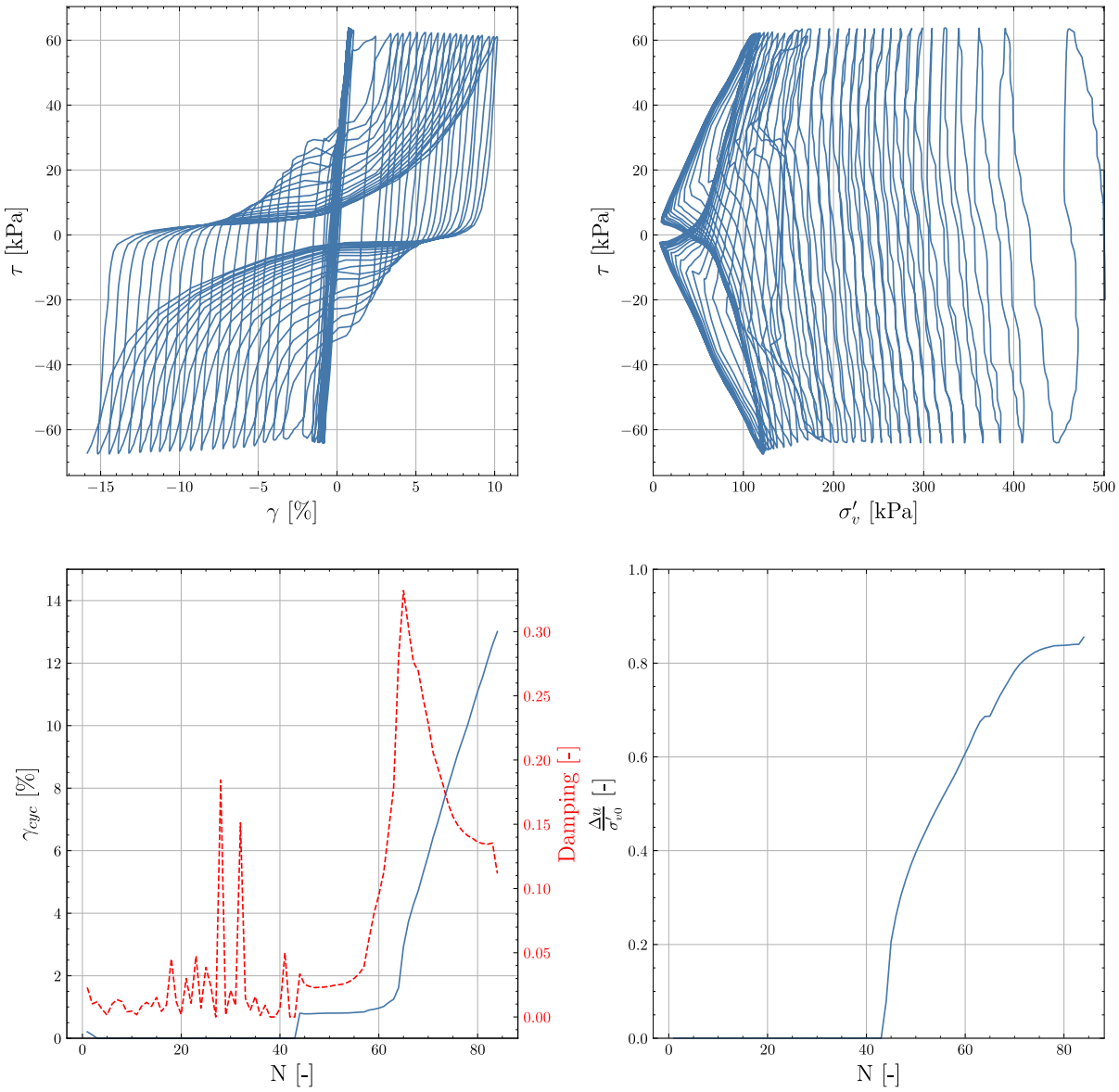

Test 17: Cyclic Behaviour of Beach Sand under CSR of 0.2, Consolidation Pressure of 100 kPa, and Relative Density of 55%

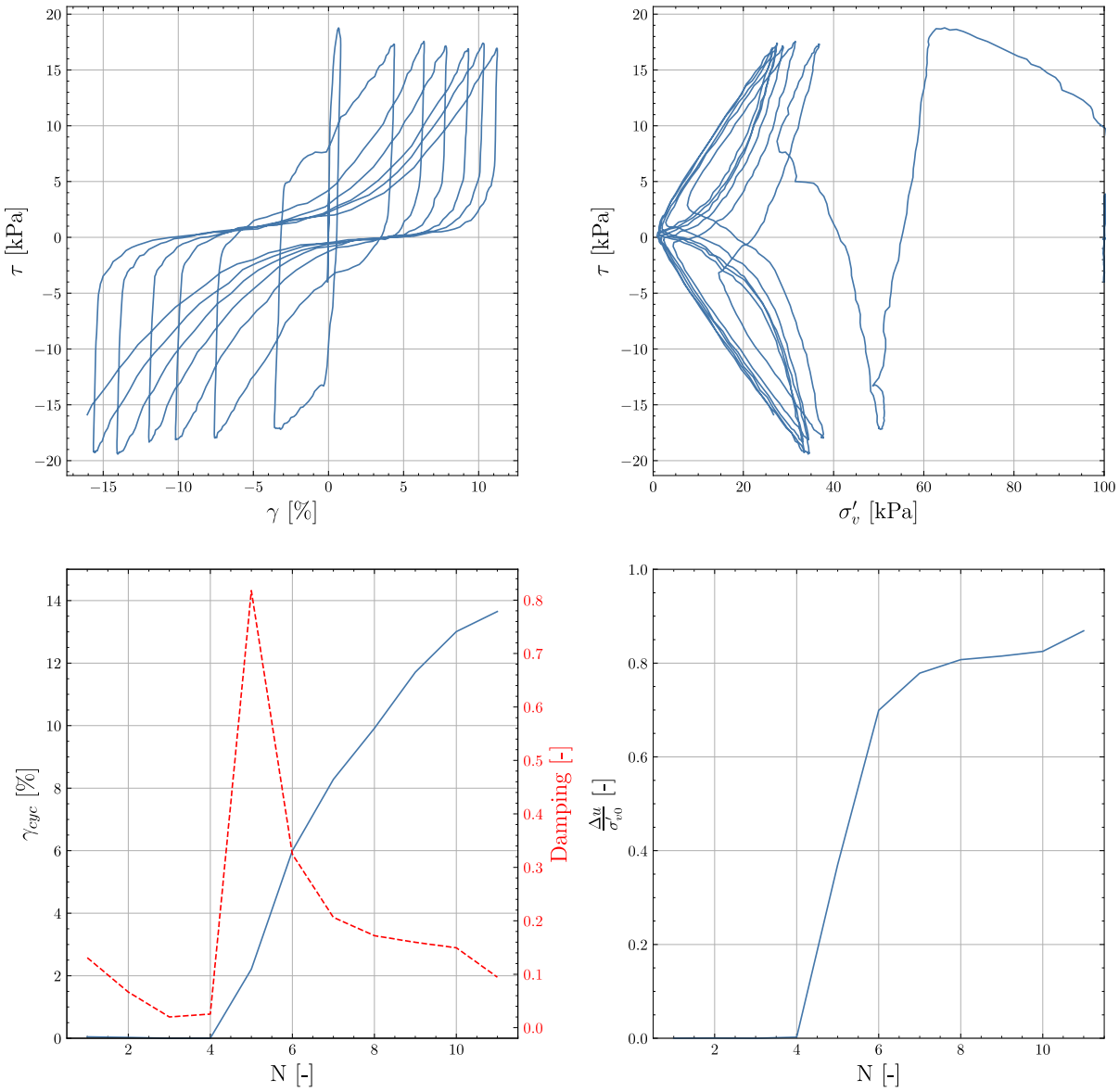

Test 18: Cyclic Behaviour of Beach Sand under CSR of 0.2, Consolidation Pressure of 100 kPa, and Relative Density of 80%

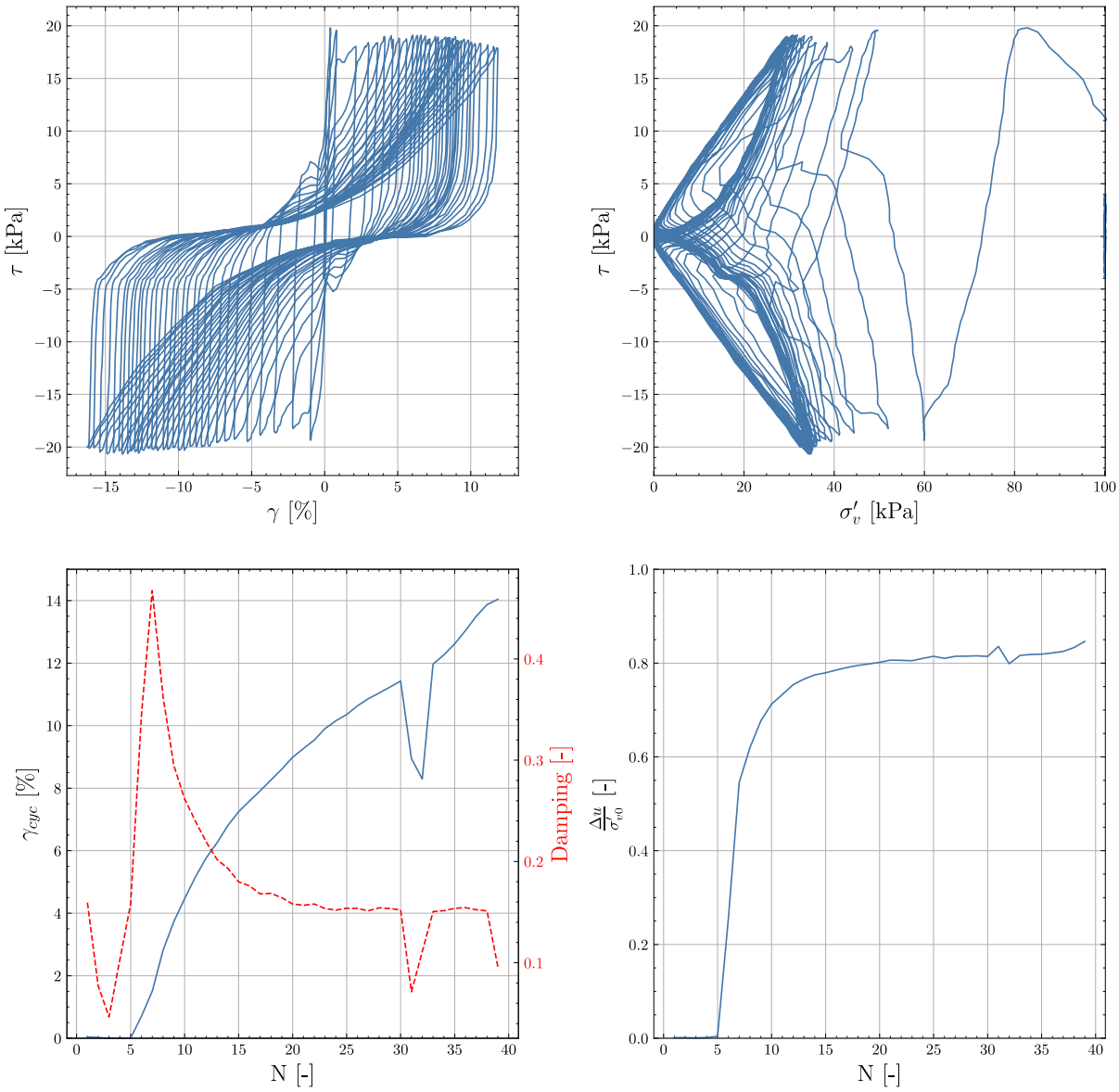

Test 19: Cyclic Behaviour of Beach Sand under CSR of 0.2, Consolidation Pressure of 150 kPa, and Relative Density of 55%

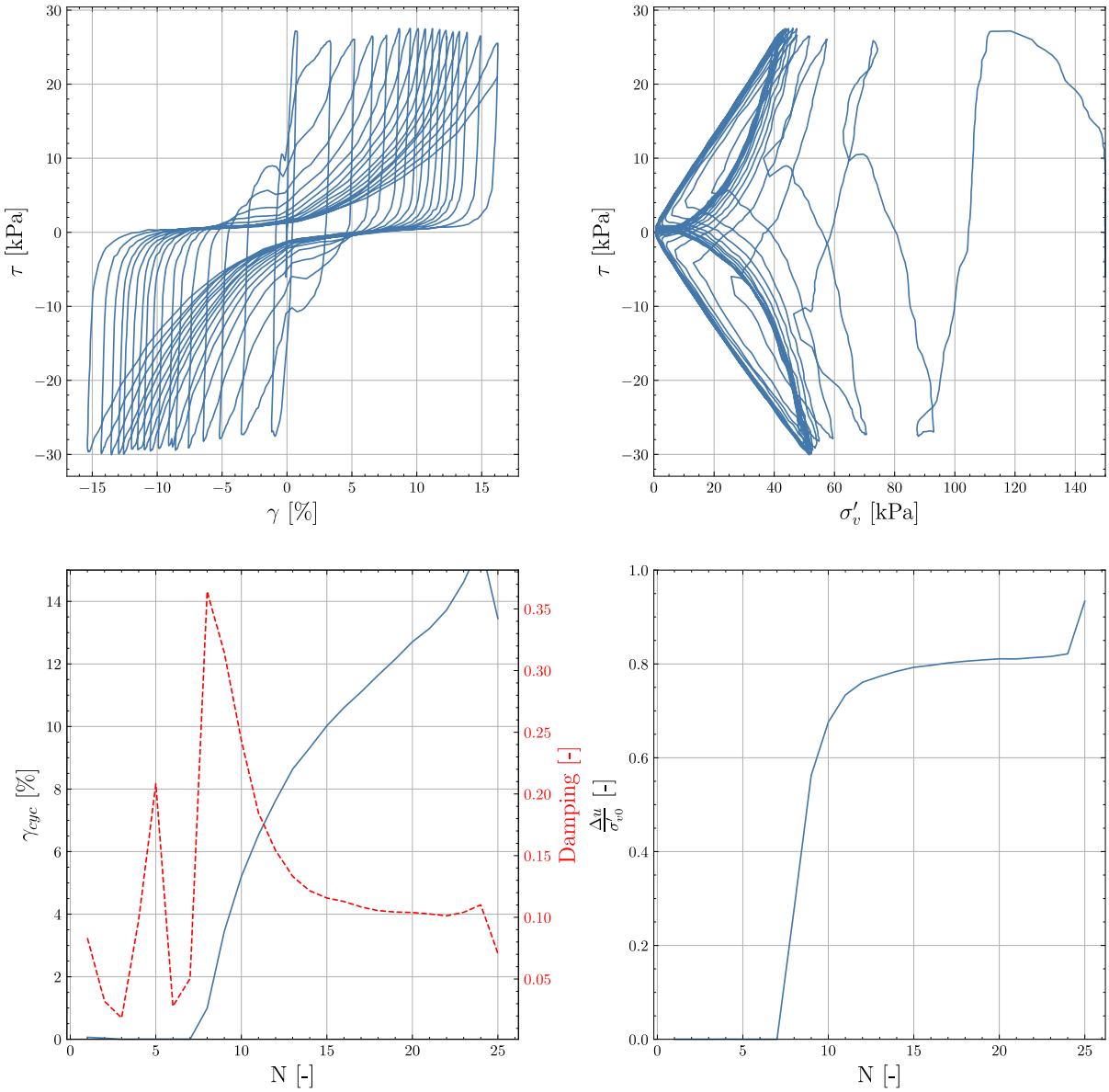

Test 20: Cyclic Behaviour of Beach Sand under CSR of 0.2, Consolidation Pressure of 150 kPa, and Relative Density of 80%

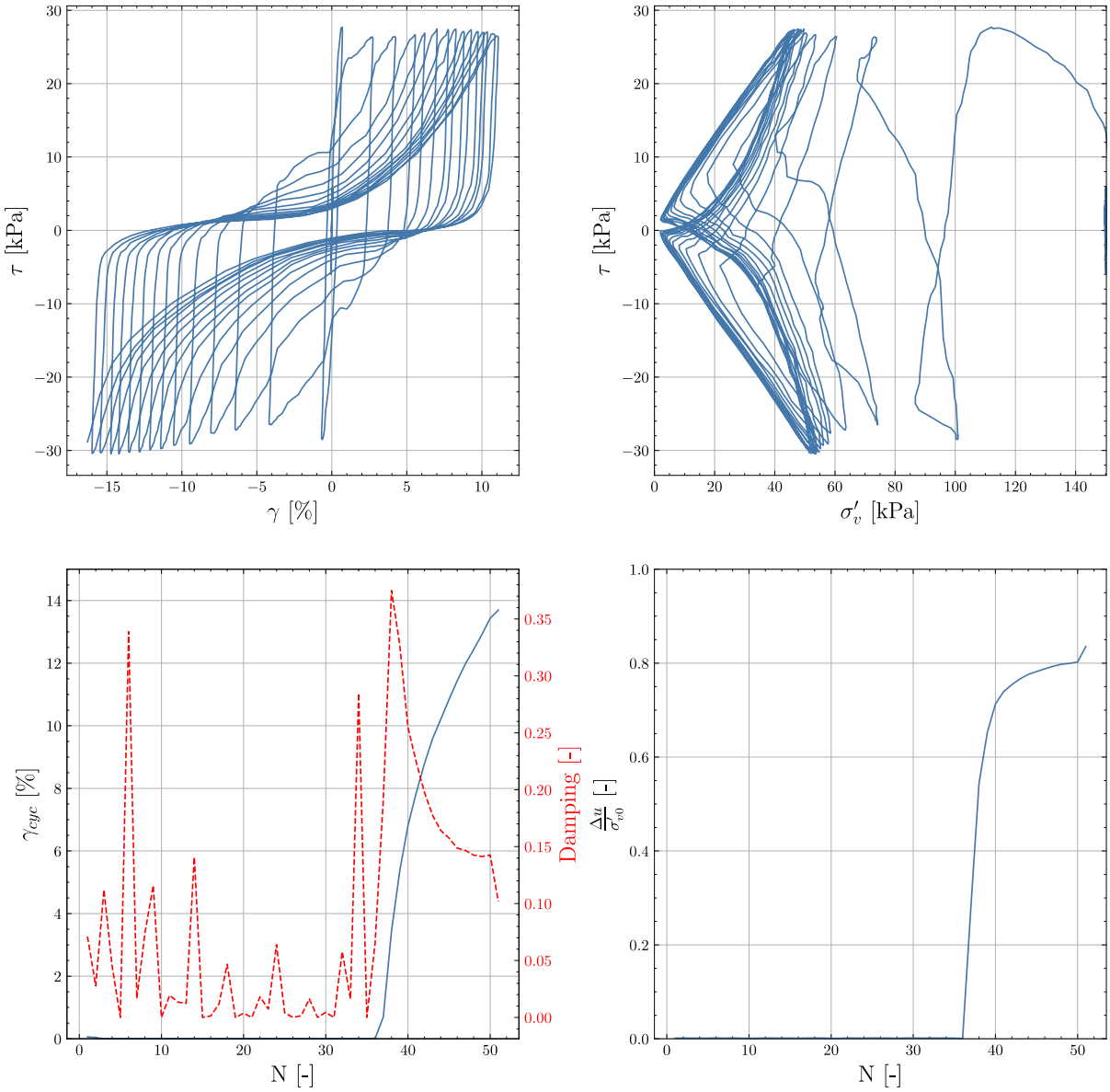

Test 21: Cyclic Behaviour of Beach Sand under CSR of 0.2, Consolidation Pressure of 250 kPa, and Relative Density of 55%

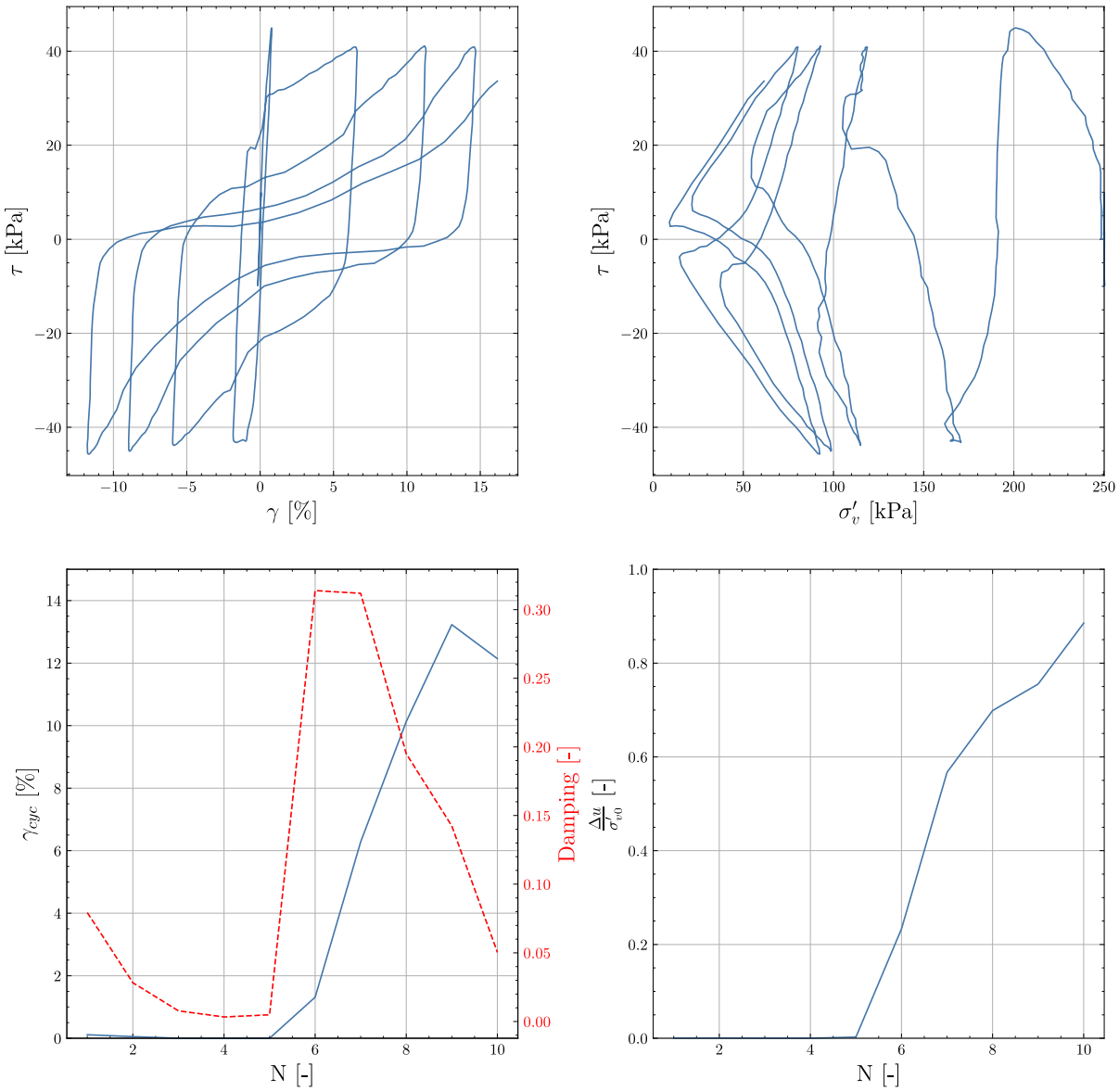

Test 22: Cyclic Behaviour of Beach Sand under CSR of 0.2, Consolidation Pressure of 250 kPa, and Relative Density of 80%

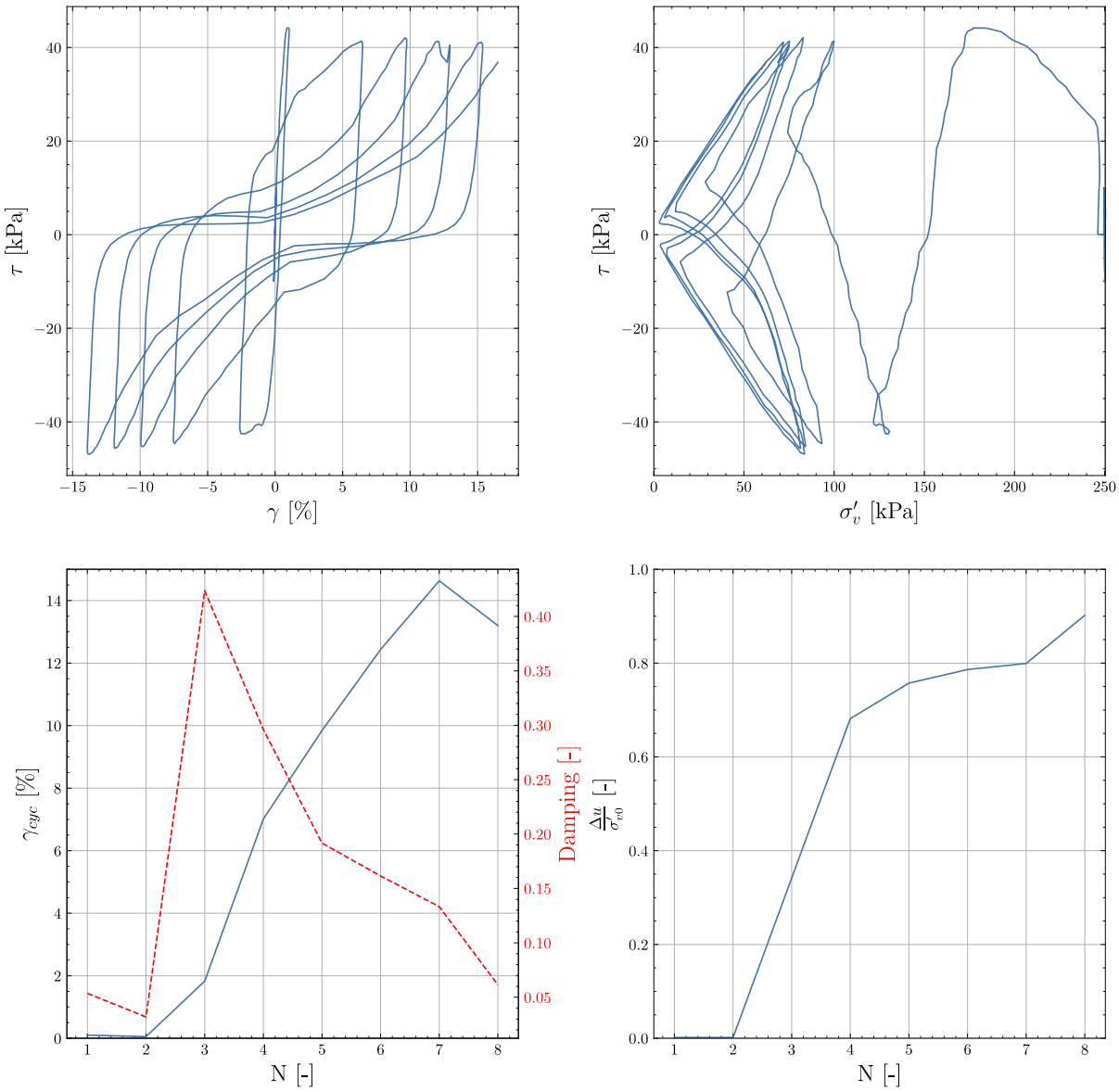

Test 23: Cyclic Behaviour of Beach Sand under CSR of 0.2, Consolidation Pressure of 500 kPa, and Relative Density of 55%

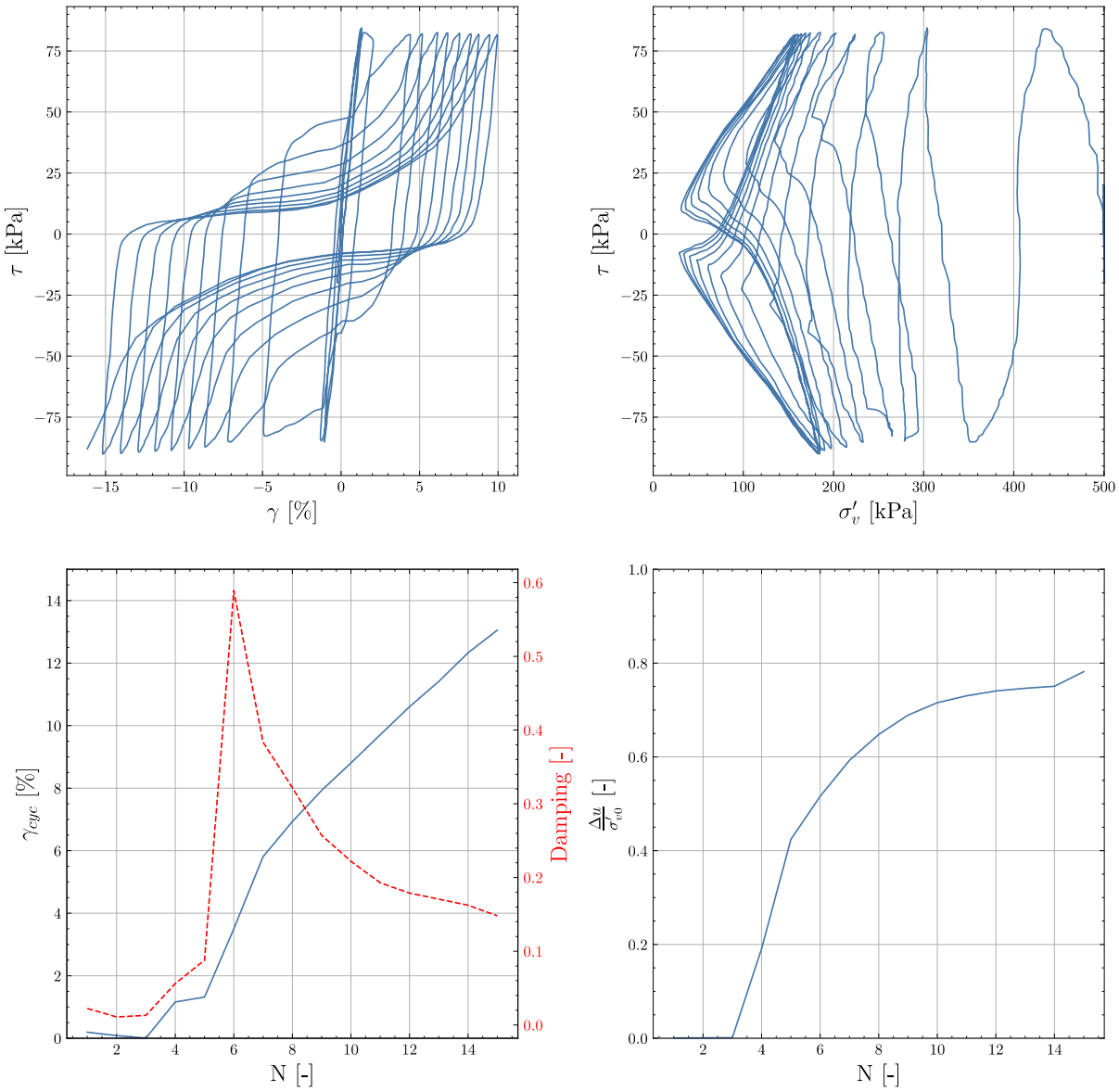

Test 24: Cyclic Behaviour of Beach Sand under CSR of 0.2, Consolidation Pressure of 500 kPa, and Relative Density of 80%

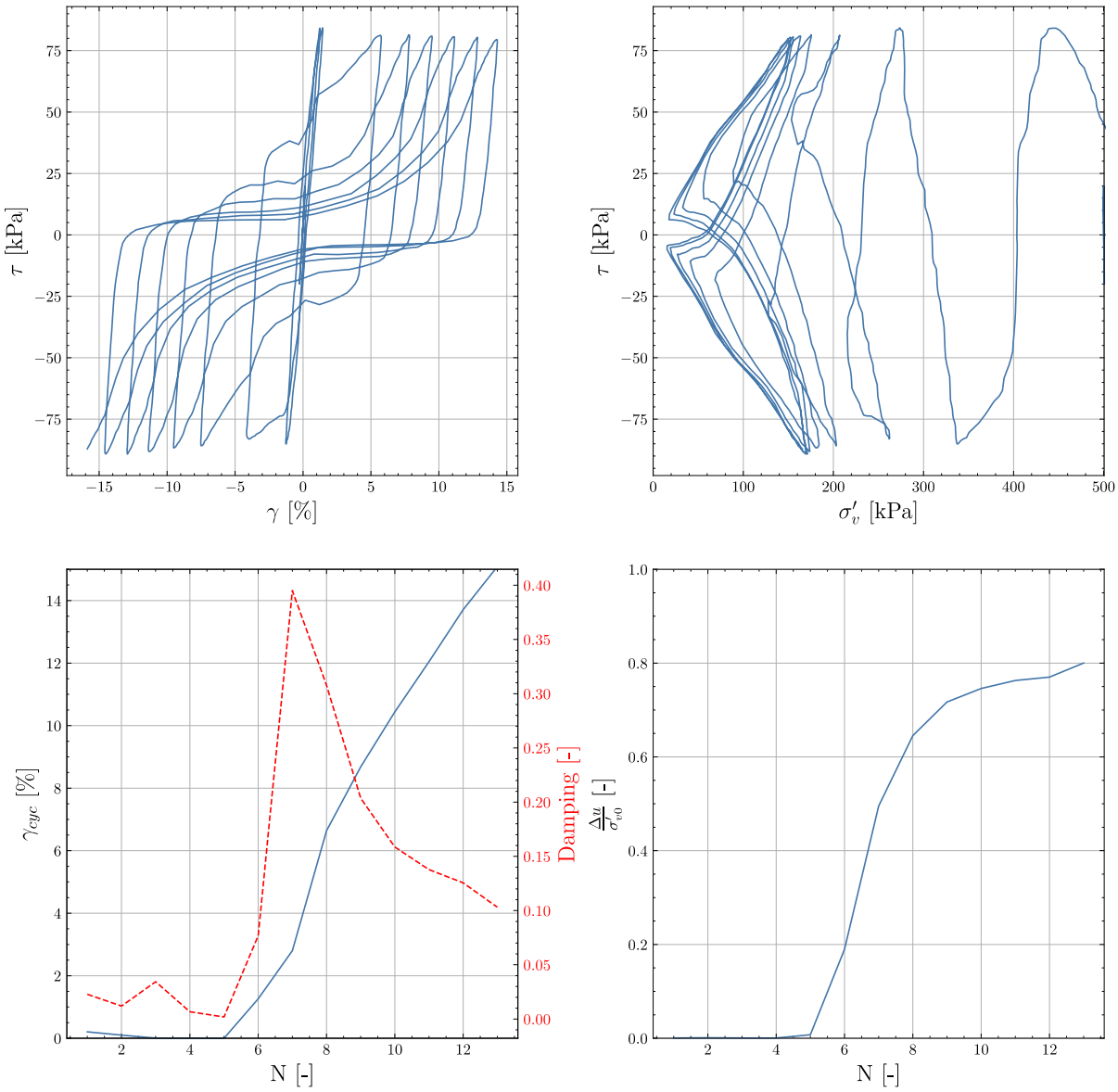

Cyclic Behaviour of Eemian Sand:

Test 25: Cyclic Behaviour of Eemian Sand under CSR of 0.1, Consolidation Pressure of 100 kPa, and Relative Density of 55%

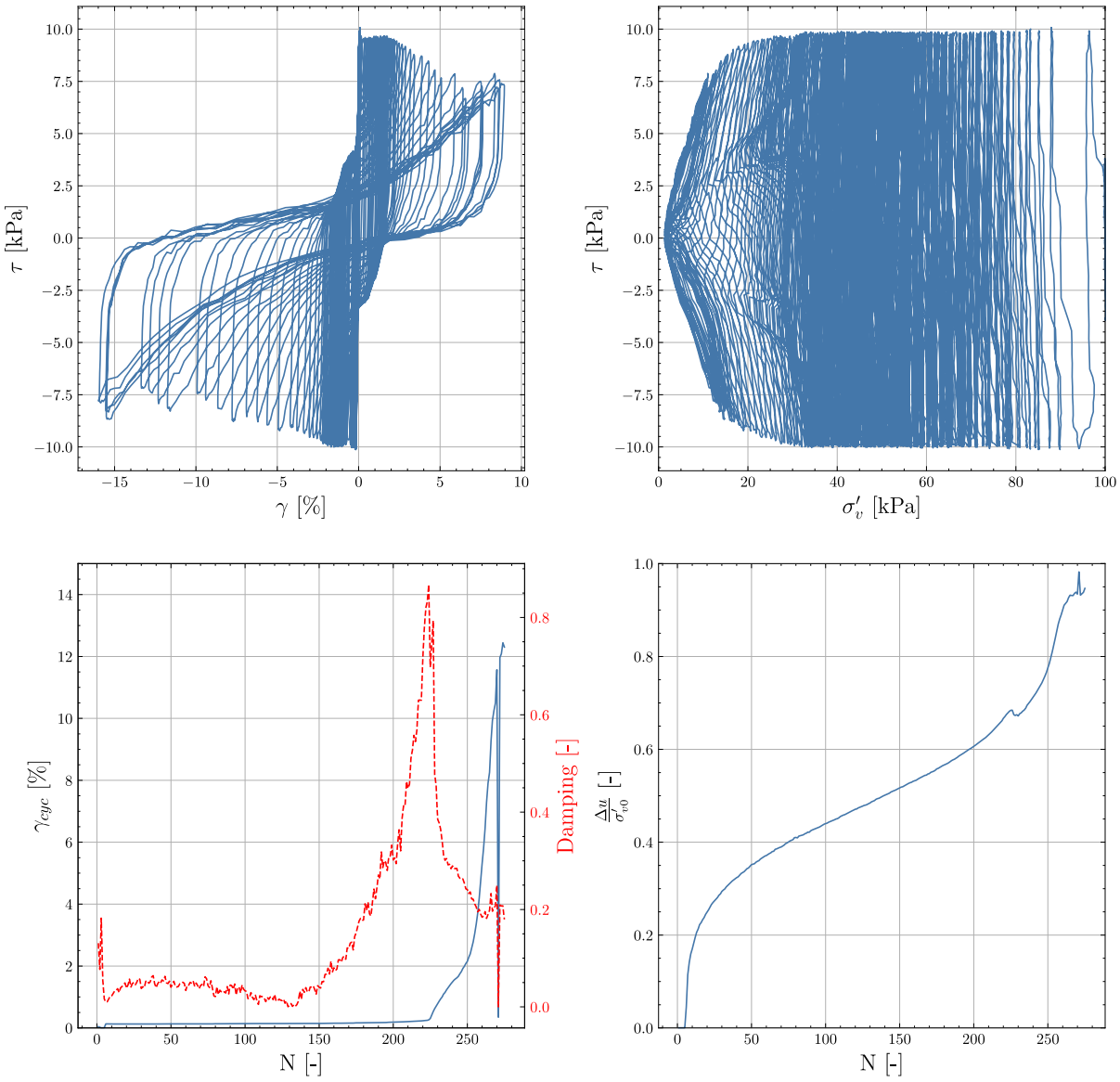

Test 26: Cyclic Behaviour of Eemian Sand under CSR of 0.1, Consolidation Pressure of 100 kPa, and Relative Density of 80%

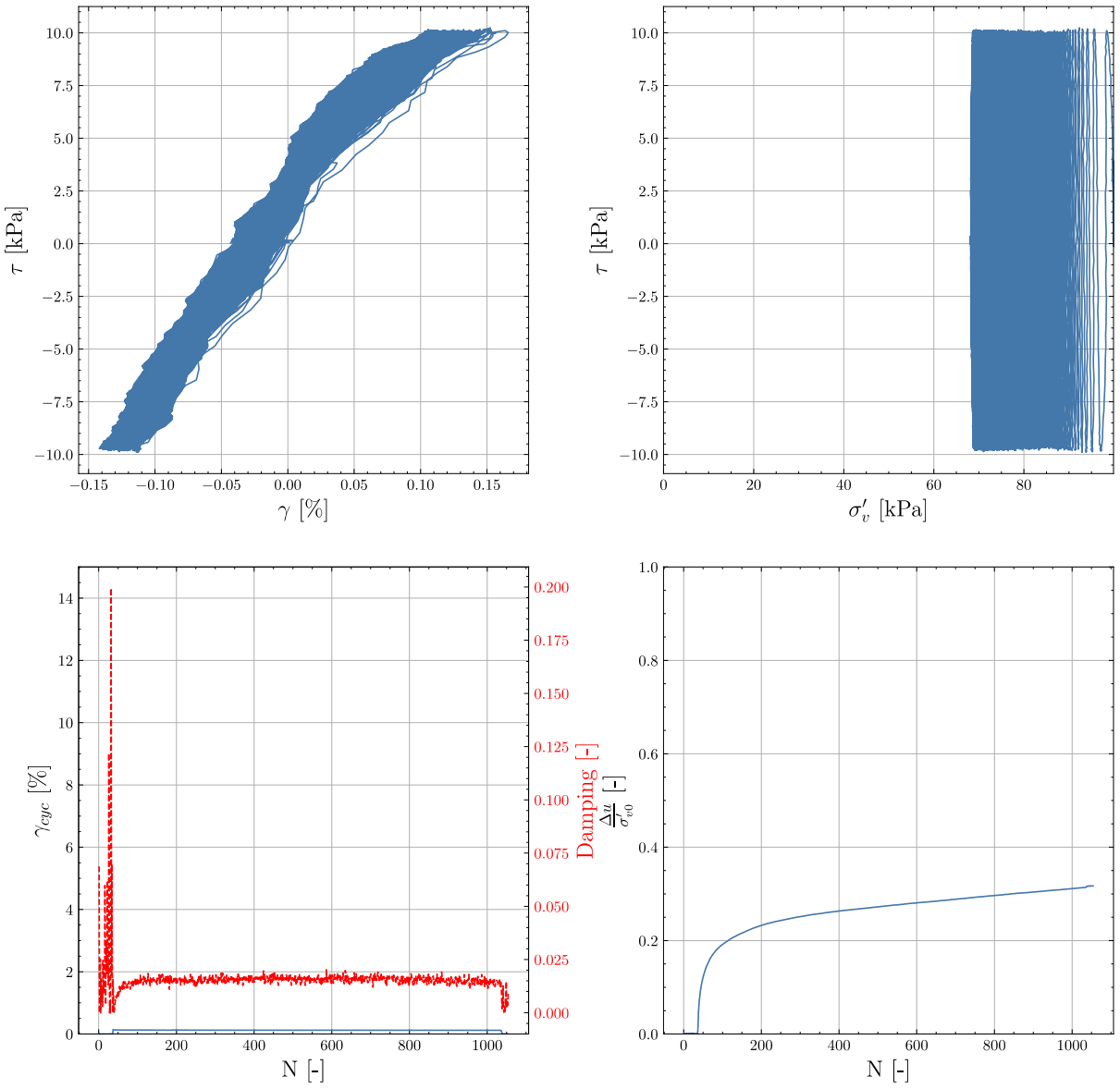

Test 27: Cyclic Behaviour of Eemian Sand under CSR of 0.1, Consolidation Pressure of 150 kPa, and Relative Density of 55%

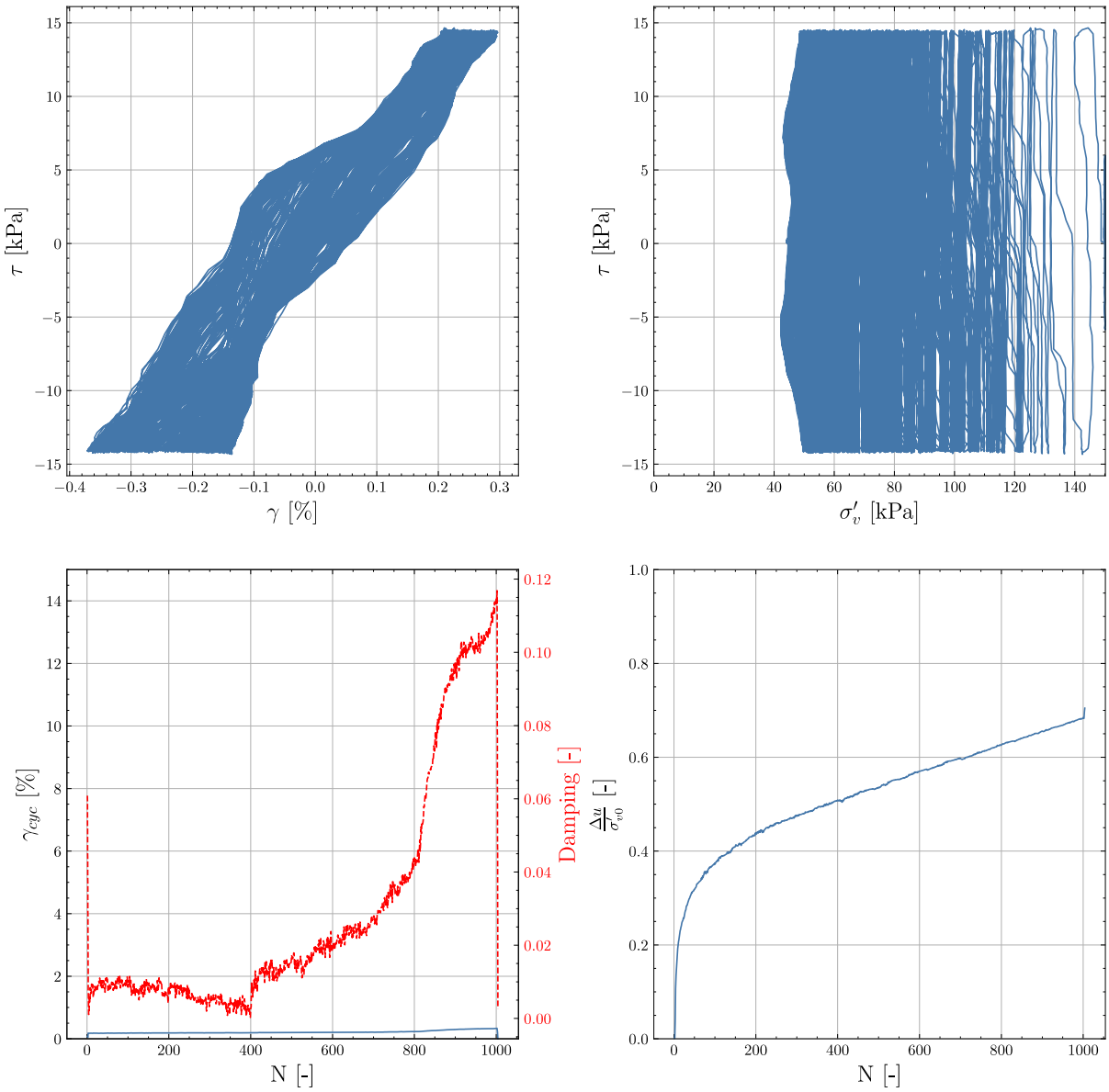

Test 28: Cyclic Behaviour of Eemian Sand under CSR of 0.1, Consolidation Pressure of 150 kPa, and Relative Density of 80%

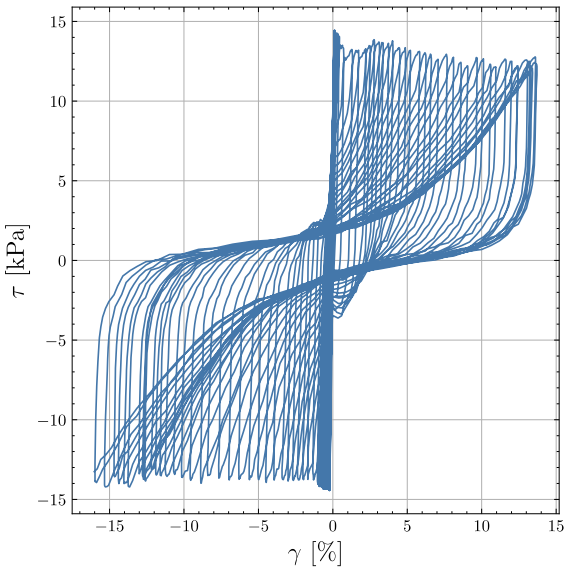

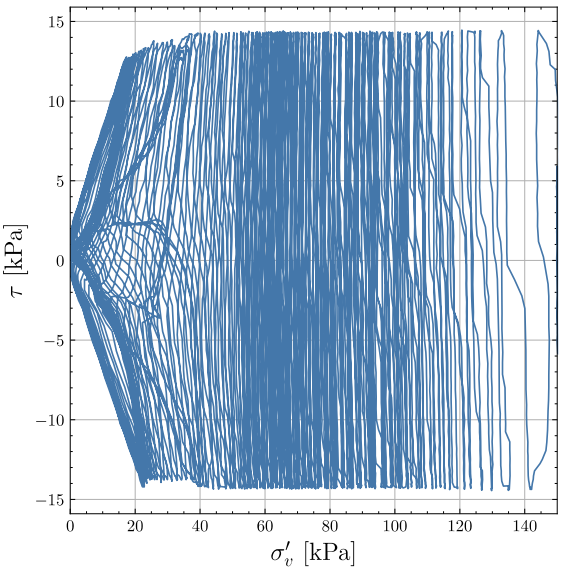

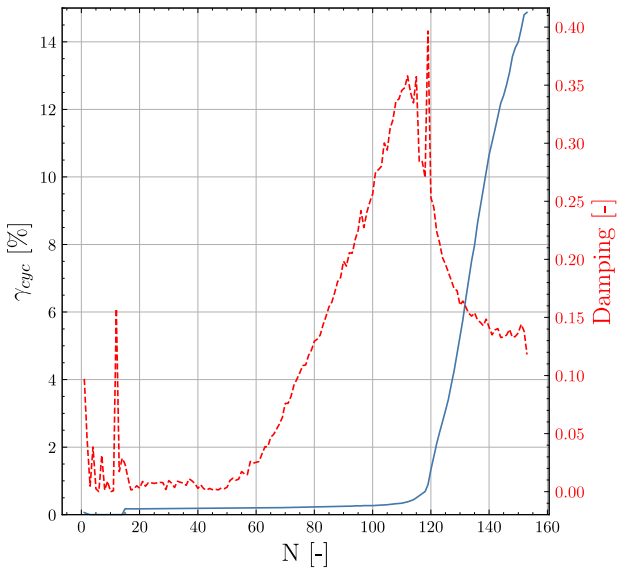

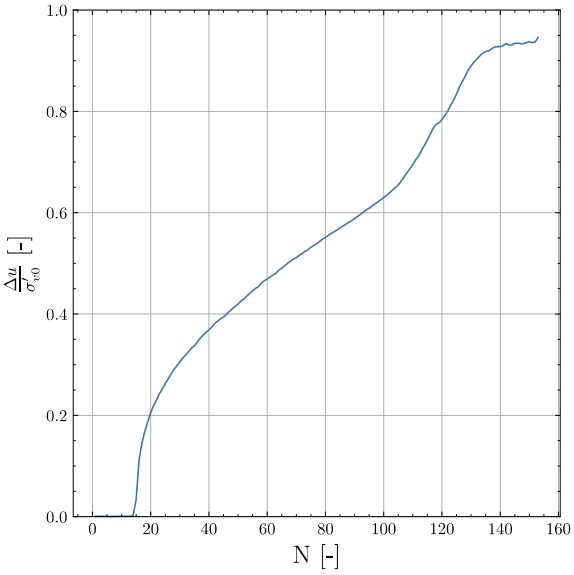

Test 29: Cyclic Behaviour of Eemian Sand under CSR of 0.1, Consolidation Pressure of 250 kPa, and Relative Density of 55%

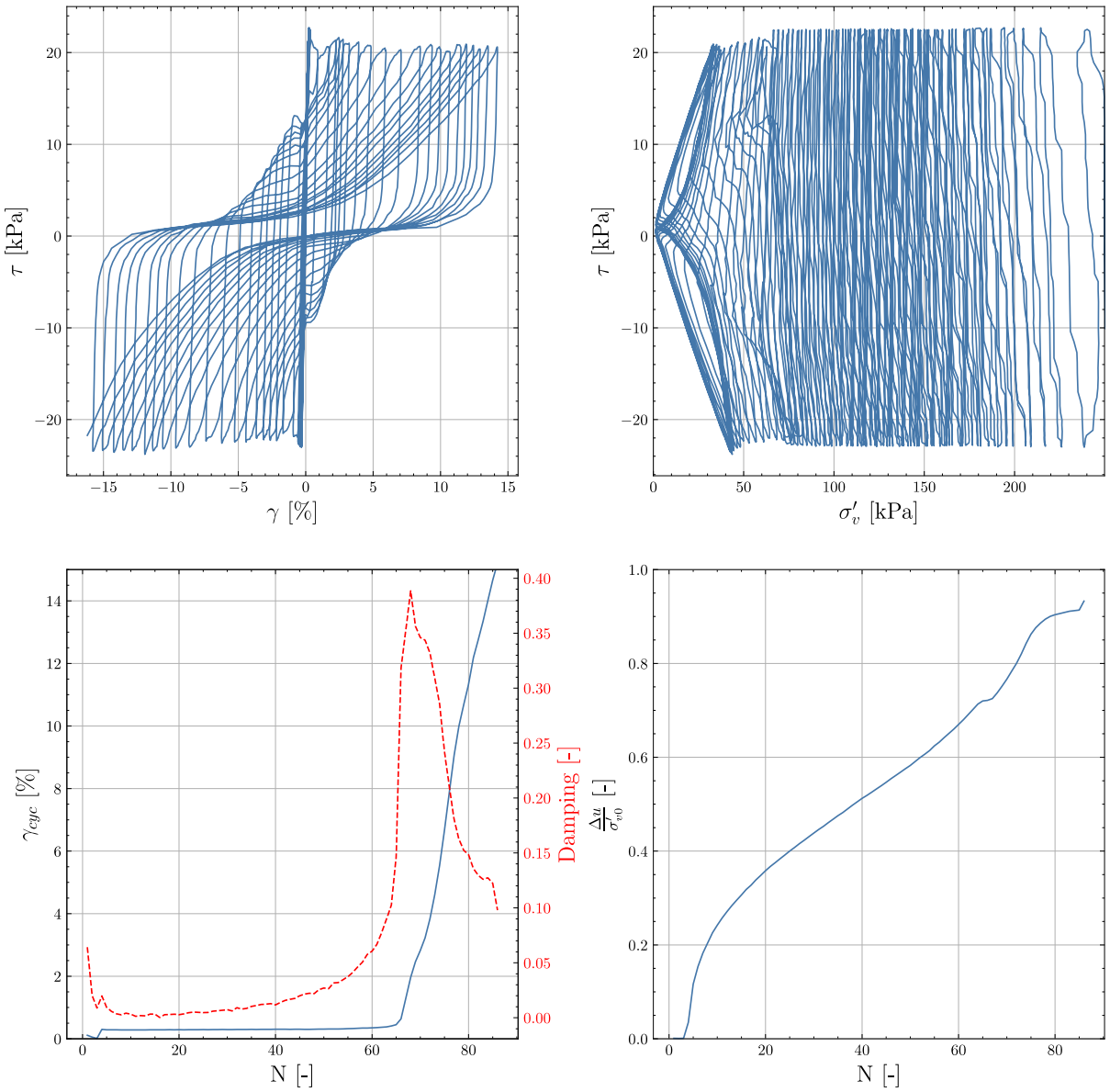

Test 30: Cyclic Behaviour of Eemian Sand under CSR of 0.1, Consolidation Pressure of 250 kPa, and Relative Density of 80%

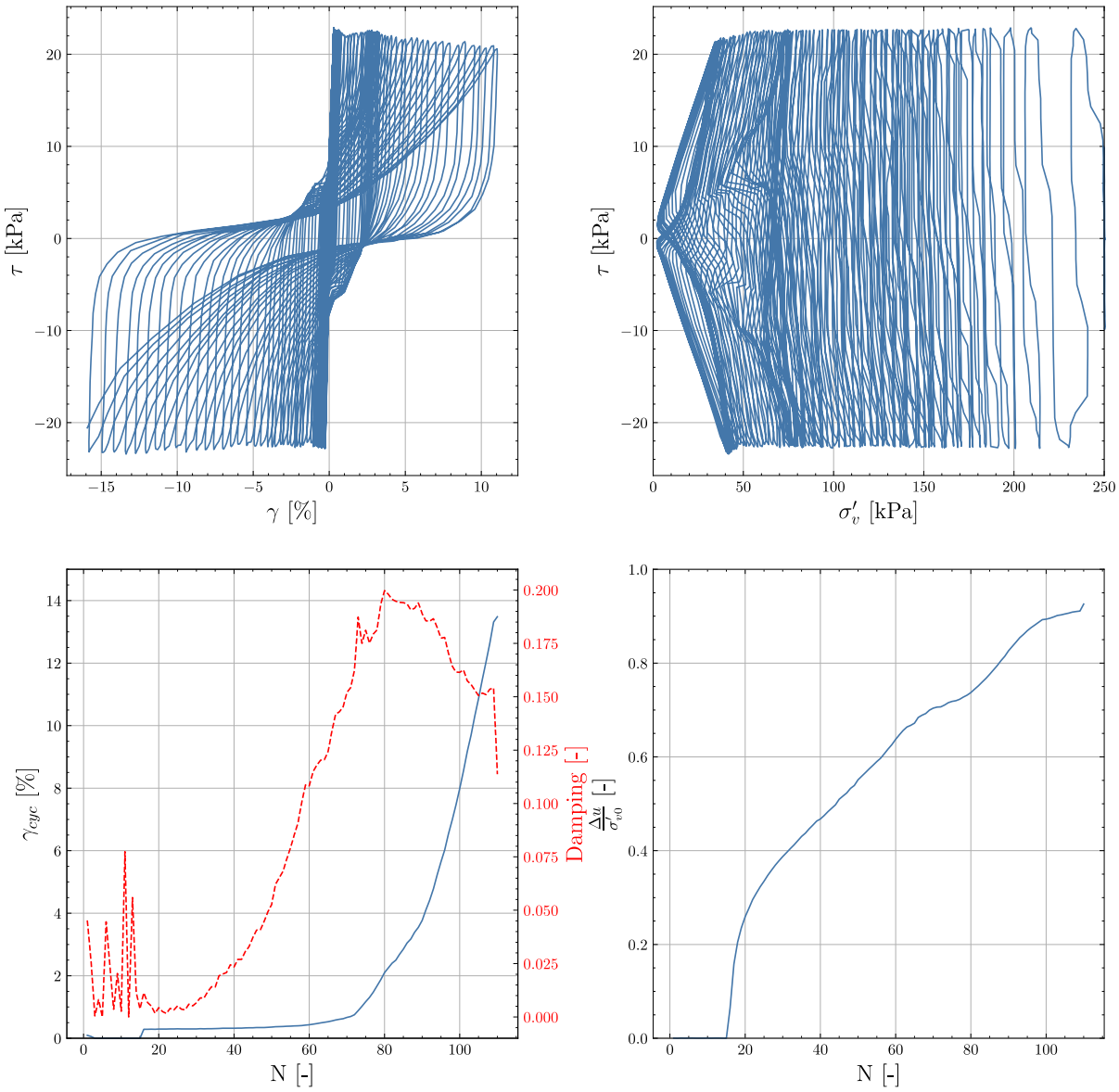

Test 31: Cyclic Behaviour of Eemian Sand under CSR of 0.1, Consolidation Pressure of 500 kPa, and Relative Density of 55%

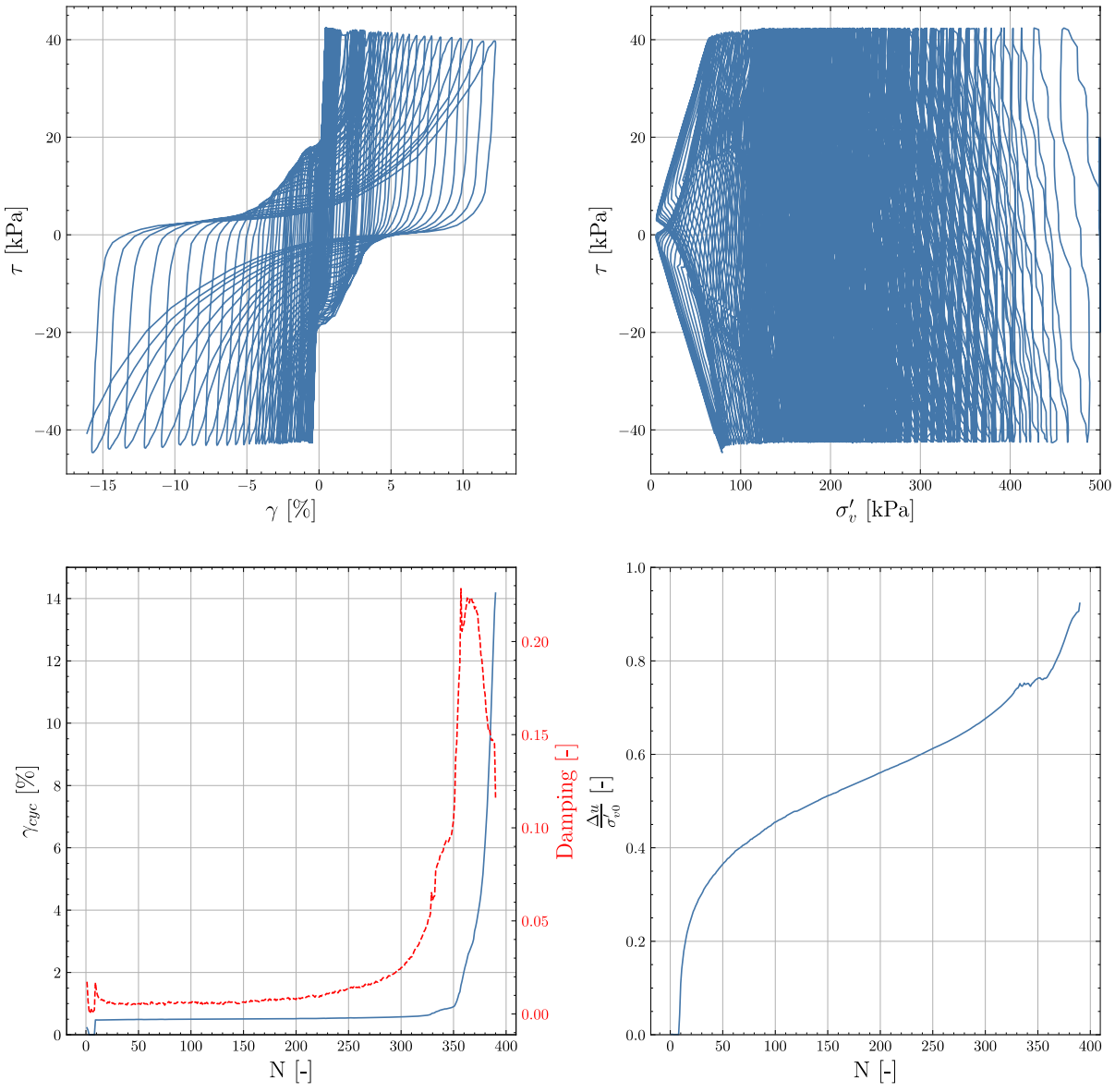

Test 33: Cyclic Behaviour of Eemian Sand under CSR of 0.15, Consolidation Pressure of 100 kPa, and Relative Density of 55%

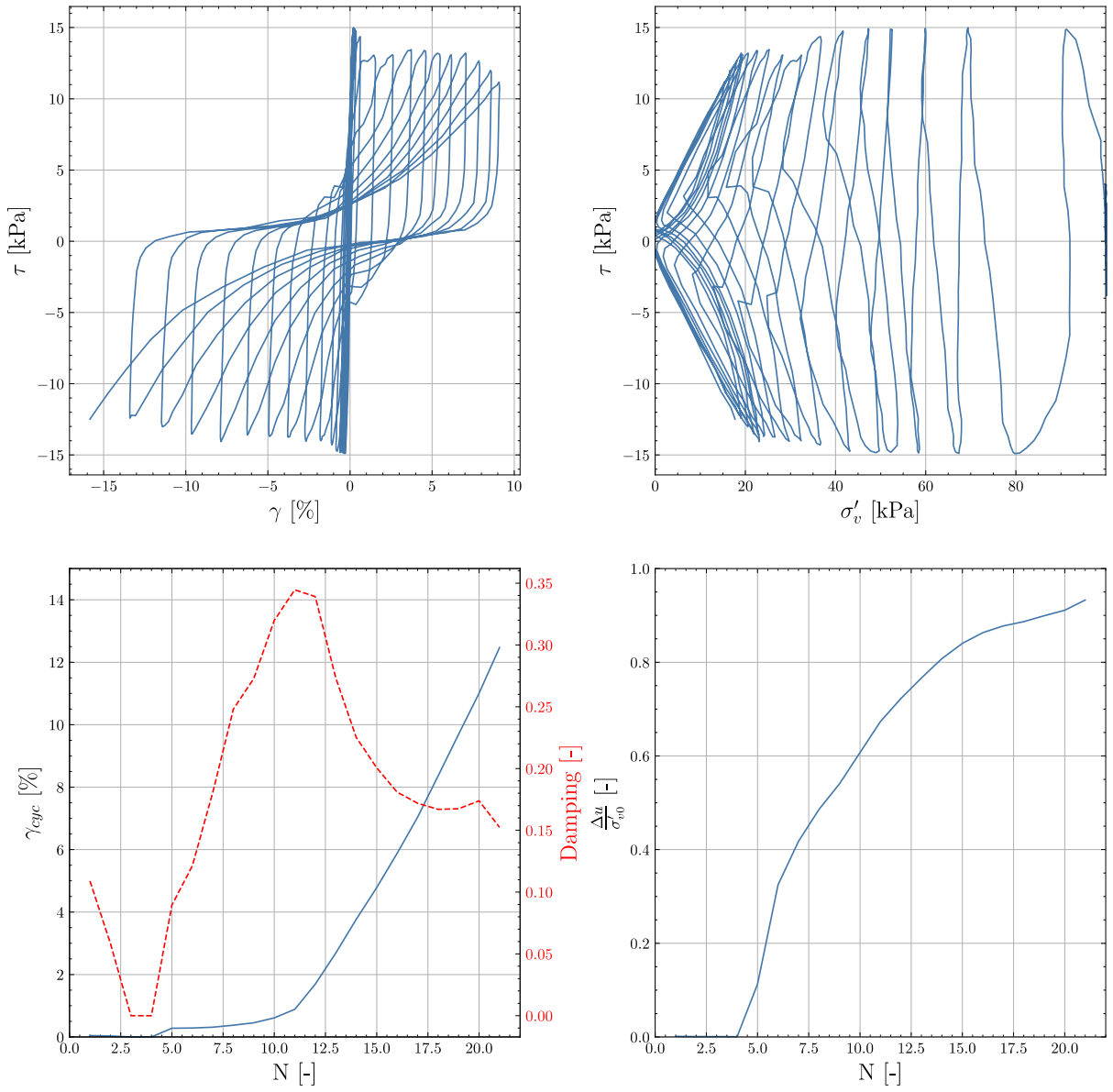

Test 34: Cyclic Behaviour of Eemian Sand under CSR of 0.15, Consolidation Pressure of 100 kPa, and Relative Density of 80%

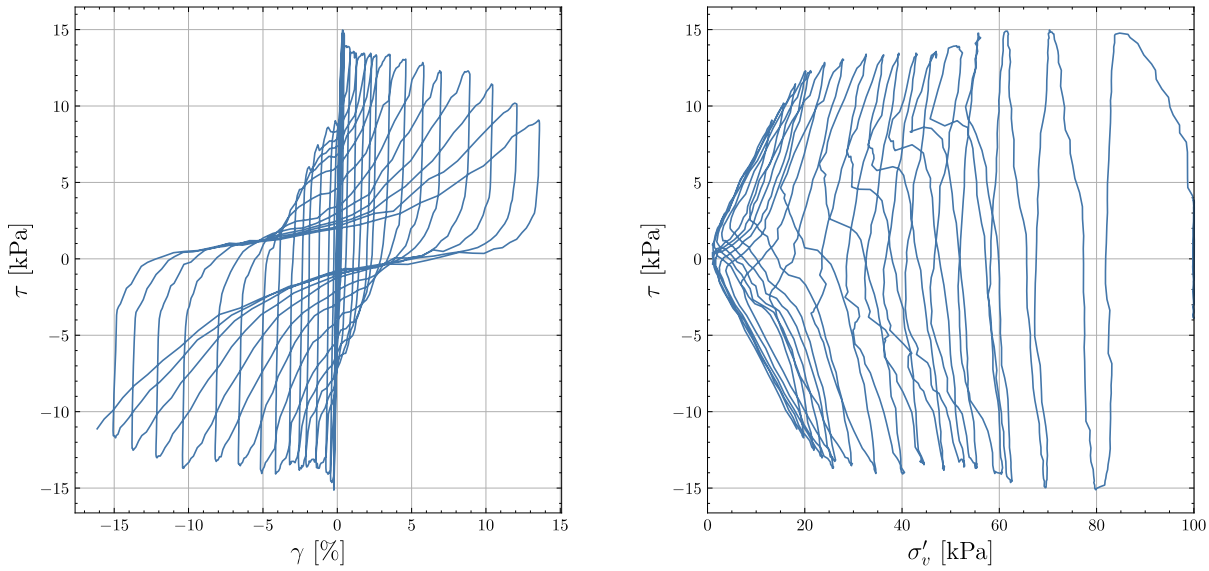

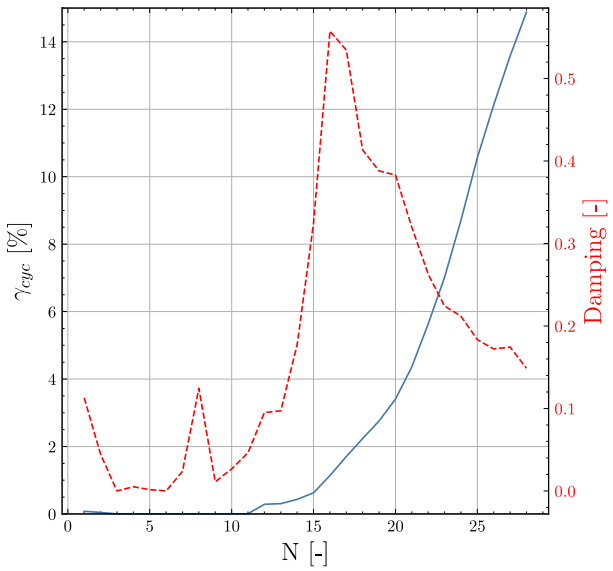

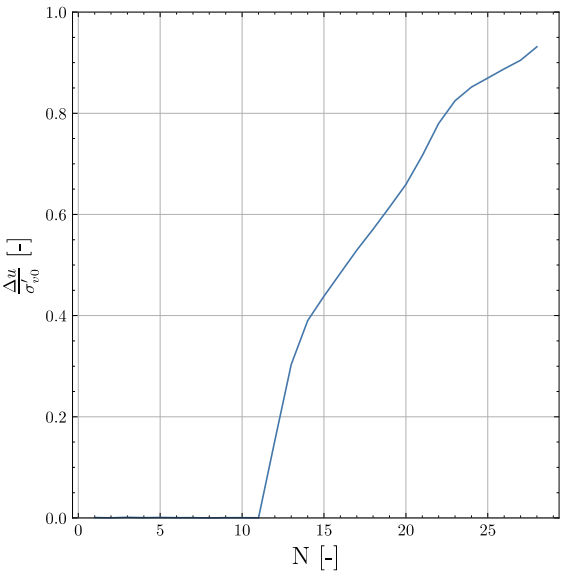

Test 35: Cyclic Behaviour of Eemian Sand under CSR of 0.15, Consolidation Pressure of 150 kPa, and Relative Density of 55%

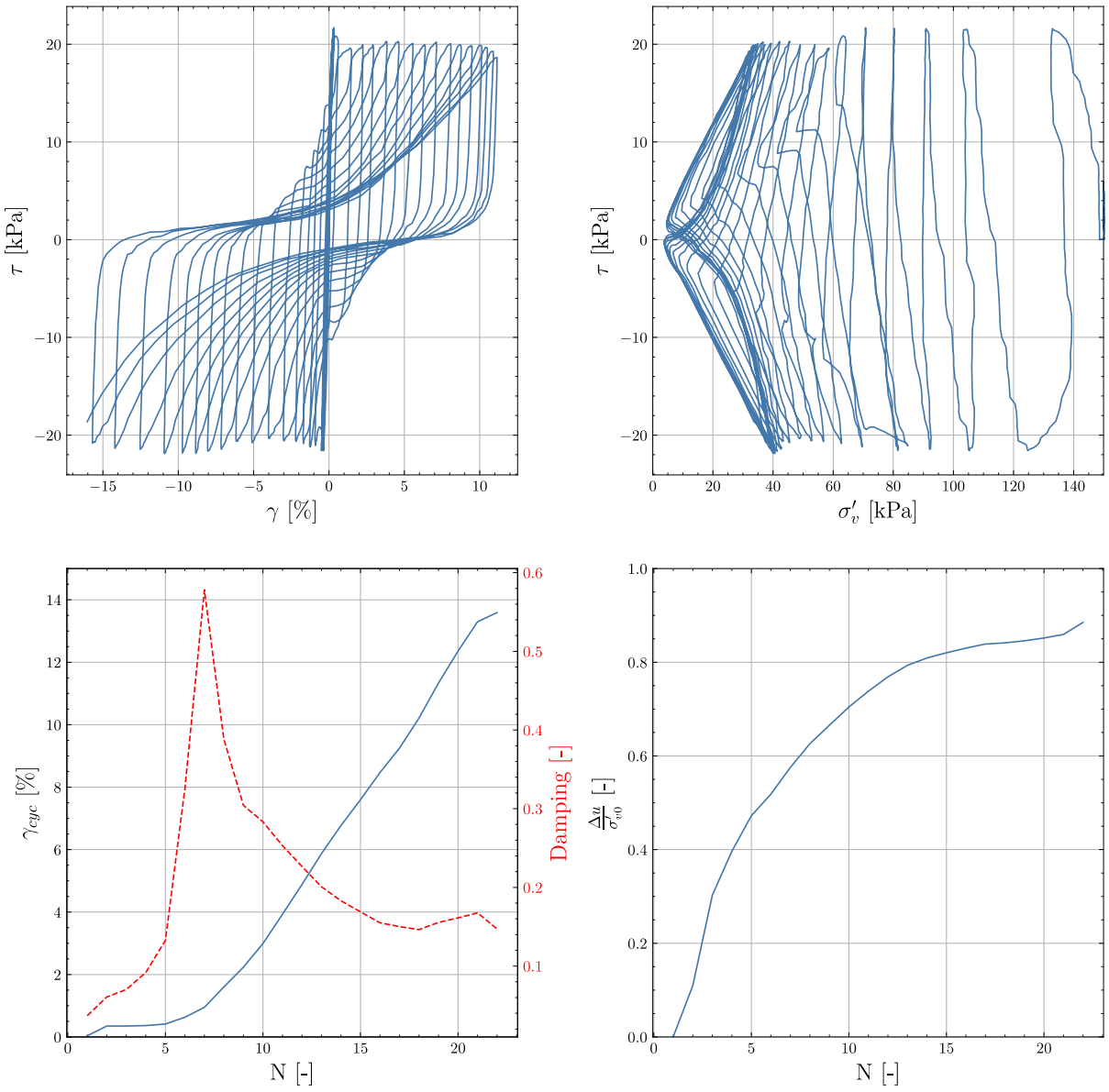

Test 36: Cyclic Behaviour of Eemian Sand under CSR of 0.15, Consolidation Pressure of 150 kPa, and Relative Density of 80%

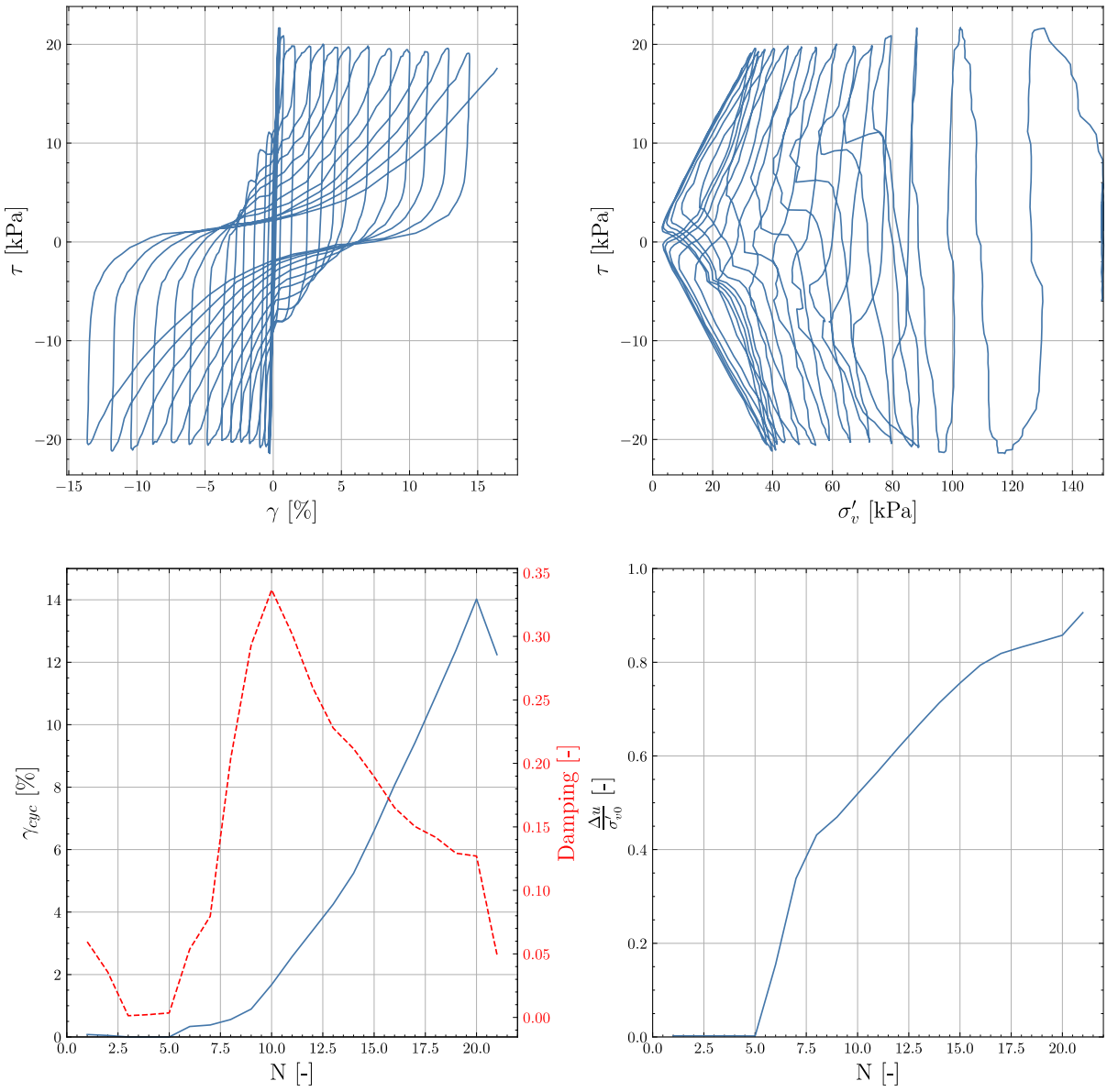

Test 37: Cyclic Behaviour of Eemian Sand under CSR of 0.15, Consolidation Pressure of 250 kPa, and Relative Density of 55%

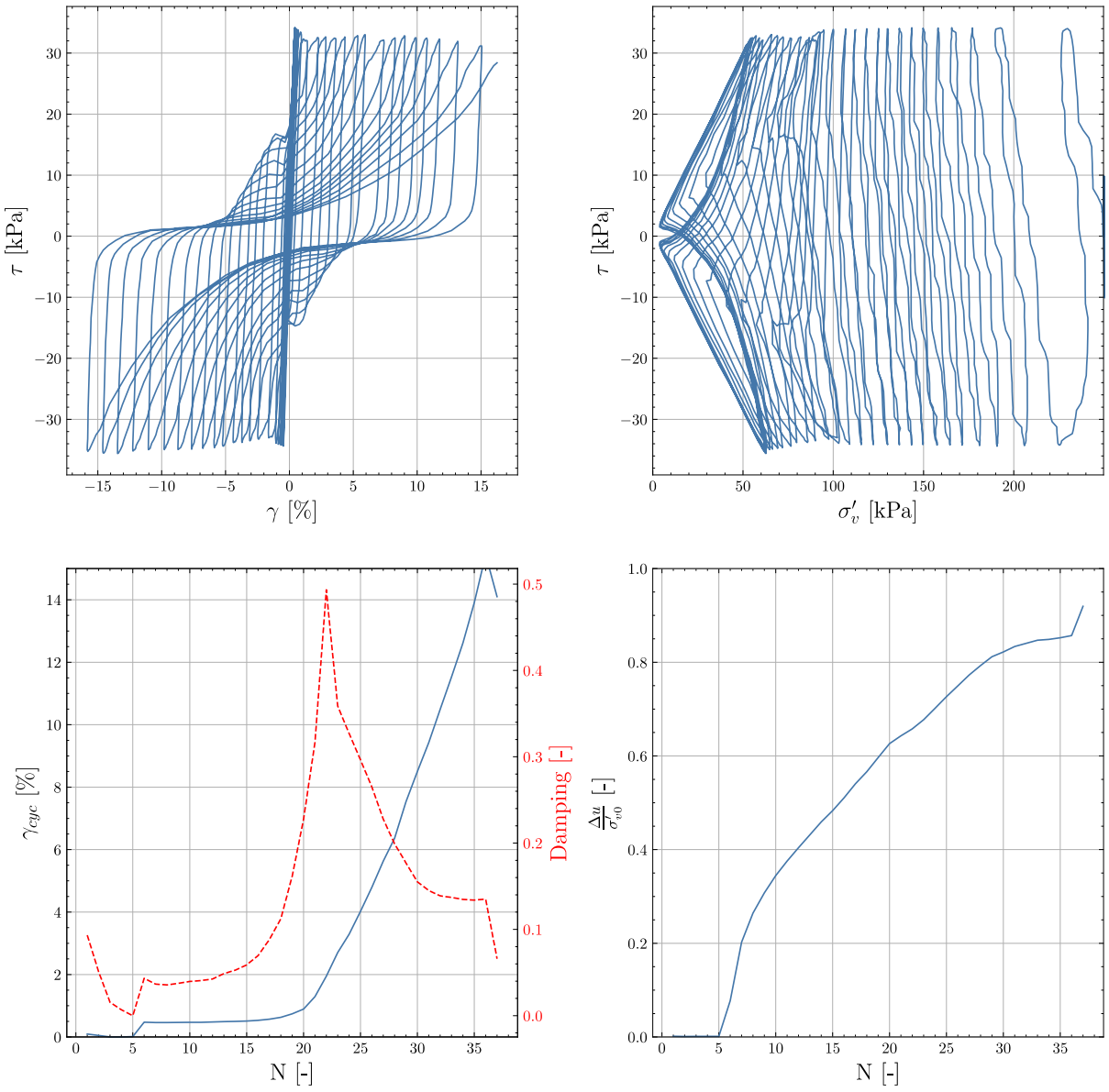

Test 38: Cyclic Behaviour of Eemian Sand under CSR of 0.15, Consolidation Pressure of 250 kPa, and Relative Density of 80%

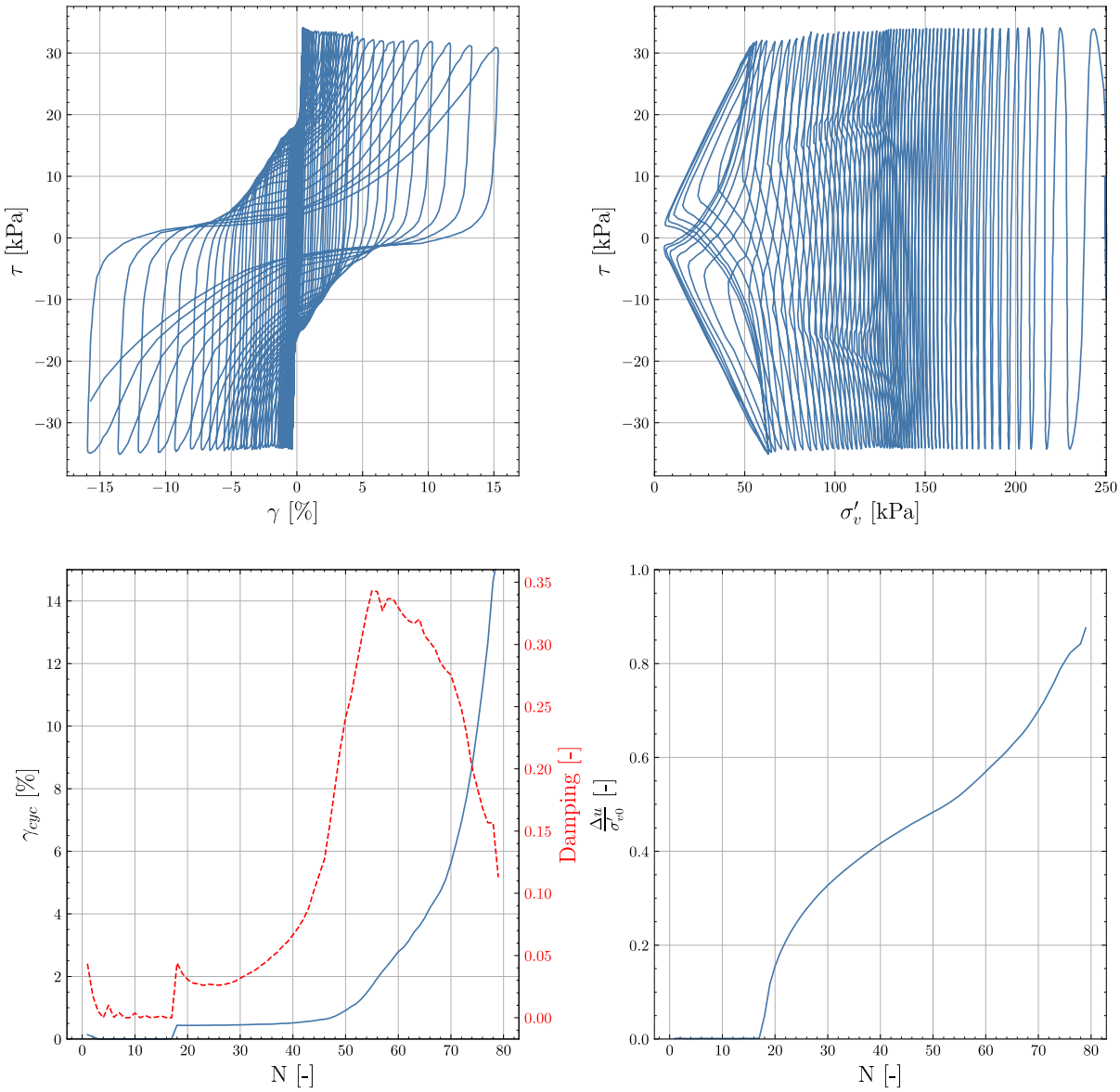

Test 39: Cyclic Behaviour of Eemian Sand under CSR of 0.15, Consolidation Pressure of 500 kPa, and Relative Density of 55%

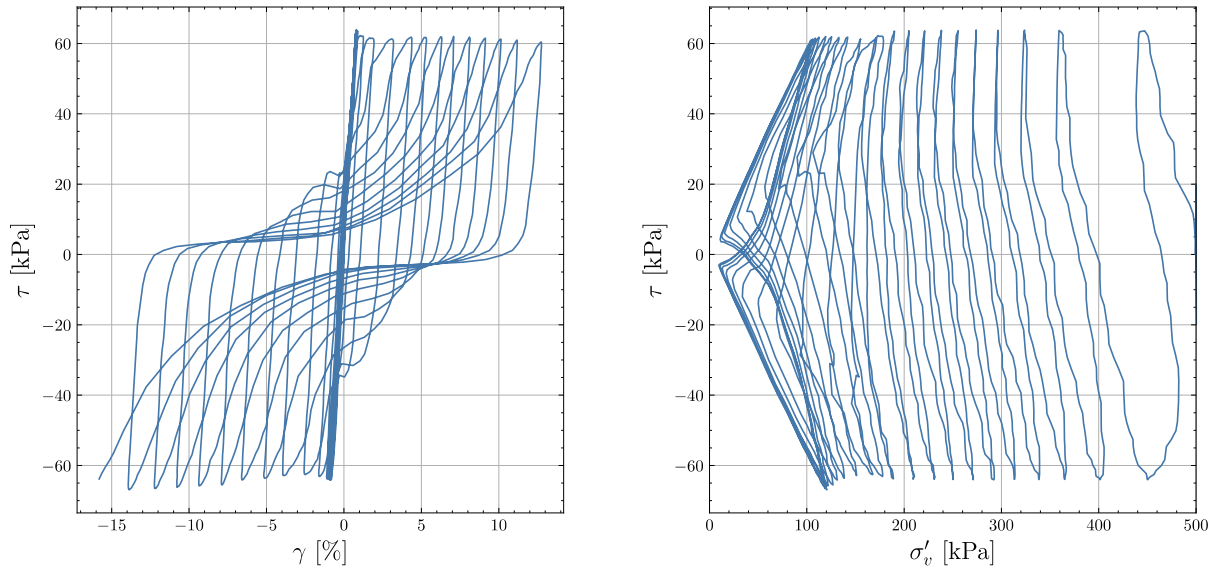

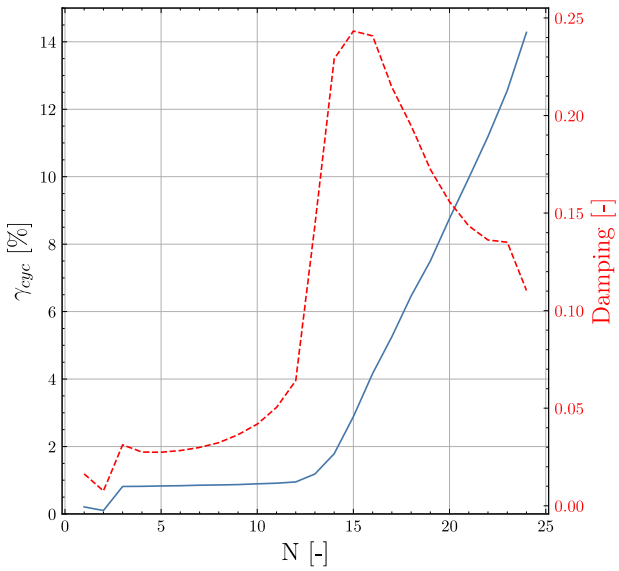

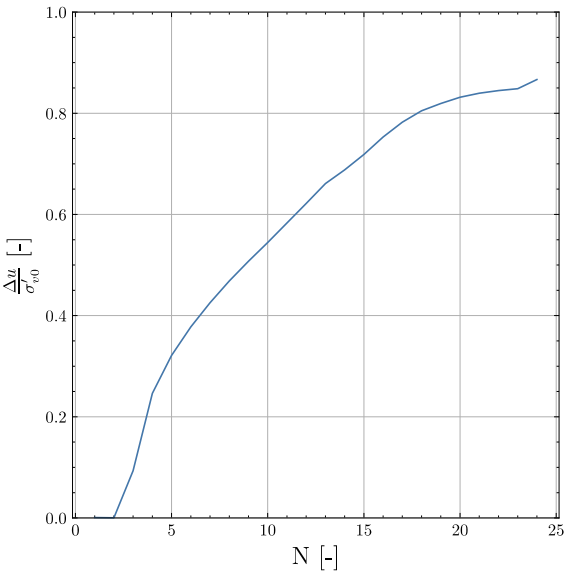

Test 40: Cyclic Behaviour of Eemian Sand under CSR of 0.15, Consolidation Pressure of 500 kPa, and Relative Density of 80%

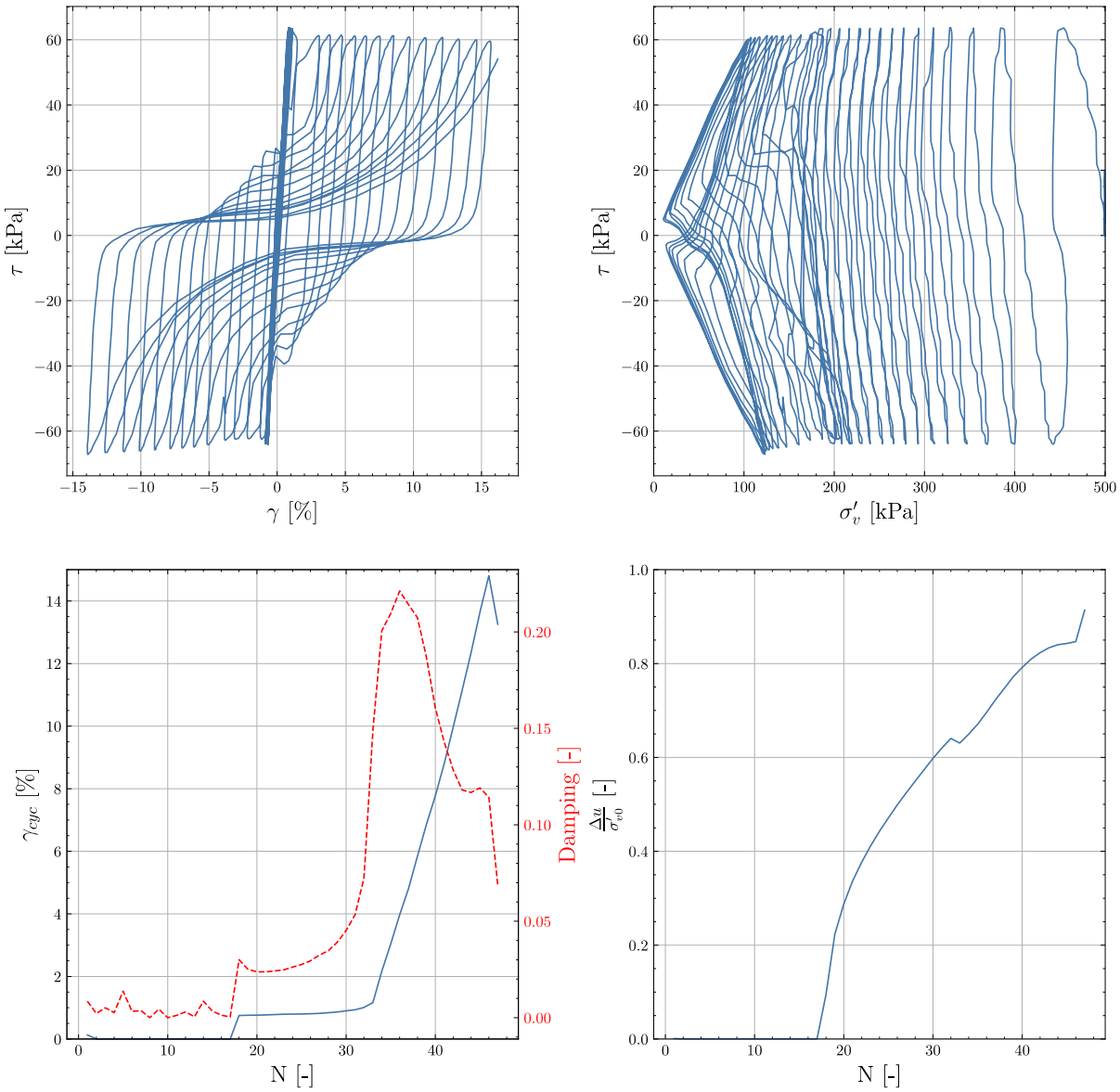

Test 41: Cyclic Behaviour of Eemian Sand under CSR of 0.2, Consolidation Pressure of 100 kPa, and Relative Density of 55%

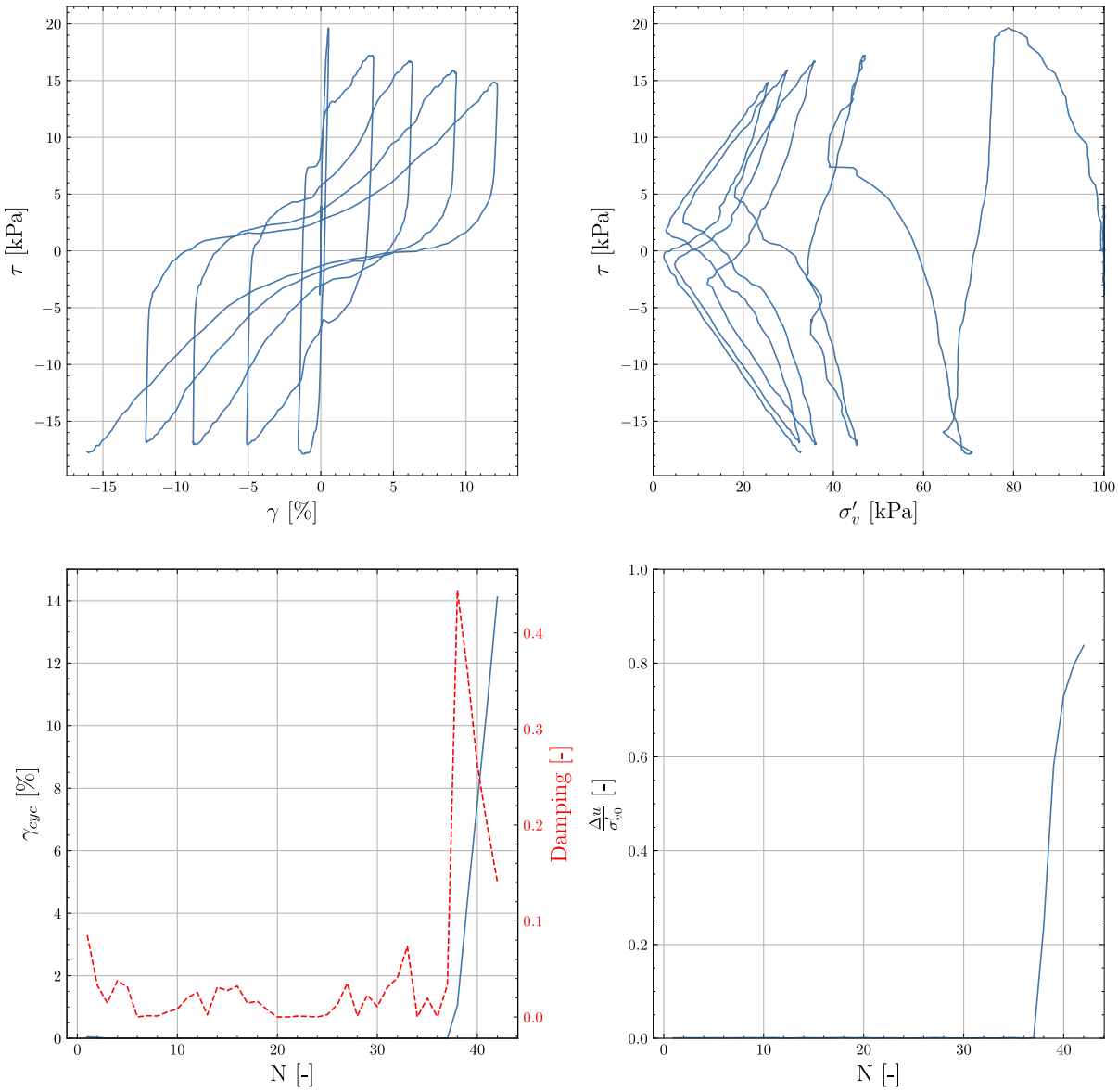

Test 42: Cyclic Behaviour of Eemian Sand under CSR of 0.2, Consolidation Pressure of 100 kPa, and Relative Density of 80%

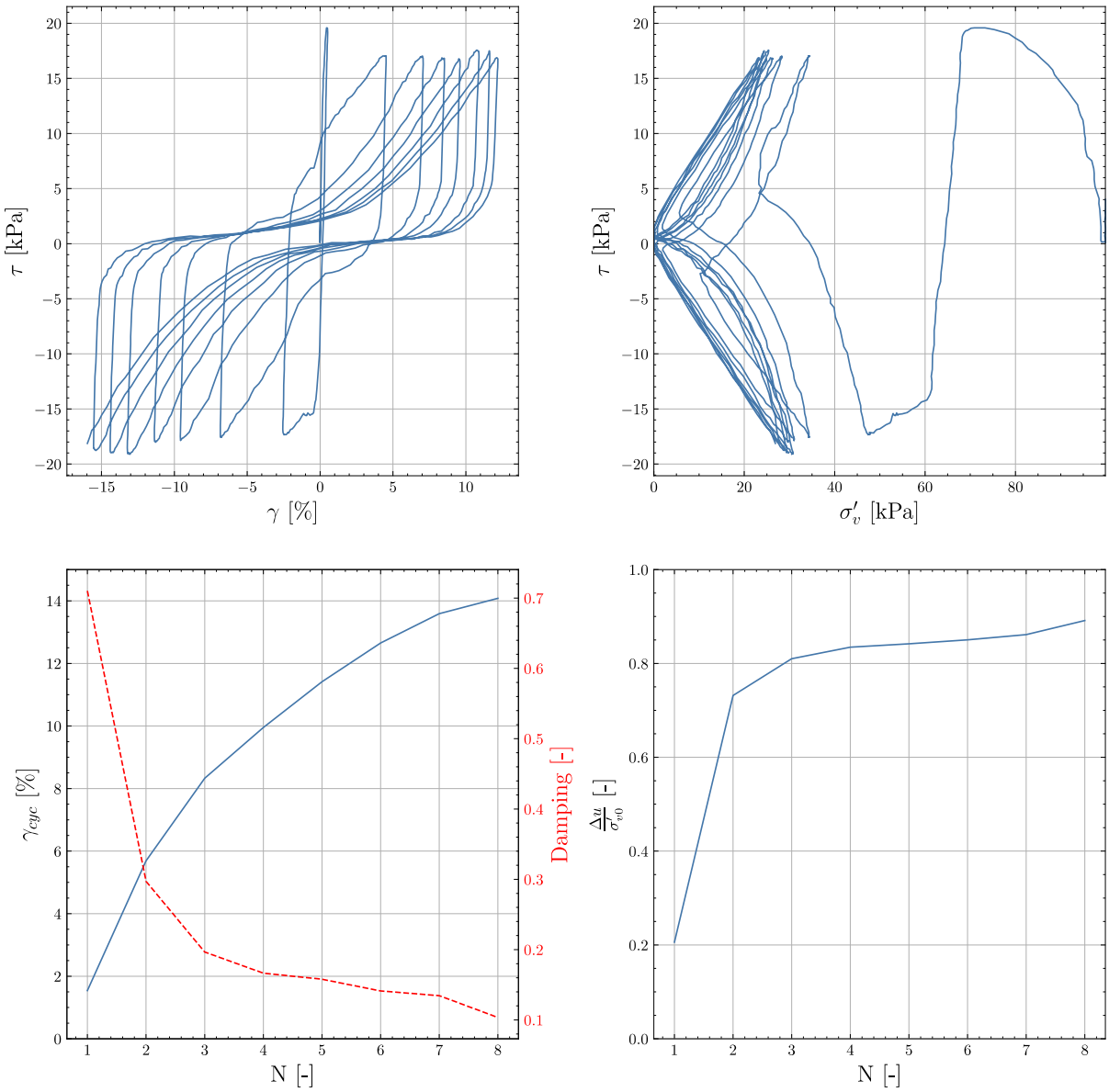

Test 43: Cyclic Behaviour of Eemian Sand under CSR of 0.2, Consolidation Pressure of 150 kPa, and Relative Density of 55%

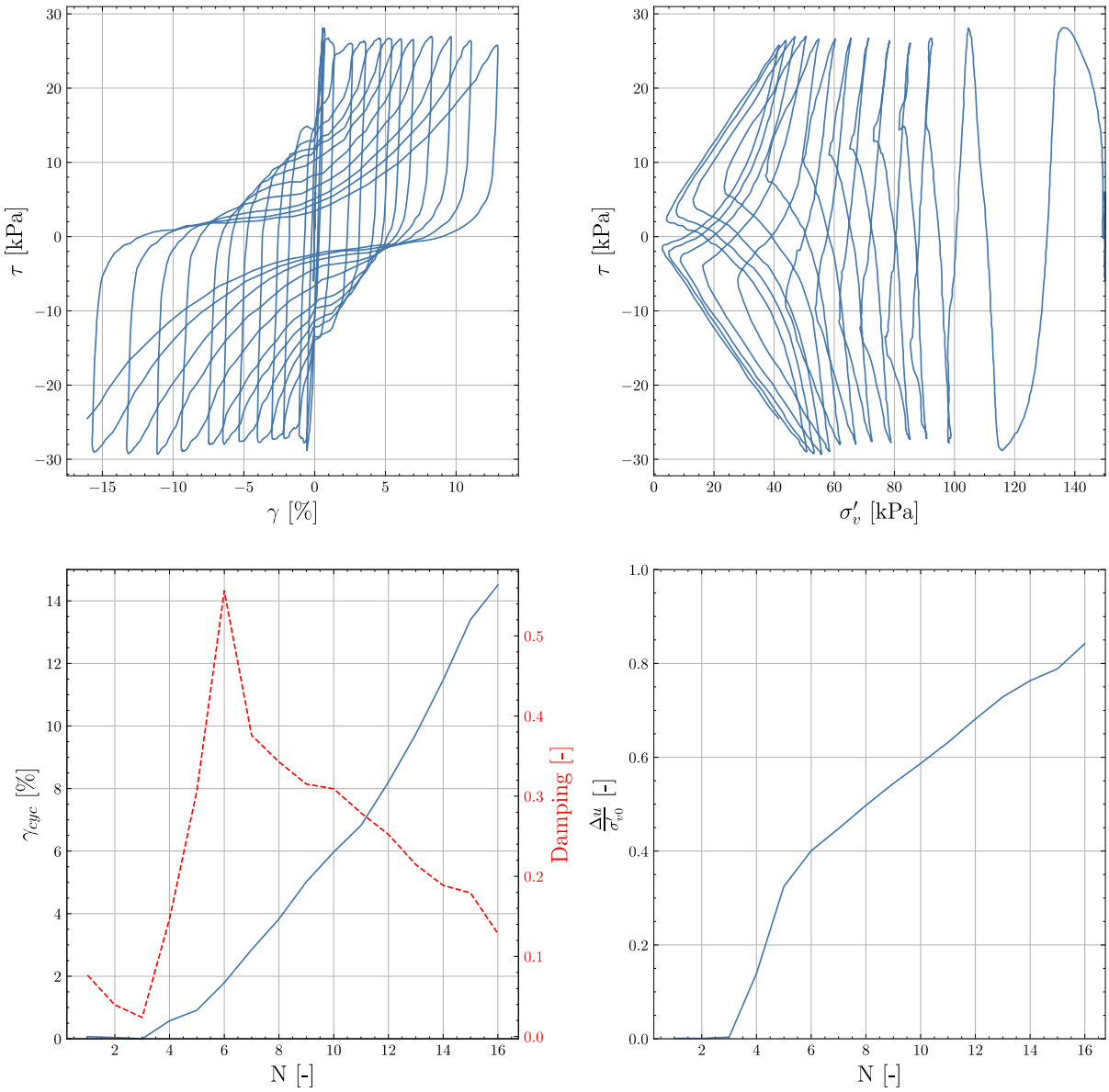

Test 44: Cyclic Behaviour of Eemian Sand under CSR of 0.2, Consolidation Pressure of 150 kPa, and Relative Density of 80%

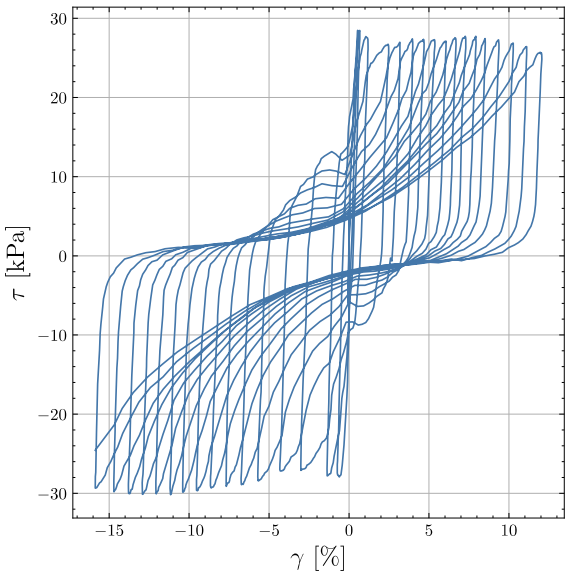

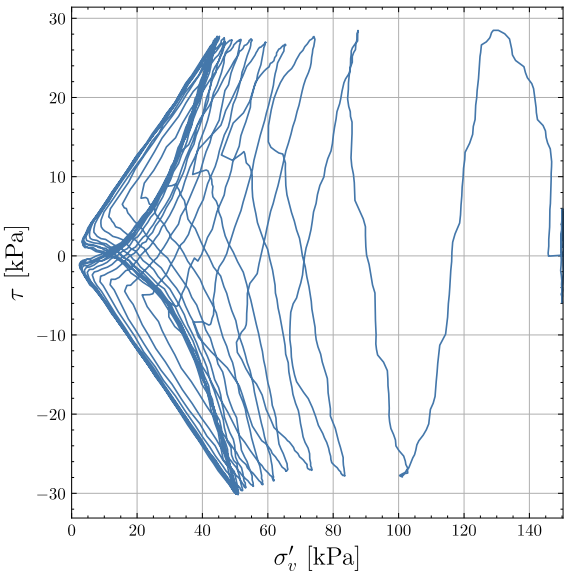

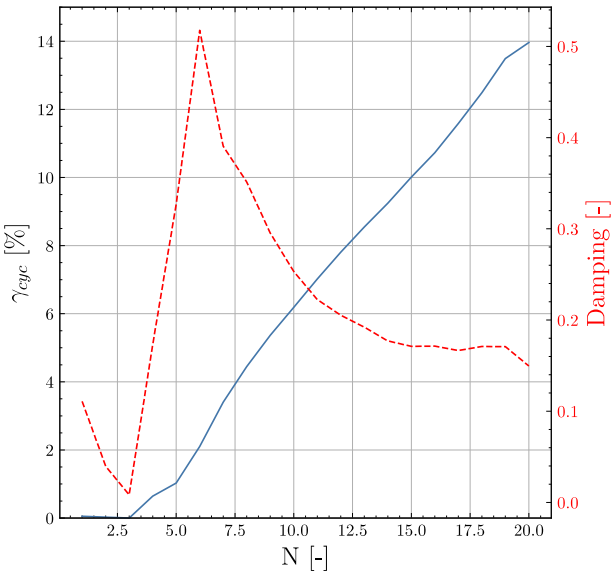

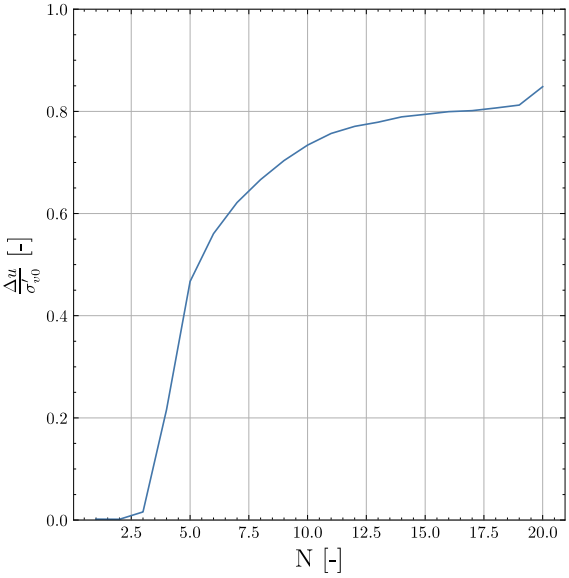

Test 45: Cyclic Behaviour of Eemian Sand under CSR of 0.2, Consolidation Pressure of 250 kPa, and Relative Density of 55%

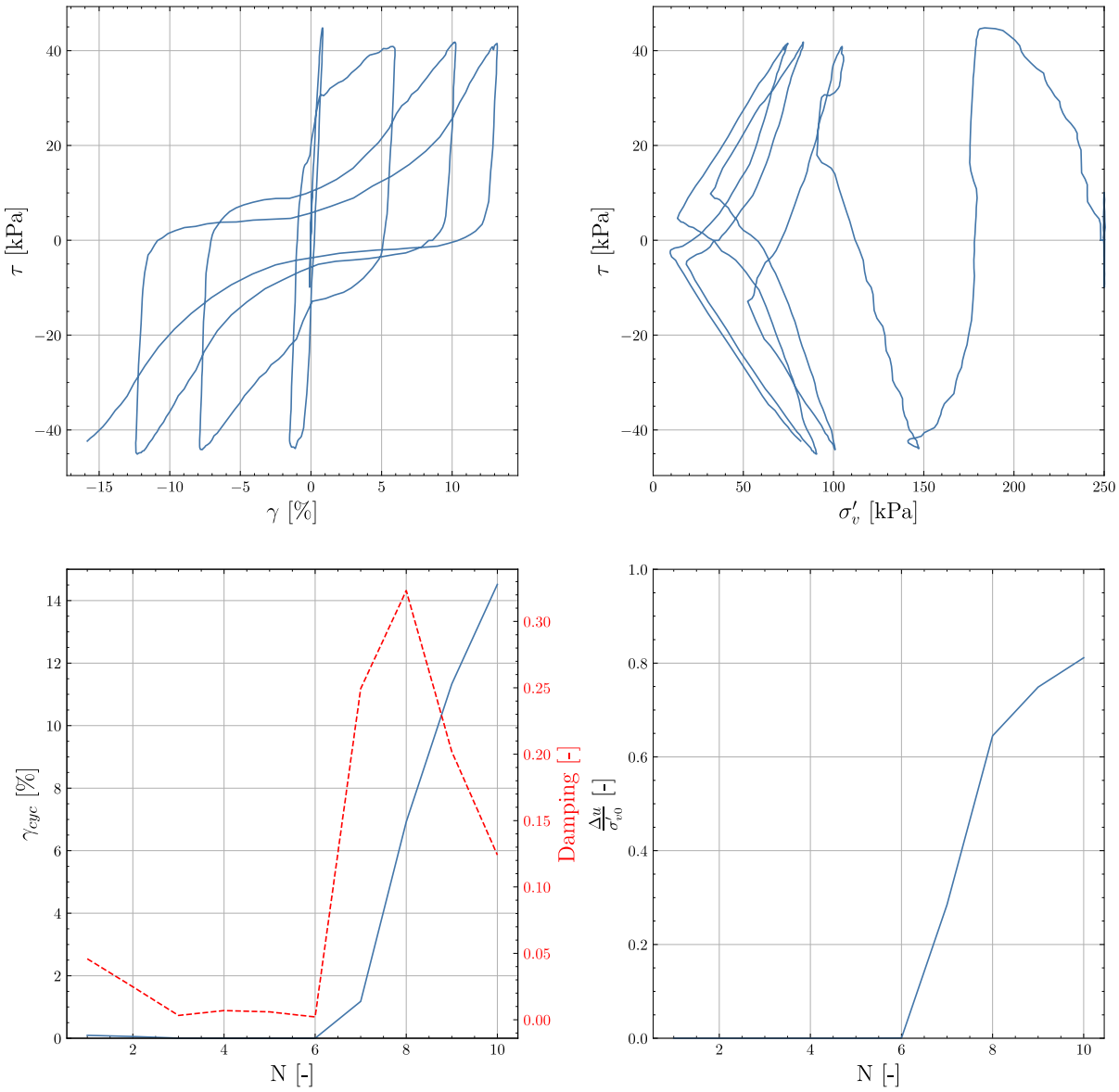

Test 46: Cyclic Behaviour of Eemian Sand under CSR of 0.2, Consolidation Pressure of 250 kPa, and Relative Density of 80%

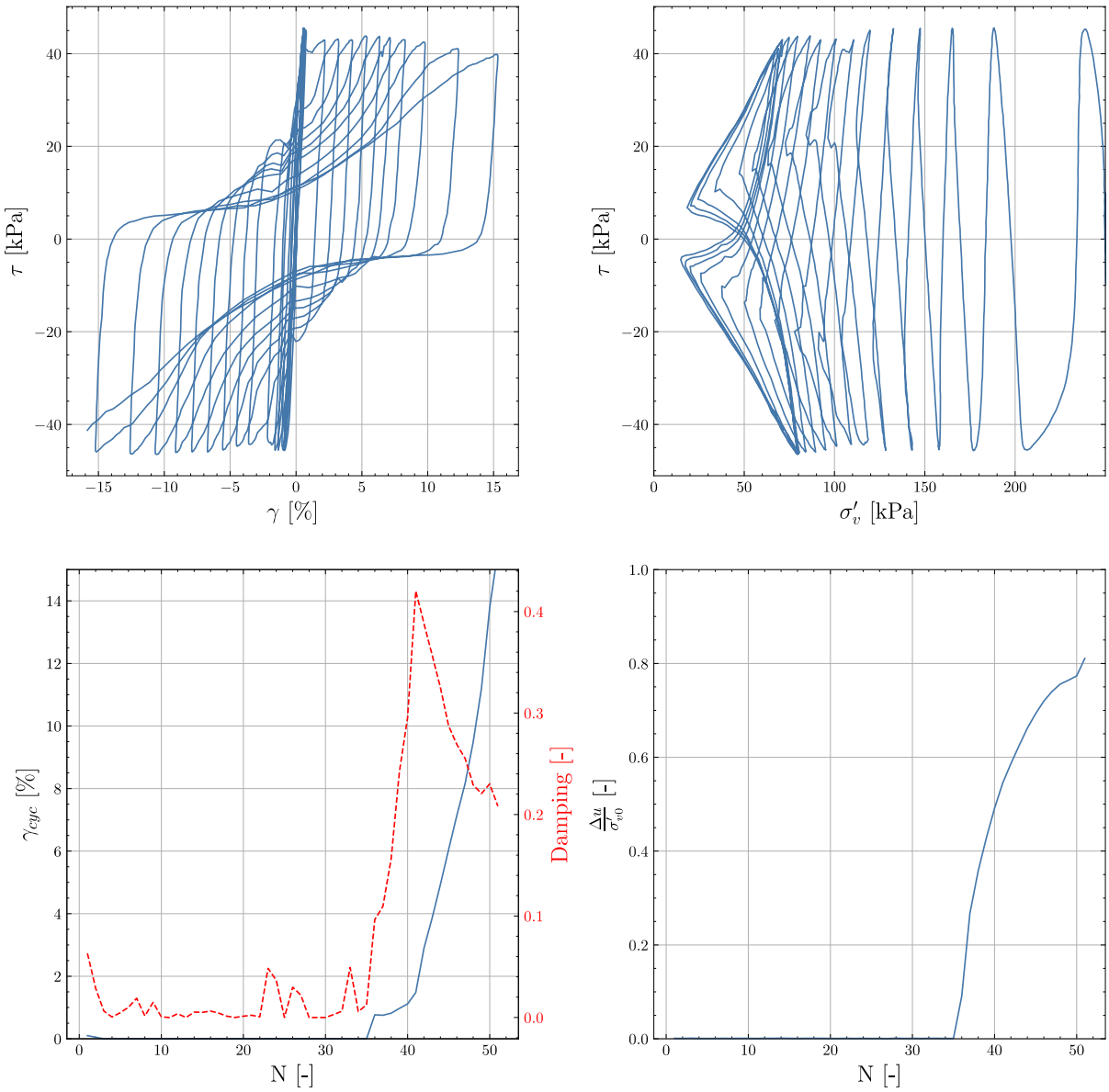

Test 47: Cyclic Behaviour of Eemian Sand under CSR of 0.2, Consolidation Pressure of 500 kPa, and Relative Density of 55%

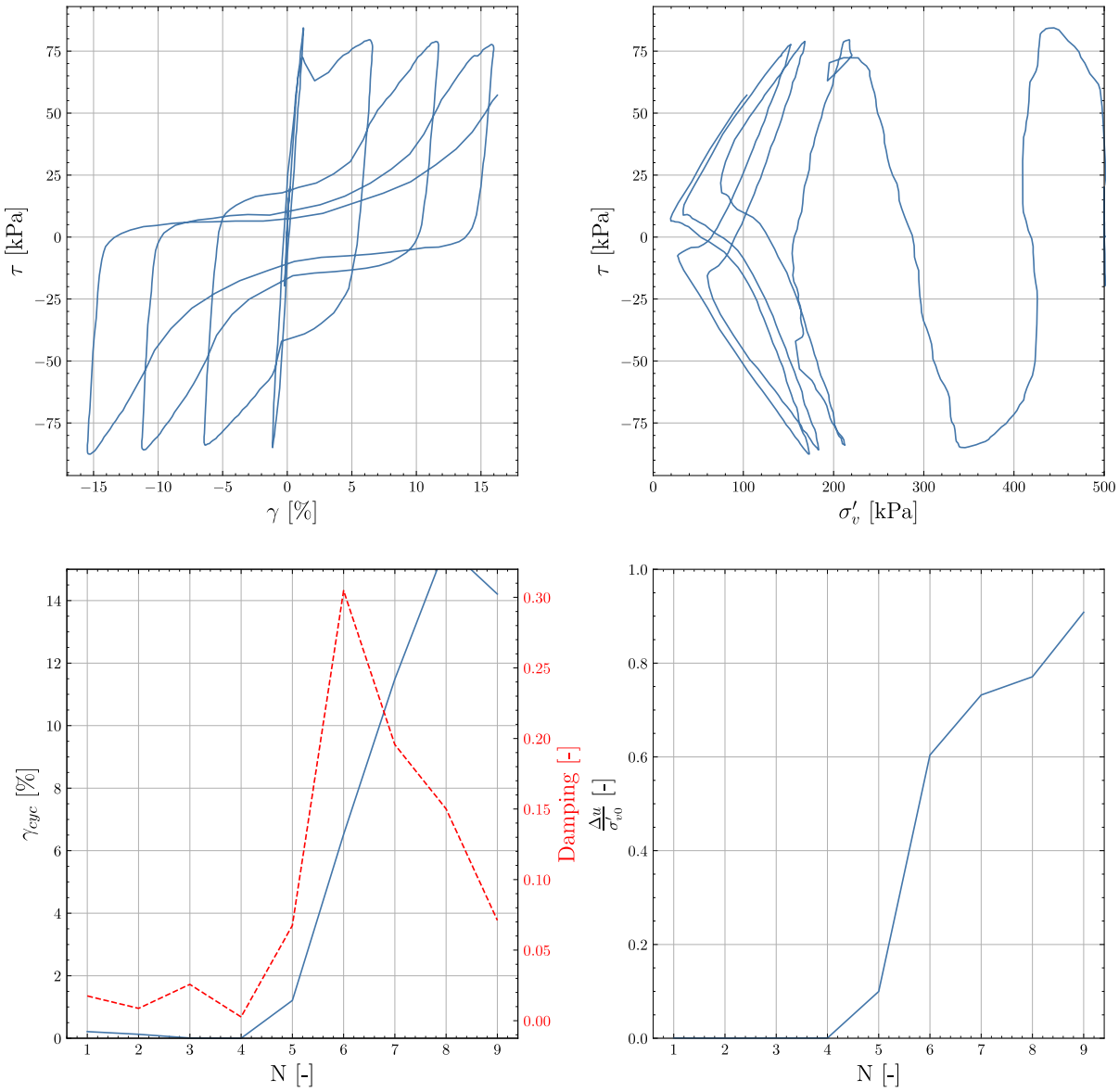

Test 48: Cyclic Behaviour of Eemian Sand under CSR of 0.2, Consolidation Pressure of 500 kPa, and Relative Density of 80%

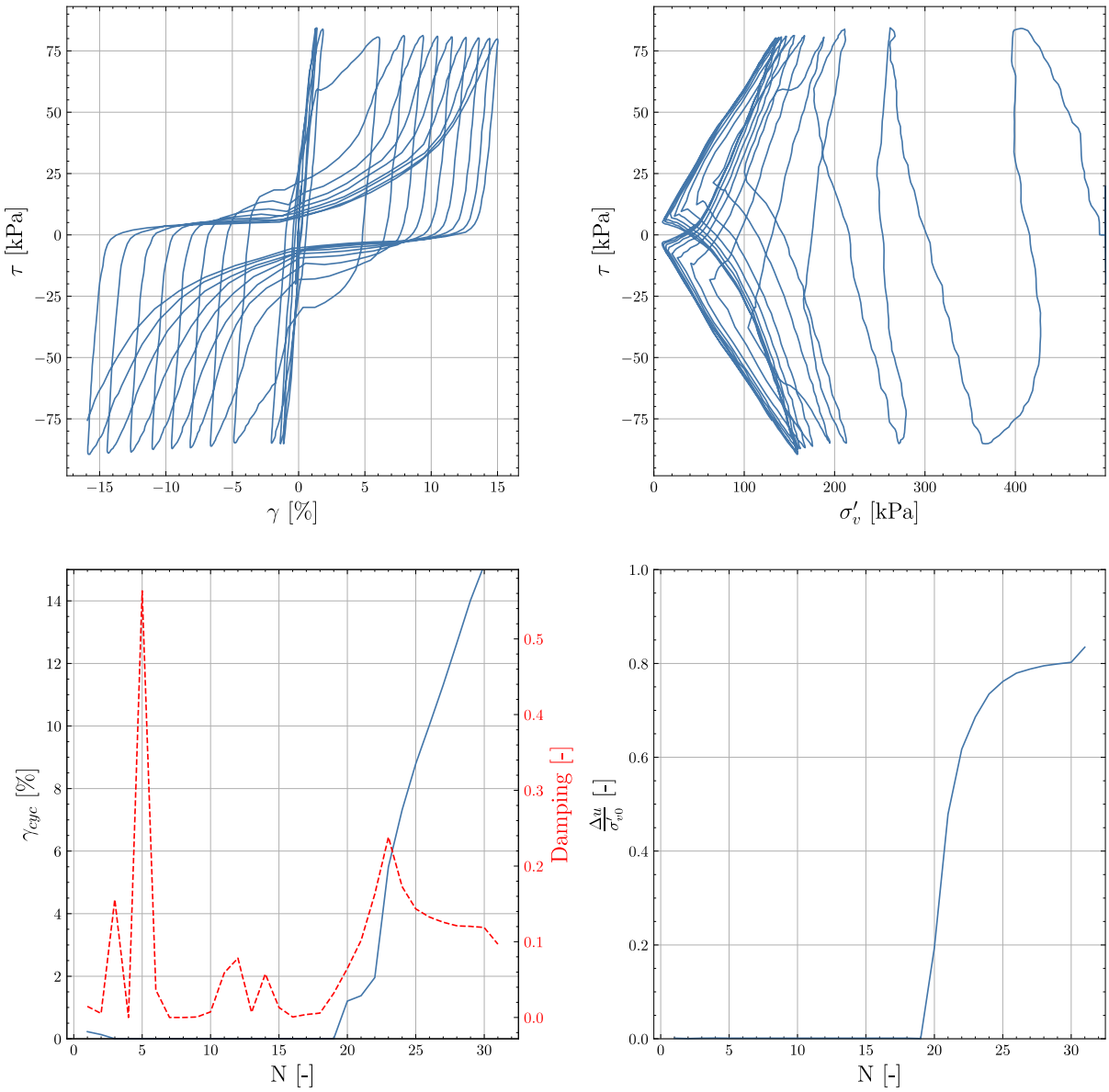

7.2 Appendix B: Strain Contours and Cyclic Response of North Sea Sands under Varied Stress Scenarios

Graph 1: Beach Sand (RD = 55%, Vertical Stress = 100 kPa)

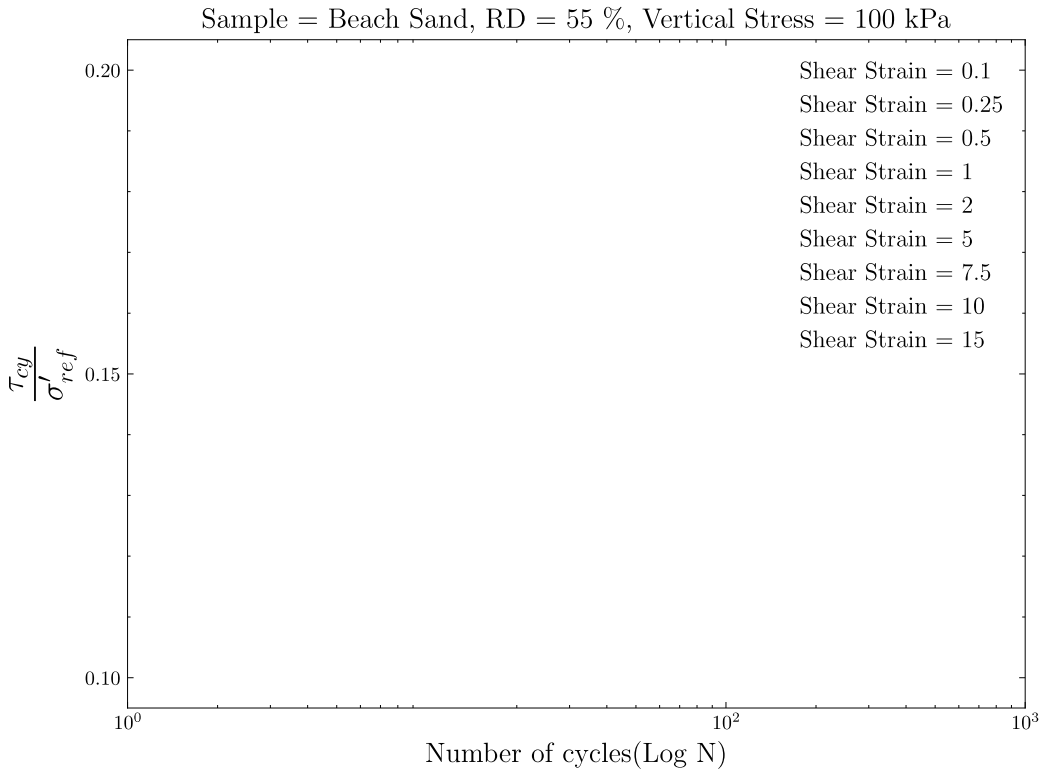

Graph 2: Beach Sand (RD = 80%, Vertical Stress = 100)

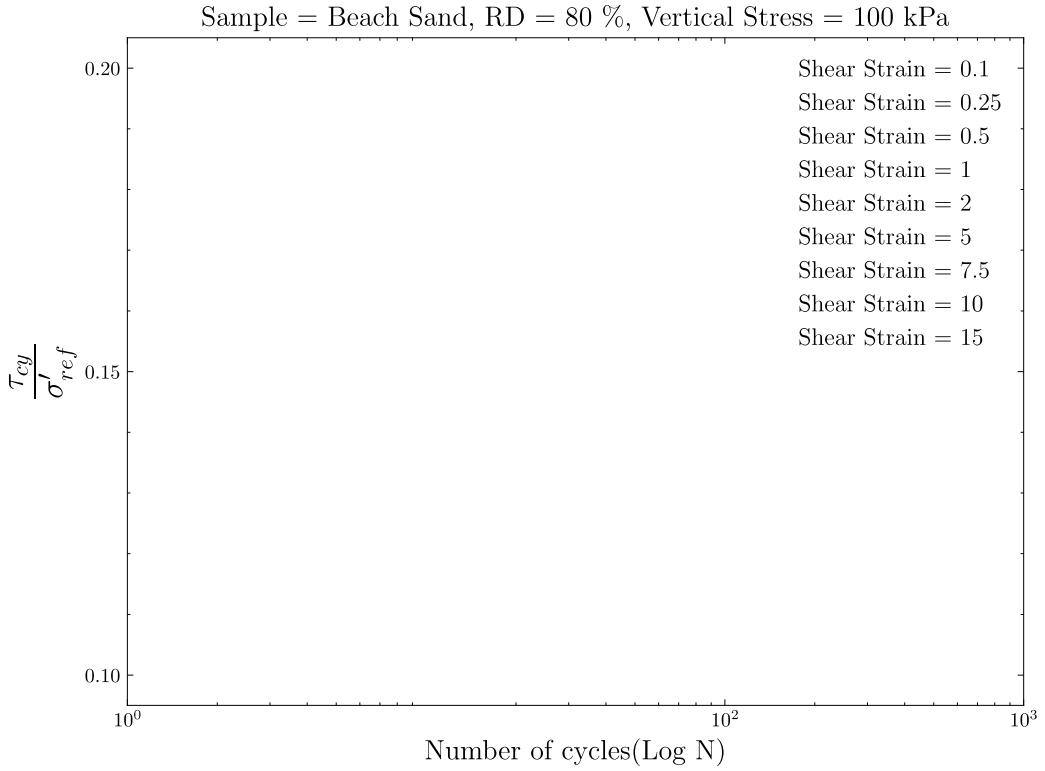

Graph 3: Beach Sand (RD = 55%, Vertical Stress = 150 kPa)

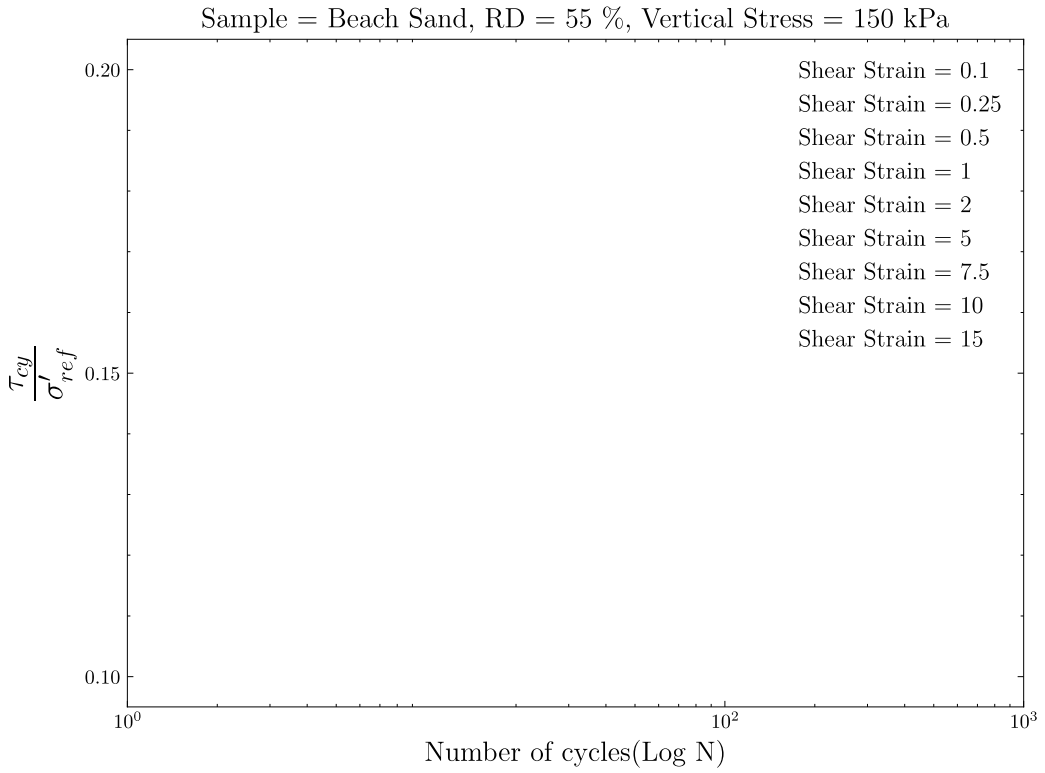

Graph 4: Beach Sand (RD = 80%, Vertical Stress = 150 kPa)

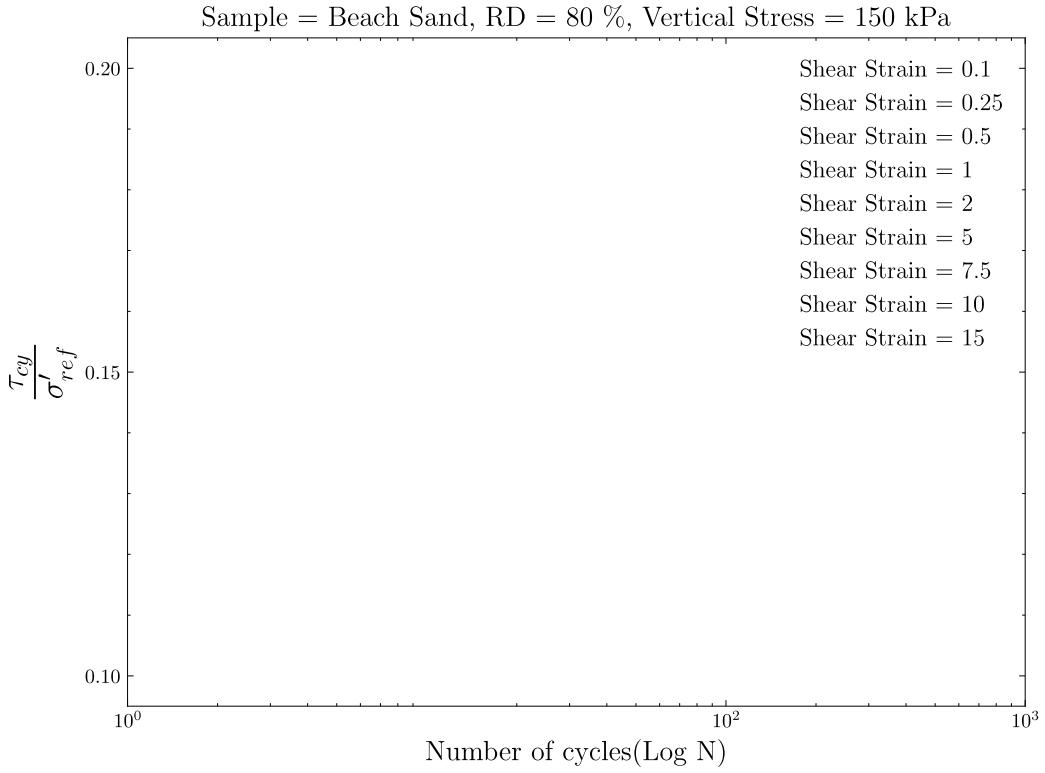

Graph 5: Beach Sand (RD = 55%, Vertical Stress = 250 kPa)

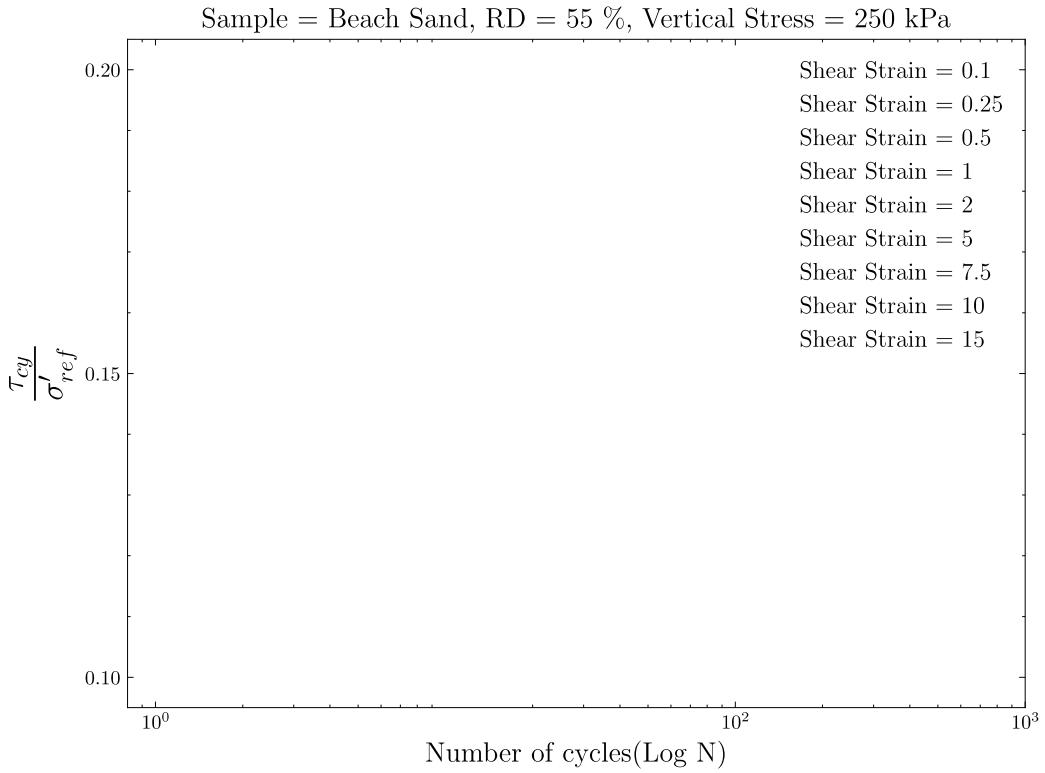

Graph 6: Beach Sand (RD = 80%, Vertical Stress = 250 kPa)

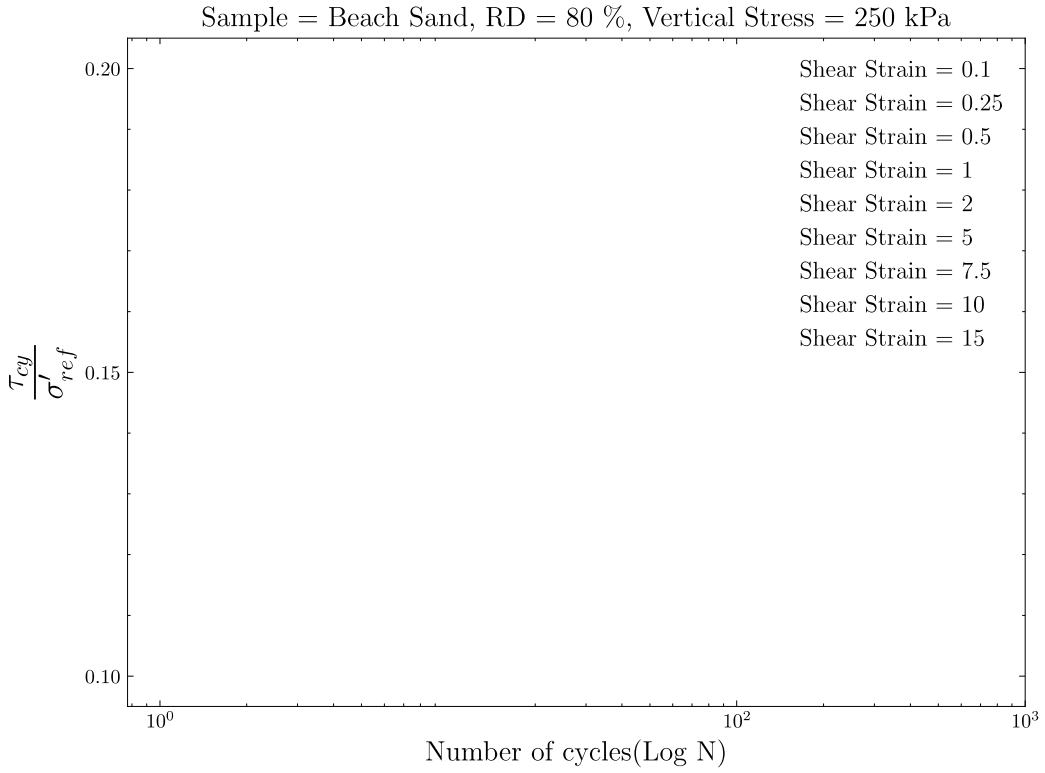

Graph 7: Beach Sand (RD = 55%, Vertical Stress = 500 kPa)

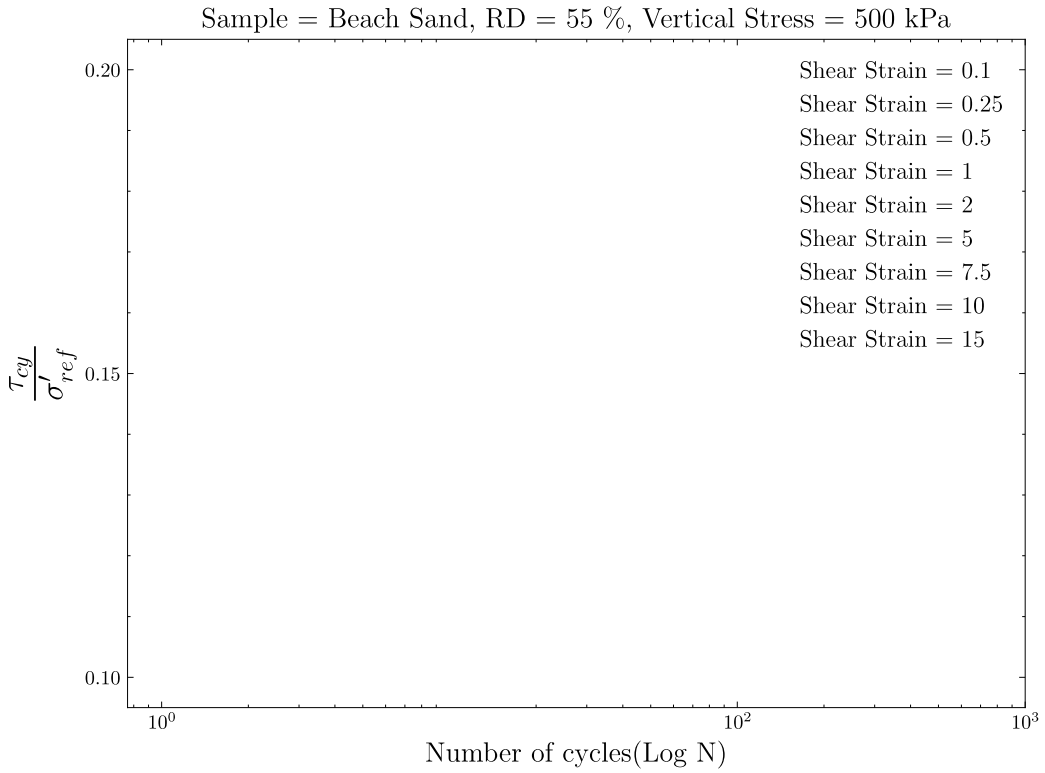

Graph 8: Beach Sand (RD = 80%, Vertical Stress = 500 kPa)

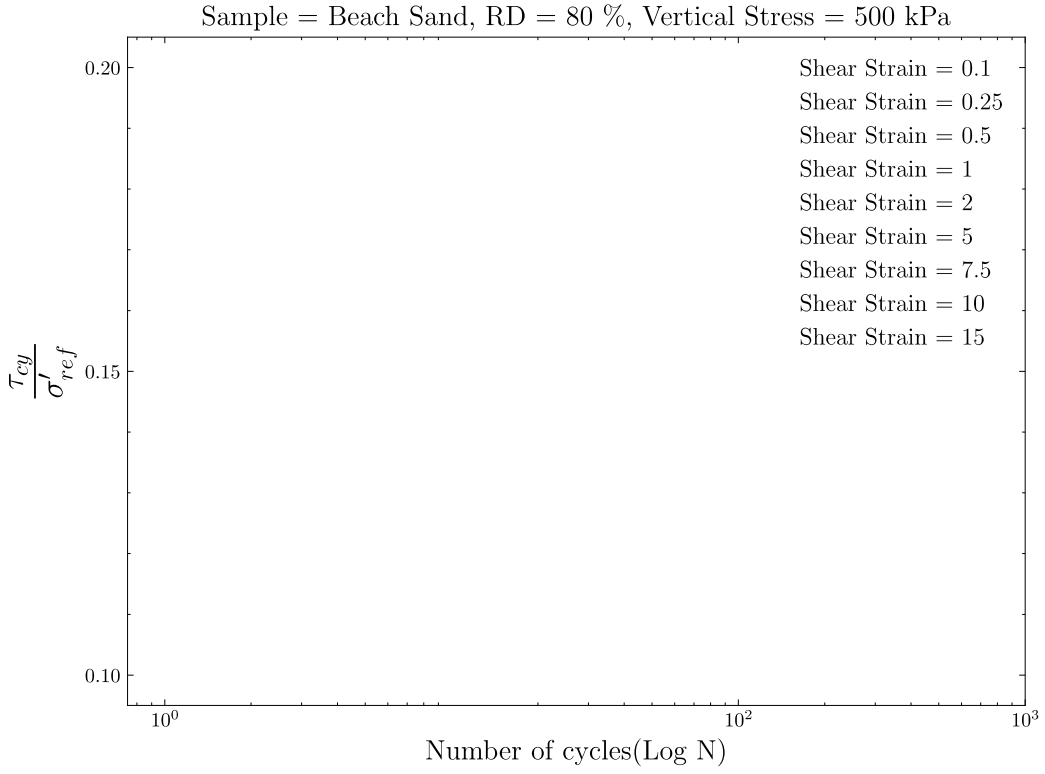

Eemian Sand:

Graph 9: Eemian Sand (RD = 55%, Vertical Stress = 100 kPa)

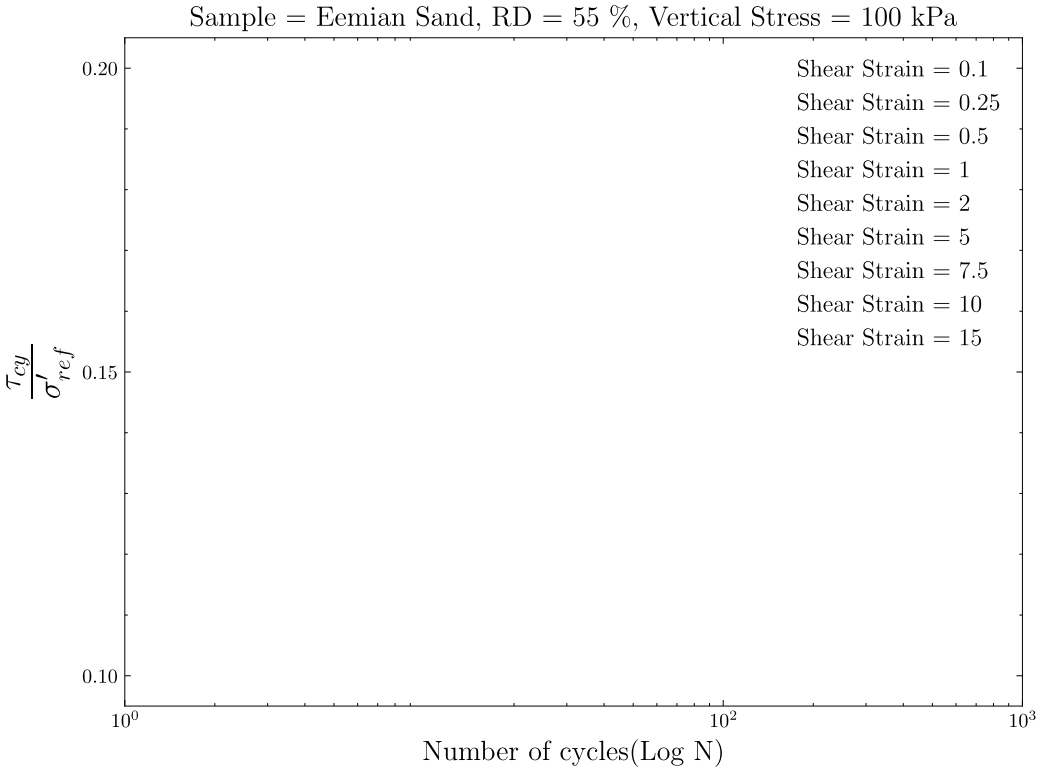

Graph 10: Eemian Sand (RD = 80%, Vertical Stress = 100 kPa)

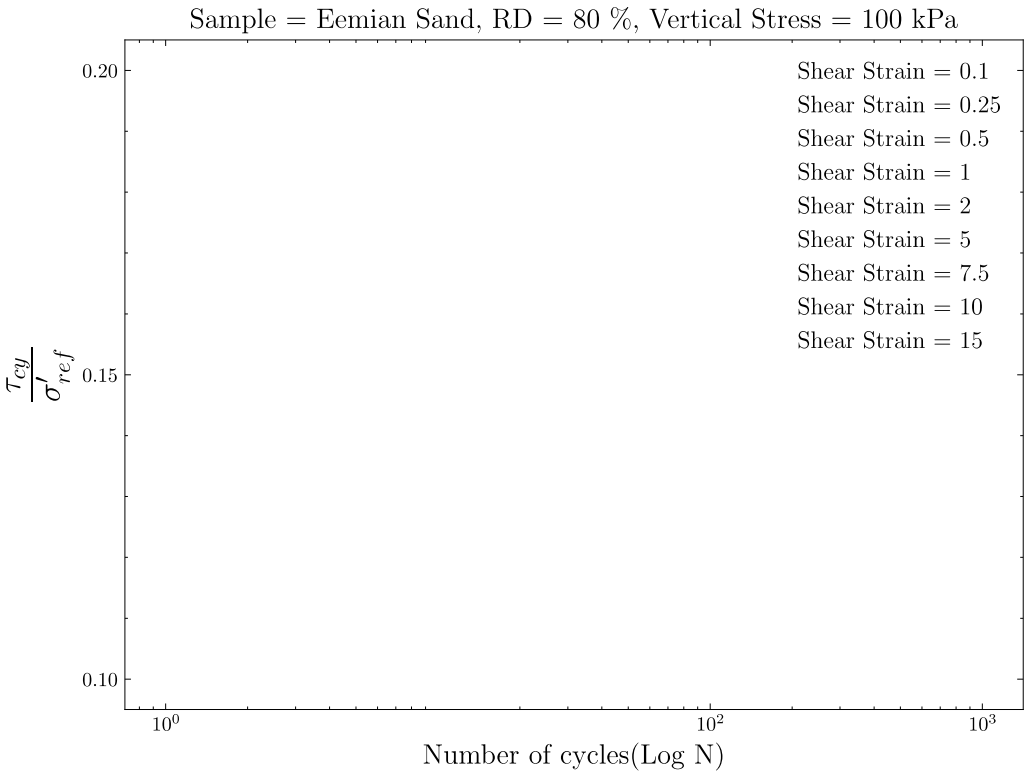

Graph 11: Eemian Sand (RD = 55%, Vertical Stress = 150 kPa)

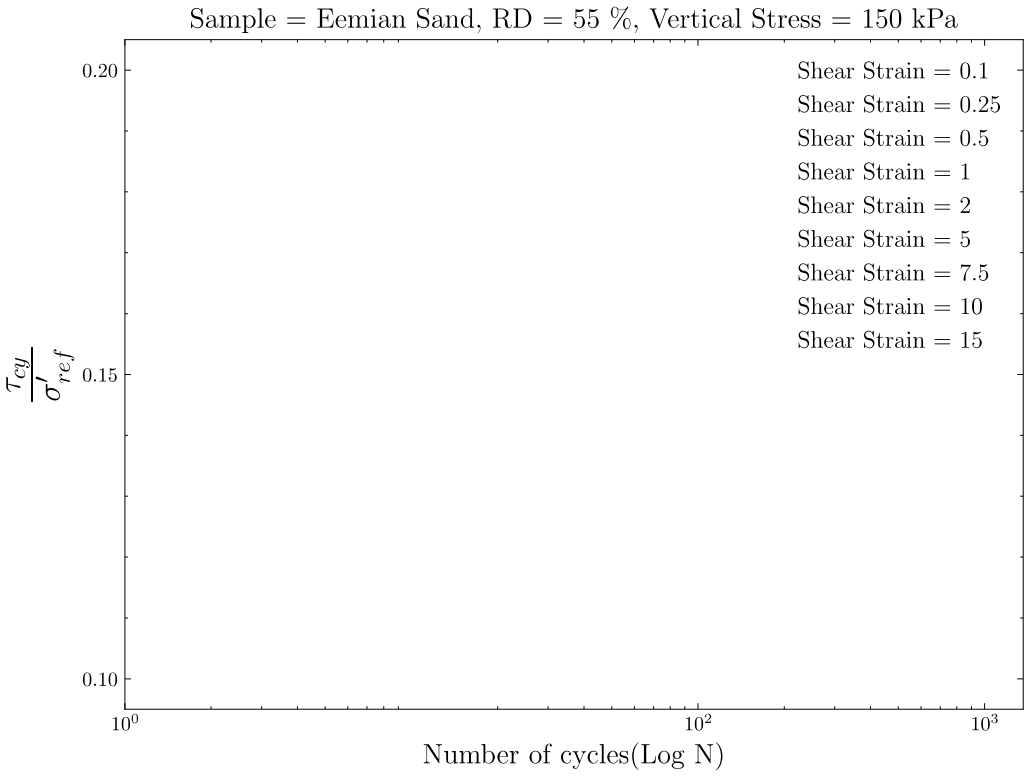

Graph 12: Eemian Sand (RD = 80%, Vertical Stress = 150 kPa)

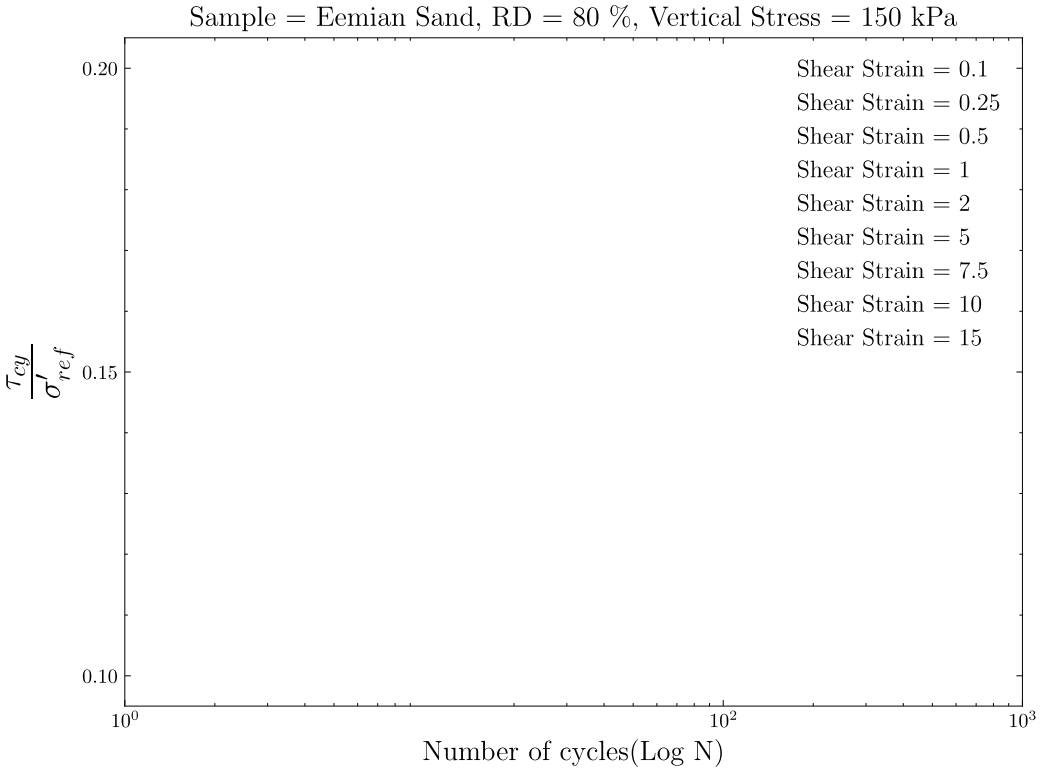

Graph 13: Eemian Sand (RD = 55%, Vertical Stress = 250 kPa)

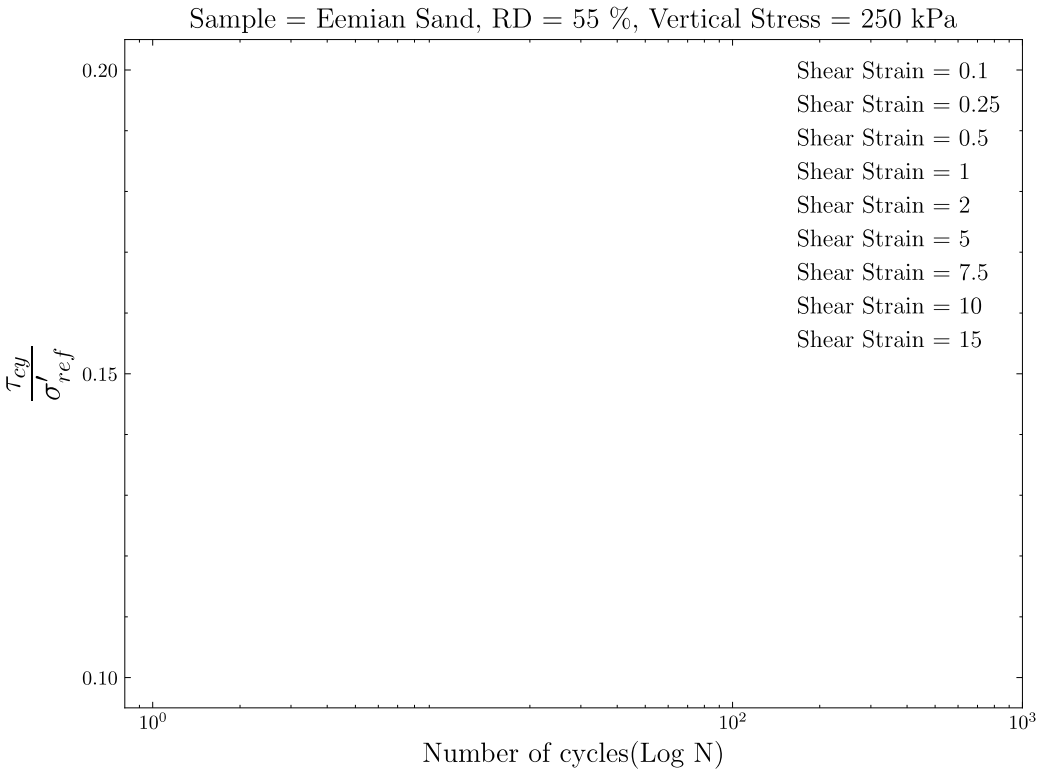

Graph 14: Eemian Sand (RD = 80%, Vertical Stress = 250 kPa)

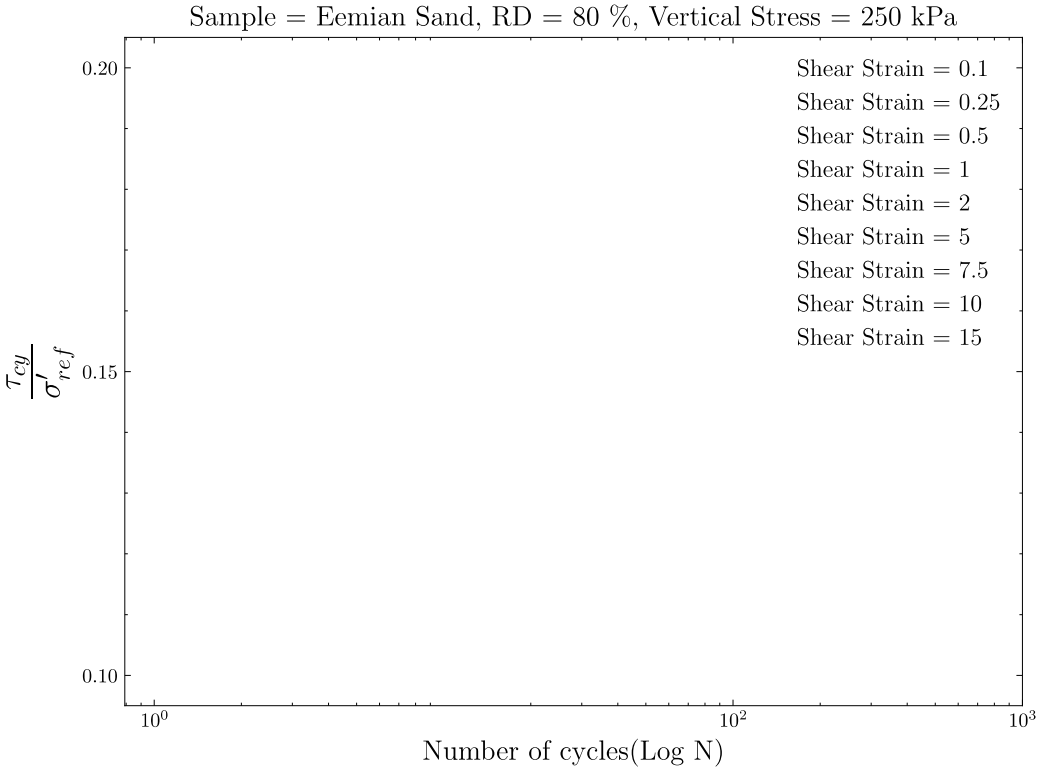

Graph 15: Eemian Sand (RD = 55%, Vertical Stress = 500 kPa)

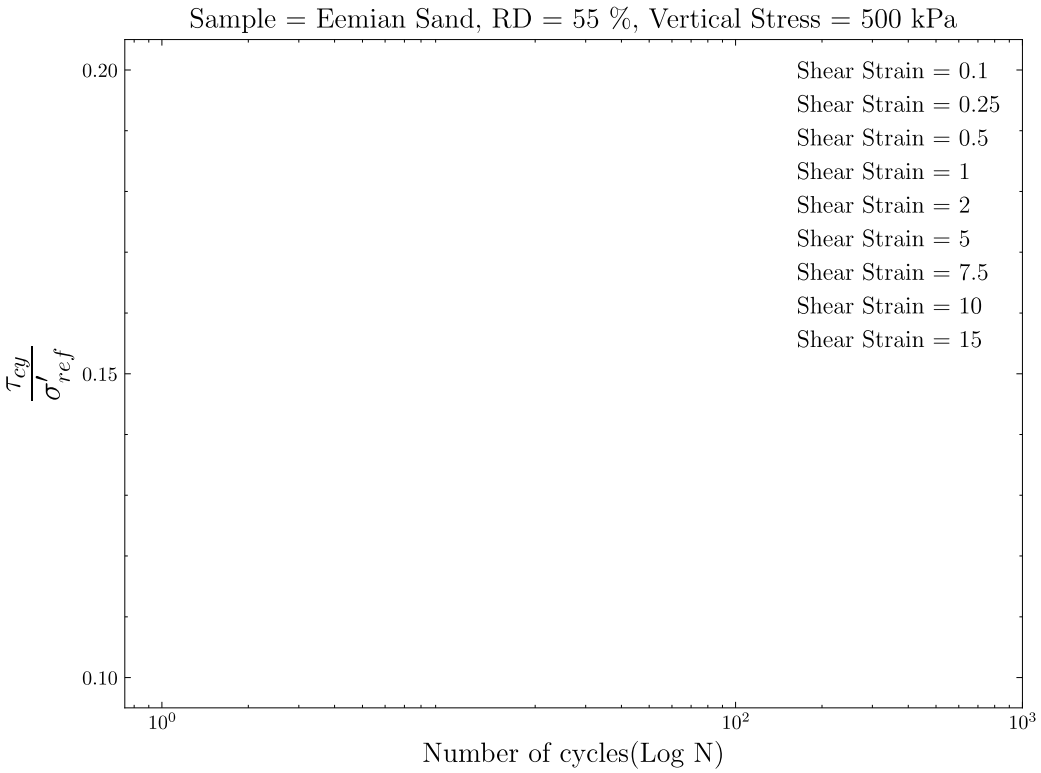

Graph 16: Eemian Sand (RD = 80%, Vertical Stress = 500 kPa)

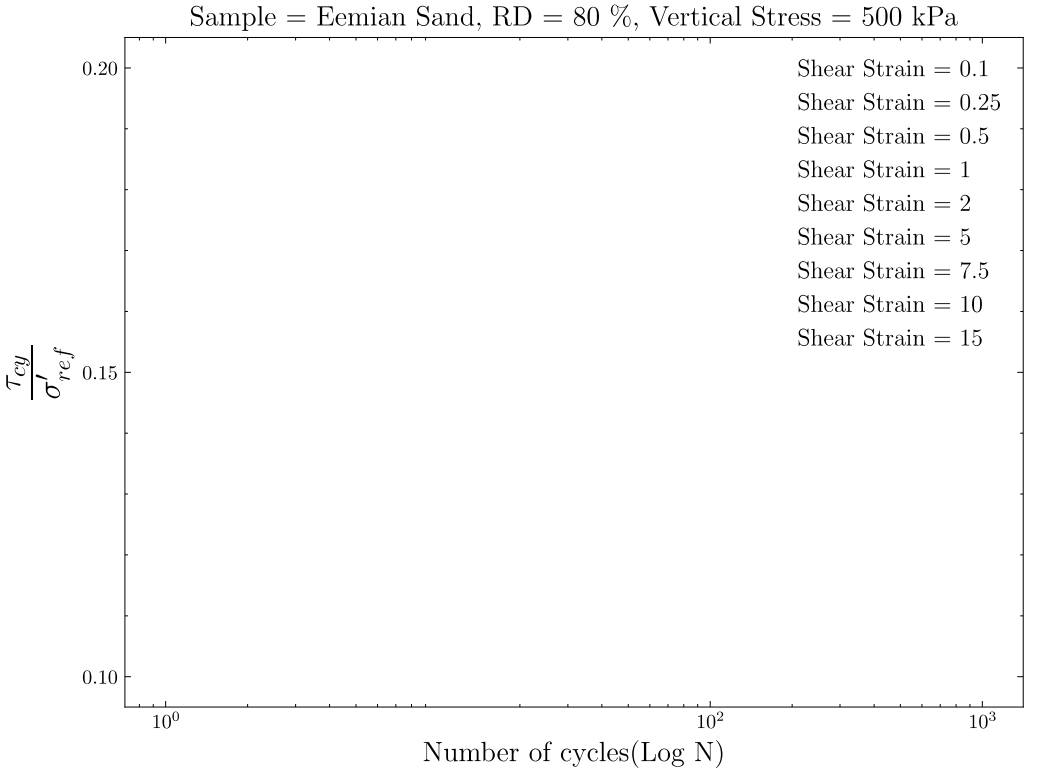

7.3 Appendix C: Average Pore Pressure Ratio and Cyclic Response of North Sea Sands under Varied Stress Scenarios

Graph 1: Beach Sand (RD = 55%, Vertical Stress = 100 kPa)

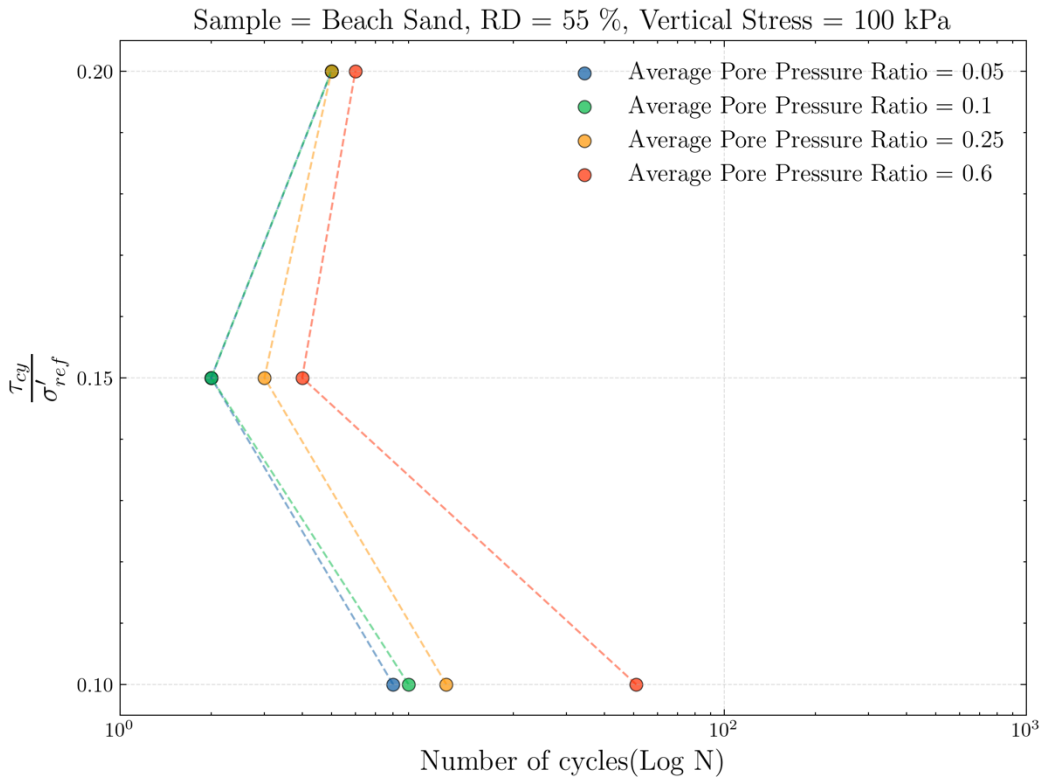

Graph 2: Beach Sand (RD = 80%, Vertical Stress = 100 kPa)

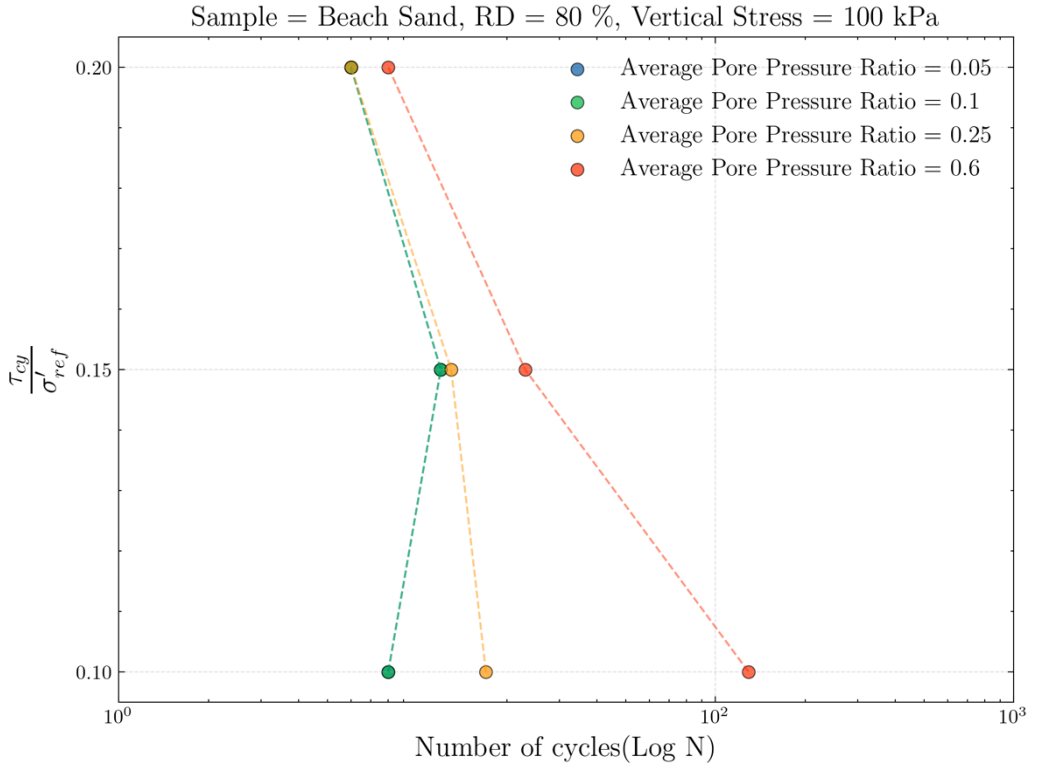

Graph 3: Beach Sand (RD = 55%, Vertical Stress = 150 kPa)

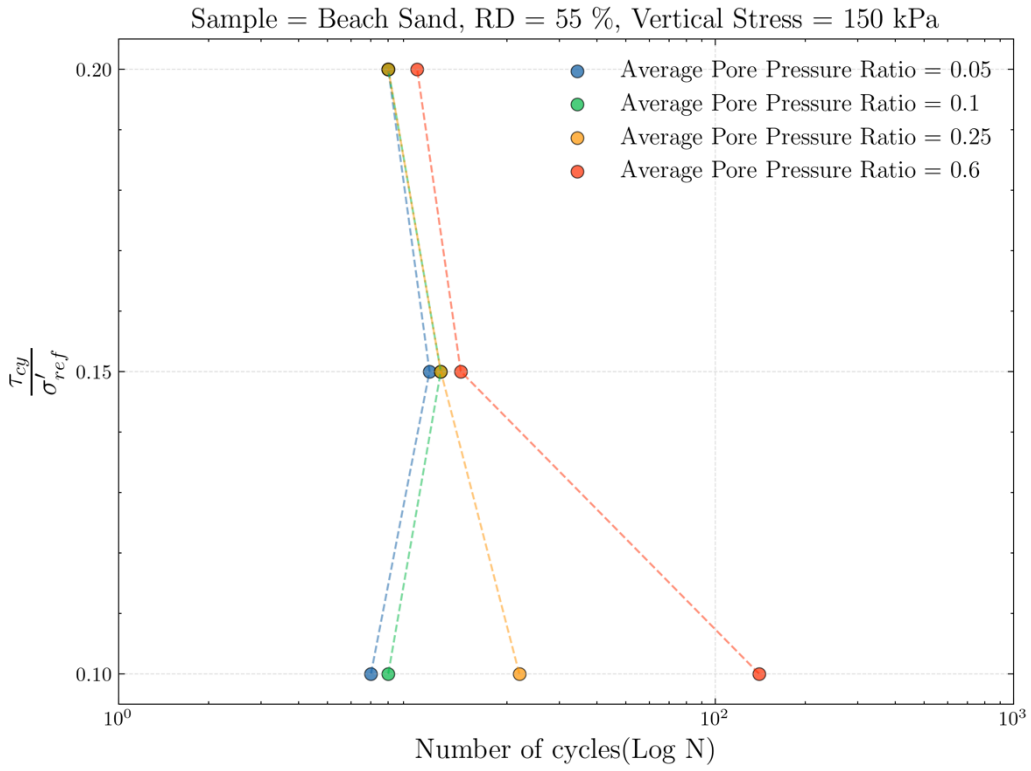

Graph 4: Beach Sand (RD = 80%, Vertical Stress = 150 kPa)

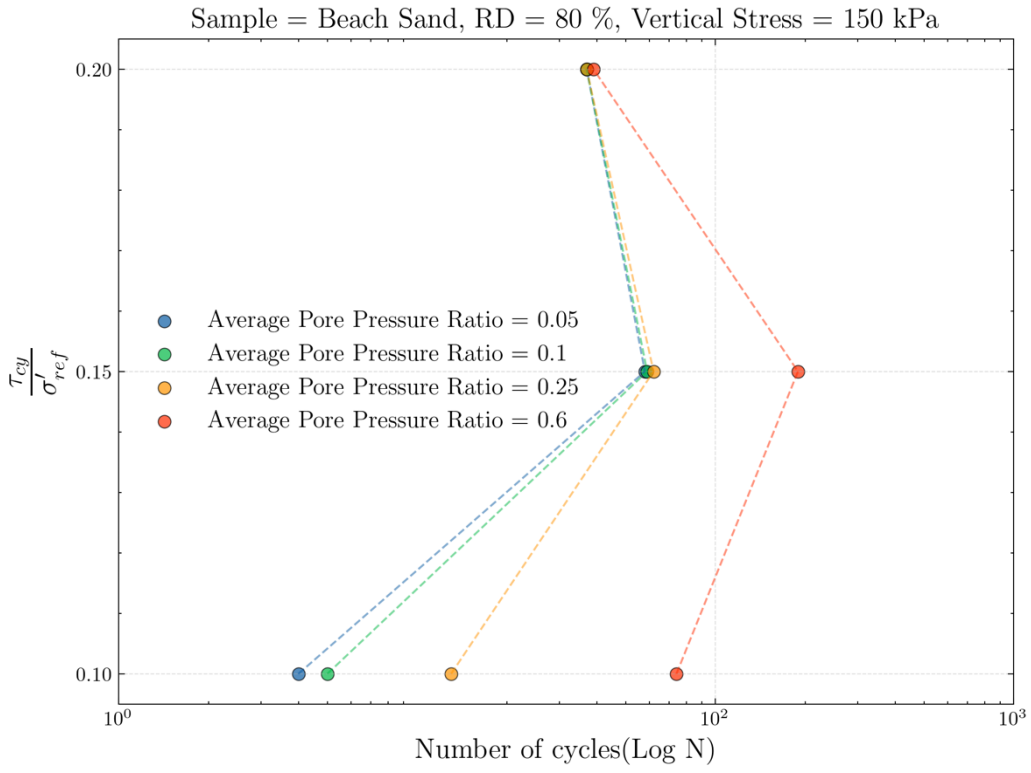

Graph 5: Beach Sand (RD = 55%, Vertical Stress = 250 kPa)

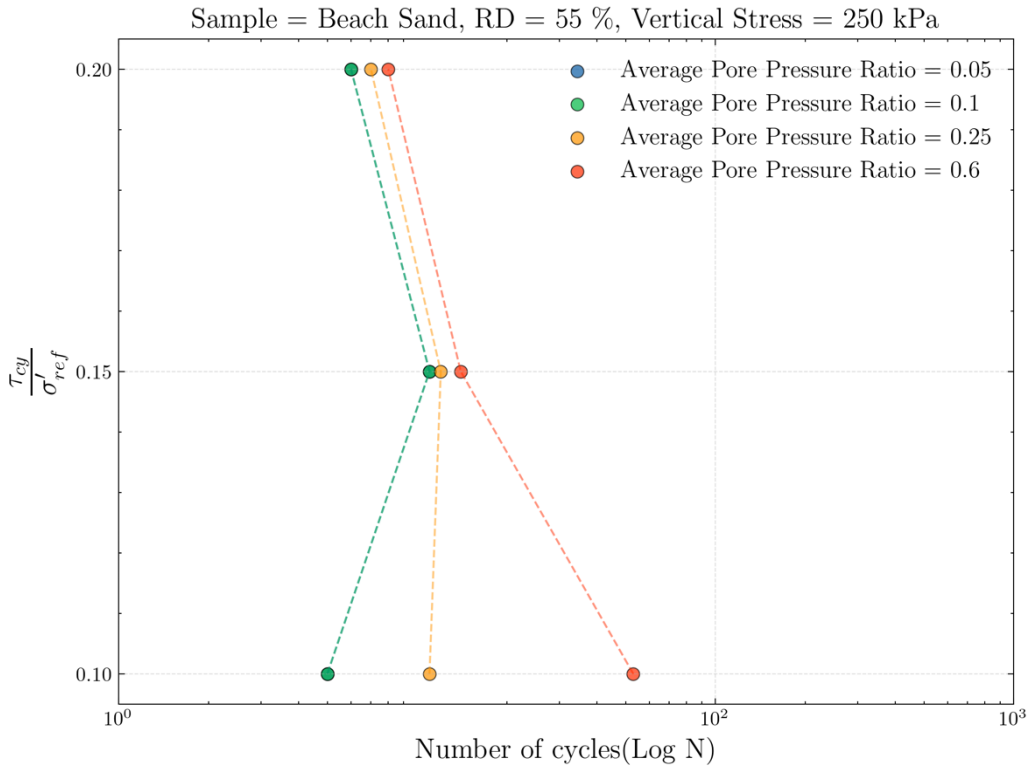

Graph 6: Beach Sand (RD = 80%, Vertical Stress = 250 kPa)

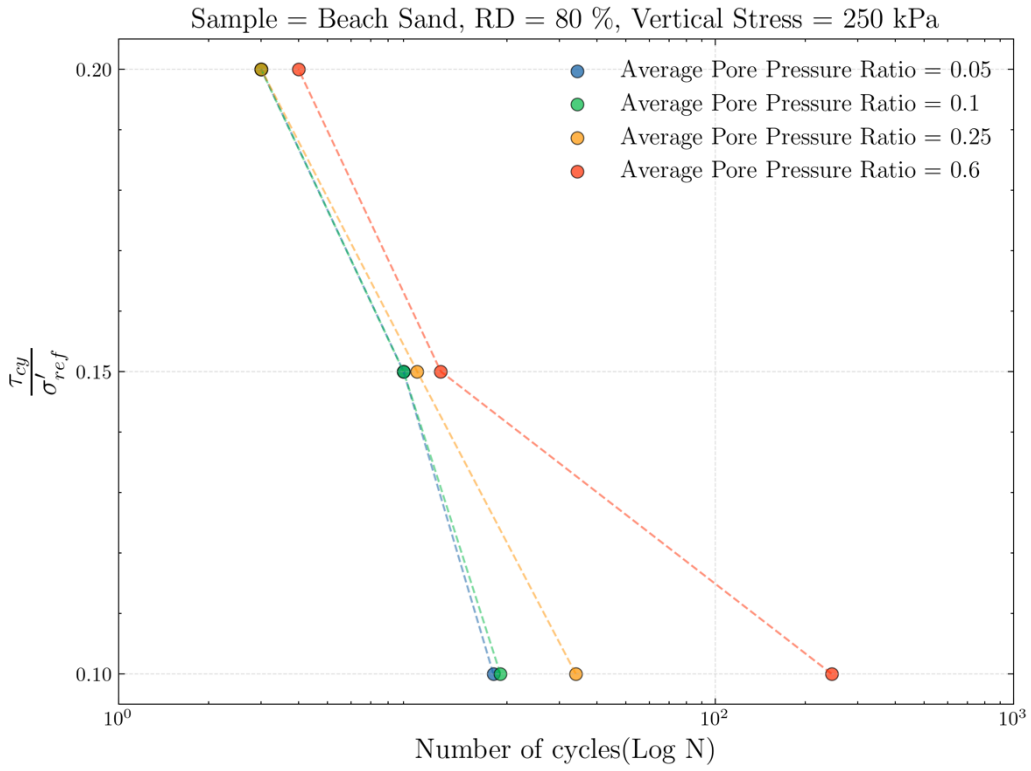

Graph 7: Beach Sand (RD = 55%, Vertical Stress = 500 kPa)

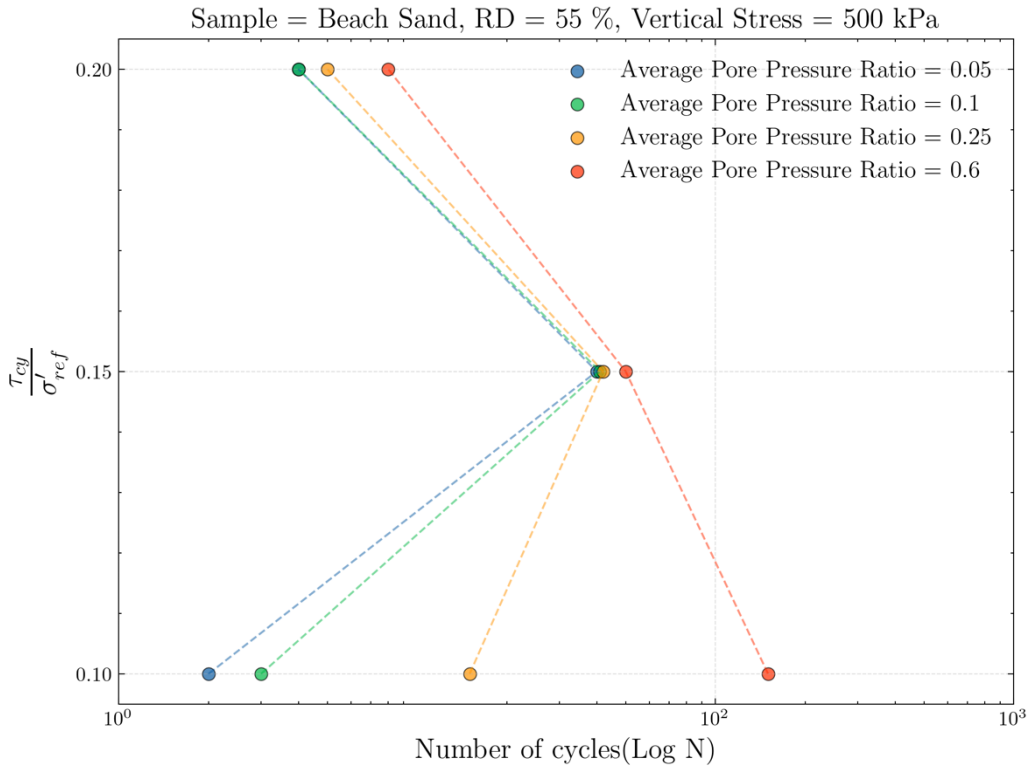

Graph 8: Beach Sand (RD = 80%, Vertical Stress = 500 kPa)

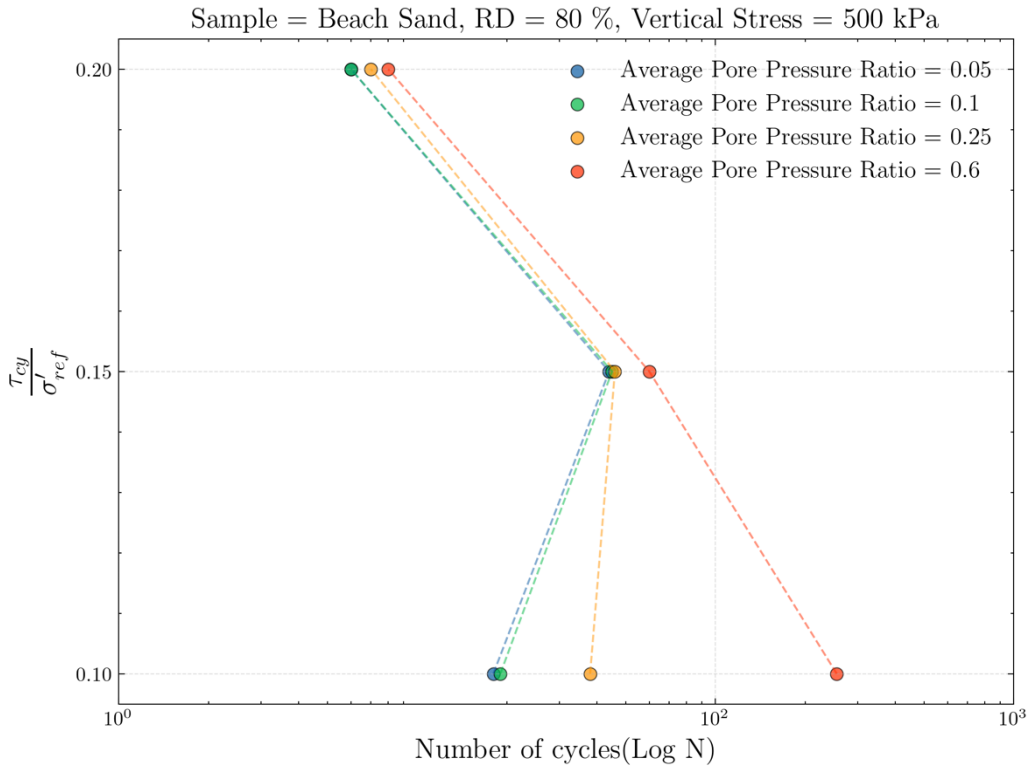

Eemian Sand

Graph 9: Eemian (RD = 55%, Vertical Stress = 100 kPa)

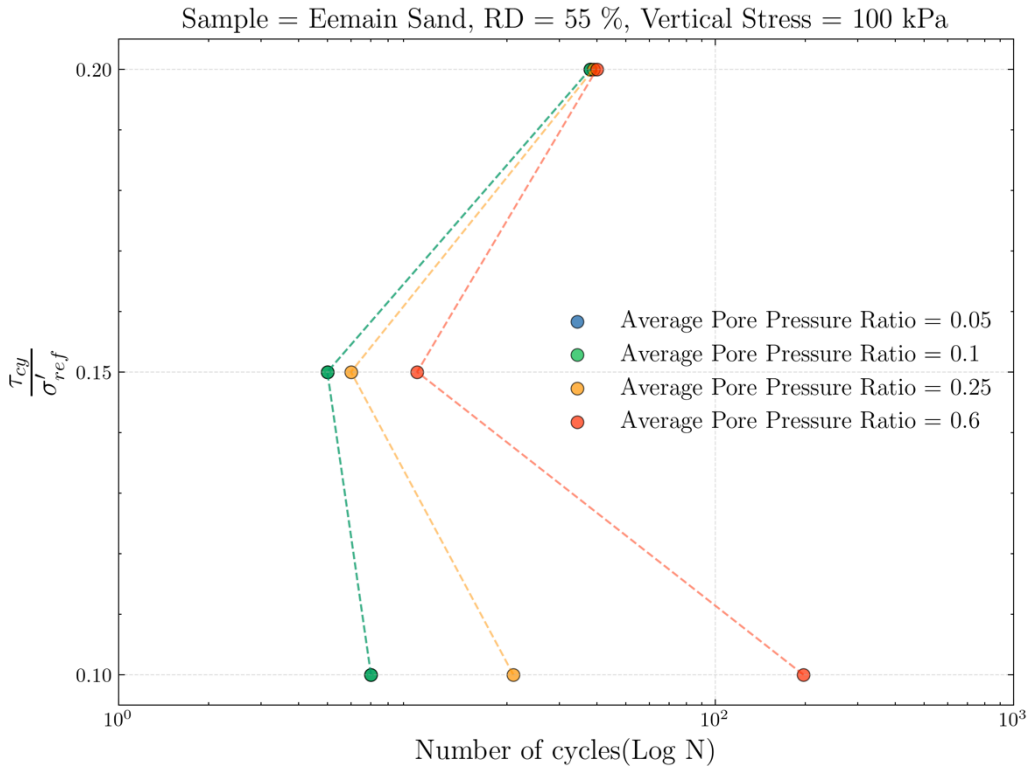

Graph 10: Eemian (RD = 80%, Vertical Stress = 100 kPa)

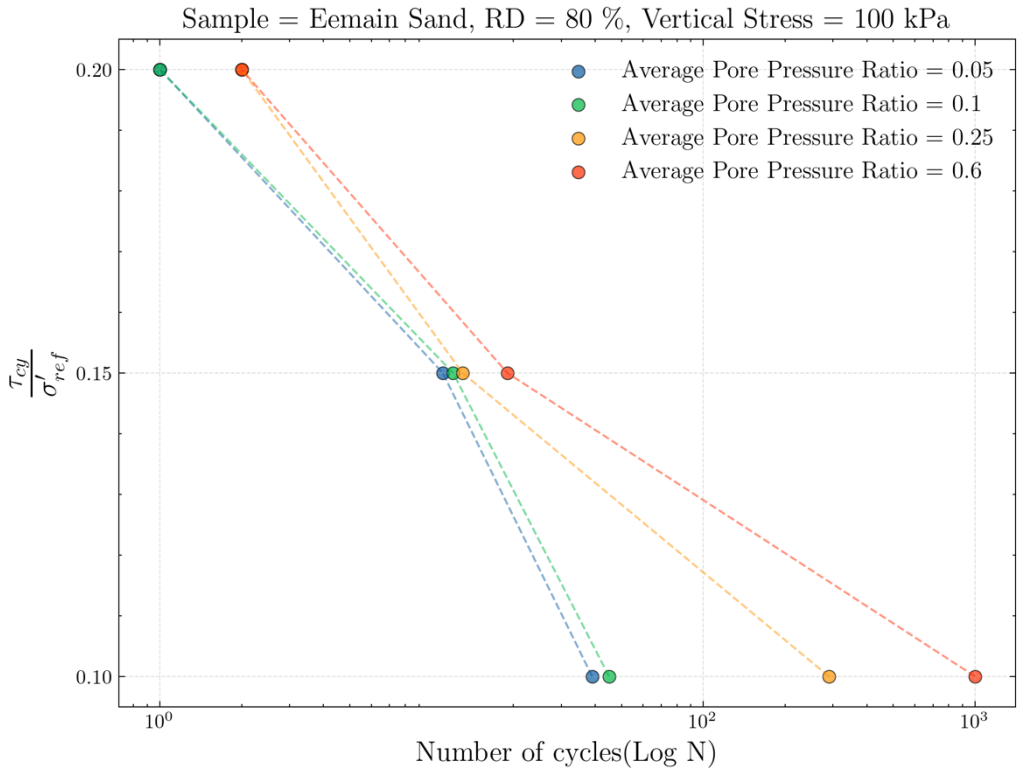

Graph 11: Eemian (RD = 55%, Vertical Stress = 150 kPa)

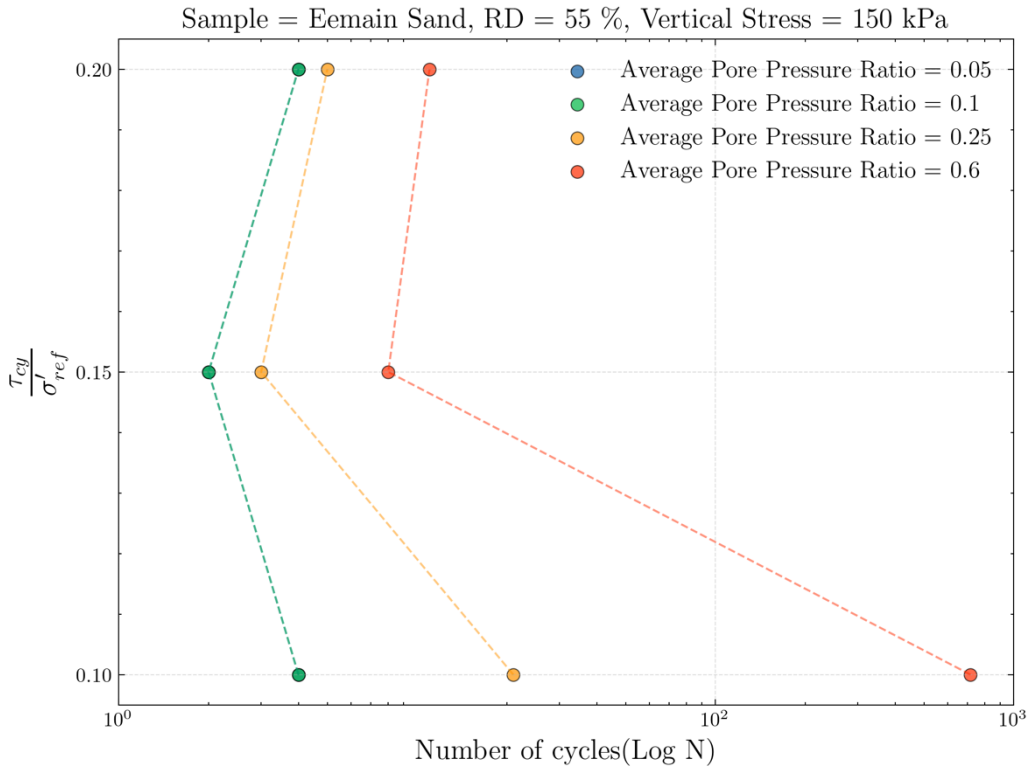

Graph 12: Eemian (RD = 80%, Vertical Stress = 150 kPa)

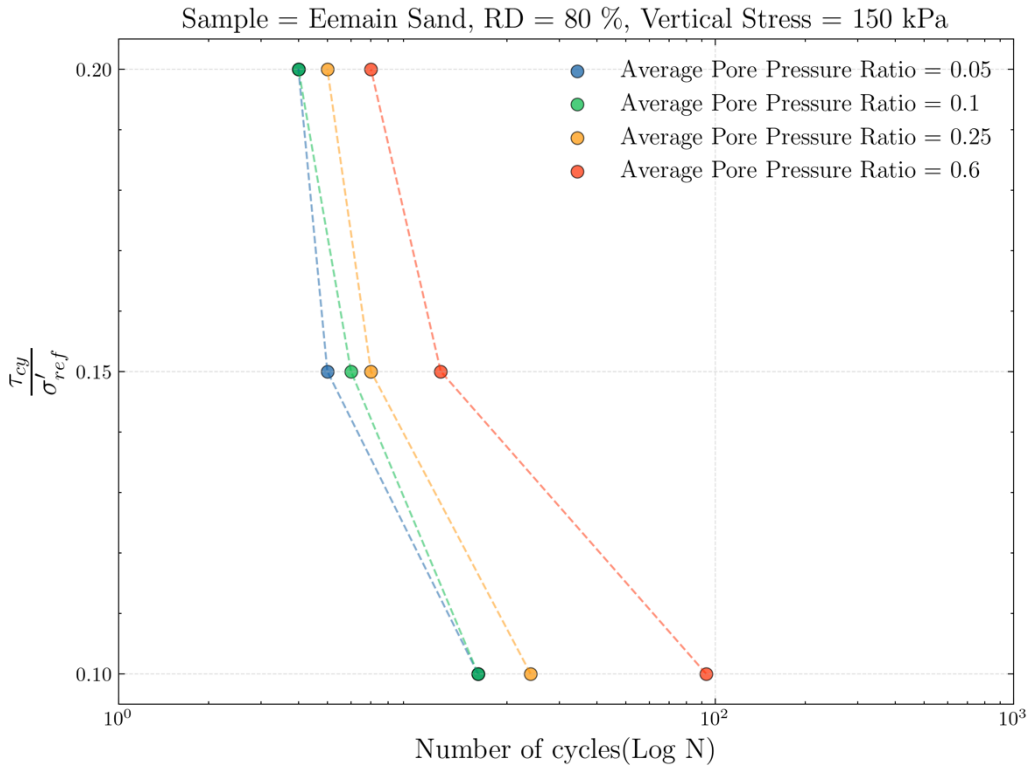

Graph 13: Eemian (RD = 55%, Vertical Stress = 250 kPa)

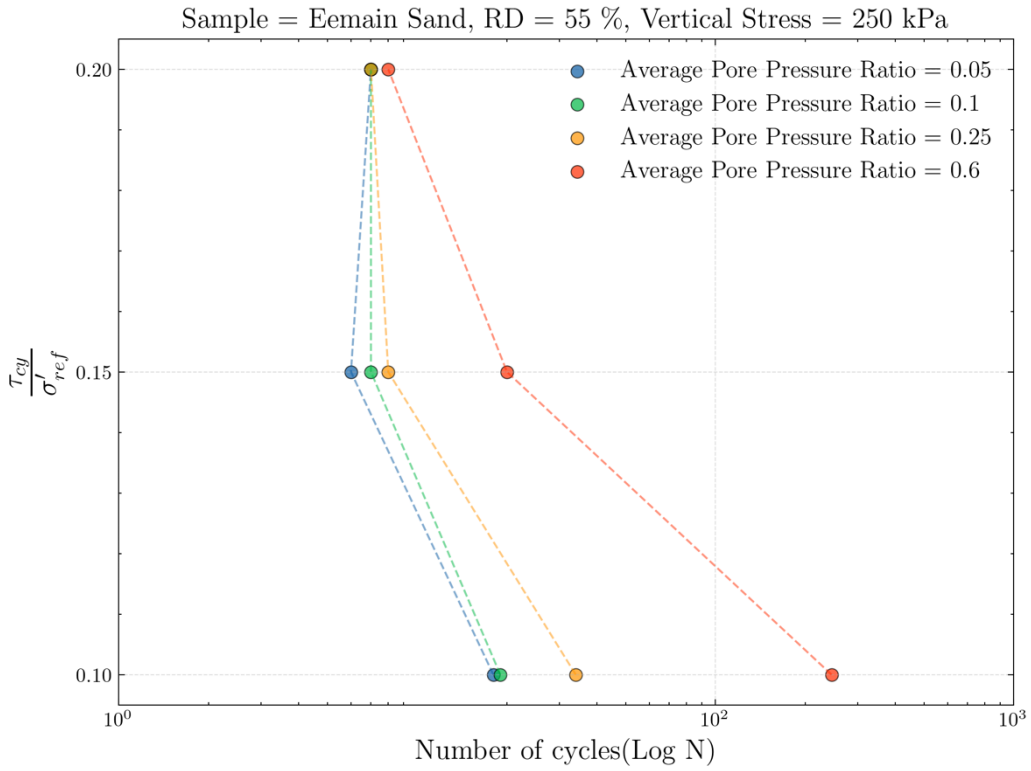

Graph 14: Eemian (RD = 80%, Vertical Stress = 250 kPa)

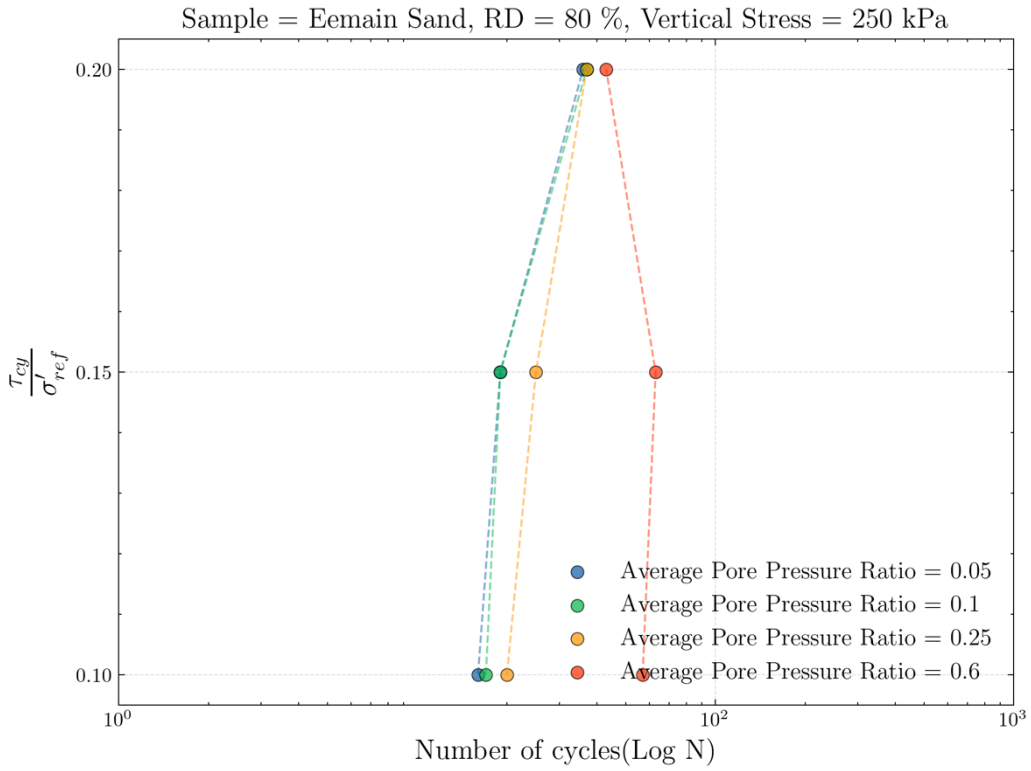

Graph 15: Eemian (RD = 55%, Vertical Stress = 500 kPa)

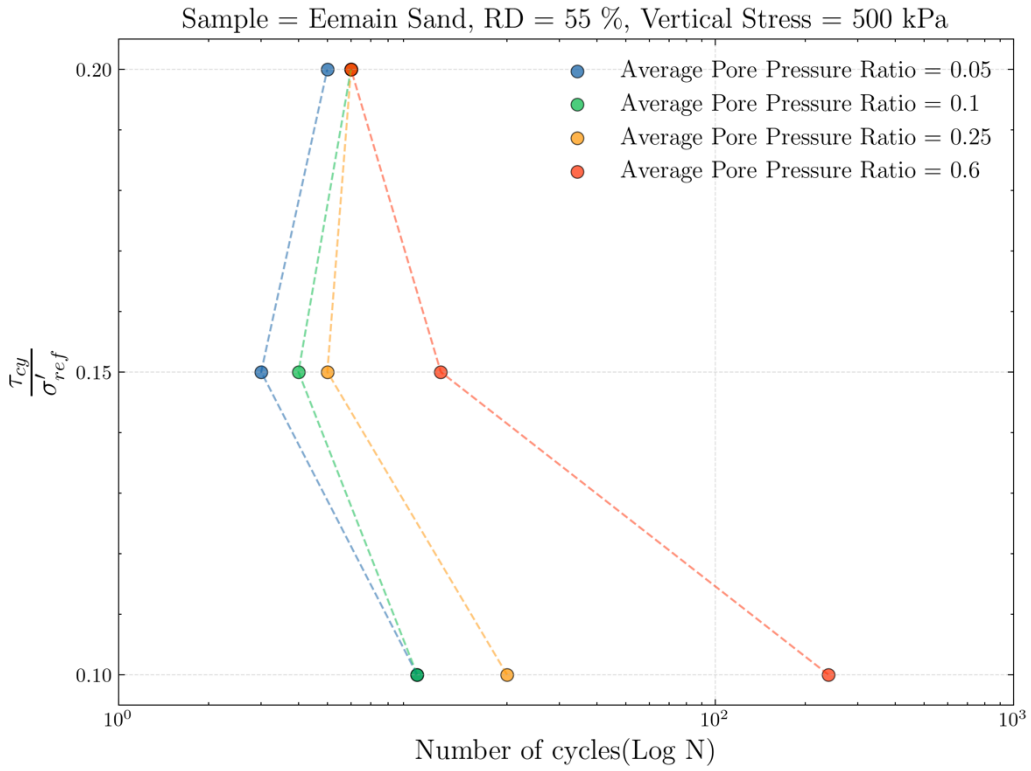

Graph 16: Eemian (RD = 80%, Vertical Stress = 500 kPa)

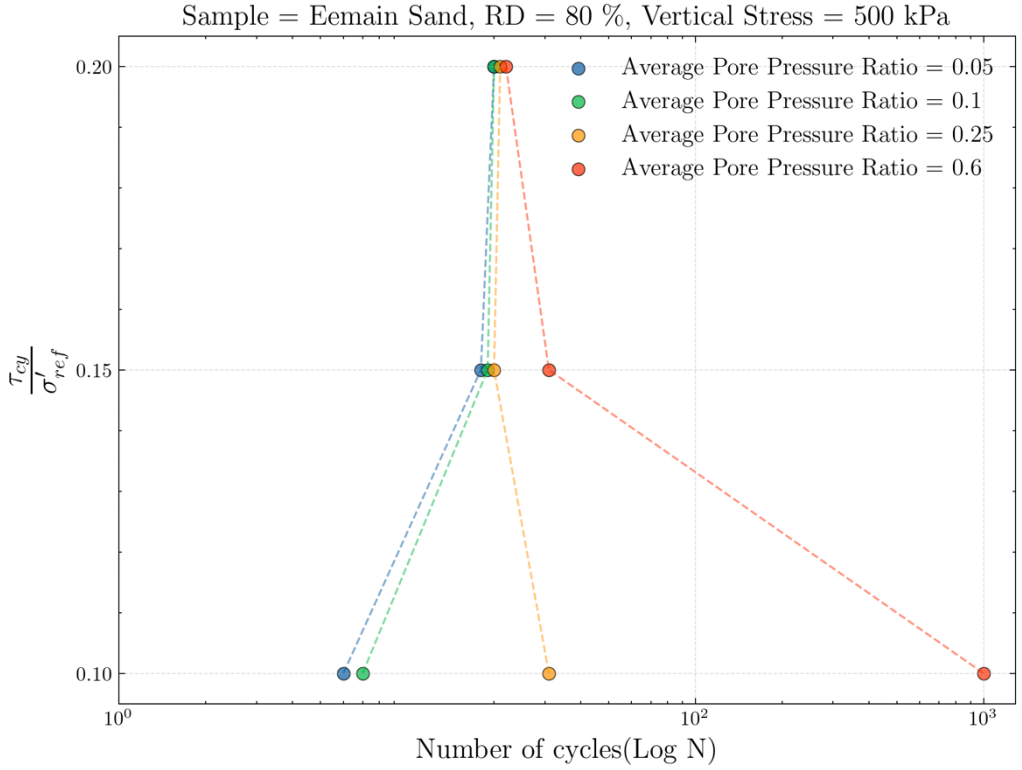

7.4 Appendix D: Effect of Relative Density on Cyclic Strength at Different CSR Levels

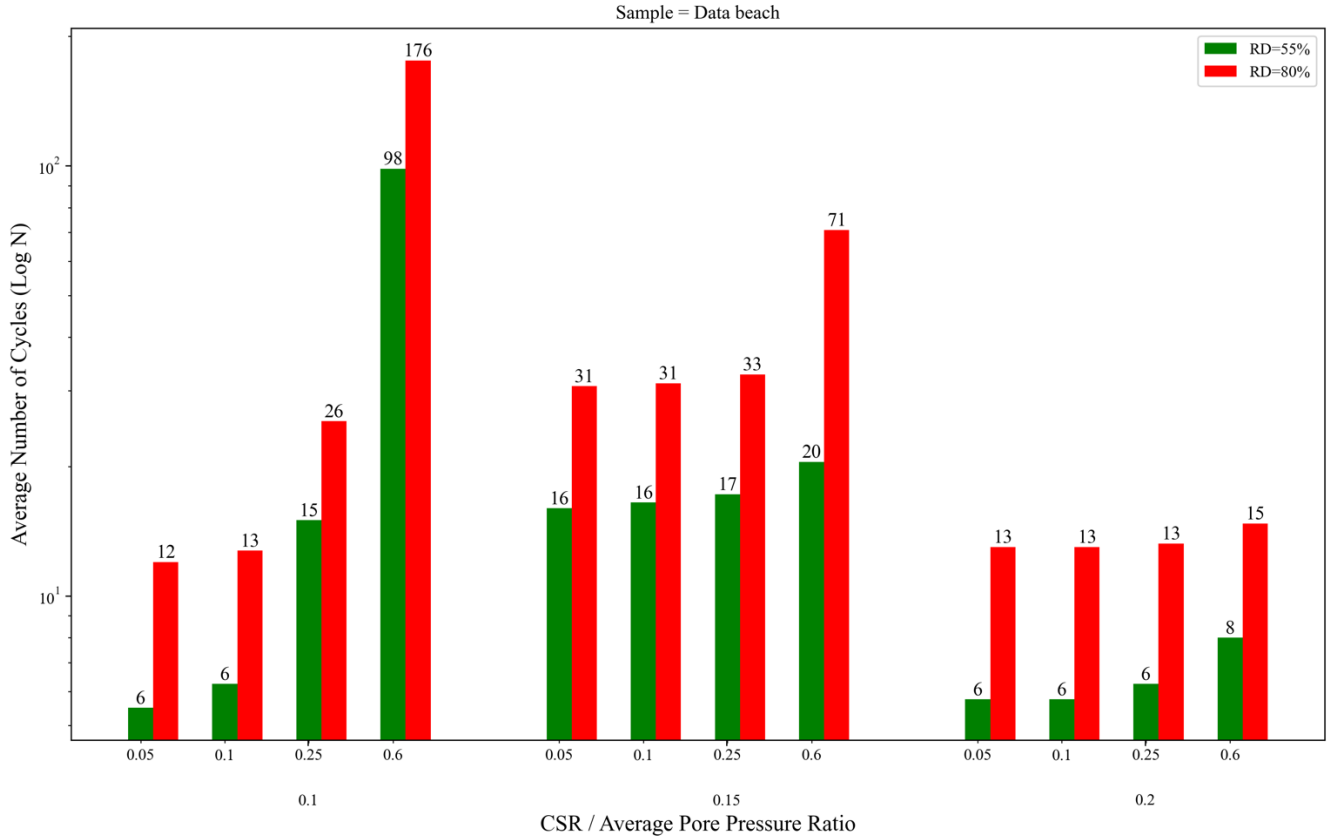

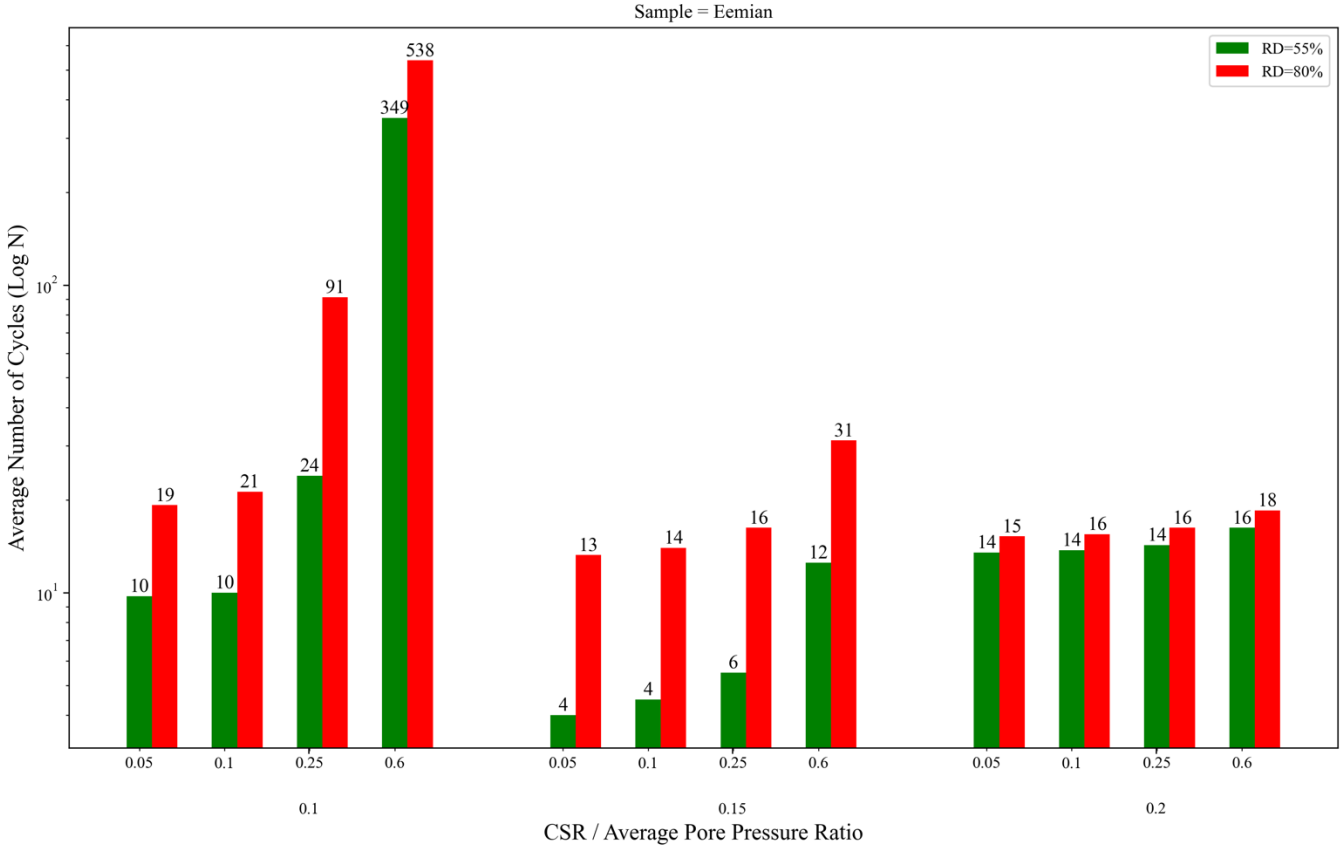
Sample = Eemian
RD=55%
RD=80%
Average Number of Cycles (Log N)
10^2
10^1
538
349
91
24
21
19
10
10
13
14
16
31
4
4
6
12
15
14
16
14
16
14
16
18
16
0.05
0.1
0.25
0.6
0.05
0.1
0.25
0.6
0.05
0.1
0.25
0.6
0.1
0.15
0.2
CSR / Average Pore Pressure Ratio

7.5 Appendix E Comparative Analysis of North Sea Sand Behavior with Andersen's Predictive Models

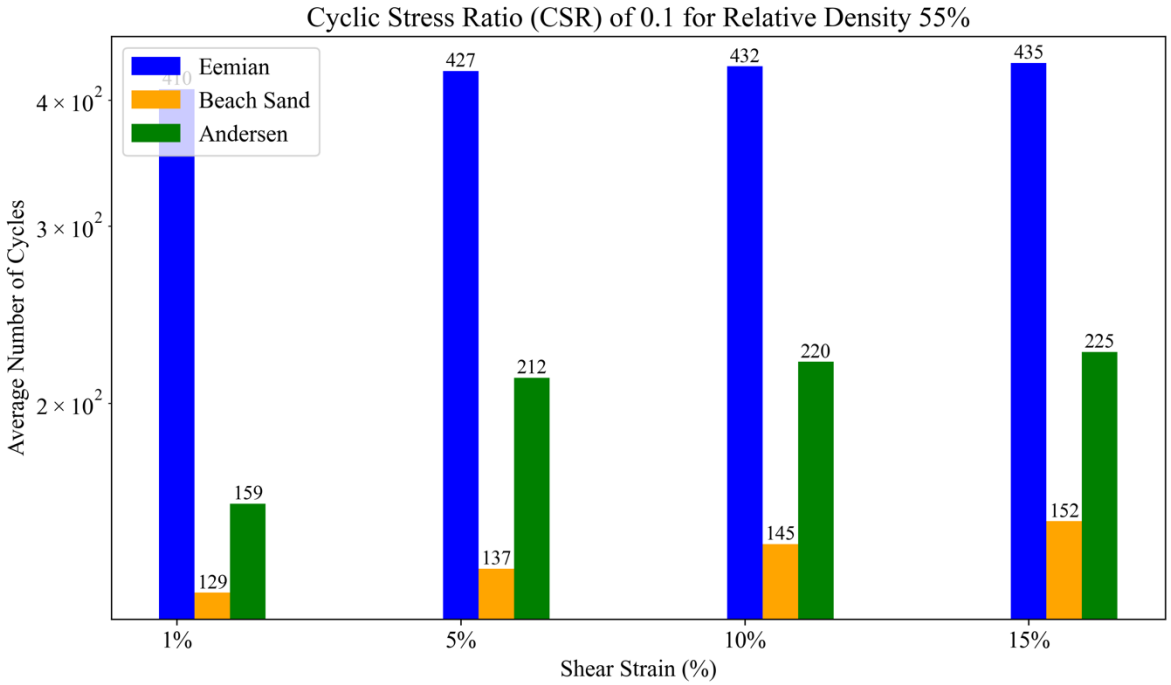

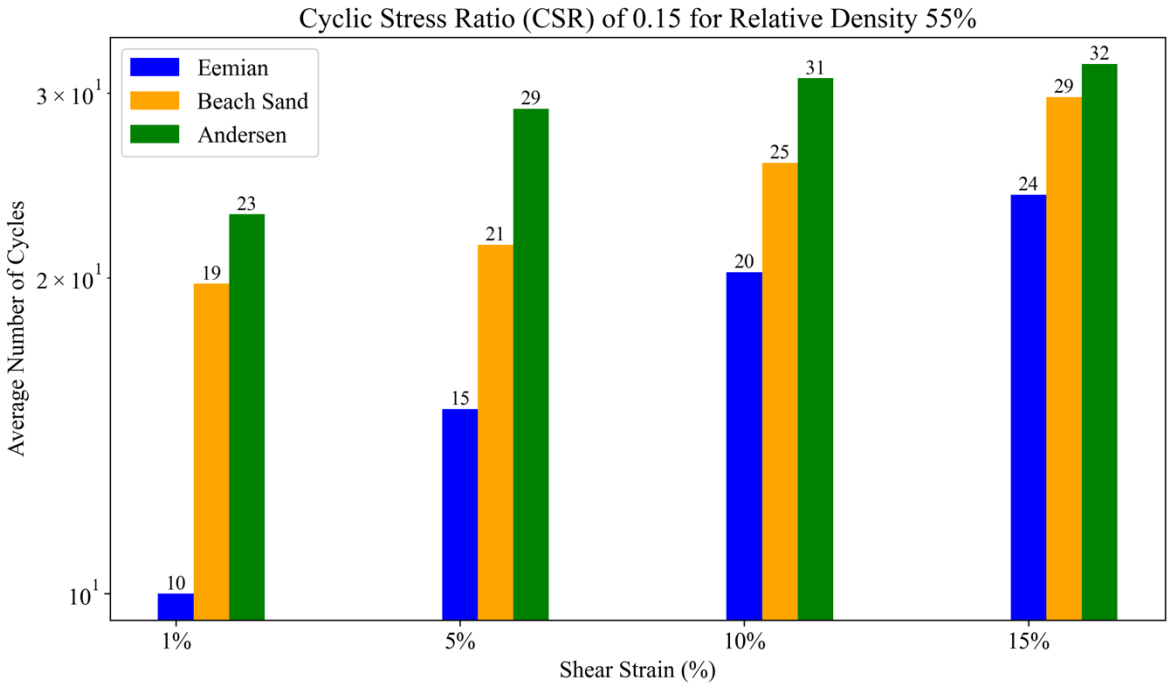

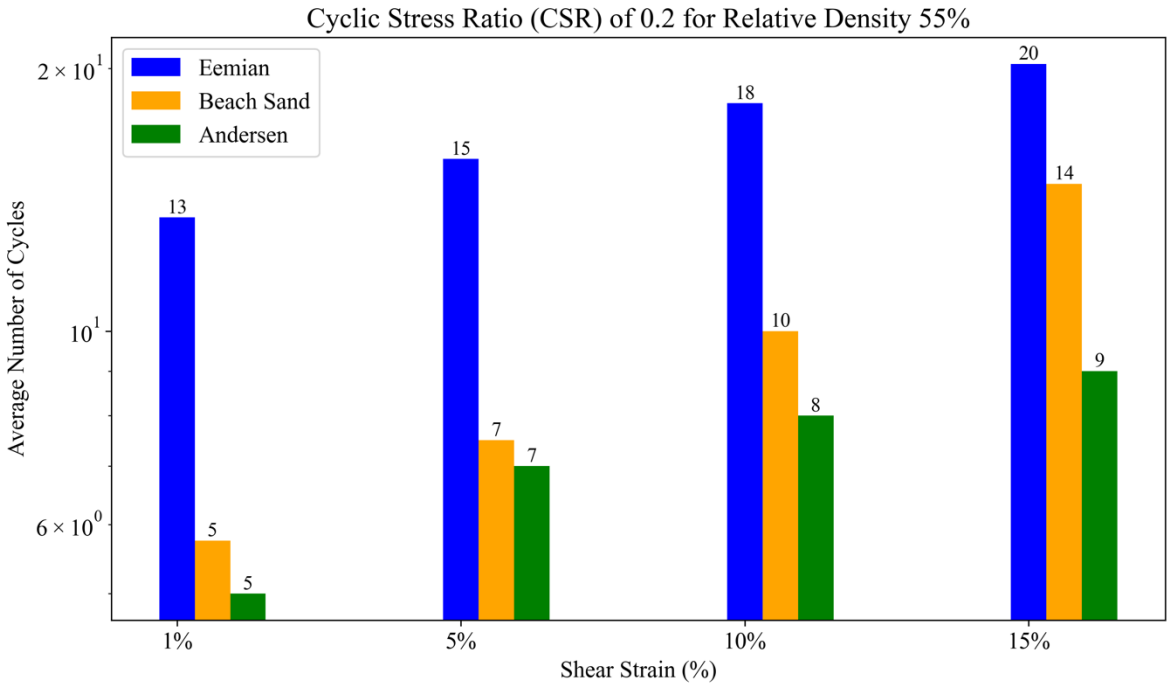
Cyclic Stress Ratio (CSR) of 0.2 for Relative Density 55%
Eemian
Beach Sand
Andersen
Average Number of Cycles
2×10^1
10^1
6×10^0
13
5
5
15
7
7
18
10
8
20
14
9
1%
5%
10%
15%
Shear Strain (%)

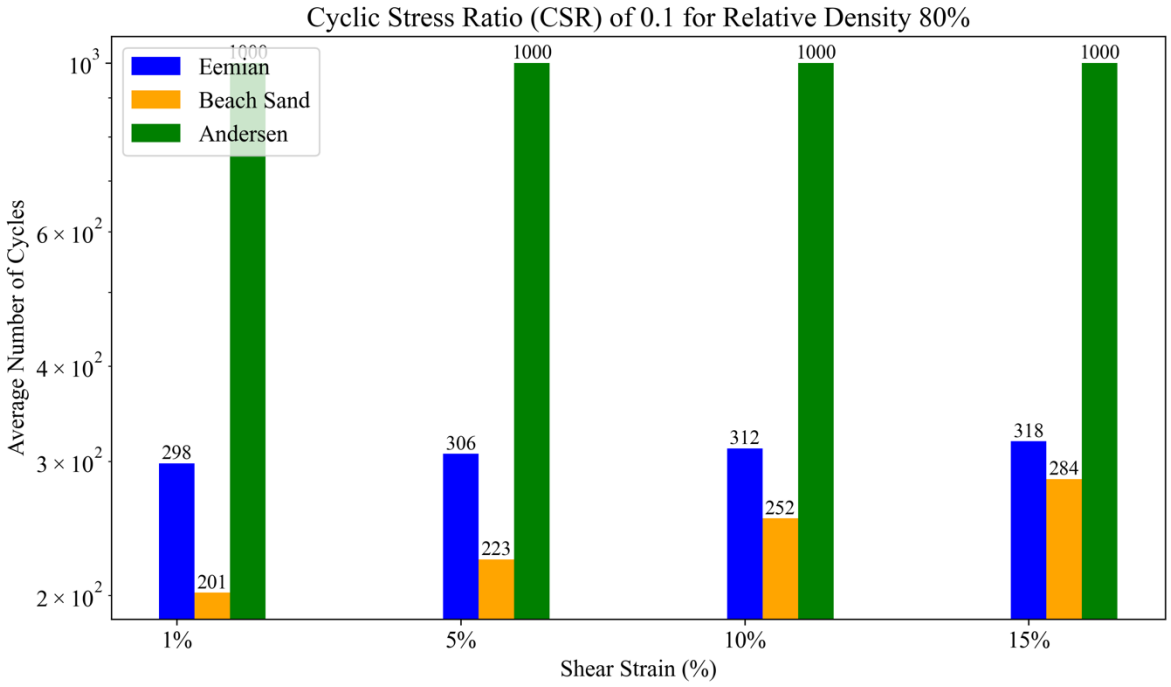
Cyclic Stress Ratio (CSR) of 0.1 for Relative Density 80%
Eemian
Beach Sand
Andersen
Average Number of Cycles
10^3
6×10^2
4×10^2
3×10^2
2×10^2
298
201
1000
306
223
1000
312
252
1000
318
284
1000
1%
5%
10%
15%
Shear Strain (%)

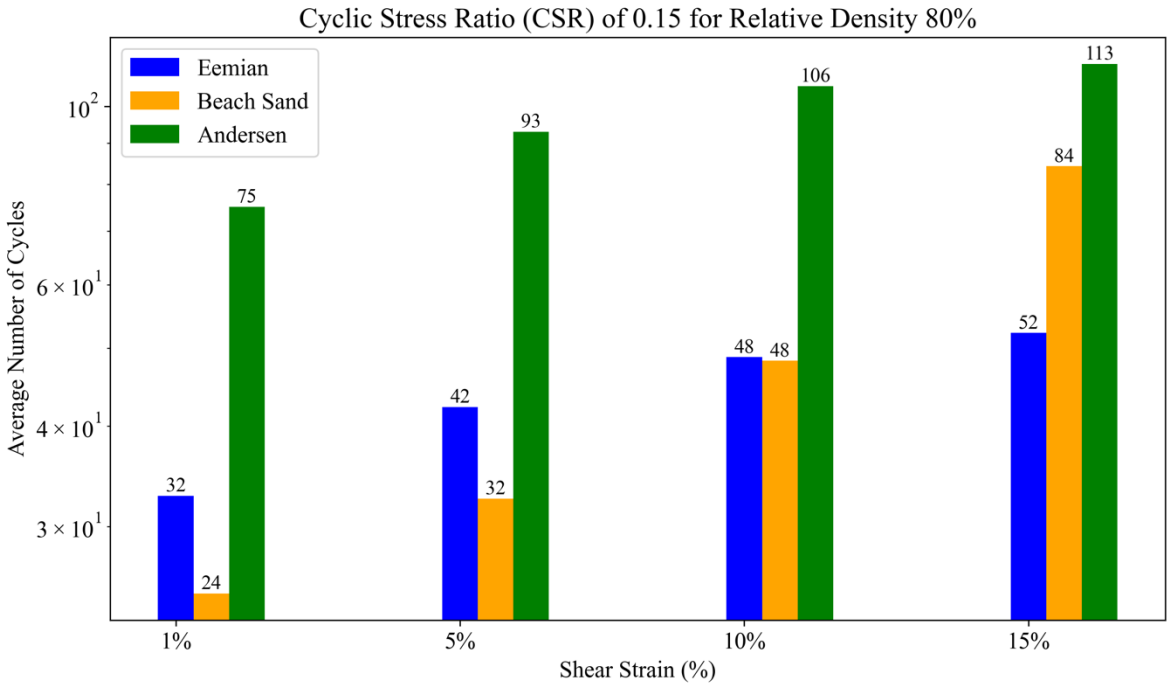
Cyclic Stress Ratio (CSR) of 0.15 for Relative Density 80%
Eemian
Beach Sand
Andersen
Average Number of Cycles
10^2
6×10^1
4×10^1
3×10^1
32
24
75
42
32
93
48
48
106
52
84
113
1%
5%
10%
15%
Shear Strain (%)